OPTIMISATION OF FLUID FLOW IN A FLAT PLATE SOLAR WATER HEATER

By

Thomas B. Grassie

A thesis submitted in partial fulfilment
of the requirements for the degree of

Doctor of Philosophy

School of Engineering

at

Napier University, Edinburgh

2001

DECLARATION

I hereby declare that the work presented in this thesis was solely carried out by myself at Napier University, Edinburgh, except where due acknowledgement is made, and that it has not been submitted for any other degree.

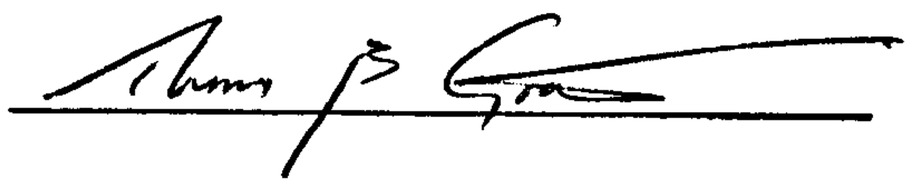

Thomas B. Grassie (candidate)

13th Sept '01

Date

ABSTRACT

At higher latitudes, where there is a lower annual solar availability, solar water heating can still make a valuable contribution towards water heating energy demand. Whereas systems at lower latitudes may use natural circulation to promote flow through the collector, at higher latitudes the collector flow rate is generally regulated by a temperature differential controller (TDC) operating a mains supplied circulation pump. With the pump switched on, the flow rate is constant. In addition, the requirement of freeze protection at higher latitudes increases system complexity, and hence cost, and can also reduce efficiency.

A new freeze-tolerant solar domestic hot water system (SDHWS) is introduced. This system, termed freeze tolerant-photovoltaic (FT-PV), through virtue of using a collector that tolerates freezing, requires neither anti-freeze nor a drain back facility to afford frost protection. In contrast to the above mentioned TDC switched circulation pump, the FT-PV system uses a small solar electric, photovoltaic (PV), module to drive a pump. As PV output varies with irradiance, so the system will operate with a low and variable flow rate. In addition, as water can be circulated directly through the collector, the collector return can be fed directly into the storage tank, with the low flow rate promoting thermal stratification therein.

For the FT-PV system storage tank, a model for defining the internal axial temperature profile in relation to that of the external wall during a cooling period is presented and validated. Furthermore, a model for simulating tank heat loss and destratification has been developed and, again, validated.

A new method for determining the collector efficiency characteristic is presented. This method is validated through a comparison with empirically defined values, and also through application in software models that have been developed for simulating the collector outlet temperature. The optimum collector flow rate profile is defined.

Presently, there are no "off the shelf" components available that will provide the above desired flow rate profile. Through considering the optimum operating condition, the present work details the selection of the most appropriate PV module/pump pairing for the present application. Through an experimental and analytical study of the FT-PV systems component characteristics and interactions, the effect of two simple methods of control on flow rate, and hence collector outlet temperature, is presented. While the flow rate profile is not ideal, the method of physical shading is seen to provide a collector outlet temperature (COT) profile that is closest to optimum.

With this control strategy, the performance of the optimised FT-PV system is compared with that of a standard anti-freeze based system. For an identical load demand, irrespective of the method of control applied to the auxiliary heat source, the FT-PV system is shown to require less auxiliary input, representing a greater saving. The FT-PV system collector outlet temperature profile, and hence the system performance is, however, highly sensitive to both the position of, and method of control applied to, the auxiliary heater. The performance of both the FT-PV and reference systems may be improved through the intelligent control of the auxiliary heater.

The above-mentioned method of analysis may be used to define the optimum degree of control for the larger commercial FT-PV system.

ACKNOWLEDGEMENTS

I would firstly like to thank my supervisory team, Kerr MacGregor, Tariq Muneer, and Jorge Kubie for their support, encouragement, and enthusiasm throughout this project. For their continued confidence, in both myself, and this work, that has helped to keep me moving forward, I am most grateful. As a team, your guidance has been invaluable, while individually you have also given most generously of your time, insights, and, most importantly, your friendship. I hope we will have the chance to work together in the future. It would again be my privilege.

Secondly, but no less importantly, I would also like to thank my office colleagues for their help and support. Dave and Nasser for helping "show me the ropes" while they themselves were "writing up", and to my current colleagues, Ana, Asif, Colin, Graeme, Imtithal, and Xiaodong. May I wish you all every success with your present work and future careers.

To the technical staff, Kevin McCann and Ian Campbell, I would also like to express my gratitude, perhaps best in the form of a beer with a bit o' foot tappin'fiddle. You have been a crucial part of the team.

Also to my wife Gillean, who has tolerated long periods of my apparent deafness while absorbed in some thought or other. I hope I can offer you the same support now that you have chosen a similar journey. Thanks for being there, always. And Sam, my son, thanks to you too, for lego, tree climbing, and camp fires, a panacea for all academic ails. Thanks also to all family and friends for your support and encouragement. I hope we all can gain a little from this work.

CONTENTS

2 REVIEW OF PREVIOUS WORK

4 MODELLING SYSTEM PERFORMANCE

5 ECONOMIC ANALYSIS

List of Publications

1 Development and Evaluation of the performance of a novel solar collector.

Pub. *UKISES Jubilee Conference.* Brighton, May 1999.

2 Optimising flow control in a novel solar domestic hot water system.

Pub. *NorthSun '99.* Solar Energy Society of Canada.

Edmonton, Alberta, August 1999.

3 Design of a PV driven low-flow solar domestic hot water system and modelling

of the system collector outlet temperature. *Accepted by Energy Conversion and*

Management, May 2001.

Articles Communicated

4 Improved performance prediction and the effect of electrical shading on the outlet

temperature of a novel direct PV driven low flow solar domestic

hot water system. *Communicated. International Journal of Solar Energy*

July 2000.

5 Side by side comparative testing of a new freeze tolerant direct, PV driven

Solar water heating system and a standard anti-freeze based system.

Communicated ASME JSEE, November 2000

LIST OF FIGURES

LIST OF TABLES

NOMENCLATURE

ΔH	dynamic head (m)
a	curve fitting perameter (-)
A_C	collector aperture area (m^2)
A_o	auxiliary energy utilised for a given load with no solar input (kWhrs)
A_{WS}	auxiliary energy utilised for a given load with solar input (kWhrs)
C_P	specific heat capacity (J/kg.K)
D_i	internal diameter (m)
f	solar fraction (-)
F_{PI}	fluid output power (W)
F_R	collector heat removal efficiency factor (-)
g	acceleration constant for gravity = 10 m/s^2
G	irradiance (W/m^2)
G_{eff}	effective irradiance (W/m^2)
G_{eq}	equivalent irradiance (W/m^2)
$Gr_{H,f}$	modified Grashoff number (-)
H	storage tank height (m)
h_{fi}	fluid side surface heat transfer coefficient ($W/m^2.k$)
I	load current (A)
I_{Afs}	PV module full sun equivalent current (mA/ [kW/m^2])
I_C	circuit current (A)
I_D	diode current (A)
I_L	light current (A)
I_{MP}	PV module current at maximum power point (A)
I_{SC}	PV module short circuit current (A)
I_{SH}	current through shunt resistance (A)
I_{TH}	threshold irradiance level (W/m^2)
L	length (m)

m_C	mass flow rate (kg/s)
Nu	Nusselt number (-)
Pe	Peclet number (-)
P_n	probe/axial nodal temperature (°C)
Pr	Prandtl number (-)
Q	volume flow rate (l/min)
q_U	useful heat output (W)
Re	Reynolds number (-)
$Ri_{H.f}$	modified Richardson number (-)
R_{LOAD}	load resistance (Ω)
R_{PL}	additional parallel resistance (Ω)
R_S	module series resistance (Ω)
R_{SH}	module shunt resistance (Ω)
S_1	transfer perameter number one (-)
S_2	transfer perameter number two (-)
T	time (s)
T_a	air temperature (°C)
T_{fm}	mean fluid temperature (°C)
T_i	collector inlet temperature (°C)
T_{IS}	inlet temperature to storage tank (°C)
T_o	collector outlet temperature (°C)
T_s	initial temperature (° C)
U_L	collector overall heat loss coefficient ($W/m^2.K$)
V	load voltage (V)
V_{MP}	PV module voltage at maximum power point (V)
V_{OC}	PV module open circuit voltage (V)
V_P	pump voltage (V)
W_n	wall nodal temperature (°C)
W_P	PV module peak output power (W)

Greek letters

τ	time constant (s)
$\tau\,\alpha$	transmissivity absorptivity product (-)
η	efficiency (-)
β	expansion coefficient (K^{-1})
ω_{IN}	tank inlet jet velocity (m/s)
ρ	density (kg/m^3)
α	thermal diffusivity (m^2/s)

LIST OF ABBREVIATIONS

BNT	Bottom Not Timed
CEC	Collector Efficiency Characteristic
EPDM	Ethylene Propylene Di Methyl
FT-PV	Freeze Tolerant – Photovoltaic
NOCT	Normal Operating Cell Temperature
PV	Photovoltaic
PWM	Pulse Width Modulation
PWPS	Photovoltaic Water Pumping System
RMSE	Root Mean Square Error
SDHWS	Solar Domestic Hot Water System
TDC	Temperature Differential Controller
TNT	Top Not Timed
TT	Top Timed
VBA	Visual Basic for Applications

1. INTRODUCTION

1.1 DOMESTIC WATER HEATING AND ENERGY DEMAND

Domestic heating accounts for approximately 30% of the United Kingdom's (UK) annual energy consumption, O.N.S. (2000). As such, this represents a significant contribution to the production of carbon dioxide, CO_2, in the UK. As old boilers, tanks, and immersions come to need replacing, more homes with mains gas supply are converting to the more efficient "combi" type gas-condensing boiler. The term "combi" refers to the fact that these systems provide heat for both the central heating and domestic hot water systems. These "combi" boilers do not generally operate with storage, and instantaneously heat the water close to point of use when there is demand. Transportation and storage losses are therefore minimised. Moreover, the boilers are often quoted as having thermal efficiencies as high as 90 %. In addition, the method of control applied to either of the older back boiler gas, or electric immersion type systems, can have a significant effect on the energy consumed for a given volume of hot water. Typically, for electric immersion systems, the bottom immersion in the tank is left on permanently to ensure a ready supply of hot water. This therefore also has a bearing on the running cost and emissions in terms of kg CO_2/ kWhr delivered.

As legislation imposes ever tighter restrictions on emissions, more pressure will ultimately be brought to bear on the consumer. All possible avenues for improving domestic hot water system efficiency and reducing emissions must be explored. One method of reducing water heating fuel bills is through installing solar water heating systems. This is obviously not an option for all households, both in terms of location, and in terms of the financial outlay required to install a system. For properties connected to the mains gas supply, the "combi" system, being cheaper to run than many alternatives, extends the payback period for a solar water heating system and therefore makes it less attractive. However, there is still a substantial proportion of the UK housing stock, particularly in more rural areas, that is not connected to mains gas supply. Using bottled gas is generally considered prohibitively expensive in respect of installing the above mentioned "combi" system. The payback period for a solar water heating system will therefore be more attractive.

1.2 INTRODUCTION TO SOLAR WATER HEATING SYSTEMS

1.2.1 Introduction

Solar domestic hot water systems (SDHWS) typically comprise a collector, mounted on a suitably appointed roof, which gathers the suns energy and transfers it to a storage medium by means of a circulating fluid. The energy delivered to the storage medium, usually a hot water tank displaces that which would otherwise have to be supplied by the primary energy. Solar energy can be converted directly to electricity by means of solar electric, photovoltaic (PV), modules. This electricity can then be used to heat the water directly. However, as these modules presently have a much lower conversion efficiency (typically 10-15%) than that of a thermal collector operating in a well-balanced system (~50%), thermal collectors constitute the vast majority of solar collectors used in SDHWS.

Generally, the stronger the sunlight, that is, irradiance, the higher the potential output for both PV modules and thermal solar collectors. The potential output is maximised during periods of clear sky with the sun's beam angle of incidence perpendicular to the collector/module surface normal. During such periods, the irradiance may approach an approximate maximum of 1000 W/m^2. However, there is still a worthwhile contribution to be gained at levels much lower than this.

1.2.2 Optimum positioning of solar collectors.

The optimum angle of tilt and orientation for a collector, from the horizontal, is approximately 0.9 times the location latitude, Duffie and Beckman (1991), with the collector facing south in the northern hemisphere, and north in the southern hemisphere. While this orientation will generally provide the maximum annual availability and yield, the yield is not overly sensitive to deviations from the above optimum position. Figure 1.2.1 shows a plot of the monthly average solar availability for different orientations and tilts. (Data obtained for Glasgow, UK, from Page and Lebens (1986))

Solar water heating systems fall into two main categories. An overview of these is now presented.

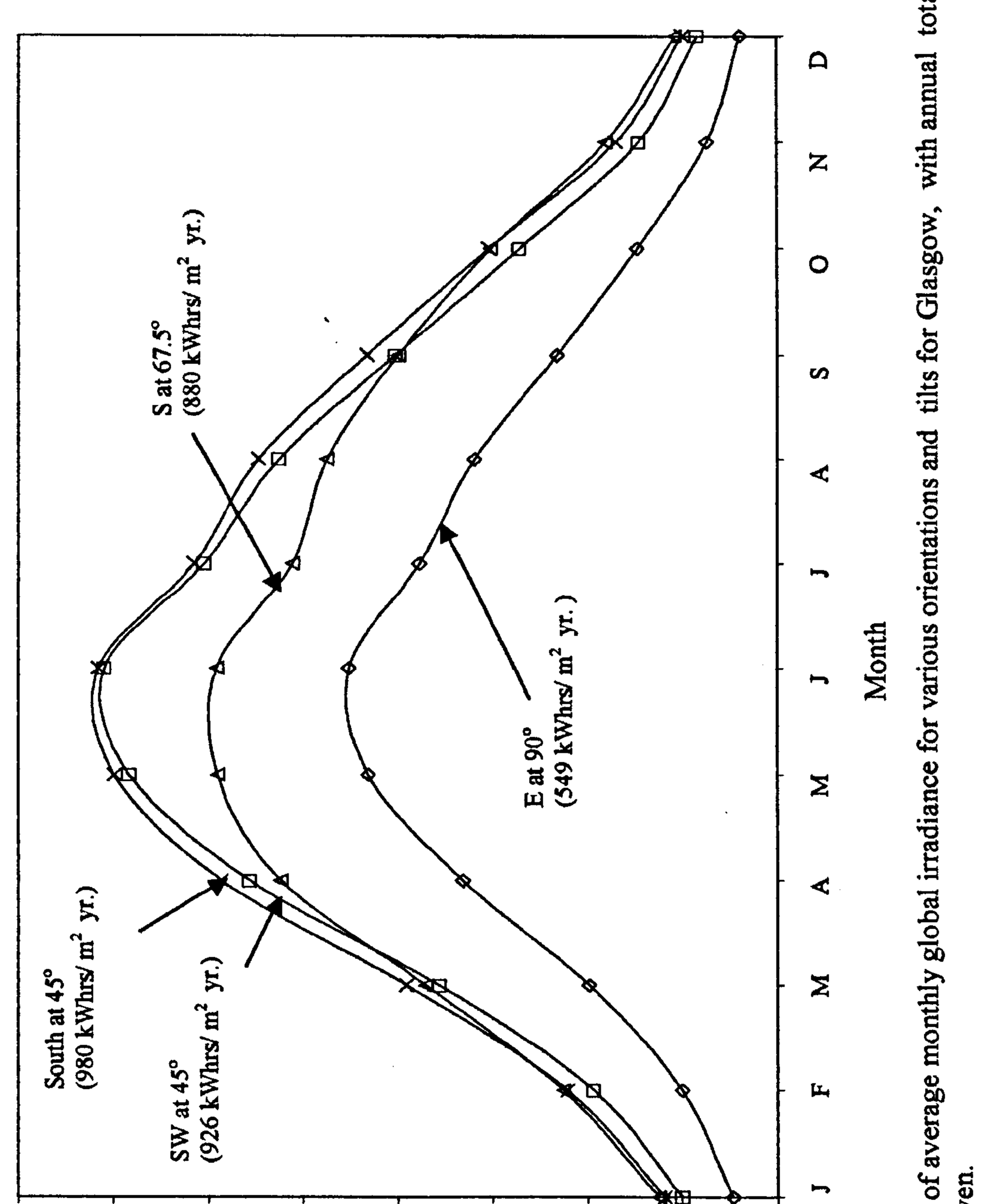

Figure 1.2.1 Plot of average monthly global irradiance for various orientations and tilts for Glasgow, with annual total also given.

1.2.3 Forced and natural circulation solar water heating systems.

While the basic principle of operation of an SDHWS, where a collector transfers heat to a circulating fluid, and thence to storage, is common to all solar thermal collector systems, this strategy may be applied in several ways. The two most distinct types of system are the natural circulation and forced circulation systems. The more simple of these is the natural circulation, or thermosyphon system. Here the buoyancy forces established through the hot fluid in the collector having a lower density than the colder water at the collector inlet cause a natural circulation of the collector fluid. Figure 1.2.2 shows a schematic of a typical thermosyphon system. It can be seen that for this system to work the storage tank must be above the collector and the piping runs kept short and at a reasonable gradient. Both the collector and tank are therefore often mounted outwith the building. This type of system is also termed direct as the water is returned directly to the storage tank after heating. It is also self-regulating, collecting heat when it is available. The fluid flow rate and collector outlet temperature are, amongst other factors, dependant on the intensity of the incident solar radiation, or irradiance.

In a forced circulation system such as that shown in Fig. 1.2.3, the collector fluid is circulated by means of a pump. Pump operation is generally regulated by a temperature differential controller (TDC) which compares the collector and tank temperatures and switches on the pump if the difference is greater than a pre-set "on" limit. Similarly, if this difference in temperature falls below the pre-set "off" limit the controller switches off the pump. This type of system, neglecting the effects of temperature on the viscosity of the collector fluid, can be said to operate with a fixed collector flow rate. While the collector inlet temperature has a significant effect, for different levels of irradaince, or heat input, the collector outlet temperature will tend to vary. The flow rate developed through using a pump is generally much greater than that established by the thermosyphon system. Considering Eq. 1.2.1, where E is the heat transferred to the collector fluid, m_C the collector mass flow rate, C_p the specific heat capacity of the collector fluid, and T_I and T_O the collector inlet and outlet temperatures respectively, it can be seen that the higher flow rate system will generally produce lower outlet temperatures.

$$E = m_C C_p (T_O - T_I) \qquad (1.2.1)$$

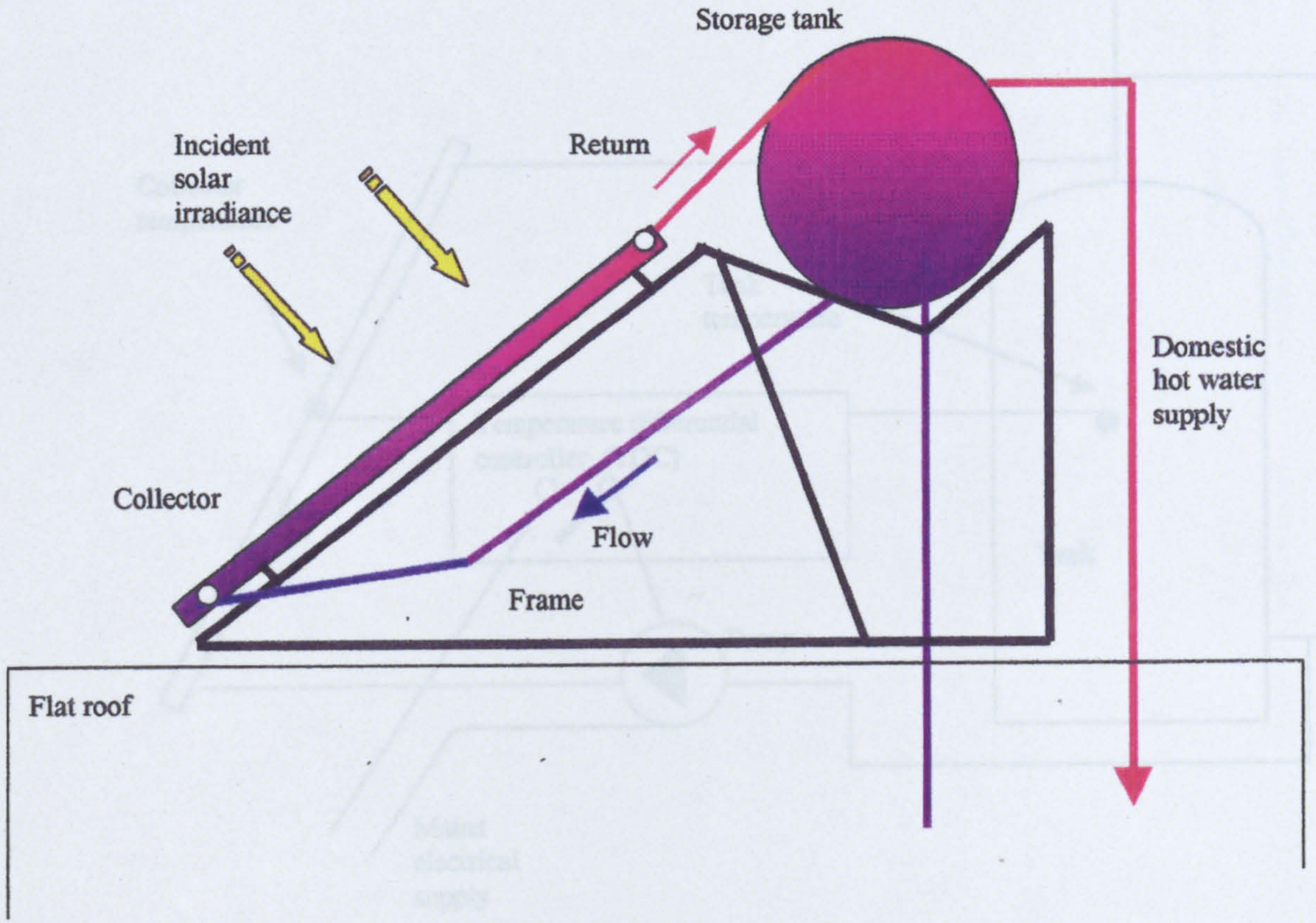

Figure 1.2.2 A flat roof mounted natural circulation (thermosyphon) system

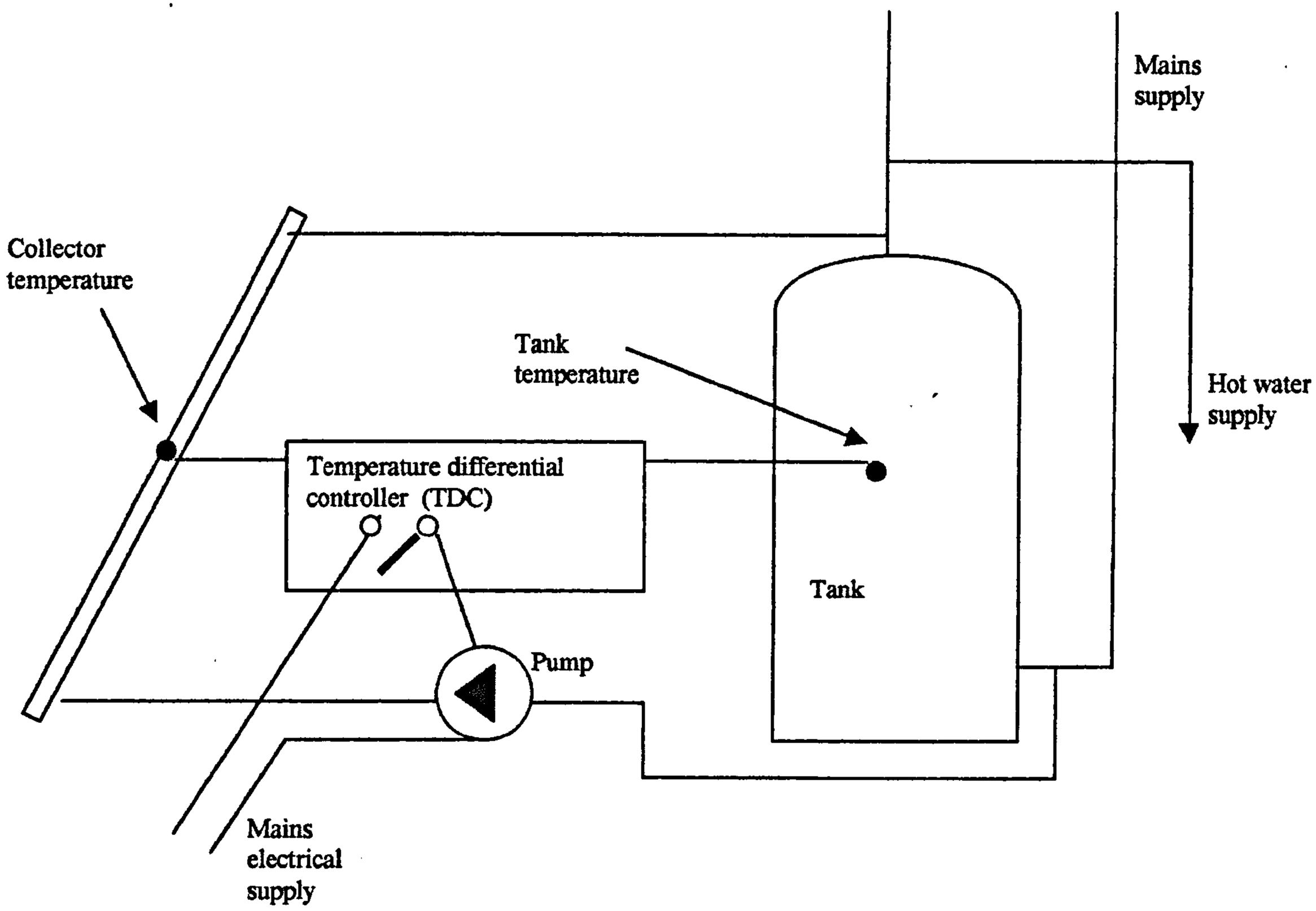

Figure 1.2.3 A simple forced circulation solar water heating system

Thus far, two simple types of SDHWS have been described. Generally, implementation of the thermosyphon system is restricted to lower latitudes where the climate provides a consistently higher number of daily sunshine hours throughout the year and annual minimum temperatures never fall below freezing point. For both the above systems, as the collector, and the tank for the thermosyphon system, are situated outwith the building, if air temperatures were to fall below freezing this could damage the systems. At higher latitudes and locations where there is the potential for freezing, the design of a solar water heating system must therefore include some form of freeze protection.

The main types of systems and the methods of freeze protection that are currently used at higher latitudes are now detailed.

1.3 APPLICATION OF SOLAR DOMESTIC HOT WATER SYSTEMS AT HIGHER LATITUDES

1.3.1 System Design.

As solar availability is generally lower and less consistent at higher latitudes than it is at lower latitudes, the thermosyphon systems outlined above do not tend to operate well in these locations. Hence, systems operating at higher latitudes are generally of the forced circulation type. In addition, at these higher latitudes, SDHW systems also need to be protected against damage from freezing. Several strategies have been developed to achieve this.

The most simple of these is to define a safe annual operating period for the location, and drain the system for the remainder of the year. This type of control is often referred to as three-season operation. With this strategy, as any potential heat gain from sunny winter periods is lost, there is therefore a thermal penalty incurred. Bradley (1997), however, through a comparative analysis of three and four-season systems found that, for certain higher latitude coastal locations, three-season operation provided a better annual system performance. In addition, it was shown that three-season system performance could be enhanced if the systems were kept operational during the first and last months of the winter period. To achieve this, hot water from the storage tank was circulated through the collector overnight to prevent freezing. The heat lost in this way was less than that gained through increasing the operational period.

One alternative method of freeze protection is to employ electric trace heating wires along the connecting pipes and inside the collector. A temperature sensor controls the electric supply on/off and warms the pipes thus preventing freezing. One of the major drawbacks of this method is that, during power cuts, which generally occur more frequently in winter, the system is unprotected. Other methods that have been considered include the addition of narrow air filled tubes within the collector fluid pipes. These tubes are designed to distort under the pressure induced through the volumetric expansion of the water in the collector pipes, and hence protect the collector pipes from freeze damage. The use of flexible collector fluid tubes and connecting pipe has also been investigated.

The two most common methods of freeze protection are firstly to use an anti-freeze solution in the collector loop, and secondly to use a drain back facility. In the first instance, as shown in Fig. 1.3.1, an anti-freeze solution is circulated through the collector with heat transferred to a solar tank via a heat

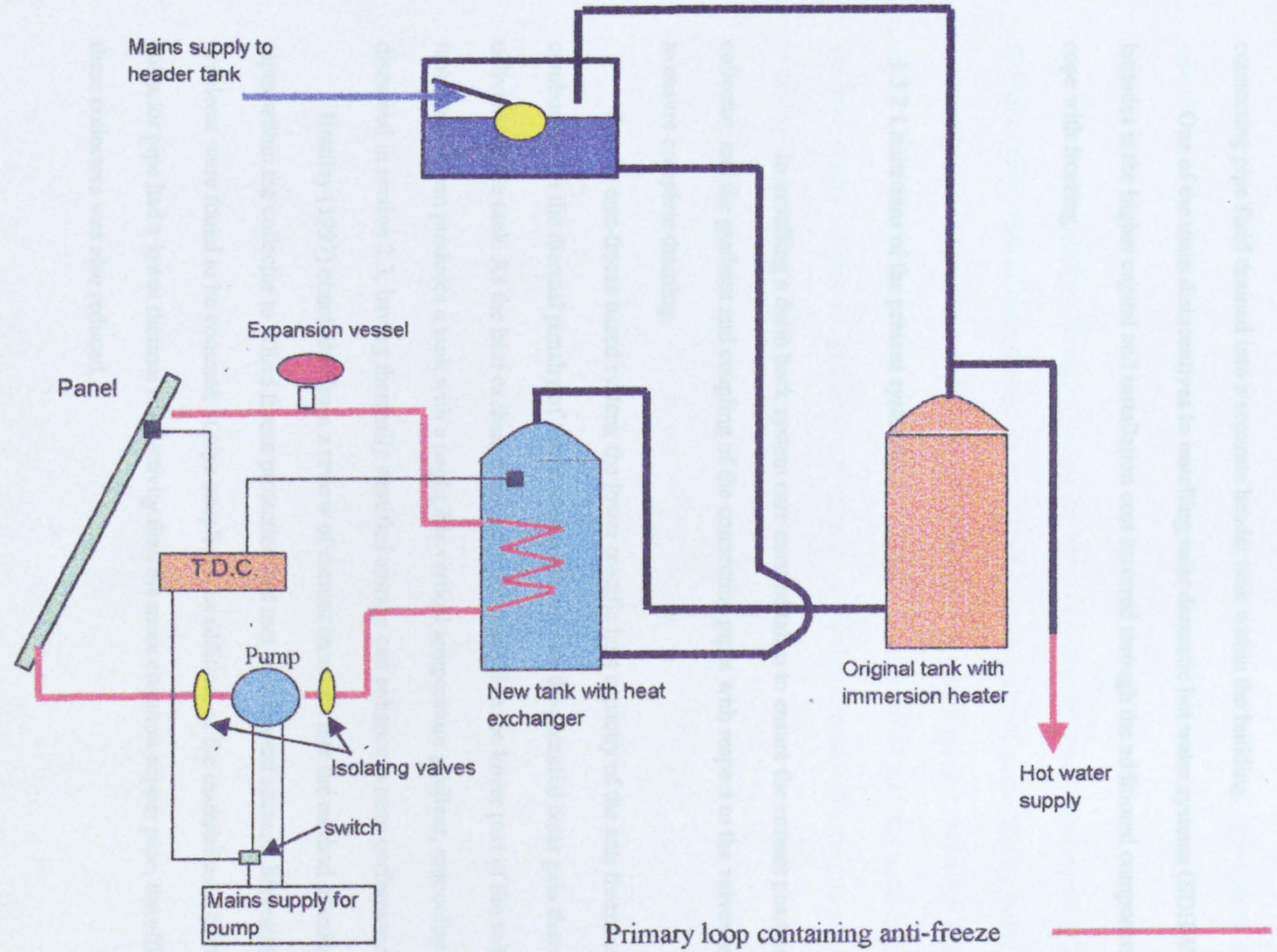

Figure 1.3.1 Anti-freeze based solar water heating system.

exchanger. Flow on/off is regulated by a temperature differential controller. In the case of the drain back system, a temperature controller again regulates the flow on/off, but also the position of flow valves. When the air temperature drops to below a pre-set value, the drain valves are opened and the collector and connecting pipe fluid drained into a separate header tank within the building.

One of the main disincentives to installing solar domestic hot water systems (SDHWS) at higher latitudes is the higher capital and installation cost incurred through the additional components required to cope with freezing.

1.3.2 Limitations of the present systems

In installing a drain back system care must be taken to ensure the correct positioning of the collector, and the gradient and coupling of the connecting pipes with respect to the valves and header tank to ensure complete draining.

For the anti-freeze based system, the lower specific heat capacity of the anti freeze solution combined with the thermal penalty of a heat exchanger reduces the potential solar gain that can be delivered to the tank. As the heat exchanger is generally situated in the lower part of the solar preheat tank, this system produces a tank with a negligible vertical temperature gradient, monocline. As will be discussed in section 2.3, having thermally stratified storage can enhance system performance.

Bradley (1997) concluded from a review of current literature that the method of using flexible pipes within the collector to afford freeze protection had met with limited success. Moreover, freezing problems were found to be common at pipe couplings. In addition, as the material used for the flexible collector pipe had a lower thermal conductivity than the more common copper pipe, the efficiency of these collectors was also reduced.

1.3.3 Range of application

Generally, at higher latitudes, the application of SDHWS is considered in relation to the heating/preheating of water for washing and bathing. While the collectors of such systems may also be used to heat water for swimming pools, often, a simpler form of collector and system is used for this application.

The use of SDHWS for space heating can provide a valuable annual energy saving. M[ac]Gregor and Balmbro (1984) showed that although the solar availability was lower, as the heating season was longer, solar water heating systems provided a greater annual energy saving at higher latitudes. This is illustrated in Fig. 1.3.2. The energy saved is represented by the shaded area. While both the heating load and annual auxiliary energy required are greater, there is a greater annual contribution from the solar heating system at the higher latitude.

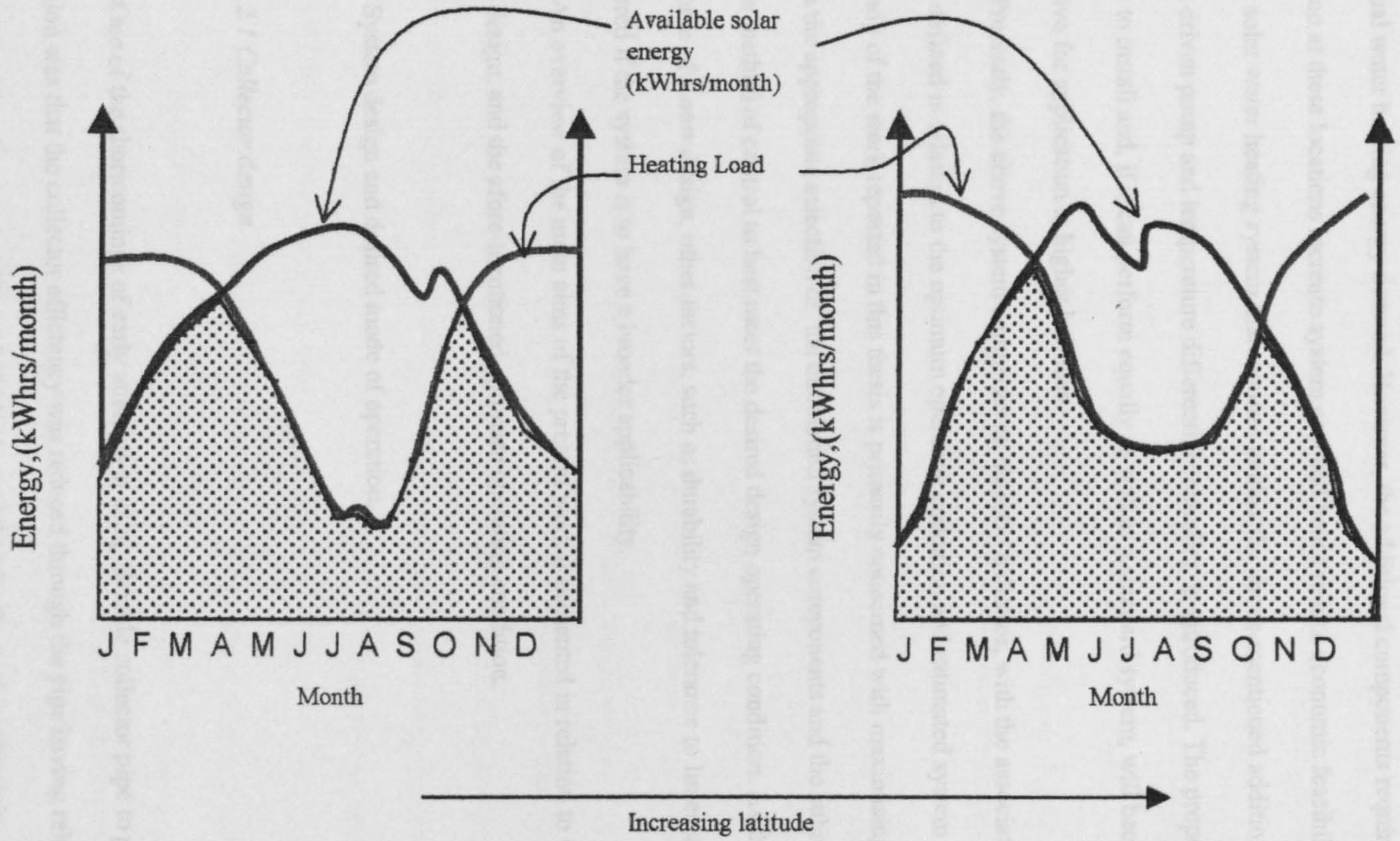

Figure 1.3.2 Potential space heating energy saving for a solar water heating system in respect of latitude

1.4 THE PRESENT WORK.

1.4.1 Introduction

Application of SDHWS at higher latitudes has been shown to provide a valuable contribution to the annual water heating energy demand. However, the additional components required to provide frost protection at these locations increase system cost and hence reduce economic feasibility. A new freeze-tolerant solar water heating system that requires neither the above-mentioned additional components, nor a mains driven pump and temperature differential controller, is introduced. The proposed system will be cheaper to install and, if it can perform equally as well as a standard system, will become a viable alternative for application at higher latitudes.

Presently, the above system comprises an untested collector, with the associated circulation system loosely defined in relation to the optimum operating condition and estimated system characteristics. The main body of the work reported in this thesis is primarily concerned with maximising system performance through the appropriate selection of the circulation system components and the subsequent application of a simple method of control to best meet the desired design operating condition. As the freeze tolerant collector is of a new design, other factors, such as durability and tolerance to limescaling, need also to be considered if the system is to have a broader applicability.

An overview of the main aims of the present work is presented in relation to the collector and system design, and the afore-mentioned optimum operating condition.

1.4.2 System design and desired mode of operation.

1.4.2.1 Collector design.

One of the shortcomings of early attempts at using flexible collector pipe to provide frost protection was that the collector efficiency was reduced through the pipe having relatively poor thermal conductivity. Bartelsen et al (1996 and 1999) showed that the thermal conductivity of EPDM pipe could be greatly enhanced through the addition of carbon black during the manufacturing process. The

conductivity of this pipe, with the additional carbon, is quoted as being between 0.8 and 0.9 W/m.k, (Bartelsen et al (1996)), whereas that of copper is given as approximately 400 W/m.K. (Incropera and Dewitt (1996))

Using this pipe, a new freeze tolerant solar water heater, hereafter referred to as the "Flexsol" panel, has been developed by Kerr MacGregor of Napier University. As the pipe is flexible, with room to deform within the absorber plate to accommodate the volumetric expansion of freezing water, mains water can be used as the primary heat transfer fluid. As such, for a retrofit system, the collector and circulation system can be plumbed directly into the existing hot water system.

Figure 1.4.1 shows a cross-sectional view of the construction of the Flexsol panel. All experimental work relating to the performance of the panel presented in section 3 was undertaken using a 2 m^2 prototype panel of the design shown in the above mentioned figure. This prototype collector measured 2.0 m by 1.0 m. The collector fluid tube is laid in a serpentine manner, making 6 passes along the 2 m width of the collector absorber plate.

Many present collectors, such as those produced by AES, (AES (1999)) and also those of Ar-Con (Ar-Con (1994)), comprise absorber plates that are fully covered with a low emmissivity coating to reduce heat loss through radiation. Only the upper half of the Flexsol panel absorber is coated. The greatest loss from a collector is in this upper region where the difference between the absorber pate and external air temperatures is greatest. During periods of high solar gain and no load draw off the collector inlet temperature can be raised to such a level that the outlet temperatures become dangerously high for domestic use. By not having the above-mentioned coating on the lower half of the absorber plate, the Flexsol collector is therefore more readily able to loose heat in such circumstances. By having the low emmissivity coating on the upper half only to maximise the benefit of reduced heat loss is maximised while affording a certain degree of overheat protection.

While it is possible to calculate the efficiency characteristic of a solar thermal collector through a consideration of its' construction, material properties and estimated flow rate, as it is intended that the system operates with a variable flow rate, it is necessary to experimentally define this characteristic in relation to the flow rate range considered. A review of collector testing methods is presented in section 2.2. The development of a new technique is outlined in section 3.4 in relation to determining the efficiency characteristic of the Flexsol panel under different operating conditions.

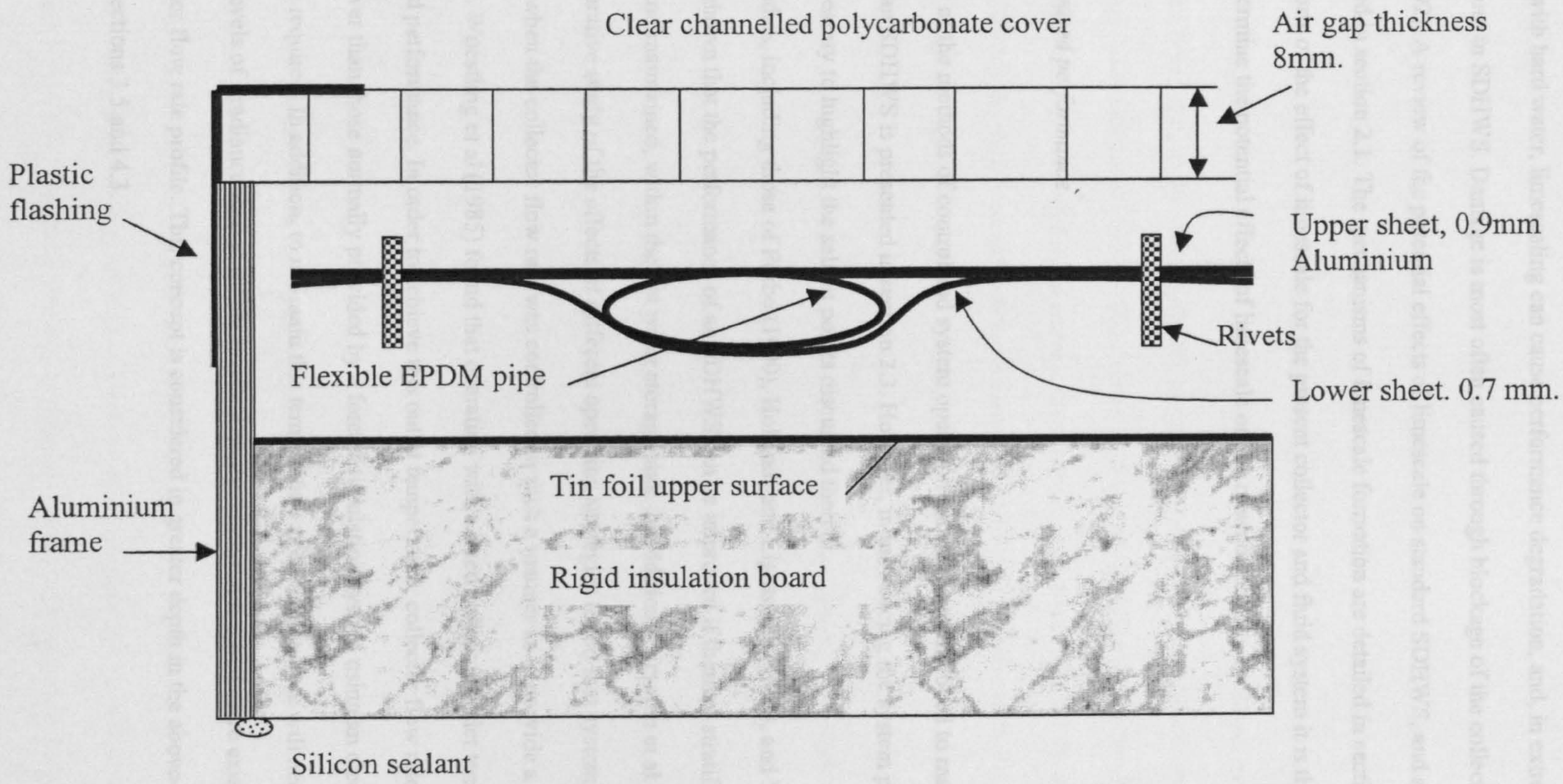

Figure 1.4.1 Cross sectional view of Flexsol collector construction.

In areas with hard water, limescaling can cause performance degradation, and, in extreme cases, components failure in SDHWS. Damage is most often caused through blockage of the collector fluid tubes, Vliet (1992). A review of the potential effects of limescale on standard SDHWS, and also in plastic pipes is presented in section 2.1. The mechanisms of limescale formation are detailed in section 3.2. As there are no reports of the effect of limescale for the present collector and fluid system it is therefore necessary to determine the potential effects of limescale on the new collector.

1.4.2.2 Optimised performance

A review of the methods of control and system operation that may be employed to maximise the performance of an SDHWS is presented in section 2.3. However, in introducing the system presently studied, it is necessary to highlight the salient points discussed therein.

Many studies, including those of Furbo (1990), Hollands and Lightstone (1989), and Wuestling et al (1985), have shown that the performance of an SDHWS can be improved if thermal stratification can be established, and maintained, within the hot water storage tank. In addition, Carvalho et al (1988), through a comparative study of the effects of different operating strategies found that system performance was maximised when the collector flow rate was controlled in such a manner as to provide a fixed temperature rise. Wuestling et al (1985) found that operating with a fixed collector outlet temperature of 55 °C maximised performance. In order to achieve this outlet temperature, collector flow rates considerably lower than those normally provided by a forced circulation system using an electric mains driven pump are required. In addition, to maintain this temperature rise, the flow rate will necessarily be lower at lower levels of irradiance than at higher levels. This therefore implies that there exists an optimum collector flow rate profile. This concept is considered in greater depth in the above-mentioned section, and in sections 3.5 and 4.3.

1.4.2.3 System design.

In consideration of the above, the new system comprises the Flexsol collector, and a solar electric, PV, module which drives a small pump. The collector flow and return are connected directly to the tank bottom and top inlets/openings respectively. A schematic diagram of the new system, termed an FT-PV (freeze-tolerant - photovoltaic driven) SDHW system, is shown in Fig 1.4.2. As the output of a PV module varies with irradaince, so the pump hydraulic output and system flow rate will also vary. Al-Ibrahim (1997) and Al-Ibrahim et al (1996, 1998) defined the PV module and pump electrical and hydraulic characteristics that were required to provide the optimum flow rate profile for the system studied. As no ideal "off the shelf" components are currently available for the present system, the PV module and pump are selected on the basis of a best match. The PV module output is subsequently controlled to obtain the specified design operating condition of a constant collector outlet temperature.

A full experimental and mathematical analysis of the effect of two simple methods of control on system performance is presented in section 3.5. The suitability of the above-mentioned control methods is considered in relation to their ability to provide the desired collector outlet temperature profile. A model for predicting the collector outlet temperature in relation to the method and degree of control is presented in section 4. The predicted collector outlet temperature profiles are compared with those measured.

1.4.2.4 Storage tank performance

As outlined in the section 1.4.2.2, the performance of solar domestic hot water systems storage tanks is pivotal to the overall thermal performance of the system. A review of the factors affecting tank performance and the rate of stratification decay and heat loss is presented in section 2.5. The present work aims to define the relationship between tank wall and internal axial temperatures for a tank with the desired dimensions for the FT-PV system. This is to enable the internal temperatures to be defined through non-intrusive measurement, and hence determine the degree of stratification within the storage tank.

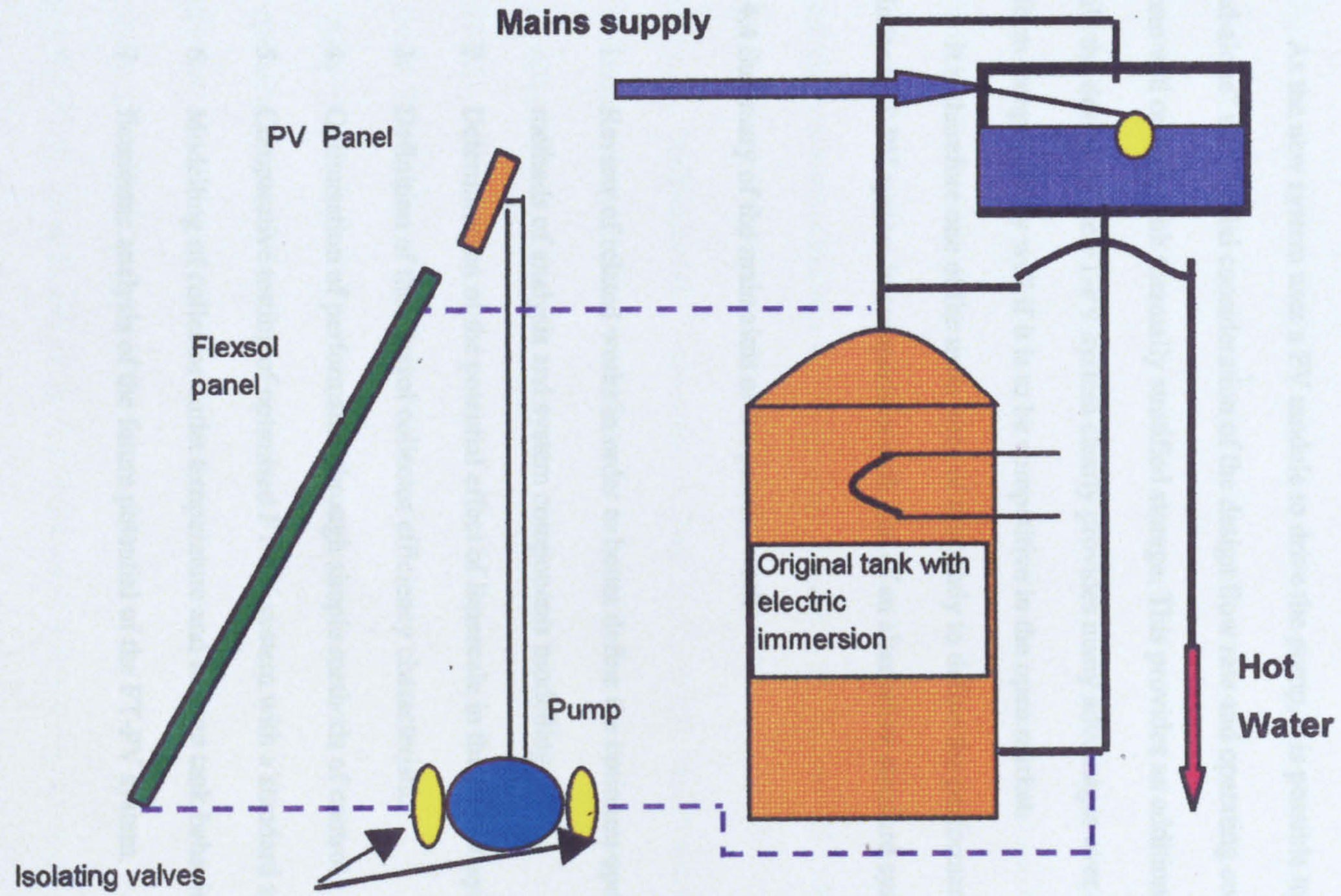

Figure 1.4.2 Schematic diagram of the FT-PV system

1.4.3 Potential benefits of the FT-PV system

The configuration of the FT-PV system greatly reduces the capital and installation costs, particularly if the system is being retrofitted, as the additional components required to prevent frost damage in alternative systems are no longer necessary. In comparison with systems employing a primary anti-freeze loop, there is an additional thermal benefit, in that, through heating the domestic hot water directly, the energy penalty incurred through using a heat exchanger and anti-freeze solution is removed.

As the new system uses a PV module to drive the pump, it is possible to operate it as an "off-grid stand-alone" unit. Initial consideration of the design flow rate and operating conditions implies that the system will operate with thermally stratified storage. This provides an additional performance benefit. While the design of the FT-PV system clearly provides many advantages over alternative systems, it must perform comparatively well if it is to be competitive in the open market.

It is therefore one of the main aims of this study to define the performance potential of the optimised FT-PV system in comparison with that of an alternative standard system.

1.4.4 Summary of the main aims of the present work

1 Review of related works in order to better define the optimum operating characteristics, methods of analysis and system components modelling

2. Determination of the potential effect of limescale in the FT-PV system.

3. Definition of the Flexsol collector efficiency characteristic.

4. Optimisation of performance through simple methods of control

5. Comparative testing of optimised FT-PV system with a standard system

6. Modelling of collector outlet temperature and storage tank behaviour

7. Economic analysis of the future potential of the FT-PV system.

REFERENCES

A.E.S., (1999), Appropriate Energy Systems, Solar Water Heating System Installation Guide. A.E.S Ltd, The Park, Forres, Scotland.

Al-Ibrahim A. M., Klein S.K., Mitchell J.W., Beckman W.A.(1998). Design procedurefor selecting an optimum photovoltaic pumping systemin a solar domestic hot water system. *Solar Energy* Vol. 64, Nos 4-6, pp.227-239.

Al-Ibrahim A.M., (1997), Optimum selection of direct coupled photovoltaic pumping system in solar domestic hot water systems. PhD thesis, University of Wisconsin-Madison.

Al-Ibrahim A.M., Klein S.K., Mitchell J.W., Beckman W.A. (1996) An Investigation of photovoltaic powered pumps in direct solar domestic hot water systems. In *Proceedings of Solar '96*, American Solar Energy Society, 13 –18 April, Asheville, North Carolina, America, Campbell-Howe R. and Wilkins-Crowder B. (Eds), pp. 141-146.

Bartelsen B., Rockendorf G., and Vennemann N., (1996), Development of an elastomer-metal-absorber for thermal solar collectors. In *Proceedings, EuroSun '96,* Section IV-1. *Pub* ISES, DGS Sonnenenergie Verlags-GmbH, Munich.

Bartelsen B., Rockendorf G., Vennemann N., Tepe R., Lorenz K., and Purkarthofer G., (1999), Elastomer-metal-absorber – development and application. In *Proceedings ISES World Solar Energy Congress,* Israel.

Bradley D., (1997) Promising Freeze protection Alternatives in Solar Domestic Hot Water Systems. MSc. thesis. University of Wisconsin-Madison.

Carvalho M.J., Collares-Pereira M., Cunha F.M., and Vitorino C., (1988), An experimental comparison of operating strategies for solar water systems. *Solar Energy,* Vol. 41, No.1, pp 33 – 39.

Duffie J.A. and Beckman W.A. (1991) *Solar Enginering of Thermal Processes,* 2nd edn, Wiley Interscience, New York . ISBN 0-471-51056-4

Furbo S., (1990), Attractive small marketed hot water solar heating systems using low flow operation. In *Proceedings of Northsun '90,* Reading, England, Sayigh A.A.M. (Ed), Pergamon Press, Oxford

Hollands K.G.T., and Lightstone M.F., (1989), A review of low flow stratified-tank solar water heating systems *Solar Energy*, Vol. 43, pp 97-105.

Incropera F.P., and DeWitt D.P., (1996), *Introduction to heat transfer*. 3rd edn, Wiley Interscience, New York . ISBN 0-471-30458-1.

M[ac]Gregor K., and Balmbro D., (1984) Why North is best for solar heating of buildings. In *Proceedings, North Sun 1984*, Napier University, Edinburgh, Scotland. p76

O.N.S., (2000), Office for National Statistics. http://www.ons.gov.uk

Page J., and Lebens R., (1986) Climate in the United Kingdom. HMSO Pubs. ISBN 0-11-412301-2

Vliet G., and Baker D., (1992), Designing solar hot water systems for scaling environments. *ASHE JSES ITSES International Solar Energy Conference*. ISBN 0791807622.

Wuestling M.D., Klein S.A., and Duffie J.A., (1985), Promising control alternatives for solar water heating systems. *ASME Journal of Solar Energy Engineering* Vol. 107.

2 REVIEW OF PREVIOUS WORK

2.1 LIMESCALING IN SOLAR DOMESTIC HOT WATER SYSTEMS.

2.1.1 Introduction

In any process that uses hard water, scaling can cause a variety of problems. That is particularly so for thermal processes where the water is hot, as this encourages salt formation and deposition. Although in some cases it is desirable to have a thin layer of scale to afford corrosion protection to internal surfaces, it is generally considered undesirable to have scaling. As the precipitation of the salts that cause scaling, (most commonly Calcium Carbonate, $Ca^{2+}CO_3^{2-}$, and to a much lesser extent, Calcium Sulphate, $Ca^{2+}SO_4^{2-}$, and Magnesium Sulphate, $Mg^{2+}SO_4^{2-}$) is dependant on temperature, scaling normally occurs on heat transfer surfaces where the potable water reaches its maximum temperature. This results in a higher heat transfer resistance and hence a decreased system efficiency. In severe cases, scaling can cause component failure. In respect of SDHW systems, Baker and Vliet (1993), the narrowing and blocking of collector tubes can cause freeze damage in drain back systems, and render a system inoperable. Burch (1994) reported a case where a deposition layer of 0.5 cm. had been built up in only one year of operation, completely blocking the collector tubes. This deposit was found to be 95% Calcium Carbonate. There is also the potential for damage to pumps and heat exchangers.

It is not within the scope of this review to detail all the mechanisms behind scale formation. However, an overview of some of the factors that influence the rate of formation is presented in relation to the configuration and materials used in SDHW systems.

2.1.2 Effect of the type of material on the rate of scale formation.

Ledion et al (1993) made a study of the comparative effects of different polymer materials on the rate of scale formation. They showed that the rate of formation was influenced by electrostatic forces built up on the polymer walls through friction between the wall and the circulating fluid. The electrostatic forces encourage the trapping of Calcium Carbonate precipitation seeds and therefore encourage the

deposition of scale. Surface roughness is also a factor. Of the materials tested it was found that the least polar polymer, being more susceptible to induced electrostatic charge, experienced a greater formation rate. For some polymer types the deposition rate was found to be greater than that for standard copper tube of the same diameter. By connecting a short length of earthed copper tube in the hydraulic circuit, the above authors showed that through discharging the aforementioned electrostatic charge, the deposition rate was reduced.

Bartelsen et al (1996 and 1998) showed that the heat transfer and strength properties of EPDM could be greatly enhanced through the inclusion of, mostly, Carbon black in the manufacturing process. The enhanced performance figures quoted by the above authors, (0.8 W/m.K), while considerably lower than those for copper, are comparable with that for water . This suggests that the new material may well be suited to heat transfer applications. There is no report of the effect that this addition has on the polarity of the new material and consequently no indication of the new materials tendency to encourage the formation of limescale. Baker and Vliet (1993) presented a model for predicting the severity of limescaling in SDHW systems. The model is based on an equilibrium water chemistry model in conjunction with the TRANSYS program developed by Klein (1985). The TRANSYS program is used to define the operating temperatures of the different systems studied. These temperatures are then used as inputs for the equilibrium analysis and an estimate of the potential severity of scaling made.

2.1.3. Methods of preventing limescale in SDHW systems.

2.1.3.1 System Design.

Vliet and Baker (1994) proposed several system designs that are more suitable for application in hard water areas. They suggest that larger diameter pipes be used for both connections and in the collector absorber plate to increase the surface area for heat absorption and reduce the hydraulic resistance of the system. In reducing the hydraulic resistance higher flow rates can be established. This lowers the mean collector fluid temperature and hence reduces the rate of scale formation. Burch et al (1998), Vliet and Baker (1994) and Baker and Vliet (1993) all suggest that the reduction in performance and the risk of

damage from scaling can be minimised through using a two tank indirect system. They maintain that using a separate solar preheat tank helps to maintain a lower collector inlet temperature, with clogging in direct system collectors being more common than in indirect system heat exchangers.

Bursch et al (1998) recommend increasing the storage volume while reducing collector size as a possible method for reducing scaling. Reducing collector size reduces the solar fraction supplied by a given system. As the primary aim of any SDHW system is to supply as large a portion of the water heating load as economically as possible, reducing the solar fraction does not appear a particularly worthwhile method of reducing scaling.

2.1.3.2 Preventative measures.

While reducing the solar fraction may seem a somewhat round about way of reducing scaling, other preventative measures may be taken. One common method employed in larger scale processes is that of electromagnetic protection. With this method scaling is actively encouraged in a certain region of the system that can be easily reached and replaced or cleaned. By encouraging deposition in one area, the concentration of the salts in solution is reduced, thus reducing the potential for deposition in other parts of the system. Other alternatives include the addition of water softeners, or regular cleaning by either mechanical means or circulation of a 1:10 diluted solution of muriatic acid to dissolve the scale. In referring to a telephone conversation Vliet and Baker (1994) quote an instance where the thermal expansion and contraction of a shell and tube heat exchanger was as marked as to cause the scale deposits to break off.

2.1.4 Summary

It has been shown that, where hard water is circulated through collector, there is the potential for deposition of limescale. Research has also shown that certain plastic polymers are susceptible to limescaling. While there is software available for predicting deposition in conventional type flat-plate collectors, there is no evidence that it is applicable to solar collectors employing plastic tubes.

2.2 MEASUREMENT OF COLLECTOR EFFICIENCY

2.2.1 Introduction

In the design and estimation of the performance of any solar water heating system, an accurate measure of the efficiency with which a given collector gathers the available solar energy is a key parameter. Various analytical and experimental procedures have been proposed and both national and international standards have been set to establish standardised methods for determining the collector efficiency characteristic. Section 2.2 therefore considers the form of the collector efficiency characteristic and the various methods that may be employed to define its parameters. Within this context, some of the factors that effect the actual collector heat output are also considered. As an introduction to this section however, a basic design common to many flat-plate solar water heaters is presented. A short analysis of the effect of environmental factors on collector performance is also given.

2.2.2 Flat-plate collector design and efficiency characteristic equations

A flat-plate solar water heater generally comprises three main components. These are, a frame of some description with an insulated backing, a transparent front cover or covers, and an absorber plate comprising pipes through which fluid is passed to remove heat gathered from the sun. Figure 2.2.1 shows a schematic of this simple configuration.

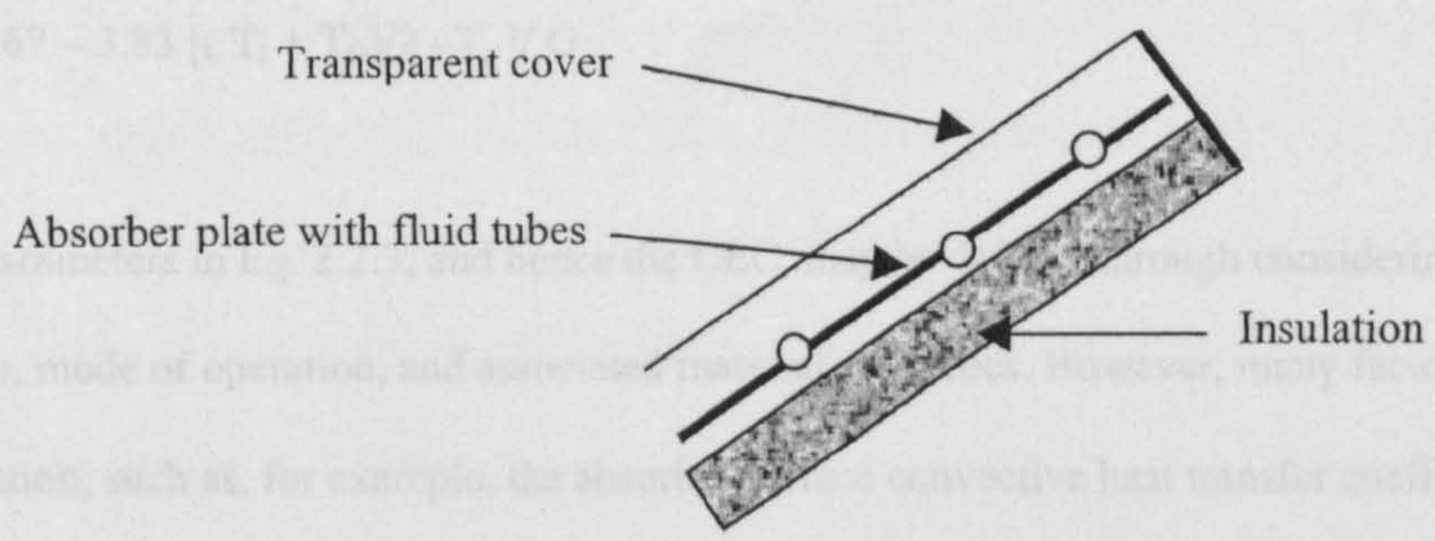

Figure 2.2.1 A cross-sectional schematic of a typical flat-plate collector.

The efficiency with which such a collector gathers the available energy is dependant on its specific construction, the materials properties, and its mode of operation. That is, the collector fluid flow rate and operating temperatures. Duffie and Beckman (1991) give a detailed analysis and derivation of the parameters that define a collector efficiency characteristic, CEC, and present this characteristic in the standard form as given in Eq 2.2.1.

$$\eta = F_R \tau\alpha - F_R U_L (T_I - T_a)/ G \qquad (2.2.1)$$

With reference to the nomenclature, the positive term represents the product of the collector heat removal efficiency factor, the cover transmissivity and the absorber absorptivity, and hence a maximum efficiency. The negative term represents the product of the collector heat removal efficiency factor, the collector overall heat loss factor and the difference in temperature between the collector inlet an ambient air, divided by the irradiance, G. In Europe this equation is often written in a slightly different form, with the inclusion of the collector outlet temperature in the negative term, as given in Eq. 2.2.2.

$$\eta = F_R \tau\alpha - F_R U_L [(T_I + T_O)/2 - T_a]/ G \qquad (2.2.2)$$

This equation therefore considers the losses in terms of the difference between the average collector fluid temperature, $(TI + T_O)/2$, and that of the ambient whereas Eq. 2.2.1 considers the losses in terms of the difference between the collector inlet and ambient air temperatures. Equation 2.2.3 below gives an actual CEC for a specific collector, Ar-Con (1994).

$$\eta = 0.67 - 3.83 [(T_I + T_O)/2 - T_a]/ G \qquad (2.2.3)$$

The parameters in Eq. 2.2.3, and hence the CEC, may be defined through considering the collector design, mode of operation, and associated material properties. However, many factors included in this derivation, such as, for example, the absorber surface convective heat transfer coefficient, are based on estimates of operating temperatures, and may only apply to a limited range of operating conditions. A review of methods used in calculating the top loss factor for a flat-plate collector is given.

2.2.3 Calculation of the collector heat loss factor

The collector heat loss factor, or U_L-value, may be considered as comprising three main parts. That is, collector edge and side losses, back losses and top losses. As the main heat transfer mechanism for heat loss through the collector sides and insulated back is conduction, calculating these components of U_L is a relatively simple operation. However, the upward, or top, heat loss factor comprises a combination of conductive, convective and radiative components, and is therefore much more complicated to define. This factor can be calculated by solving the governing heat transfer equations iteratively, or approximately from semi-empirical equations. Samdarshi and Mullick (1991) through a review of various models and software concluded that the approximate method was the more popular of the two. While numerous models for calculating the top loss factor have been proposed many are developments based on an initial equation presented by Hottel and Woertz (1942).

As many of the properties included in the estimation of the top heat loss factor are temperature dependant the magnitude of the negative term in the CEC will therefore also be dependant on the temperatures assumed for the above estimation. While Klein (1975) improved the above mentioned basic equation and extended its temperature range of application, Cooper and Dunkle (1981) considered the overall loss coefficient to be a linear function of the difference in temperature between the collector fluid and the ambient. This produced a non-linear collector efficiency characteristic. While this model was shown to improve accuracy, Cooper and Dunkle (1981) concluded that the linear model as presented in Eq. 2.2.2 was more than adequate for most operating circumstances. Whillier (1977) presented a detailed method for computing the overall heat loss value, U_L that included the cover refractive index, and the extinction coefficient, that is, the cover absorption losses. Grossman et al (1977) undertook an analysis of the effect of an absorber surface low emissivity selective coating on heat loss and hence collector efficiency. Other models, Agarwal and Larson (1981), Hollands et al (1981), Garg and Datta (1984) highlighted further developments and gave detailed analyses of the convective and radiative parameters affecting the top heat loss factor. Samdarshi and Mullick (1991) described an analytical equation for the top heat loss factor for a double glazed collector. They showed that, compared to the more accurate iterative method, the computational error could be as high as 30% if the equation proposed by Klein (1975) was used. Their method calculated the top heat loss factor to within three percent of the value

obtained by the iterative method. The basic equations used in determining the top loss coefficient vary depending on the design of the collector, and therefore must be carefully selected. Dayan (1996) gives a detailed analysis of the effect of the collector configuration and design on the collector heat removal efficiency and outlines the above mentioned appropriate equations.

It has been shown that the top heat loss factor may presently be predicted with reasonable accuracy. However, the semi-empirical method applied here, and also that for estimating the collector heat removal efficiency factor, are both mathematically laborious and do not take account of any material or construction irregularities. For example, the collector heat removal efficiency factor is dependant on, among other parameters, the fluid side surface heat transfer coefficient. This coefficient in turn is dependant on the Nusselt No. For a collector with a serpentine type pipe the Nusselt No, as described by Dayan (1996), is given in Eq 2.2.4.

$$Nu = 3.7 + \frac{0.0534\,(Re\ Pr\ D_i/L)^{1.15}}{1 + 0.335\,(Re\ Pr\ D_i/L)^{0.82}} \qquad (2.2.4)$$

The Nusselt No is seen to be dependant on the Reynolds No, the Prandtl No, and the diameter and length of the collector pipe, dimensions D_i and L respectively. Any physical irregularities in either of these defined dimensions will affect the internal flow profile and hence the actual efficiency of the collector. In addition, Duffie and Beckman (1991) highlight the fact that, for certain designs of collector, such as the header and riser type, the flow is not distributed evenly through the tubes. This results in a different heat removal efficiency factor from that calculated empirically.

While the above approach may be very useful in ascertaining the general effects of altering a specific design, most methods and standards commonly used to define the efficiency characteristic of a specific collector rely on the interpretation of experimentally generated data.

2.2.4 Introduction to collector efficiency characteristic and time constant measurement

There are presently several national and international standards, for example, the ASHRAE 93-86 standard, ASHRAE (1978), and the BS 6757, BS (1986), that define experimental methods for determining the CEC equation for solar collectors. The methods proposed fall into two main categories. Namely, steady state and transient testing. The ASHRAE standard, as cited by Amer and Nayak (1999), refers to a steady state method of testing under clear sky conditions whereas the BS 6757 standard, enables the CEC to be determined from data obtained under variable weather conditions.

Due to the transient nature of irradiance and a collector having a thermal capacitance, using instantaneous values of outdoor measured data to calculate the CEC, such as collector inlet and outlet temperatures and irradiance, would provide an inaccurate estimate. Wang et al (1987) give a detailed account of the effect of using instantaneous values on the derived efficiency characteristic. Outdoor, or transient, testing, therefore requires that limits be imposed on the variance, within a defined time period, of certain measured parameters in order to better define the CEC. Imposing such limits generally increases the amount of time required for outdoor testing.

In this respect, the benefits of steady state indoor testing are therefore apparent. However, there are both arguments for and against indoor testing. Muschaweck and Spirkl (1999) showed that, while it is possible to generate a steady irradiance indoors, this steady state operation is not typical of outdoor operation. It is difficult to simulate a true sky temperature and match the exact spectral distribution of outdoor irradiance. In contrast, Govaner (1988) showed experimentally that, provided the irradiance was properly quantified, an accurate measure of the CEC could be determined by indoor testing with an incandescent simulator. In addition, Bourges et al (1997), through an analysis of measurement errors, concluded that, in outdoor testing, as the temperature of the environment seen by the collector is ill-defined, the scatter of data could be reduced, and hence accuracy improved, by indoor testing. However due to the high costs associated with establishing an indoor solar simulator test facility, many simplified methods, aimed at reducing the testing time and improving the accuracy of outdoor testing have been proposed.

In considering the form of the CEC given in Eq.2.2.2, a reasonable spread of data points is required to provide an accurate measure of the CEC. The above mentioned standards therefore specify

that successive constant collector inlet temperatures be used, with time allowed for settling, before data is gathered. As the collector heat removal efficiency factor, F_R, being dependant on the fluid side surface heat transfer coefficient, h_{fi}, is related to the collector fluid flow rate, the manufacturers specified flow rate must be used during testing. Hausner and Fechner (1998) highlight the dependence of h_{fi}, on the flow rate, and also the flow condition, that is, either laminar or turbulent. In addition, they show that, for the same flow rate h_{fi} can be reduced by as much as 20% for a typical collector anti-freeze solution as compared to water. The manufacturers specified heat transfer fluid must therefore also be used. As the collector cover transmissivity, τ, decreases for beam angles of incidence greater than 30°, Duffie and Beckman (1991), the optimum optical efficiency, denoted by $F_R\tau\alpha$, also decreases beyond this angle. Testing is therefore restricted to periods for which the beam angle of incidence is less than 30°, with results from pairs of tests symmetrical about solar noon combined to provide a more accurate determination of the CEC. Beam incidence angle modifiers, being dependant on the collector cover properties, may later be applied when considering the CEC for angles greater than 30^0.

In defining a method of measurement, limit setting and averaging times, it is necessary to define the collector time constant or response function. Pierson and Padet (1990) define the time constant, τ_t, as the time taken for the collector outlet temperature to change by 63.2 % of the total change in response to a step change in irradiance. This relationship is defined mathematically in Eq 2.2.5.

$$T(\tau_t) - T(0) = 0.632\,[T(\infty) - T(0)] \qquad (2.2.5)$$

The above authors state that if the collector flow rate is high, ($m_c > 0.06$ kg/s.), then τ may be considered to be constant for any step change in irradiance. However, for lower flow rates, τ, was found to vary with flow.

2.2.5 Transient methods of collector testing.

Transient test methods for testing flat-plate collectors may be classified in six main groups: namely, (1) simple methods, (2) response function methods, (3) multi-node methods, (4) multi-test methods, (5) indoor methods, and, (6) unvalidated methods. In consideration of the collector presently studied, and the facilities available for testing, a brief review of methods 1 to 4 is given.

2.2.5.1 Simple methods of testing

One of the more simple methods is that developed by Talarek and Stein (1978). Here the irradiance and collector output are integrated over a long period, usually about an hour, and an average efficiency calculated. However, in assuming that the residual heat in the collector is the same at both the start and end of the test period, this method provides room for error. In addition, it takes a long time period to get one data point.

Aranovitch (1977) proposed a method where a collector thermal capacity term was included in the basic characteristic equation to account for the thermal response. This relationship, in terms of useful heat output per unit area, is given in Eq. 2.2.6.

$$q_u = F_R(\tau\alpha)\, G - F_R\, U_l(T_{fm} - T_a) - (mc)\, dT_{fm}/\, d\, t \qquad (2.2.6)$$

where $T_{fm} = (\, T_I + T_O)/2$

While this method does not require the control of the collector inlet temperature, an additional experiment is required to determine the value of (mc). In order to minimise error it is necessary to keep the term $(mc)\, dT_{fm}/\, d\, t$ small in relation to q_u. To keep $(mc)\, dT_{fm}/\, d\, t$ small Amer et al (1997) consider that the variance limit as given in Eq 2.2.7. should be imposed.

$$dT_{fm}/\, d\, t <= 12\ ^0C/hr. \qquad (2.2.7)$$

Wang et al (1987) suggest that the transient in this method is limited to 20 °C. Imposing either of these limits implies that this method is only applicable to slowly varying irradiance and is therefore not universally applicable.

Souproun (1992) proposed a transient procedure where the efficiency characteristic parameters were determined through an analysis of collector heating and cooling processes. To initiate cooling, the collector was covered to shield it from the sun. During both periods, the solar radiation and ambient conditions need to be constant. This implies that a sufficiently long period of stable conditions is required for accurate measurement, and hence this method is not suitable for variable weather conditions.

2.2.5.2 Response function methods

Rogers (1981) outlined a method, which uses a response function to apply a weighting factor to the irradiance incident on the collector. In comparing the efficiency characteristics for three different collectors obtained by this method, Emery and Rogers (1984), found that predicted collector parameters were slightly lower than values obtained from steady state testing.

Wang et al (1987) presented a filter method based on a dynamic collector model, Duffie and Beckman (1991). A second order differential equation is assumed to adequately describe the collector. The collector impulse response function, h (τ), as given in Eq. 2.2.8. may be combined with the above-mentioned differential equation to determine a transfer function for the collector.

$$h(\tau) = \begin{cases} (\exp(-\tau/S_2) - \exp(-\tau/S_1))/(S_2 - S_1), & \tau \geq 0 \\ 0, & \tau < 0 \end{cases} \qquad (2.2.8)$$

The parameters defined by the transfer function can then be used to program a recursive digital filter. Assuming that the variance in collector cover transmissivity with beam incidence angle is known, a wider range of beam and diffuse conditions may be used to determine an equivalent normal irradiance. This greatly reduces the amount of time required for testing as a greater variance in the instantaneous irradiance and beam angles of incidence can be tolerated. From this equivalent normal irradiance, an effective irradiance may be defined by Eq. 2.2.9.

$$G_{eff} = \int_0^{\infty} h(\tau) G_{eq}(\tau - t) dt \qquad (2.2.9)$$

The steady state performance can be estimated from the transient testing results by use of Eq. 2.2.9. and a "best fit" applied to the generated data. This method has been validated through comparison, and found to be in good agreement, with measured data gathered from steady state testing. In considering the source of errors in their proposed model, the above mentioned authors conclude that the main sources are from the mathematical model (the aforementioned second order differential equation), fluctuation in collector inlet temperature, and from diffuse solar radiation effects. The error in collector efficiency induced by the filter method is estimated as:

for $500 \leq G_{eff} < 700$, $\Delta\eta = 0.048$

for $G_{eff} > 700$, $\Delta\eta = 0.03$

2.2.5.3 Multi-node methods

Wijeysundera and Hawlader (1984), and Hawlader and Wijeysundera (1987) have proposed an iterative method where the collector is considered as having two nodes, namely, the collector material, and the circulating fluid. The two nodes are considered as having an independent thermal capacitance.

The experiment involves shielding the collector from the sun and circulating a stream of hot fluid through it. The variations of absorber plate and fluid outlet temperatures are monitored. A set of collector efficiency parameters is estimated. Theoretical values are obtained for the above mentioned plate and outlet temperatures through considering the efficiency characteristic parameters and individual capacitance of the two nodes. The theoretical results are then compared with measured values. The procedure of estimating the efficiency parameters and comparing with measured results is continued until a good agreement is obtained.

2.2.5.4 Multi-test methods

The method proposed by Saunier and Chungpaibulpatana (1983) requires both day and night-time tests. During the day, the collector is exposed to the sun, while during the night period it is subjected to several heating and cooling cycles, the heat being supplied by means of an auxiliary heater. The night test is used to define the collector heat loss coefficient and thermal capacitance. Incorporating these parameters in the analysis of the day results affords the definition of the collector heat gain parameter. With this method, an additional experiment is required to determine the auxiliary heater characteristics. The collector parameters are determined through a non-linear regression technique applied to the test data. Chungpaibulpatana and Exell (1990) modified the above method to exclude the night testing through undertaking two shading tests and one auxiliary heating test during the day. The individual efficiency characteristic parameters are then calculated in a similar manner to those previously.

2.2.6 Comparison of collector test methods.

While the above methods are able to predict the CEC parameters with reasonable accuracy, certain models are more applicable for general use. In a review of transient test methods for flat-plate collectors Amer et al (1997) consider the model of Arranovich (1977) to be unsuitable as the variance limit imposed, Eq. 2.2.7., requires that the irradiance must remain effectively constant for the time period. In effect, this equates to almost steady state testing and cannot be used under varying solar conditions. The method proposed by Talarek and Stein (1978) requires a long time to get one data point, while that of Rogers (1981), although applicable during periods of varying irradiance requires both a prior response function test, and successive calculations to determine the aforementioned weighting parameters (section 2.2.5.2). The response function method postulated by Wang et al (1987), while requiring an initial test to define the collector response function and thence construction of the digital filter, is claimed by the authors to give good agreement with steady state results.

Hellstrom and Perers (1998) compared two standard collector test methods, namely, a steady state test (SST) and a one-node capacitance model. As the capacitance model incorporates both the diffuse

irradiance and beam angle of incidence it can use data from non-stationary conditions. It is therefore termed a quasi-dynamic test (QDT) method. This method is included in the current European Standard (1998) for solar collector testing. The above investigators found that, using the defined data sets, the QDT method gave a more consistent set of results than the SST.

2.2.7 Summary

Estimation of the efficiency characteristic of a flat plate solar collector by mathematical interpretation can be laborious. Due to the potential effect of material and construction irregularities on collector performance, the degree of accuracy of the mathematically defined parameters can be uncertain. The methods of testing specified by recognised standards require the use of specialised equipment for both indoor and outdoor testing, and also require long periods of operation for data acquisition.

A short review of alternative methods that may be employed to reduce testing time and expense has been presented. This has shown that transient methods employing data filtering techniques appear to be in good agreement, with measured data gathered from steady state testing.

2.3 OPTIMISING THE PERFORMANCE OF SOLAR WATER HEATING SYSTEMS

2.3.1 Introduction.

It has been demonstrated by, among many others, Hollands and Lightstone (1989), Furbo (1989) and, earlier by Bowman et al. (1981) and van Koppen et al (1979), that systems employing a low-flow strategy, where stratification is promoted in the storage tank, generally perform better than systems operating with higher flow rates and non stratified storage. That is, for a given consumer load where the solar contribution does not fully meet the demand, the amount of auxiliary energy required to meet this load will be less for a system operating with a well stratified storage tank. For a SWHS operating with an antifreeze loop and heat exchanger at the bottom of a primary storage tank however, there is no stratification. Due to convective mixing, this type of system generally produces a tank with a minimal vertical temperature gradient. This design of system is therefore not suitable for consideration within the context of stratified storage.

A review of the different methods employed to enhance stratification is presented, and optimum solar collector flow rates and control strategies are considered. The effects of the position of the auxiliary heater within the system, and the pattern of consumer use, or load profile, on systems performance are also outlined.

2.3.2 Methods for enhancing stratification

Many tank and inlet design modifications have been suggested for enhancing and maintaining thermal stratification in the storage tank. Van Berkel (1996) states that it is purely the difference in the hot and cold fluid densities that keeps the fluid bodies apart, with the tendency to mix being inversely proportional to the temperature difference between the bodies. Gari and Loehrke (1982) proposed various designs of porous inlet distribution manifolds. For direct systems where potable water from the collector outlet is fed directly to the top of the storage tank, these manifolds were intended to reduce the velocity of the inlet stream and allow this water to diffuse, through buoyancy forces, into a region of similar

temperature within the tank. Experimental results showed a marked reduction in entrainment, that is, cooler water entering and drawing hotter water downwards as it descends, and reduced mixing at the density interface.

Jesch and Braun (1984) found that stratification could be enhanced through employing a variable volume storage container. However this method was deemed practicable only for larger scale systems.

Adams and Davidson (1993) found that a flexible manifold was preferable to a rigid one as it was able to react to differences in pressures between the tank and the incoming fluid by altering the cross sectional-area. Davidson and Adams (1994) proposed a new quantitative measure of tank stratification which they termed the mix number. This number is based on the energy in the storage tank weighted by vertical location. In respect of this measure, they found that stratification was best enhanced by using a vertically suspended flexible close-knit synthetic tube. Ghaddar (1994) implemented a distribution ring type inlet manifold in the tank top and reported a simulated and validated 15-20% improvement in system performance through enhanced stratification. Van Koppen et al (1979) proposed a floating flexible inlet pipe mounted mid-way along the vertical side of the cylindrical storage tank, as shown in Fig 2.2.1.

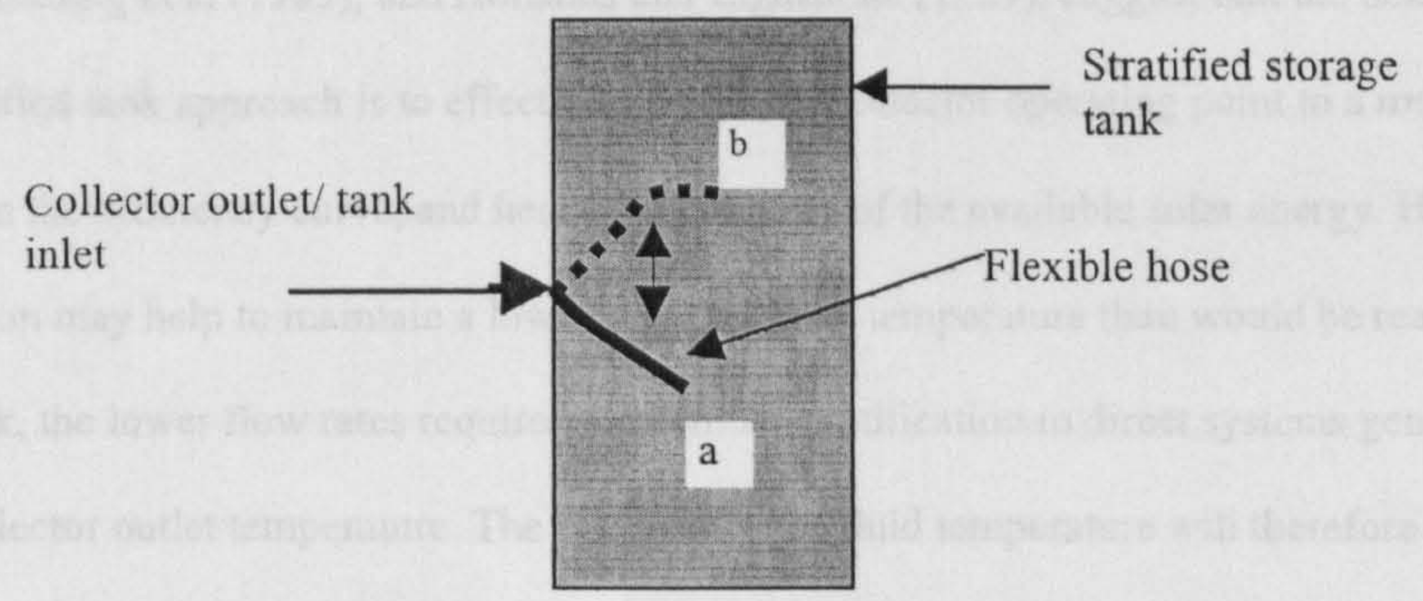

Figure 2.2.1. The flexible inlet pipe method proposed by van Koppen et al. (If cool water enters the tank the hose will settle closer to position "a". If the inlet temperature rises it will move upwards towards position "b".)

Through buoyancy forces the water entering the tank will cause the hose to settle at a level in the tank that is at the same temperature as the inlet water, and hence promote stratification. The authors

highlight the point that the inlet flow rate must be kept lower than $0.1ms^{-1}$ to stop the hose from swinging and causing mixing. Jordan et al (1998) proposed a complex system where heat was delivered to the load via a semi-enclosed heat exchanger mounted in the upper section of the stratified storage tank. When load is drawn and a flow established in the heat exchanger coil, the tank water is cooled, falls, and is collected beneath the heat exchanger. It then descends through a central pipe with the flow rate regulated by means of a butterfly type valve so as not to cause mixing on exiting the pipe at the tank bottom.

While it is possible to enhance stratification through employing the above methods, the majority require expensive tank modifications. Van Koppen et al (1979), in their early study, conclude that, promoting stratification is best served by employing lower collector flow rates. Employing a lower flow rate can reduce pumping costs and negate the requirement for more expensive storage designs .

2.3.3 Optimum solar collector fluid flow rates.

2.3.3.1 The effect of low flow rates on system performance.

Wuestling et al (1985), and Hollands and Lightstone (1989), suggest that the benefit of the low flow-stratified tank approach is to effectively move the collector operating point to a more favourable position on the efficiency curve, and hence collect more of the available solar energy. However, while stratification may help to maintain a lower collector inlet temperature than would be realised for a fully mixed tank, the lower flow rates required to promote stratification in direct systems generally produce a higher collector outlet temperature. The mean collector fluid temperature will therefore not necessarily be lower for a low flow stratified system than for the fully mixed system. Considering Eq 2.2.1, and assuming a similar mean collector fluid temperature for a fully mixed and a stratified low flow system, this implies that the collector efficiency is not necessarily enhanced through operating with storage stratification.

Hausner and Fechner (1998) showed that the fluid side surface heat transfer coefficient, h_{fi}, and hence the collector heat removal efficiency factor, is dependant on the flow condition, that is, either laminar or turbulent. This implies that for the same collector and mean fluid temperatures, the collection

efficiency will decrease as flow rates decrease. Berg and Furbo (1990) found that good agreement between predicted and measured values of system performance was only obtained if the effect of flow rate on collector efficiency characteristic was taken into consideration. In view of these considerations the benefit to system performance is more likely to come through the stratified systems ability to provide a better quality of energy to the load.

Tabarra and Bowman (1985), through an experimental comparison, showed that, operating with a flow rate of approximately one third of standard (0.0033 l/s.m^2 compared to 0.01 l/s.m^2) reduced the solar energy collected by 5% while increasing system performance by 7%. This therefore implies that the reduction in collector efficiency is outweighed by the performance benefits of stratification. Hollands and Lighstone (1989) suggest that improvements in performance of up to 38% may be realised in practice. More recently Tsilingris (1996), through simulation studies suggests that similar improvements in performance are obtainable. However, Furbo (1989), working with mantle type storage tanks, showed that these benefits were dependant on the solar fraction, or percentage of the load provided by the solar input. As the solar fraction increases for both types of system, conventional and low flow, so the benefits of the low flow system diminish. At lower solar fractions, the thermal performance of the low flow system was approximately 27% better than that of the standard flow rate system

2.3.3.2 Optimum solar collector flow rates for systems operating with a mains driven pump.

In the above mentioned study of the relative performance of systems operating with mantle type storage tanks, Furbo (1989) found that, in comparing the effect on performance of a range of low flow rates, a constant collector flow rate of between 0.00167 l/s.m^2 and 0.00333 l/s.m^2, as compared to any other range, produced optimum system performance. Typically, manufacturers of high flow SDHW systems suggest flow rates of the order of 0.020 l/s.m^2. A.E.S. (1998). The optimum flows specified by Furbo (1989) are in the range 12 to 17% of those specified in the aforementioned higher flow systems. Similarly, Fanney and Klein (1988) also found that, for the specific configuration of the direct solar water heating systems studied, the optimum flow rate was between 10% and 20% of that typically used in forced circulation direct systems. Both of these above studies, Furbo (1989) and Fanney and Klein (1988) consider

the effect of a constant low flow rate. Other investigators have considered alternative/variable flow strategies.

Wuestling et al (1985) carried out simulation studies on the effect of both low and variable low collector flow rates. The system studied, as shown in Fig. 2.3.2, comprised a separate solar preheat tank and second auxiliary tank with immersion heater. The above authors found that system performance was maximised when the flow rate was controlled so as to provide a constant collector outlet temperature of 55 °C. While the efficiency characteristic of the panel used is not stated, considering that the characteristic is similar to that quoted in Eq 2.3.1 below, implies that, for an inlet temperature of 15 °C, a flow rate of approximately 0.0033 l/s.m^2 would be required at full sun to provide the desired rise.

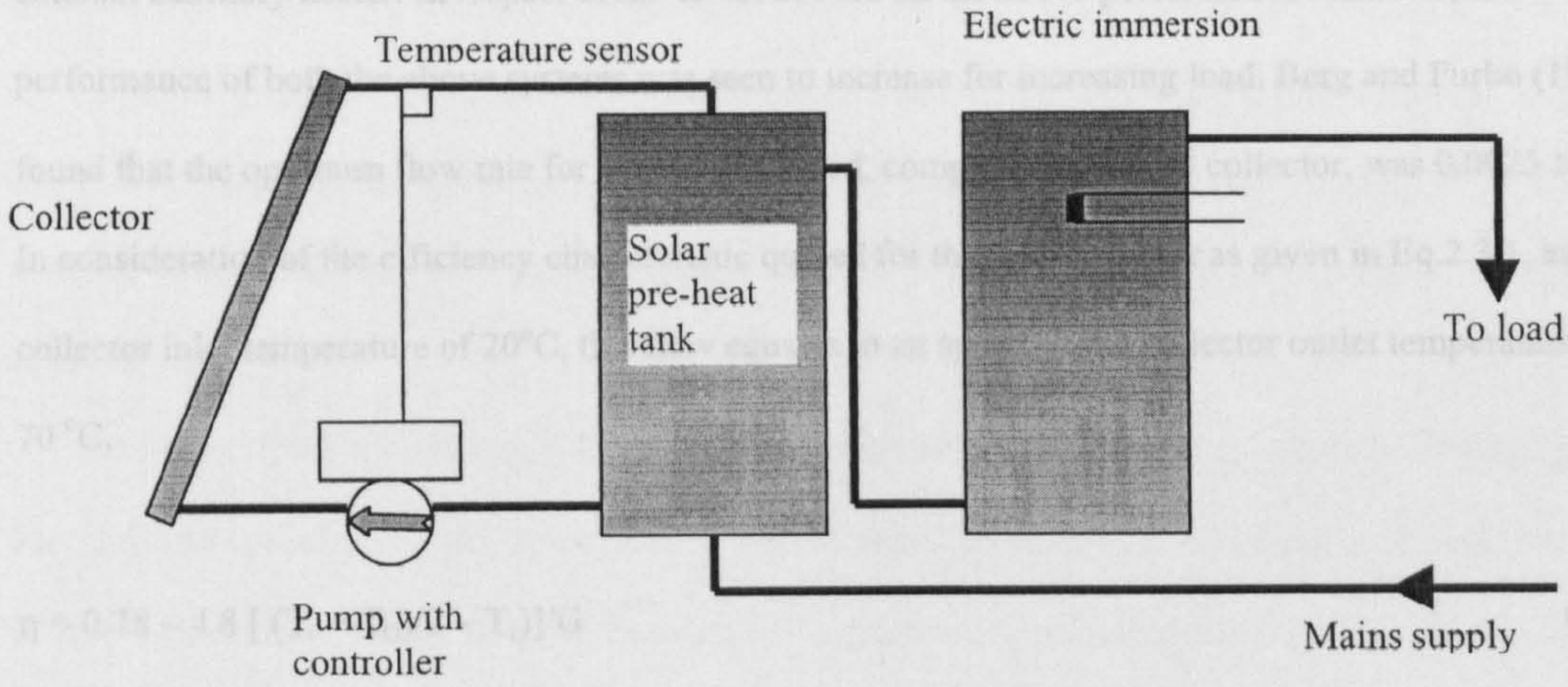

Figure 2.3.2 Schematic of the test apparatus employed by Wuestling (1985) and Csordas et al (1992)

Csordas et al (1992) undertook a simulation study on the effects of different flow control strategies on the performance of the same system as studied by the above authors. This analysis revealed that controlling the collector flow rate in such a manner as to produce a fixed temperature rise across the collector, FCTR, gave a better performance than controlling flow to provide a pre-set specified collector outlet temperature, SCOT, (as defined by Wuestling et al (1985) to optimise performance). Csordas et al (1992) considered that, for the SCOT strategy, if the temperature at the bottom of the storage tank were at

or above the SCOT value, then no more solar energy would be collected. On the other hand, the FCTR strategy assumed that, if there was enough solar energy available to produce the desired rise, then it would always be collected irrespective of collector inlet temperature. It is possible however that through the selection of an appropriately sized and stratified preheat tank, a lower collector inlet temperature may be maintained. This would therefore improve the predicted performance of the system operating with the SCOT strategy.

Furbo and Shah (1996) compared the thermal performance of two SWHS employing mantle type storage tanks, (where the only difference between the systems was the addition of an auxiliary immersion heater in one of the tanks). They found that, for the same delivered load, the net utilised solar energy was maximised for both systems when the flow rate through the collector and mantle was approximately 0.2 l/min.m^2. In addition, the net utilised solar energy was greater for the system with an external auxiliary heater. In respect of the effect of load on the above performance indicator, the performance of both the above systems was seen to increase for increasing load. Berg and Furbo (1990) found that the optimum flow rate for the system tested, comprising a 4.3 m^2 collector, was 0.0025 l/s.m^2. In consideration of the efficiency characteristic quoted for that test collector as given in Eq.2.3.1, and a collector inlet temperature of 20°C, this flow equates to an approximate collector outlet temperature of 70 °C.

$$\eta = 0.78 - 4.8\,[\,(T_I + T_O)/2 - T_a)]/G \qquad (2.3.1)$$

However, as the collector fluid is not passed directly to the tank but is instead circulated through a mantle jacket, the internal tank temperatures will necessarily be lower than this apparently high collector outlet temperature. In addition, the desired load delivery temperature was not specified. In relation to the operation of low flow systems all of the above research has been undertaken with pumps driven directly by mains electricity, with the hydraulic output controlled where applicable by throttling or other means.

While Furbo and Shah (1996) employed an "intelligent" pump which could be programmed to automatically vary flow in proportion to temperature, Furbo (1998) concluded that further work relating to the optimisation of flow through employing a small solar electrically driven pump, PV/pump, would be worthwhile.

2.3.3.3 Optimum solar collector flow rates for systems operating with a PV driven pump.

Early work undertaken by Parker (1976) considered the use of a PV driven pump to provide a more standard flow rate. Consequently the measured collector temperature rise was of the order of 10 ^{0}C. The pumping unit comprised a screw-type impeller housed in a length of standard copper tube, driven by a small motor rated at 3V, 0.95 A, at 6900 rpm, with an effective resistance of 2Ω. Each PV unit was rated as having a nominal output of 2 V, 0.6 A at full sun, (1000 W/m^2). Testing showed that when two PV units were used to drive the pump motor, the threshold, or cut in, irradiance was 450 W/m^2 due to the requirement of a high starting current by the motor. The cut out level was 200 W/m^2. Using three PV modules was found to give a more acceptable cut in of 300 W/m^2, and a cut out of 150 W/m^2. It is not clear from the literature whether the PV modules were connected in series or parallel. However, as the main barrier to pump cut in was the requirement of a high starting current, it is more likely that the modules would be connected in parallel to increase the current, rather than series for voltage enhancement.

Cromer (1983), on sizing, selection and matching of PV components for use in SDHW systems, found that an optimised PV driven circulation system was, in relation to both thermal performance and cost, a viable alternative to a mains driven system. As with the system studied by Parker (1976), Cromer (1983) utilised the PV/pump unit to generate more standard flow rates, typically of the order of 0.02 l/s.m^2, producing a solar loop temperature rise of 10°C at full sun.

More recently, in defining the optimum flow rate versus irradiance profile, in order to maximise the thermal performance off a PV-SDHW system, Al-Ibrahim et al (1996), presented a search methodology and defined the desired electrical characteristics of the PV module and pump motor to best match the defined optimum profile for the given system. They did not specify the collector outlet temperature in the reported literature. Although the initial model presented in the above mentioned paper assumed a constant pump hydraulic efficiency across the full range of operating conditions, a more recent article by the above authors, Al-Ibrahim et al (1998), does consider a variable pump efficiency, and optimum components parameters are defined accordingly. From this analysis, using a 6.5 m^2 collector,

the optimum flow rate profile presented implies a flow rate of approximately 0.0166 l/s at full sun, (approximately 1000 W/m^2). This figure agrees well with those presented earlier by Furbo (1989), Berg and Furbo (1990) and Furbo and Shah (1996).

While the studies so far reported specify either an exact optimum flow rate, control strategy, or, as is the case for the recently studied PV-driven system, Al-Ibrahim et al (1996 and 1998), an optimum flow rate profile, other investigators have considered the optimum flow rate in relation to the delivered load and also an optimum collector area to storage volume.

2.3.4 Effect of storage volume, load profile, and position of the auxiliary heater on system performance.

2.3.4.1 Effect of storage volume on system performance

Many studies have been undertaken in relation to determining the optimum storage volume to collector area ratio, Sv: Ca. In a review of early work Bowman et al (1981) found different estimates of this optimum ratio ranging from 30 l/m^2 to a maximum of 208 l/m^2, Carter (1978). The average value however appears to lie between 50 to 100 l/m^2. More recently, Tsilingris (1996) and Furbo (1998) have both specified a value of 50 l/m^2 as being the optimum.

In considering the relative performance of direct systems operating with an Sv:Ca ratio of 67 l/m^2, Carvalho et al (1988) found that system thermal performance was maximised when the daily collector flow was equal to the storage volume. This is termed a single pass type system. For a daily solar collection time of 8 hours this equates to an average flow rate of 0.0023 l/s.m^2. This is comparable to the optimum low flow rates reported in section 2.3.3.1 and 2.3.3.2. For the system detailed in Fig 2.3.2, Wuestling et al (1985) found that, in addition to regulating the flow rate such that the collector outlet temperature was fixed at 55 °C, performance was maximised when the daily collector flow equalled the daily load. Jesch and Braun (1984) also found that performance was maximised when the daily collector flow equalled the daily load volume.

2.3.4.2 Effect of load profile on system performance

Hollands and Lighstone (1989) showed that the performance benefits of low flow stratified systems are potentially sensitive to the pattern and rate of draw off. As lower draw off rates produce less mixing in the bottom of the tank this improves the relative performance for the systems operating with stratified storage. With respect to the effect of the pattern of draw off on system performance, Tabara and Bowman (1985) showed that changing the peak draw from evening to noon produced a 17% increase in the solar fraction, while the shift from a noon to a morning peak reduced the solar fraction by 30%. For a direct low-flow system, changing the peak from evening to noon generally has the effect of providing a lower collector inlet temperature during the afternoon period. Tsilingris (1996) also found that performance was maximised for a midday peak load. Furbo (1989) also showed that system performance was affected by the draw off pattern, with the low flow stratified system appearing more sensitive than the higher flow system. The relative performance of the two system was however not affected, with the low flow system outperforming the other for all load profiles studied. Morrison et al (1992) undertook an analysis of the effect of load profile and auxiliary boosting in a single tank system where the solar loop inlet was two thirds of the way up the vertical height of the tank and the auxiliary heater situated above this point. These investigations showed that system performance was maximised by the application of an evenly distributed load, with an evening peak load providing a better performance than a morning peak.

2.3.4.3 Effect of the position of the auxiliary heater on system performance

While the requirement of a constant availability of a large quantity of hot water would dictate the position and control of an auxiliary heater this demand scenario is not necessarily common to many commissioned SDHW systems. It is generally accepted, Wuestling (1985), Michaelides and Wilson (1997), that the performance of the solar loop is maximised when the auxiliary heater is external to the solar tank. Operating with a bottom electric immersion heater in a single tank system would cause

convective mixing and so destroy any stratification, and its benefits. However, if a two tank system is considered there are greater standing losses, with the solar preheated water only transferred to the secondary tank after load has been drawn. There have been no reported studies of the relative performance gains and losses as outlined above that are incurred through employing a second tank with auxiliary heater.

Overall system thermal performance is maximised, when an external instantaneous auxiliary heater is used to provide the top up during load demand. If it is not possible to have such an external heater, where the load requirement is such that smaller quantities of hot water are required at any given time a top immersion heater is preferable to a lower. Morrison et al (1992) showed that system thermal performance was worst when an evening auxiliary boost was applied, irrespective of the load profile. Prud'homme and Gillet (1998) propose a tank top three element electric auxiliary immersion heater, the three elements having different lengths and ratings and a combined rating equal to the original single element. They consider that a combined element like this affords a better control of, and hence minimises, the auxiliary input. This method requires the use of an "intelligent" controller, with the requirement of pre-defined load demand temperature and profile.

2.3.5 Summary.

Systems operating with stratified storage generally out perform those with fully mixed tanks. While many different strategies for improving stratification have been proposed, for many systems, operating with a lower collector flow rate can enhance overall performance. From the above review the consensus of opinion is that employing a collector flow rate of approximately 0.2 l/min.m^2 will maximise performance. Where a variable flow rate strategy may be employed, controlling the flow rate so as to maintain a relatively constant collector outlet temperature of around 55 °C can further enhance performance. The effect of system design and load profile on relative performance has also been discussed.

2.4 CHARACTERISATION AND PERFORMANCE OF PHOTOVOLTAIC PUMPING SYSTEMS.

2.4.1 Introduction.

While Durisch et al (2000 and 1996) considered that photovoltaic technology was not commercially competitive for the high volume generation of electricity, the use of solar electric modules to provide power for water pumping is common, Langridge et al (1996). In areas where grid power is unavailable and solar energy is plentiful, photovoltaic water pumping systems, PWPS, can offer several advantages over alternative systems; such as those powered by petrol or diesel generators, Jafar (2000). There are no pollutants, maintenance is generally reduced, and system lifetime is also increased. Many experimental and theoretical investigations have therefore been undertaken in order to better predict and optimise the performance of PWPS. While much of this work specifically relates to stand alone type systems, where the main criteria is to maximise flow rate and volume delivered, some investigators, Cromer (1984), Miller and Hittle (1993), and Al-Ibrahim et al (1996), have considered the application of PWPS for use in forced circulation SDHWS. To optimise the performance of this type of system, as outlined in section 2.3 , a controlled flow rate is desirable.

Section 2.4 presents a review of PWPS design, components modelling and performance analysis, and discusses the application of PWPS for use in forced circulation SDHWS

2.4.2 Characterisation of photovoltaic modules.

Photovoltaic, PV, modules generally comprise a number of units called cells which are connected in self contained groups to form a module. Modules may be connected in series or parallel to make an array of the desired size. The design of a PWPS requires that the electrical characteristics of the PV module or array be known.

2.4.2.1 Characterisation of polycrystalline silicon modules.

The equivalent circuit shown in Fig. 2.4.1, presented by, among others, Eckstein et al (1990), Duffie and Beckman (1991), and Lawrence and Wichert (1994), is derived from a consideration of the PV cell construction and material properties

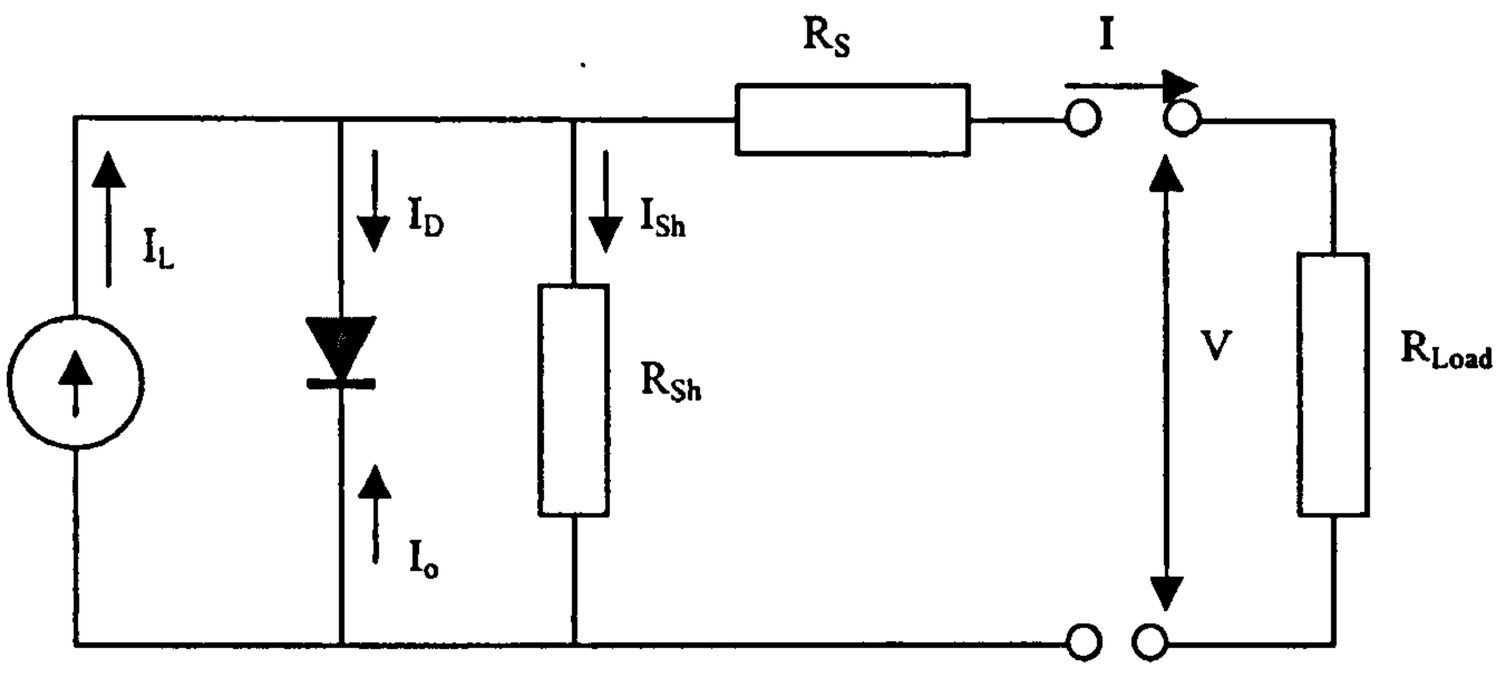

Figure 2.4.1 The equivalent circuit for a PV generator.

For a fixed temperature and solar radiation, the current-voltage characteristic of this model is given by Eq. 2.4.1, and the power given by Eq. 2.4.2.

$$I = I_L - I_D - I_{Sh} = I_L - I_o\{\exp[(V + IR_S) / a\,] - 1\} - (V + IR_S)/ R_{Sh} \qquad (2.4.1)$$

$$P = IV \qquad (2.4.2)$$

It can be seen from Eq. 2.4.1 that to define the I-V characteristic, 5 parameters need to be known. These are, namely, the light current, I_L, the diode reverse saturation current, I_O, the series resistance, R_S, the shunt resistance, R_{Sh}, and a curve fitting parameter, a. As the shunt resistance, R_{Sh}, is generally much larger than the numerator in the last term of Eq 2.4.1, $(V + IR_S)$, Moussi et al (1999) and Al-Ibrahim

(1996) consider this last term to be equal to zero, and hence simplify the equation to the four parameter problem, as given in Eq 2.4.3.

$$I = I_L - I_D - I_{Sh} = I_L - I_o\{\exp[(V + IR_S) / a\,] - 1\} \qquad (2.4.3)$$

As manufacturers generally only quote three operating points on the performance curve for a specific module, namely the open circuit voltage, V_{OC}, the short circuit current I_{SC}, and the current and voltage values at the maximum power point, I_{MP} and V_{MP}, other measurements are required to define the series resistance R_S. For the module operating at the normal cell operating temperature, NOCT, application of Eq 2.4.3 produces a set of module performance curves of the nature as shown in Fig. 2.4.2.

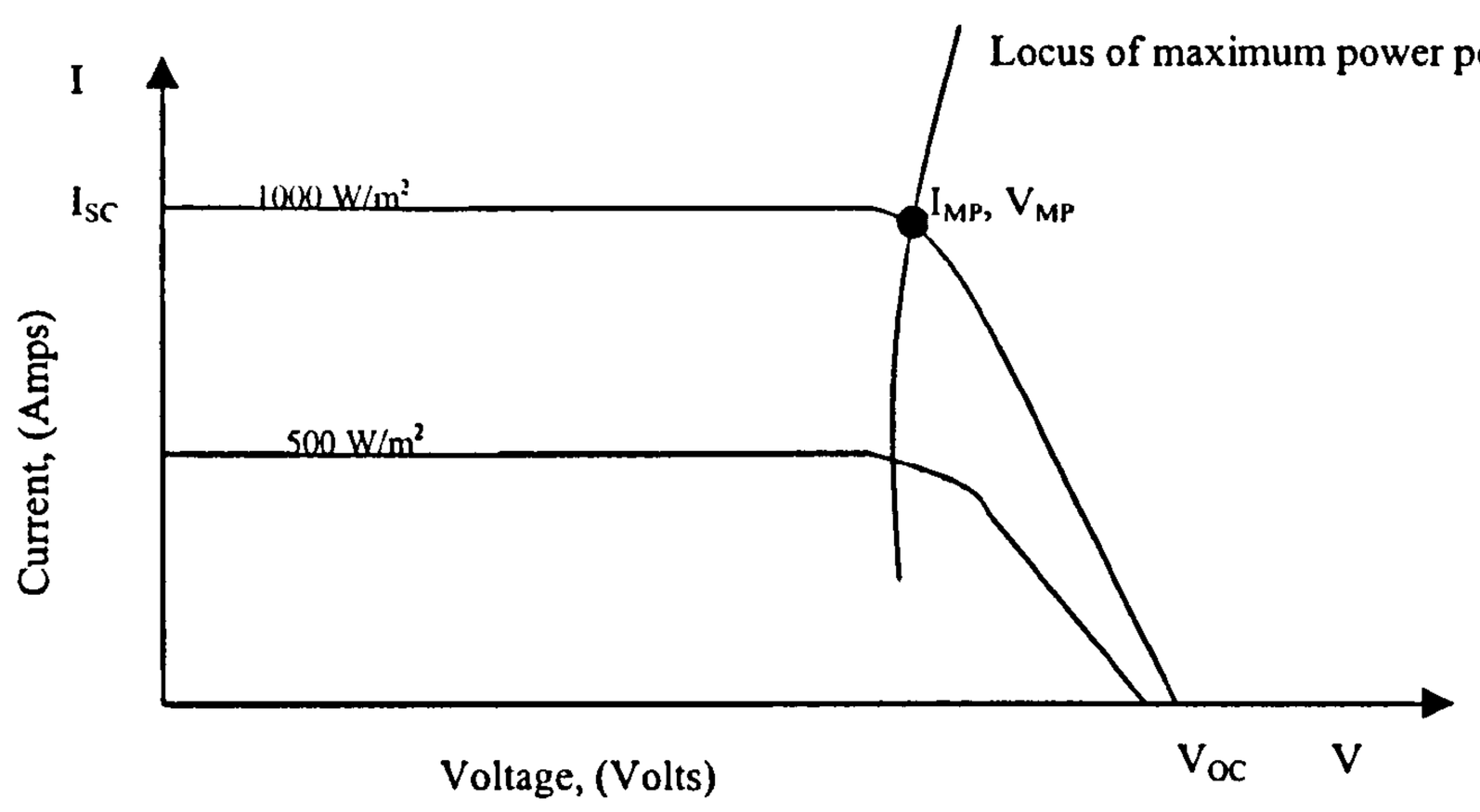

Figure 2.4.2 Typical performance curves for a PV module derived from NOCT data.

It can be seen from Fig 2.4.2 that the short circuit current is shown as being proportional to the incident radiation, with I_{SC} at 1000 W/m^2 equal to twice its value at 500 W/m^2. This is only true if the spectral distribution of radiation remains constant for all irradiance levels. Hirata and Tani (1995), through an experimental investigation in Japan, showed that this distribution had a marked effect on module performance. For the same measured global irradiance, between summer and winter, module output power was seen to vary by 5 % for polycrystalline modules and 14% for amorphous silicon modules. This

difference was attributed to the seasonal difference in spectral distribution in respect of the modules wavelength response band. The amorphous modules were more susceptible due to their more limited range of wavelength response.

2.4.2.2 The effect of temperature on module performance.

Paretta et al (1998) considered that the reference conditions defined by the NOCT and irradiance parameters were unattainable in practice as they combined, "the irradiance of a clear summers day with the module temperature of a clear winters day, and the spectral distribution of a clear spring day". The model presented in the previous section assumes a constant cell operating temperature. As temperature increases, cell efficiency decreases. Therefore, when the effect of temperature is included in the analysis an altered profile, as shown in Fig 2.4.3 is obtained for the performance curves. Both the short circuit current and open circuit voltage are seen to decrease for the higher operating temperatures that are generally experienced at higher insolation levels. That is, the short circuit current at 1000 W/m^2 at 40 °C is less than twice that at 500 W/m^2 and 30 °C.

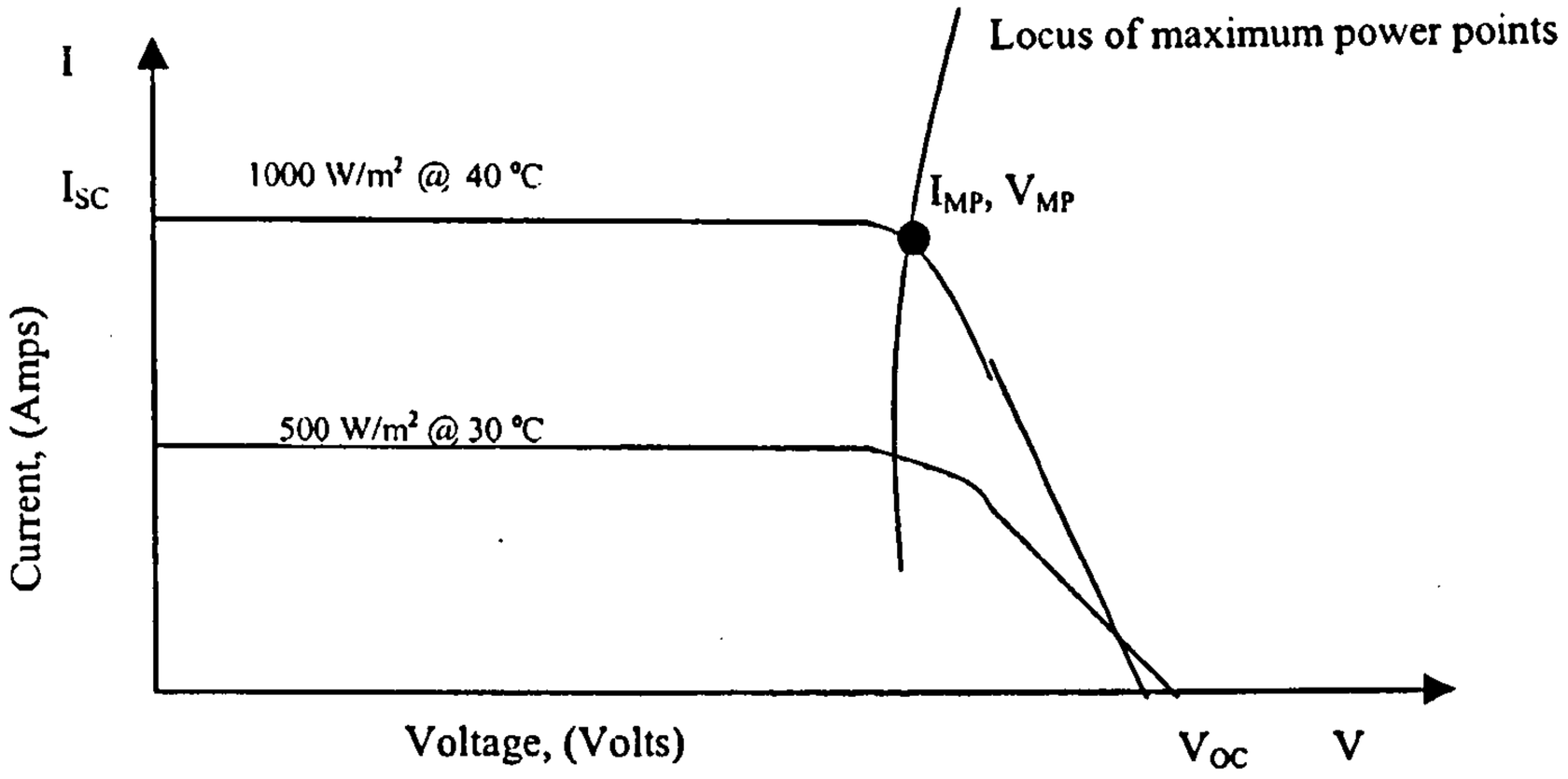

Figure 2.4.3 Performance curves for a PV module including the effect of temperature.

Lawrence and Wichert (1994) provided a mathematical analysis defining the effect of temperature on cell performance. Their improved model was shown to predict module characteristic values to within 2.5% of measured values.

2.4.3 The performance of photovoltaic pumping systems.

Narvarte et al (2000) stated that it was possible to predict the water output from pump manufacturers data and PV array power alone. However, Jafar (2000) concluded that, as there was only limited data available from most pump manufacturers, it was necessary to test each particular system and develop a model that could predict the output for any combination of head and irradiance.

The hydraulic output of a PWPS system depends on the electrical power available for pumping, motor efficiency, and the efficiency of the pump for the given hydraulic conditions. In selecting an appropriate PV module/pump combination Section 2.4.3 therefore considers the development of a model in relation to components selection with respect to the PV module characteristics outlined above.

2.4.3.1 The electrical power available for pumping.

Figures 2.4.2 and 2.4.3 show the locus of maximum power points as defined from the PV module characteristics. The electrical power delivered to the load is derived from a combined analysis of the pump motor electrical characteristics and the PV module characteristic curves. Figure 2.4.4 shows two motor electrical load characteristics superimposed on the module characteristic plot as given in Fig 2.4.3.

The electrical power delivered to the load, as shown by points 1 and 2 for motors A and B respectively, is defined from the intersection of the motor and PV characteristic curves. Clearly, in the above case, the electrical input will be greater to motor B. Careful selection, or load matching, will therefore result in a more efficient system, Kou et al (1998). The motor load lines in Fig 2.4.4 show an over simplified case. Generally, at starting, they do not exhibit a straight-line characteristic, and also require a minimum irradiance, or threshold level, before a flow rate is established.

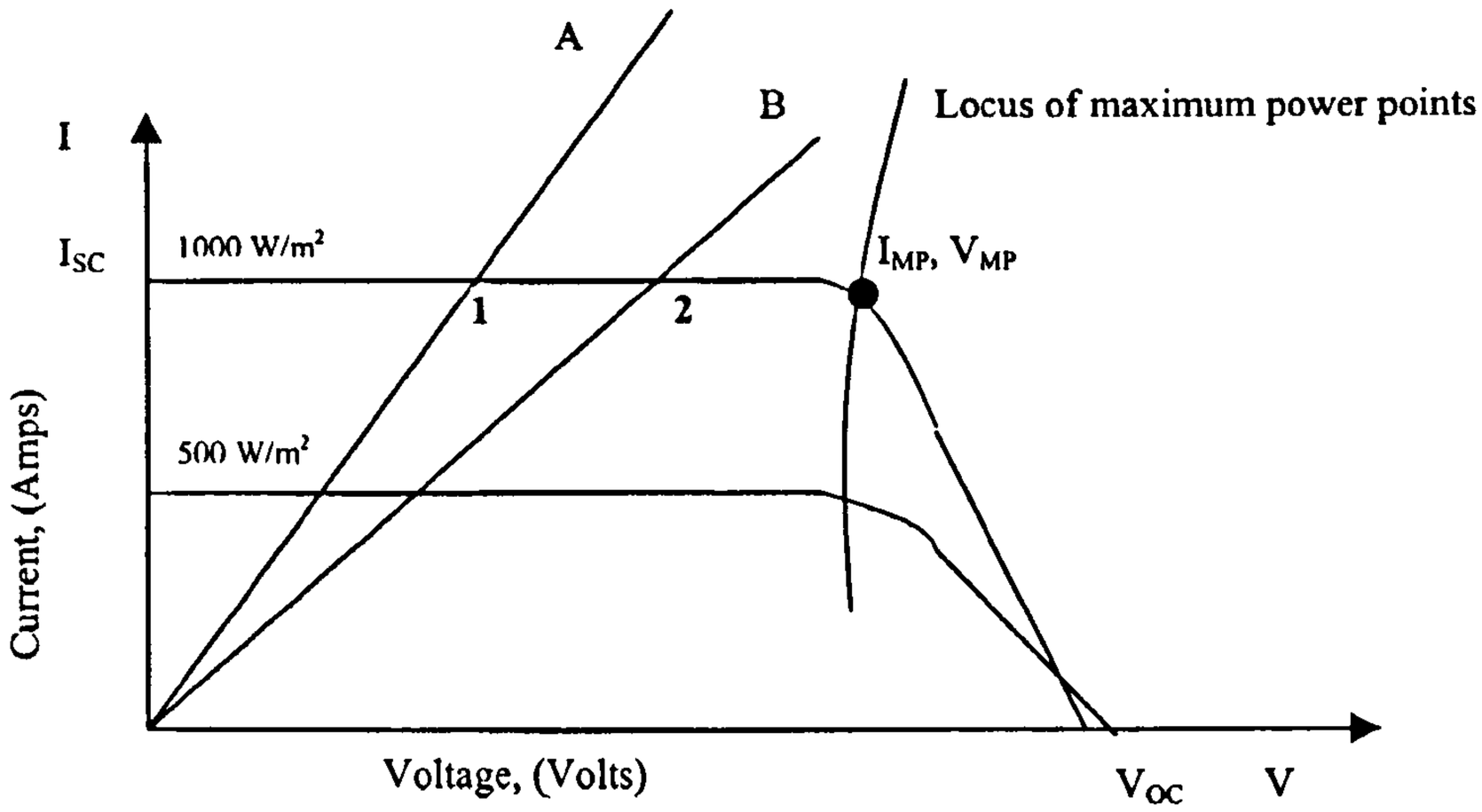

Figure 2.4.4 Two motor electrical load characteristics with PV module characteristic curves

2.4.3.2 PV/pump matching for efficient operation.

Cromer (1984) undertook an analysis of the starting characteristics of direct coupled PV pumps and highlighted the importance of matching for efficient operation. He showed that while the four test pumps required a similar power input to produce the same flow rate in the test system, 2.8 W, 2.4 W, and two at 3.0 W, the individual pump motor I-V characteristics, and hence load line, implied that very different irradiance levels were required to produce the desired flow rate for each pump. Singer and Appelbaum (1993) used a maximum power point tracker, MPPT, to improve system performance and motor starting. (An MPPT has the effect of shifting the operating load line to the right and therefore closer to the locus of the PV module maximum power points.) Zaki and Eskander (1996) also considered the appropriate matching of components for maximum efficiency operation. They concluded that using a separately excited d.c. motor to drive a centrifugal pump provided the greatest output for a given PV module.

Kou et al (1998) in considering manufacturers pump efficiency and meteorological data used a similar analysis to that presented in Fig 2.4.4 to predict the long term output of a PWPS. While other

estimates of system performance have been undertaken, Anis and Metwally (1994), specific case studies and systems analyses have also been presented, Pulfrey et al (1987), and Herrmann et al (1987).

2.4.4 PV powered SDHWS.

There are two very distinct types of PV powered SDHWS. The first of these uses the output from the PV modules to directly heat water in the storage tank, whereas the second uses the PV module to drive a pump and circulate water through thermal solar collectors.

In respect of the first type of system, Fanney et al (1997) incorporated a microprocessor controller to adjust the resistive load of the heating element in relation to the insolation to best match the load required for operation at the PV module maximum power point. To make a valuable contribution to the heating load, due to a lower conversion efficiency, a much larger area of PV modules was required than would be thermal collectors for a similar contribution. The current work is concerned with the second type of system. A review of PV pumped SDHWS has been presented in section 2.3.3.3.

2.4.5 Summary

A model for defining the electrical power available for pumping in relation to the PV cell/module and electric motor characteristics has been presented. The majority of past research has been concerned with maximising system hydraulic output by appropriately matching PV modules and pump motors for maximum efficiency of operation.

In respect of obtaining an optimum collector flow rate profie, Al-Ibrahim (1996) defined the optimum set of component parameters for operation in a low flow PV powered SDHWS. In relation to the present system, comprising a smaller collector than that of the afore-mentioned investigator, a review of standard components available suggested that some form of control would be required to provided the optimum flow profile.

2.5 COMPARATIVE TESTING OF SOLAR WATER HEATING SYSTEMS

2.5.1 Introduction

The comprehensive systems simulation package TRANSYS, TRANSYS (1990), is able to accurately predict the performance of different systems when subjected to different operating conditions. It is therefore able to compare the performance of these systems, thus allowing an informed choice to be made for a given application. However, it is possible to define the thermal performance of solar water heating systems in many different ways, with the performance indicator and method of testing making specific designs of SWHS appear more favourable than others.

Some of the factors affecting the relative performance of solar water heating systems have already been discussed in section 2.3. For example, the effect of collector flow rate and load profile on performance have been outlined.

Section 2.5 considers some of the other factors that need to be considered in order to provide an unbiased assessment of the comparative performance of SWHS.

2.5.2 Definition and selection of collector area

Presently, commissioned by the Department of Trade and Industry (UK) (2000), the comparative testing of several types of SWHS is being undertaken. Commentators on the proposed testing strategy, including M^{ac}Gregor (2000) have highlighted flaws in the methodology, where a certain procedure or system specification may favour one particular design or manufacturer. For example, if all the collectors are required to have the same area, specifying aperture or absorber area can have a marked effect on the perceived performance of the systems. If one considers equal absorber areas, vacuum tube type collectors will appear to have a higher efficiency than that of flat plate absorbers. However, to provide the same absorber area as a flat plate collector, the required aperture area is generally greater for the vacuum tube array. In practical applications, the limiting factor for collector area will often be the available area, and hence aperture size. M^{ac}Gregor (1996) showed that if the aperture area is taken as the common factor, the

perceived collector efficiency characteristic of the vacuum tubes examined is then less than for conventional flat plates.

2.5.3 System design.

The original methodology, DTI (2000), proposed that all systems to be tested should use a solar preheat tank with an internal heat exchanger, with the solar hot water then transferred to a second tank during draw off. While this is a design common to many systems operating with an antifreeze loop and a fully mixed solar tank, it would disadvantage systems that are designed to operate with a direct tank and stratified storage.

2.5.3 Performance indicators

For systems where the solar input does not provide the whole of the annual load, as is typically the case for economically sized applications at higher latitudes, a common indicator of system performance is to compare the solar fraction, or the portion of the heating load supplied by solar contribution. Duffie and Beckman (1991) define the solar fraction, f, as equal to the energy saved through solar input, divided by the auxiliary energy that is required to provide the same load when there is no solar input. This relationship is outlined in Eq. 2.5.1.

$$f = (A_o - A_{WS})/ A_o \qquad (2.5.1)$$

In studying the effect of different control and operation strategies on system performance, the solar fraction, as defined above, may seem a reasonable indicator of performance. However, it is not always possible to get an accurate measure of the "auxiliary with no solar" consumption for an in situ system, and hence an inaccurate estimation of the solar fraction may be made.

Beale (1987), in citing the Canadian Standards Association standard F 379.1, defines the net daily solar energy as the daily solar energy minus the auxiliary or parasitic energy. In considering the effect of flow rate on the solar energy gathered, section 2.3 showed that while a low flow stratified system may gather less solar energy, to deliver the same load, it may also require less auxiliary input. The above defined "net daily solar energy" may therefore give an incorrect estimation of the relative performance of two systems where one is of the low-flow/stratified type.

2.6 MODELLING OF SDHW SYSTEMS.

2.6.1. Introduction.

A model that can accurately simulate a physical system, and predict the values of system parameters as a result of different operating scenarios is obviously a valuable design tool. In respect of solar water heating, if it is possible to predict system performance and output, cost scenarios can be considered, relative performances compared, and appropriate systems installed for a given location and function. As many of the present systems component parameters, such as the collector efficiency, are unknown it is not possible to fully simulate this system with existing models. As it is the intention of the research to develop and validate a model specifically for the present system, section 2.6 gives only a brief review of some current models. As discussed in section 2.3, however, it is intended that the new system operates with stratified storage. A review of models relating to thermal stratification in storage tanks is therefore presented.

To accurately simulate system performance, in addition to having a validated model, site meteorological data is also required. Beckman, Duffie and Klein (1977) highlighted the lack of good, consistent, hourly beam and diffuse radiation data that is required for full performance simulation. Since that time, much more data has been made readily available through both national and international measurement programmes. Data is available "on-line" from many sources including the Florida Solar Energy Centre (2001) and the Solar Energy Research Institute at the National Renewable Energy Laboratory (2001) for many locations across the United States of America, and from the Word-wide Information system for Renewable Energy (2001) and the European Solar Radiation Atlas (2001) for European and United Kingdom data. In addition, where there are inconsistent data sets, there are models available, Gul et al (1998), which can determine solar radiation data from other meteorological data. These models can be used to complete fragmented data sets making them suitable for application in modelling of SDHW systems.

2.6.2 Present models

Many early system performance analyses were undertaken using the "f-chart" method developed by Klein (1978). This method requires the user to manually compute many parameters at various stages in the analysis. As it does not allow for the consideration of stratification in the storage tank, it is limited, and laborious if several systems are to be compared. There are many models for individual systems that comprise mathematical definitions of specific component characteristics, such as the flat-plate collector described in section 2.2. However, many investigators, including, for example Uecker et al (1998), consider the TRANSYS, (Transient simulation) program, also developed by Klein (1980), to be the most comprehensive and best validated tool for simulating solar thermal systems. This software is continually being developed, with new updates, and modular additions superseding previous units. The program is subdivided into "TYPES", with each "TYPE" performing a specific function. For example, TYPE 4 and TYPE 60, as cited by Al-Ibrahim (1996) are related to storage tank type, configuration, and performance. Other units, or TYPES, consider collector efficiency, flow rates, load profile and so on, making the TRANSYS software applicable to many types of system and associated application.

2.6.3 Modelling of storage tank charging and discharging

While the above mentioned model is used for full performance simulation, other investigators, Al-Nimir (1993), Eldessouky (1993), and Yoo and Pak (1993,) among many others, have presented models specific to the behaviour of stratified storage tanks. In considering the manner in which a direct system stratified tank is charged by a solar collector, Duffie and Beckman (1991) presented two distinct models. These are termed the Plug flow and Node flow models respectively.

2.6.3.1 The plug flow model.

In the case of plug flow, the model considers that during charging, the fluid in the tank moves continuously downwards, with the hot return from the collector settling on top of the cooler water with no mixing. For a constant collector outlet temperature, as shown in Fig 2.6.1, this model assumes that, at any time during charging, there are two distinct temperature zones within the tank. T_o is the collector outlet temperature, and T_i the initial tank temperature. For variable inlet temperature the model assumes that a new disc or zone of fluid at the new temperature is formed at each time step.

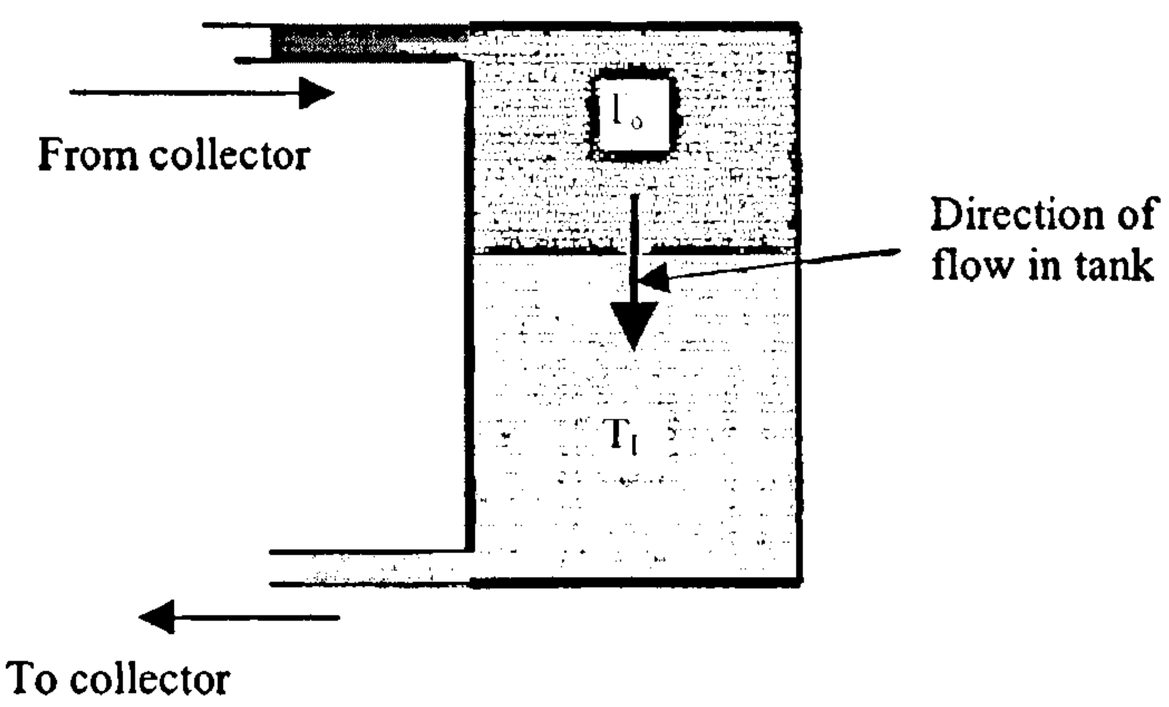

Figure 2.6.1 Schematic representation of the plug flow model.

Bowman et al (1981) showed that a stratified storage container behaved more like a three-segment system. They also showed that the greater the temperature difference between the zones, the more stable they became. Van Berkel (1996) also showed that the degree of mixing was reduced for a greater difference in density between the respective zones. While Eldessouky (1993) also found that the tank behaved as a three-segment system, Hoogendorn et al (1985), through an experimental analysis found that, in most cases, ten or more nodes were required for describing tank behaviour.

When cooler mains water enters the bottom of a tank during load delivery, there is necessarily mixing and a degradation of the quality of some of the stored energy. Mavros et al (1994), in simulating the draw off temperature profile of a fully mixed tank found that model accuracy improved with the number of segments considered. While the number of segments affects the performance of the model, a

greater number also demands greater computational effort. While a large benefit in performance was observed for an increase in segment numbers for up to twenty segments, the benefit rapidly decreases for increasing numbers above this value.

2.6.3.2 The Multinode model

The second of the aforementioned models is the multinode model. The tank is considered as consisting of a number of nodes of equal and constant volume. At each time-step, in relation to the temperature of water entering and leaving the tank, an energy balance is written for each node. Heat loss to the surroundings and heat transfer between adjacent nodes is also taken into account. Load is assumed to be delivered from the uppermost node, with mains and collector inlet adjacent to the bottom node. For this model, for a variable collector outlet temperature, the inlet fluid is assumed to settle in the node with the temperature closest to but lower than its own, without any mixing. Gari and Loehrke (1982) showed that this was achievable in practice through using a low velocity inlet manifold. A schematic of a multinode model is shown in Fig. 2.7.2. A more detailed description of the multinode method and the aforementioned nodal energy balance is presented in chapter 4 section 5.

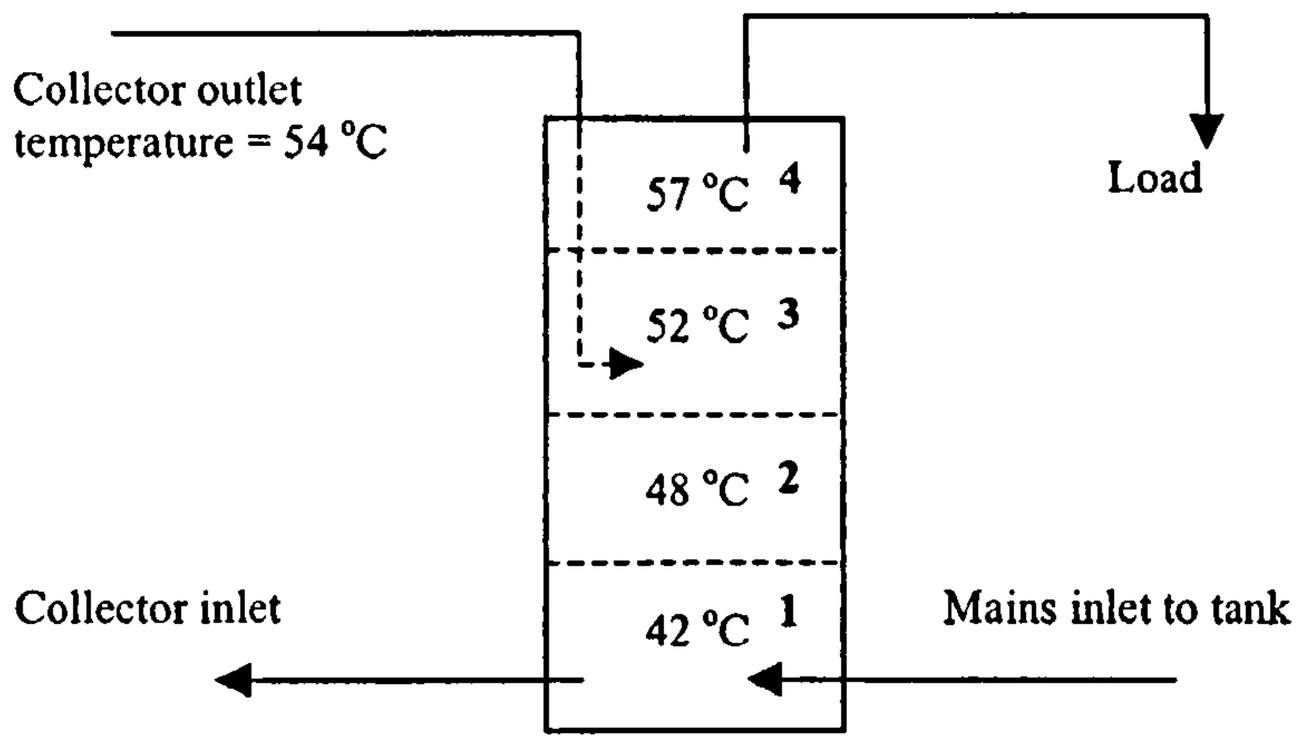

Figure 2.7.2. Schematic representation of the multinode model for a four node tank. For the case shown water from the collector is assumed to settle in node 3.

In their review of one-dimensional models Zurigat et al (1989) consider that the model, in the above form, as presented by Cabelli (1977) and Sharp (1978) is limited as it does not take account of any local mixing effects at the tank inlets. From an analysis of storage tank temperature profiles, Jaluria and Gupta (1982) concluded that the tank temperature field was one dimensional, varying only in relation to the vertical dimension. This, they claimed, was sufficient to allow the assumption that simple one-dimensional models were adequate in defining the temperature profile in stratified storage tanks. While Hoogendorn et al (1985) also found that there was a negligible horizontal temperature gradient, through an experimental investigation Issa and Al-Nimir (1989) found that the radial temperature distribution was an important factor. They showed that while the gradient was negligible near the bottom of the tank, it increased in relation to the vertical height within the tank.

When the effects of plume entrainment, Lightstone et al (1989), and localised mixing are included in the analysis, Guo and Wu (1985), Zurigat et al (1989) concluded that this model better reflects the real situation. Kleinbach et al (1993) recommend the use of the multinode model in preference to the plug flow model as they found that the plug flow model overestimated the energy quantities within the tank. However, Yoo and Pak (1996), and Yoo et al (1999) through the derivation of an analytical solution for stratified storage with variable inlet temperature and momentum induced mixing presented a complex yet robust and accurate solution for the tank thermocline profile based on the plug flow model.

2.6.4 Factors affecting tank performance and rate of destratification.

The above models give an overview of the two main methods that are employed to model the temperature profile within the stratified tank. While additional considerations required to provide an accurate estimation are also outlined, section 2.6.4 presents a more detailed account of the effect of flow rate, temperatures, and tank wall conductivity on the performance of the tank.

2.6.4.1 Effect of wall properties on tank performance.

In comparing the effects of a finite and theoretically infinite tank wall thickness Al-Nimir (1993) concluded that, for the finite thickness case, there was a greater tendency to decrease stratification in the tank. For thin, high thermal conductivity walls, as is the case for domestic copper hot water stores, Al-Nimir (1993) also considered that the temperature of the wall could be lumped radially and assumed equal to the temperature of the fluid. Hoogendorn et al (1985) showed that increasing the heat capacity of the wall produced a widening of the mixing front between adjacent zones at different temperature. Shyu et al (1989) while agreeing with the findings of Hoogendorn et al (1989) also demonstrated that the addition of internal insulation could help to maintain stratification. In addition, they stated that, while the removal of external insulation would help reduce the rate of decay, the increase in axial conduction, and hence heat loss would outweigh any benefits gained through this reduction. Satyanaryana Murthy et al (1989) also conclude that using a material of lower thermal conductivity for the walls will also enhance stratification.

2.6.4.2 Effect of flow rate and temperature on tank performance.

Hahne and Chen (1998) proposed that the modified Richardson number be used as a measure of the effect on stratification of the combined maximum collector flow/tank inlet velocity, and inlet temperature. As can be seen from Eq. 2.6.1 the modified Richardson number, $Ri_{Hf,}$ is the ratio of the modified Grashoff number, Gr_{HF}, and the modified Reynolds number $Re_{Hf.}$ The term "modified" is applied to each of these numbers to signify that they have been adapted for use in relation to the dimensions and configuration of storage tanks.

$$Ri_{H,f} = Gr_{H,f} / Re^{2}_{H,f} \qquad (2.6.1)$$

The modified Grashoff number, as given in Eq 2.6.2, is a measure of the ratio of buoyancy to viscous forces induced in the tank through temperature differences, and the modified Reynolds number, Eq 2.6.3, the ratio of the inertial to viscous forces, Incropera and DeWitt (1996).

$$Gr_{Hf} = g\beta(T_{IS} - T_S)H^3 / \nu^2 \quad (2.6.2)$$

$$Re_{Hf} = \omega_{IN}H / \nu \quad (2.6.3)$$

Based on the modified Richardson number Hahne and Chen (1998) defined the tank charging efficiency as "the ratio of the net stored thermal energy in a store at the end of a charging process to the thermodynamic maximum storable energy", that is, the ratio of the energy contained to the total energy delivered by the collector. The above authors showed that, for a high $Ri_{Hf,}$ where the buoyancy forces outweighed the momentum forces a good thermal stratification was established. They showed that for Ri_{Hf} greater than 0.25, the charging efficiency was greater than 97%.

Yoo and Pak (1993) express the charging / storage efficiency analytically in terms of the Peclet number. The Peclet number, as given in Eq 2.6.4, is a measure of the ratio of heat transfer by convection to that by conduction. It is quoted by the above authors, Yoo and Pak (1996) as being of the order of 10^2 or greater for typical storage tanks.

$$Pe = V H / \alpha \quad (2.6.4)$$

Issa and Al-Nimir (1989), and Al-Nimir (1993) also consider the magnitude of the Peclet number as an indicator for charging efficiency, with an increase in Peclet number leading to a decrease in the heat transfer between adjacent nodes.

2.6.5. Summary

In respect of modelling SDHWS the TRANSYS software suite of programs is the most versatile and best validated simulation tool. While the benefits of the plug flow model have been outlined it appears that the multi-node variable inlet tank model is preferred. This model can be easily adapted to take account of the effects of wall thermal conductivity and plume entrainment to more accurately predict the performance of tanks where these factors are likely to have an influence. An indicator of tank performance based on the Peclet and modified Richardson numbers has also been presented.

REFERENCES

Adams D.E., and Davidson J.H., (1993) Tank stratification with a flexible manifold. In *Proceedings of ASES Annual Conference, Solar '93,* Washington, DC, USA.

Agarwal V.K., and Larson D.C., (1981), Calculation of top-loss coefficients of a flat-plate collector. *Solar Energy,* Vol. 27, pp. 69-71.

Al-Ibrahim A. M., Klein S.K., Mitchell J.W., Beckman W.A.(1998). Design procedurefor selecting an optimum photovoltaic pumping systemin a solar domestic hot water system. *Solar Energy* Vol. 64, Nos 4-6, pp.227-239.

Al-Ibrahim A.M., (1997), Optimum selection of direct coupled photovoltaic pumping system in solar domestic hot water systems. PhD hesis, University of Wisconsin-Madison.

Al-Ibrahim A.M., Klein S.K., Mitchell J.W., Beckman W.A. (1996) An Investigation of photovoltaic powered pumps in direct solar domestic hot water systems. In *Proceedings of Solar '96*, American Solar Energy Society, 13 –18 April, Asheville, North Carolina, America, Campbell-Howe R. and Wilkins-Crowder B. (Eds), pp. 141-146.

Al-Nimir M.A., (1993), Temperature distribution inside a solar collector storage tank of finite wall thickness. *Transactions of the ASME JSEE,* Vol. 115, pp 112 – 116.

Amer E.H., Nayak J.K., and Sharma G.K., (1997), Transient test methods for flat – plate collectors: review and experimental evaluation. *Solar Energy,* Vol. 60, No.5, pp 229 – 243.

Anis W.R., and Metwally M.B., (1994), Dynamic performance of a directly coupled PV pumping system. *Solar Energy,* Vol. 53, No. 4, pp 369 – 377.

Arranovich E., (1977), The joint solar collector testing programme of the European Community. In *Proceedings UK/ISES Conference C11, Testing of solar collectors and systems,* pp 49 – 70.

ASHRAE 1982, "Standard 95-1981, Methods of testing to determine the thermal performance of solar domestic hot water systems." *Proc. 1982 ASES Passive Solar Conference,* ASES.

B.S., (1986), British Standard 6757: method of test for thermal performance of solar collectors. British Standards Institute.

Baker D., Vliet G., and Lawler D., (1996), SOLSCALE: Software to predict scaling in solar domestic hot water systems. In *Proceedings of Solar '96, 25th ASES Conference,* Asheville, NC, USA.

Bartelsen B., Rockendorf G., and Vennemann N., (1996), Development of an elastomer-metal-absorber for thermal solar collectors. In *Proceedings, EuroSun '96,* Section IV-1. *Pub* ISES, DGS Sonnenenergie Verlags-GmbH, Munich.

Bartelsen B., Rockendorf G., Vennemann N., Tepe R., Lorenz K., and Purkarthofer G., (1999), Elastomer-metal-absorber – development and application. In *Proceedings ISES World Solar Energy Congress,* Israel.

Beckman W.A., Duffie J.A., and Klein S.A., (1977), Simulation of solar heating systems. Chapter IX, in *ASHRAE- Application of solar energy for heating and cooling of buildings.*

Berg P. and Furbo S. (1990), Calculation of the thermal performance of small hot water solar heating systems using low flow rates. In *Proceedings of Northsun '90,* Reading, England, Sayigh A.A.M. (Ed) Pergamon Press, Oxford.

Bourges B., Rabl A., Leide B., Carvalho M.J., and Collares-Pereira M., (1991), Accuracy of the European solar water heater test procedure. Part 2, prediction of long term performance. *Solar Energy,* Vol. 47, No. 1, pp 17-25.

Bowman N.T., Redferne W.B., and Eldessouky E., (1981), Stratified solar storage for use in domestic scale systems. *Sun at Work in Britain,* No. 12/13.

Burch J., Egrican N., and Carlisle N., (1990), Calcium carbonate scaling in solar domestic hot water systems. In *Proceedings of ASES Annual Conference.* Austin, TX, USA.

Cabelli A., (1977), Storage tanks – a numerical experiment. *Solar Energy,* Vol. 19, pp 45 – 54.

Camani M., Cereghetti N., Chianese D., and Rezzonico S., (1998) Comparison and behaviour of PV modules. In *Proceedings EuroSun '98,* 14-17 September, Portoroz, Slovenia, Goetzberger A. and Krainer A. (Eds) Volume 2 Section V.1.1, The Franklin Company Consultants Ltd, Birmingham, UK.

Carvalho M.J., Collares-Pereira M., Cunha F.M., and Vitorino C., (1988), An experimental comparison of operating strategies for solar water systems. *Solar Energy,* Vol. 41, No.1, pp 33 – 39.

Chungpaibulpatana S., and Exell R.H.B., (1990), Transient method for testing flat-plate solar collectors. In *Proceedings Energy and the Environment into the 1990's,* Vol.2, Sayigh A.A.M., (Ed.) Pergamon Press, Oxford, pp 699 – 703.

Cooper P.I., and Dunkle R.V., (1981), A non-linear flat plate collector model. *Solar Energy,* Vol. 26, pp 133 –140.

Cromer C.J., (1984), Design of a DC-pump, photovoltaic powered circulation system for a solar domestic hot water system. In *Proceedings of the ASES Solar 1984 conference*, Anaheim,CA, pp.233-238.

Csordas G.F., Brunger A.P., Hollands K.G.T., and Lightstone, M.F., (1992), Plume entrainment effects in solar domestic hot water systems employing variable flow rate control strategies. *Solar Energy,* Vol. 49, No.6, pp 497-505.

Davidson J.H., and Adams D.A., (1994) Fabric stratification manifolds for solar water heating. In *Transactions of ASME JSEE,* Vol. 116, pp 130 – 136.

Dayan M., (1997), High performance in low flow solar hot water systems. M.S. Thesis, University of Wisconsin – Madison.

DTI, 2000, Communication from Department of Trade and Industry, UK, Details in the document ETSU S/P3/00268/REP.

Duffie J.A. and Beckman W.A. (1991) *Solar Enginering of Thermal Processes,* 2nd edn, Wiley Interscience, New York . ISBN 0-471-51056-4

Durisch W., Tlle D., Worz A., and Plapp W., (2000), Characterisation of photovoltaic generators. *Applied Energy,* Vol. 65, pp 273 – 284.

Durisch W., Urban J., and Smestad G., (1996), Characterisation of solar cells and modules under actual operating conditions. In *Proceedings World Renewable Energy Congress,* Denver, Vol. 1, p 389.

Eckstein J., Townsend T., Beckman W.A., and Duffie J.A., (1990), Photovoltaic powered energy systems. In *Proceedings* American Solar Energy Society conference. Austin Texas 1990.

Eldessouky E.A.E., (1985), Comparison of measured and predicted results for a domestic thermally stratified solar storage container. *Proceedings of INTERSOL '85.* 9th biennial congress of the ISES. Vol. 2, Bilgen E., Hollands K.G.T., Eds. Pergamon Press.

Emery E., and Rogers B.A., (1984), On a solar collector thermal performance test method for use in variable conditions. *Solar Energy,* Vol. 33, pp 117 –

European Solar Radiation Atlas, (2001), Internet address, http://www.helioserve.cma.fr/esra

Fanney A.H., and Klein S.A., (1988) Thermal performance comparisons for solar hot water systems subjected to various collector and heat exchanger flow rates. *Solar Energy,* Vol. 40,No.1, pp 1 – 11.

Fanney A.H., Dougherty B.P., and Kramp K.P., (1997), Field performance of photovoltaic solar water heating systems. In *Proceedings ASME International Solar Energy Conference.* pp 171 – 182.

Florida Solar Energy Centre, (2001), Internet address, http://www.logger.fsec.ucf.edu/net

Furbo S., (1989), Solar water heating systems using low flow rates.- experimental investigations. Internal Report No. 89-9, Thermal Insulation Laboratory, Technical University of Denmark.

Furbo S., (1990), Attractive small marketed hot water solar heating systems using low flow operation. In *Proceedings of Northsun '90,* Reading, England, Sayigh A.A.M. (Ed), Pergamon Press, Oxford

Furbo S., (1998) Present and future SDHW technology. In *Proceedings EuroSun '98,* 14-17 September, Portoroz, Slovenia, Goetzberger A. and Krainer A. (Eds) Volume 2 Section III.3.5, The Franklin Company Consultants Ltd, Birmingham, UK.

Furbo S., and Shah L.J., (1996), Optimum solar collector fluid flow rates. In *Proceedings, EuroSun '96,* Section II-46. *Pub* ISES, DGS Sonnenenergie Verlags-GmbH, Munich.

Garg H.P., and Datta G., (1984), The top loss calculation of flat-plate solar collectors. *Solar Energy,* Vol. 32, pp. 131-133.

Gari H.N., and Loehrke R.I., (1982), A controlled buoyant jet for enhancing stratification in a liquid storage tank. *Journal of Fluids Engineering,* Vol. 104, 475 – 481.

Ghaddar N.K., (1994), Stratified storage tank influence on performance of solar water heating system tested in Beirut. *Renewable Energy,* Vol. 4, No. 8, pp 911 – 925.

Govaner D., (1988) Indoor collector testing with an incandescent simulator. *Solar Energy,* Vol. 40, No.4, pp 363-368.

Grossman G., Shitzer A., and Zvirin Y., (1997), Heat transfer analysis of a flat-plate solar energy collector. *Solar Energy,* Vol. 19, pp. 493-502.

Gul M.S., Muneer T., and Kambezedis H.D., (1998), Models for obtaining solar radiation from other meteorological data. *Solar Energy,* Vol. 64, Nos. 1-3, pp 99 – 108.

Guo K.L., and Wu S.T., (1985), Numerical study of flow and temperature stratification in a liquid thermal storage tank. *Transactions of the ASME JSEE,* Vol. 107, pp 15 – 20.

Hahne E. and Chen Y., (1998), Numerical study of flow and heat transfer characteristics in hot water stores. *Solar Energy,* Vol. 64, Nos. 1 – 3, pp 9 - 18.

Hammad M.A., (1994), Experimental study of a solar thermal-photovoltaic integrated system. *Renewable Energy,* Vol. 4, No.8, pp 897 – 905.

Hausner R., and Fechner H., (1998), Influence of the flow condition (laminar/ turbulent) in the fluid tube on the collector efficiency factor of a fin absorber. In *Proceedings of EuroSun 1998,* 14-17 September,

Portoroz, Slovenia, Goetzberger A. and Krainer A. (Eds)Volume 2 Section III.2 13. The Franklin Company Consultants Ltd, Birmingham, UK.

Hawlader M.N.A., and Wijeysundera N.E., (1987) Solar collector testing. *Renewable Energy Review Journal.* Vol. 9, pp 11 – 28.

Hellstrom B., and Perers B., (1998), Comparison of two standard collector test methods. In *Proceedings EuroSun '98,* , 14-17 September, Portoroz, Slovenia, Goetzberger A. and Krainer A. (Eds)Volume 2 Section III.2 17. The Franklin Company Consultants Ltd, Birmingham, UK.

Herrmann B., Karl H., Kopf E., and Lehner G., (1987), Realistic indoor testing of photovoltaic water pumping systems. *Solar Energy,* Vol. 38, No.4, pp 275 – 279.

Hirata Y., and Tani T., (1995), Output variation of photovoltaic modules with environmental factors – 1. The effect of spectral solar radiation on photovoltaic module output. *Solar Energy,* Vol. 55, No.6, pp 463 – 468.

Hollands K.G.T., and Lightstone M.F., (1989), A review of low flow stratified-tank solar water heating systems *Solar Energy*, Vol. 43, pp 97-105.

Hollands K.G.T., Unny T.E., Raithby G.D., and Konicek L., (1981), Free convective heat transfer across inclined air layers. *ASME Journal of Heat Transfer,* Vol. 98, No.2 May, pp. 189-193.

Hottel H.C., and Woertz B.B., (1942), The performance of flat-plate solar heat collectors. *Transactions of the ASME,* Vol. 64, pp. 94-102.

In *Proceedings of ASES Annual Conference.* Austin, TX, USA.

Incropera F.P., and DeWitt D.P., (1996), *Introduction to heat transfer*. 3rd edn, Wiley Interscience, New York . ISBN 0-471-30458-1.

Issa M., and Al-Nimir M., (1989), Temperature distribution inside hot water storage tanks of solar collectors. *Transactions of the ASME JSEE,* Vol. 111, pp 311 – 317.

Jafar M., (2000), A model for small scale photovoltaic solar water pumping. *Renewable Energy,* Vol. 19, pp 85 – 90.

Jaluria Y., and Gupta S.K., (1982), Decay of thermal stratification in a water body for solar energy storage. *Solar Energy,* Vol.28, No. 2, pp 137 – 143.

Jesch L.F., and Braun J.E., (1984), Variable volume storage and stratified storage for improved water heater performance. *Solar Energy,* Vol. 33, pp 83 - 87.

Jordan U., Vajen K., Hilmer F., Knopf B., and Spieler A., (1998) A stratified storage tank with an internal thremosyphonically driven fin-tube heat exchanger. In *Proceedings EuroSun '98,* 14-17 September, Portoroz, Slovenia, Goetzberger A. and Krainer A. (Eds) Volume 2 Section III.3.6, The Franklin Company Consultants Ltd, Birmingham, UK.

Kiatsiriroat T., Namprakai P., and Hiranlabh J., (1993), Performance estimation of a PV water pumping system with utilizibility function. *International Journal of Energy Research,* Vol.17, pp 305 – 310.

Klein S.A., (1975), Calculation of flat-plate collector loss coefficients. *Solar energy* Vol. 17, pp 79-80.

Klein S.A., Beckman W.A., and Duffie J.A., (1976), A design procedure for solar heating systems. *Solar Energy,* Vol. 18, No.2, pp

Klein S.A., et al (1990) TRANSYS 13.1 User's manual. Engineering experiment station report 38-13, Solar Energy Laboratory, University of Wisconsin-Madison.

Kleinbach E.M., Beckman W.A., and Klein S.A., (1993) Performance study of one-dimensional models for thermal storage tanks. *Solar Energy,* Vol. 50, No. 2, pp 155 – 166.

Kou Q., Klein S.A., and Beckman W.A., (1998), A method for estimating the long-term performance of direct-coupled PV pumping systems. *Solar Energy,* Vol. 64, Nos. 1-3, pp 33 – 40.

Langridge D., Lawrence W., and Wichert B., (1996), Development of a photovoltaic pumping system using a brushless d.c. motor and helical rotor pump. *Solar Energy,* Vol. 56, No. 2, pp 151 – 160.

Lawrence W.B., and Wichert B., (1994), A versatile PV module simulation model based on PSI/e. *Solar Energy,* Vol. 52, No.2, pp 191 – 195.

Ledion J., Gueugnon Y., Ribal C., and Combaz P., (1993), Encrustation of the surface of plastic materials. *Techniques, Sciences, Methodes,* Vol. 88, Nos.7/8, pp 355 – 360. (In French)

Lightstone M., Hollands K.G.T., and Hassani A.V., (1988), Effect of plume entrainment in the storage tank on calculated solar system performance. Proc 14th Annual conference of SESCI, Energy Solutions for Today, Ottawa pp 236 - 241.

MacGregor K., 1996, "Comparison Between Flat-Plate and Vacuum-Tube Solar Collectors". *Proc* Eurosun 1996, 12-14 July 1996, Freiburg, Germany.

MacGregor K., 2000, private communication, Napier University, Edinburgh, Scotland.

Mavros P., Belessiotis V., and Haralambopolous D., (1994), Stratified energy storage vessels: characterization of performance and modelling of mixing behaviour. *Solar Energy,* Vol. 52, No. 4, pp 327 – 326.

Michaelides I.M., and Wilson D.R., (1997), Simulation studies of the position of the auxiliary heater in thermosyphon solar water heating systems. *Renewable Energy,* Vol. 10, No.1, pp 35 – 42.

Miller J.A., and Hittle D.C., (1993), Yearly simulation of a PV pumped, wrap-around heat exchanger, solar domestic hot water system. In *Proceedings ASME Joint Solar Engineering Conference,* Washington, pp 67 – 73.

Morrison G.L., Gilliaert D., and Tebaldi P., (1992) Outdoor testing of solar water heaters- effects of load pattern and auxiliary boosting. *Solar Energy,* Vol. 49, No. 4, pp 299 – 308.

Moussi A., Betka A., Azoui B., (1999), Optimised photovoltaic pumping system. In *Proceedings of the 34th Universities Power Engineering Conference.* University of Leicester, Vol. 1, pp 86 – 90.

Muschaweck J., and Spirkl W., (1993), Dynamic solar collector performance testing. *Solar Energy Materials and Solar Cells.* No. 30 pp.95-105.

Narvarte L., Lorenzo E., and Caamano E., (2000), PV pumping analytical design and characteristics of boreholes. *Solar Energy,* Vol. 68, No.1, pp 49 – 56.

Parker G.J., (1976), A forced circulation system for solar water heating. *Solar Energy,* Vol. 18, pp 475 – 479.

Parretta A., Sarno A., and Vicari L.R.M., (1998), Effects of solar irradiation conditions on the outdoor performance of photovoltaic modules. *Optics Communications,* Vol. 153, pp 153 – 163.

Pierson P., and Padet J., (1990), Time constant of solar collectors. *Solar Energy,* Vol. 44, No. 2, pp 109-114.

Prud'homme T., and Gillet D., (1998) Optimization of solar domestic hot water systems. *EuroSun '98,* , 14-17 September, Portoroz, Slovenia, Goetzberger A. and Krainer A. (Eds)Volume 2 Section III.3.9. The Franklin Company Consultants Ltd, Birmingham, UK.

Pulfrey D.L., Ward P.R.B., and Dunford W.G., (1987), A photovoltaic powered system for medium head pumping. *Solar Energy,* Vol. 38, No.4, pp 255 – 265.

Rogers B.A., (1981), A method of collector testing under transient conditions. In *Proceedings Solar World Forum, ISES Congress,* Brighton, England, Vol.1, Hall D.O., and Morton J., (Eds.) Pergamon Press, Oxford, pp 898 – 902.

Samdarshi S.K., and Mullick S.C., (1991), Analytical equation for the top heat loss factor of a flat plate collector with double glazing. *ASME Journal of Solar Energy Engineering,* Vol. 113 pp117-122, 1991.

Satyanaryana Murthy S., Nelson J.E.B., and Sitharama Rao T.L., (1992), Effect of wall conductivity on thermal stratification. *Solar Energy,* Vol. 49, No. 4, pp 273 – 277.

Saunier G.Y., and Chungpaibulpatana S., (1983), A new inexpensive dynamic method of testing to determine solar thermal performance. In *Solar World Congress,* Vol.2, Szokolay S.V. (Ed.). Pergamon Press, Oxford, p 910.

Sharp M.K., (1978), Thermal stratification in liquid sensible heat storage. *M.S. Thesis,* Colorado State University, Fort Collins, Colorado.

Shyu R-J., Lin J-Y., and Fang L-J., (1989), Thermal analysis of stratified storage tanks. *Transactions of the ASME JSEE,* Vol. 111, pp 54 – 61.

Singer S., and Appelbaum J., (1993), Starting characteristics of direct current motors powered by solar cells. *IEEE Transactions on Energy Conversion,* Vol. 8, No.1, pp 47 – 52.

Solar Energy Reasearch Institute, (2001), Internet address, http://rredc.nrel.gov/solar

Souproun A.V. (1992), Dynamic method of solar collector testing. *ASME JSEE,* Vol. 2, pp 1149 – 1154.

Tabarra M., and Bowman N.T., (1985), The effect of load profiles on stratified solar storage tanks. In *Proceedings of INTERSOL '85.* 9th biennial congress of the ISES. Vol. 2, Bilgen E., Hollands K.G.T., Eds. Pergamon Press.

Tsilingris P.T., (1996), Solar water-heating design – a new simplified dynamic response. *Solar Energy,* Vol. 57, No.1, pp19 – 28.

Uecker M., Hampel M., Krause M., Ratka A., Vajen K., and Ackermann H., (1998), A comparison of simulation studies and measurements of a medium scale solar thermal system. In *Proceedings EuroSun '98,* 14-17 September, Portoroz, Slovenia, Goetzberger A. and Krainer A. (Eds) Volume 2 Section III.2.49., The Franklin Company Consultants Ltd, Birmingham, UK.

Van Berkel J., (1996), Mixing in thermally stratified energy stores. *Solar Energy,* Vol. 58, Nos. 4-6, pp 203 – 211.

van Koppen C.W.J, Simon Thomas J.P. and Veltkamp W.B., (1979) The actual benefits of thermally stratified storage in a small and a medium size solar system. In *Sun II -Proceedings of ISES* Biennial Meeting, Atlanta, GA, Vol. 2, pp. 576-584.

Vliet G., and Baker D., (1992), Designing solar hot water systems for scaling environments. *ASHE JSES ITSES International Solar Energy Conference.* ISBN 0791807622.

Wang X.A., Xu Y.F., and Meng X.Y., (1987), A filter method for transient testing of collector performance. *Solar Energy.* Vol. 38, No. 2, pp. 125-134.

Whillier A., (1977), Prediction of performance of solar collectors. Chapter VIII, in *ASHRAE- Application of solar energy for heating and cooling of buildings.*

Wijeysundera N.E., and Hawlader M.N.A., (1984), Indoor transient tests on solar collectors. In *Proceedings ENERGEX '84,* Regina, Canada, pp 181 – 185.

Worldwide Infromation network for renewable Energy, (2001), Internet address, http://www.wire0.ises.org

Wuestling M.D., Klein S.A., and Duffie J.A., (1985), Promising control alternatives for solar water heating systems. *ASME Journal of Solar Energy Engineering* Vol. 107.

Yoo H., and Pak E., (1996), Analytical solutions to a one-dimensional finite domain model for stratified thermal storage tanks. *Solar Energy,* Vol.56, No. 4, pp 315 – 322.

Yoo H., and Pak E-T., (1993), Theoretical model of the charging process for stratified thermal storage tanks. *Solar Energy,* Vol. 51, No. 6, pp 513 – 519.

Yoo H., Kim C-J., and Kim C.W., (1999) Approximate analytical solutions for stratified thermal storage under variable inlet temperature. *Solar Energy,* Vol. 66, No. 1, pp 47 – 56.

Zaki A.M., and Eskander M.N., (1996), Matching of photovoltaic motor-pump systems for maximum efficiency operation. *Renewable Energy,* Vol.7, No.3, pp 279 – 288.

Zurigat Y.H., Maloney K.J., and Ghajar A.J., (1989), A comparison study of one-dimensional models for stratified thermal storage tanks. *Transactions of the ASME JSEE,* Vol. 111, pp204 – 210.

BLANK IN ORIGINAL

3 SYSTEM PERFORMANCE ANALYSIS

3.1 INTRODUCTION TO EXPERIMENTAL WORK

The main body of this work covers an analysis of the system components performance. Central to this is the experimental evaluation of the Flexsol collector efficiency characteristic, and the subsequent selection of a suitable pump and PV module pairing based on the desired operating condition. A study of the effect of two simple methods of flow control on the collector outlet temperature profile is presented. The best method, and degree, of control are selected on the basis of their ability to meet the condition of a constant collector outlet temperature. The rationale behind the side by side comparative testing of the optimised FT-PV system with a good standard anti-freeze based solar water heating system is outlined. The results of this testing are presented and conclusions drawn regarding the performance of the FT-PV system.

Initial consideration of the likely maximum design flow rate and collector outlet temperature suggested that the system would promote stratification within the storage tank. An experimental investigation of storage tank temperature profiles was undertaken to confirm these implications. Testing was carried out in order to define the relationship between axial internal and external wall temperatures. This is to allow an estimation of the energy within the tank to be made from external measurement alone. Measurements of the tank external wall temperature profile during charging and subsequent cooling/destratification were made to afford an estimation of the tank embodied energy during these periods. The results of this work are used in section 4 for comparison with values obtained through modelling the collector outlet temperature, flow rate, and storage tank charging and cooling.

As limescale can affect system performance, it was necessary to investigate the potential effect of the carbon doped EPDM collector pipe on the rate of scaling within the FT-PV system. The results of this investigation are now presented.

3.2 ANALYSIS OF THE POTENTIAL EFFECTS OF LIMESCALE IN THE NEW SYSTEM

3.2.1 Introduction

It has been shown in section 2.1 that where hard water is circulated through a solar collector, there is the potential for the deposition of limescale. In severe cases these deposits can reduce system performance and damage components. A review of related work, Ledion et al (1993), revealed that some polymer materials are more prone to limescaling than others. The Flexsol collector has carbon doped EPDM fluid pipes and may therefore be susceptible to limescaling. Section 3.2 presents a summary of the mechanism behind the formation of limescale and details the experimental procedure developed to determine the likelihood of limescale formation in the fluid tubes of the Flexsol collector.

3.2.2 The mechanism of limescale formation.

Limescaling is the term used to describe the deposition of salts on the walls of fluid filled channels and pipes. It is a phenomenon most usually associated with hard, or alkaline, water in which the salts and their constituents naturally occur in solution.

The main constituents of lime-scale are Calcium Carbonate, Ca (CO_3), and Magnesium Carbonate, Mg (CO_3), with other salts and compounds, including Calcium Phosphate Ca (PO_4) and Silicon Dioxide, Si O_2. Typically there is a much greater proportion of Ca (CO_3) than Mg (CO_3) in the scale as most "source" hard water is drawn from limestone and chalk areas.

In defining the hardness of water, for ease of comparison of different water samples, rather than give the concentrations of both the above salts, the relative concentrations of the metal ions in solution are combined to produce a hardness equivalent of Ca (CO_3), as given in Eq 3.2.1

$$Ca\ (CO_3)\ (mg/l) = 2.497*Ca\ (mg/l) + 4.118*Mg\ (mg/l) \qquad (3.2.1)$$

While hardness is a useful measure for comparison, it does not, however, give an indication of a particular samples' readiness, or ability, to form scale. This is because the quantity of $CO3^{2-}$ ions in ordinary water is usually very low compared to Ca^{2+} ions, and both are required for scale to form. The equilibrium balance is given in Eq. 3.2.2

$$Ca^{2+} + (CO_3)^{2-} \rightleftharpoons Ca(CO_3) \qquad (3.2.2)$$

There are several factors that affect the rate of scale formation., namely;

1. The concentration of the ions and salts in solution; - the higher the concentration, the more easily they will precipitate out. If there are any suspended solids in the solution, or Ca (CO_3) "seeds", the rate of deposition will be greatly enhanced. (Vliet and Baker (1994))

2. The water temperature; - the salts become less soluble as the temperature increases.

3. The fluid flow rate; - the higher the stream velocity, the less readily the salts can settle. The Reynolds number is also important, as there will obviously be a marked change in the rate of deposition between laminar and turbulent flow.

4. The pipe material; - a rougher surface will enable settling, and electrostatically induced charges on the pipe walls will encourage salt formation.

3.2.3 Rationale.

In view of the above considerations, accelerated testing was carried out over a period of four months to establish whether there was likely to be a problem created by thermal limescaling through long term circulation of hot hard water through the tubes/pipes in question.

A saturated hard water solution, the "make-up" of which is given in Table 3.2.1, was circulated at a flow rate of 0.5 l/min and a temperature of 60 ° C. The solution was prepared using constituent salts and quantities as outlined by Thames Water Board, Bryant (1998), for make up of "very hard" water. The salt quantities, when added to distilled water provide water with a hardness factor of 280 – 320 (mg Ca CO_3 / litre). This is approximately three times the maximum allowed for domestic supply within Britain. (110 mg Ca CO_3 / litre). This flow rate, as shown in section 3.5, implies that the flow will be laminar in all samples, thus increasing the potential for scaling.

Table 3.2.1. Constituent quantities for make up of very hard water

Component	Na HCO_2	Ca $SO_4 - H_2O$	Mg SO_4	K Cl
Quantity (mg/litre)	384	240	240	16

For a $2m^2$ collector, from the literature, section 2.3, the above flow rate represents an approximate maximum for a low flow system. The temperature is above the design optimum outlet of 55 °C. While under normal operating conditions the collector outlet temperature may be at this value, the average collector fluid temperature will be lower. Testing at this elevated temperature will tend to further enhance scale formation.

Vliet and Baker (1994) quoted a case where the thermal expansion and contraction of a heat exchanger fragmented and removed the scale that would have otherwise formed on it. In considering the construction of the Flexsol collector and circulation system, it is possible that the variable flow rate may cause expansion and contraction of the fluid tubes, and hence affect scale formation.

Three 0.4 m samples of pipe were examined: namely, a 15mm copper pipe sample, used as a standard, and two different configurations of the carbon doped EPDM. The first EPDM sample was clamped/sandwiched as it would be in the collector absorber plate, and the second was held rigid in a jacket. This second sample was held rigid to reduce the chance of any flow fluctuations causing the pipe

walls to flex and disturb any deposits. The pump was set on a timer to switch off for a duration of 15 minutes 8 times per day. All samples were weighed prior to, and after testing with a set of calibrated electronic scales, (tolerance +/- 0.0005 g.)

3.2.4 Results

After four months continuous testing the samples were removed and initially examined by eye. All three samples were seen to have a thin whitish deposit of scale on the walls, with a slightly darker /thicker deposit on the lower surface.

If there were very strong electrostatic influences in the EPDM samples it is likely that the deposit would be seen to be more even on the interior surface. As there is the same pattern of deposition on all samples this would tend to indicate that there is not a larger electrostatic influence for the EPDM pipe.

Although a deposit was visible to the naked eye, on weighing, none of the samples recorded an increase in weight. This implies that a maximum of 0.0005g may have been deposited for any of the samples.

A 1 cm. section of each pipe sample was carefully removed from each of the original 40 cm. lengths, and prepared for examination by electron microscope. Analysis of the samples by electron microscopy revealed that the deposits had a similar surface roughness and maximum particle size of approximately $3 * 10^{-6}$ m for all samples.

3.2.5 Conclusions.

While it has not been possible to definitively quantify the potential effect of limescale within the Flexsol collector with respect to a conventional system using copper pipes, electron microscopy has revealed a similar surface roughness between the three samples in the above analysis. As the roughness is similar for the two EPDM samples, this implies that the flexing of the collector absorber tube, caused by pump cycling, has little affect on the rate of scale formation under the test conditions applied.

As the sample solution is three times the hardness of that allowable for domestic supply, and testing was continuous as opposed to an average maximum of 8 hours per day for an installed system, it may be assumed that the surface roughness/particle size represents approximately nine times that which would be seen for an installed system. Over an operational period of 20 years, in an area supplied with maximum hardness water, assuming a linear deposition rate, the measured particle size suggests that there would be a layer of limescale approximately 0.02 mm in depth deposited over this period. This would have a minimal effect on the heat transfer properties of the collector pipe. Assuming an average pipe width of 4mm (with the pipe sandwiched in the collector plate) this figure also represents a 1% blockage. The effect on flow rate will also therefore be negligible.

As systems comprising the Flexsol collector have only recently become commercially available, (January 2000), no systems have been operational in areas with hard water for more than 1 year to date. It is therefore not possible to validate the above assumptions on the long term rate of deposition at the present time.

3.3 STORAGE TANK PEROFRMANCE.

3.3.1 Introduction

The mechanisms and some of the factors affecting the rate of stratification decay in hot water storage tanks were discussed in section 2.6. Al-Nimir (1993) presented an analytical solution for the heat transfer in a hot water store with a finite wall thickness. He stated that the assumption that the fluid could be lumped radially, that is, no radial temperature gradient, was justified for tanks where the radius to length ratio was much less than unity, and the Peclet number (section 2.6.4.2) was less than 50. For the present tank and design conditions, the Peclet number, as calculated using the formula presented by the above author, Eq. 3.3.1, is calculated as having a value of 66 for an approximate optimum full sun flow rate of 0.4 l/min. This therefore suggests that the fluid cannot be lumped radially in this instance.

$$Pe = \rho C_p V r_1 / k \qquad (3.3.1)$$

In addition, Al-Nimir (1993) also stated that, for a thin high conductivity wall, the wall could also be lumped radially with the fluid. This implies that a measure of temperature on the wall external surface would give an accurate indication of the internal bulk temperature, and hence energy stored within the tank. The above outlined limits relating to wall thickness, are, however, not detailed enough to determine the suitability of the lumped wall approach in the present situation. Also, earlier work, Issa and Al-Nimir (1989), showed that, for some tanks there was a horizontal temperature gradient, and that this was dependant on the height within the tank at which measurement was made.

In consideration of the effect on stratification of the likely maximum design flow rate and collector outlet temperature the modified Richardson number, ($Ri_{H.f} = Gr_{H.f} / Re^2_{H.f}$), as described by Hahne and Chen (1998) and presented in section 2.6, was calculated as having a value of 11.6 for the present system. The above authors found that if Ri_{Hf} was greater than 0.25, then the flow field in the tank tended to be an ideal piston flow, and good thermal stratification was developed. This therefore implies that the design operating conditions will promote stratification in the tank.

As part of systems performance simulation, the collector outlet temperature, tank charging and subsequent destratification are modelled. In order to determine the validity of the proposed model the computed values were compared with measured profiles. The main aims of the current investigation were therefore to determine the relationship between the external wall and internal axial fluid temperature, and determine the validity of the lumped approach outlined above. This was to enable the definition of the internal temperature profile, and the tank energy, from these external measurements alone.

As the inlet flow rates considered are very low, during tank charging, the internal temperature fields will move very slowly. It is therefore assumed that the relationship between the external wall and internal axial temperatures will be the same during tank charging as for destratification.

Under real operating conditions, after load has been drawn and cooler mains water is delivered to the bottom tank, thus lowering the collector inlet temperature, the collector outlet temperature may be lower than that at the top of the tank. On entering the tank, the cooler water can cause a falling plume, and promote mixing and destratification. While it is an over simplification to ignore these potential effects for full simulation, it is not within the scope of this work to study and define the effect of load profile, and hence plume entrainment, on stratification. The present work is primarily concerned with defining the validity of the lumped approach, and the relationship between the internal and external temperatures during charging and destratification.

3.3.2 Storage tank temperature measurement.

3.3.2.1 Rationale

Some investigators, for example Bowman et al (1981) and Eldessouky (1993), found that, during charging, a storage tank could be accurately modelled if considered as a three segment system. Others, such as Hoogendorn et al (1985) and Mavros et al (1994), found that ten or more nodes were required to accurately describe tank behaviour. With these considerations, for system simulation, a model based on a ten node tank was constructed, and the tank, as shown in Fig 3.3.1, was set with ten equally spaced

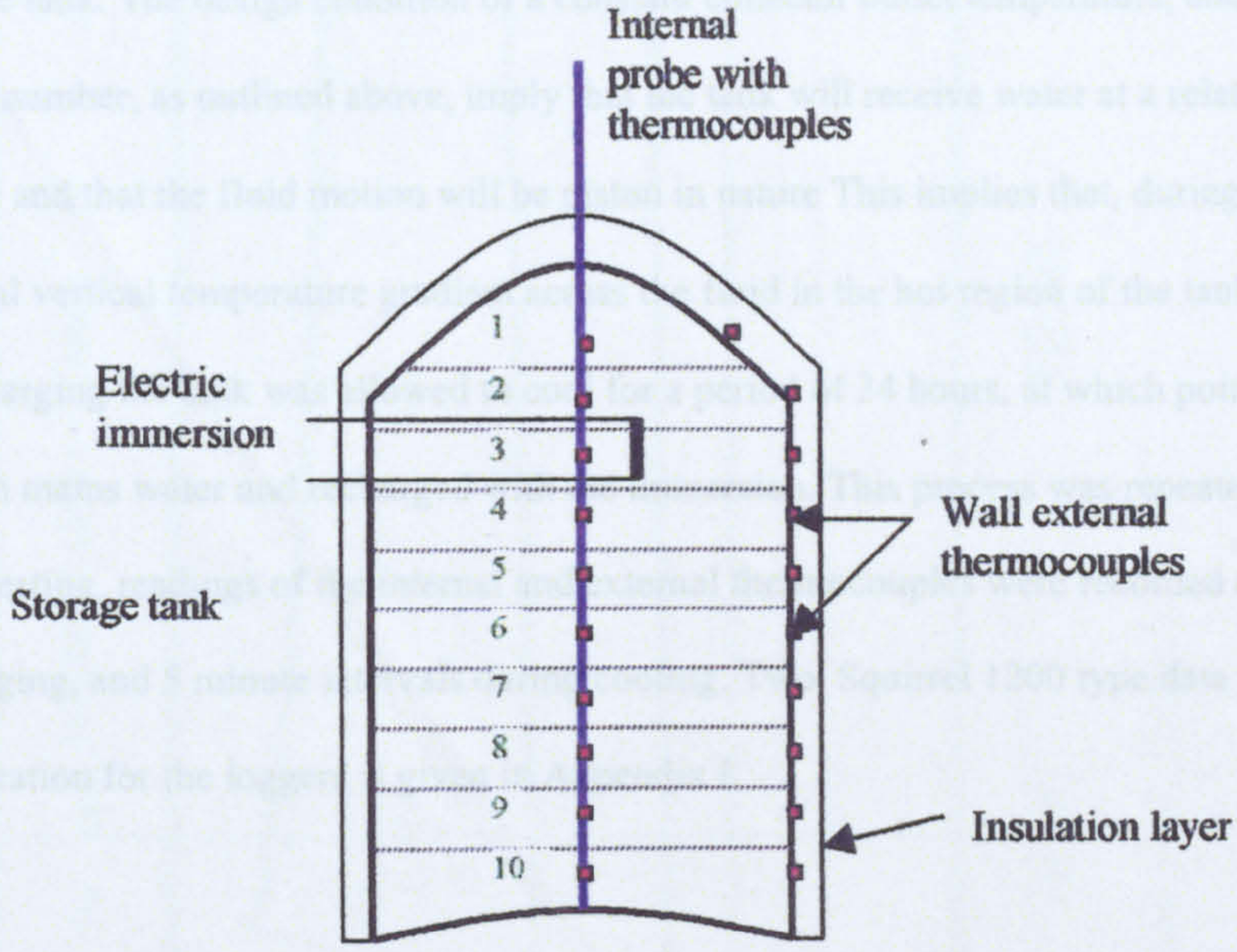

Figure 3.3.1 Schematic diagram of storage tank with immersion heater and internal and external thermocouples.

internal and external thermocouples. The respective internal and external thermocouples were set at the same vertical height from the tank bottom. For the external thermocouples, to ensure good surface contact and accurate readings, the tank wall was lightly centre punched to locate the thermocouple bead.

In the first instance, the tank was charged using the 3 kW upper electric immersion heater for a period of 2 hours to provide a marked thermocline step within the tank. The electric immersion was used raise the temperature to such a point as there was observed to be a minimal vertical thermocline in the upper region of the tank. The design condition of a constant collector outlet temperature, and the modified Richardson number, as outlined above, imply that the tank will receive water at a relatively constant temperature and that the fluid motion will be piston in nature This implies that, during charging, there will be a minimal vertical temperature gradient across the fluid in the hot region of the tank.

After charging the tank was allowed to cool for a period of 24 hours, at which point it was fully flushed with mains water and recharged with the immersion. This process was repeated three times. During all testing, readings of the internal and external thermocouples were recorded at 1 minute intervals during charging, and 5 minute intervals during cooling. Two Squirrel 1200 type data loggers were used. The specification for the loggers is given in Appendix I.

3.3.2.2 Charging profile

Figure 3.3.2 shows a plot of the internal thermocouple temperatures during the second half of the charging phase. It can be seen that by the end of charging a high degree of stratification has been established within the tank. Due to convective mixing within the tank, caused by the immersion heater, the upper portion of the tank is close to being at a single bulk temperature, with the plot for the temperatures of the three upper thermocouples superimposed. The corresponding wall temperatures, as seen by comparison of the plots obtained for the upper external wall and internal tank temperature profiles in Fig 3.3.3, while they follow the trends observed for the internal axial temperatures, are lower. At the end of the charging period the greatest difference between respective internal and external temperatures was observed to be at the node immediately below the hot region. Figure 3.3.4 shows a plot of the respective temperature differences for the 10 tank nodes.

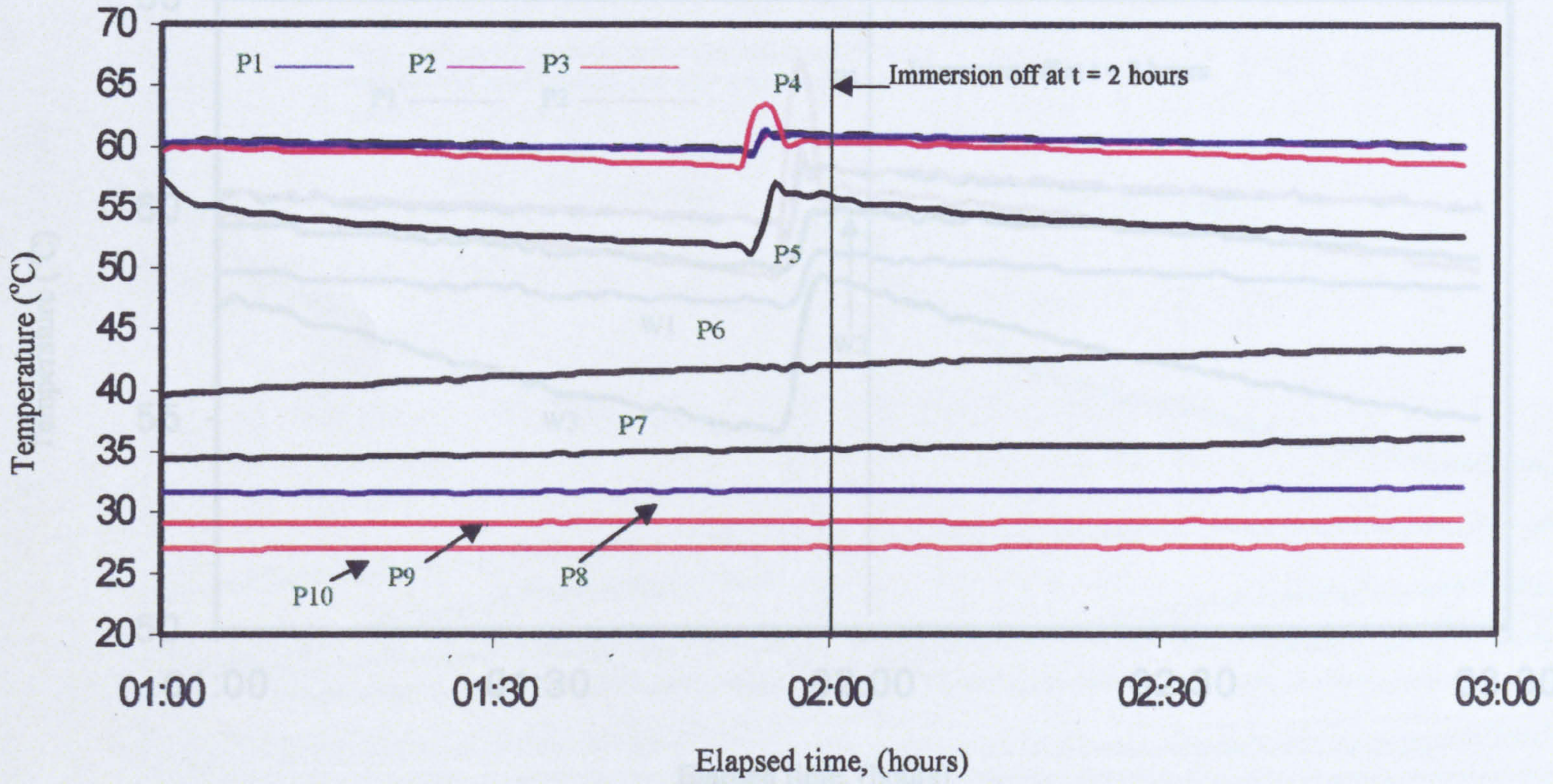

Figure 3.3.2 Plot of internal/probe thermocouple temperatures during the tank charging phase.
(the plots for probe thermocouple numbers 1, 2 and 3 are effectively superimposed in the above figure)

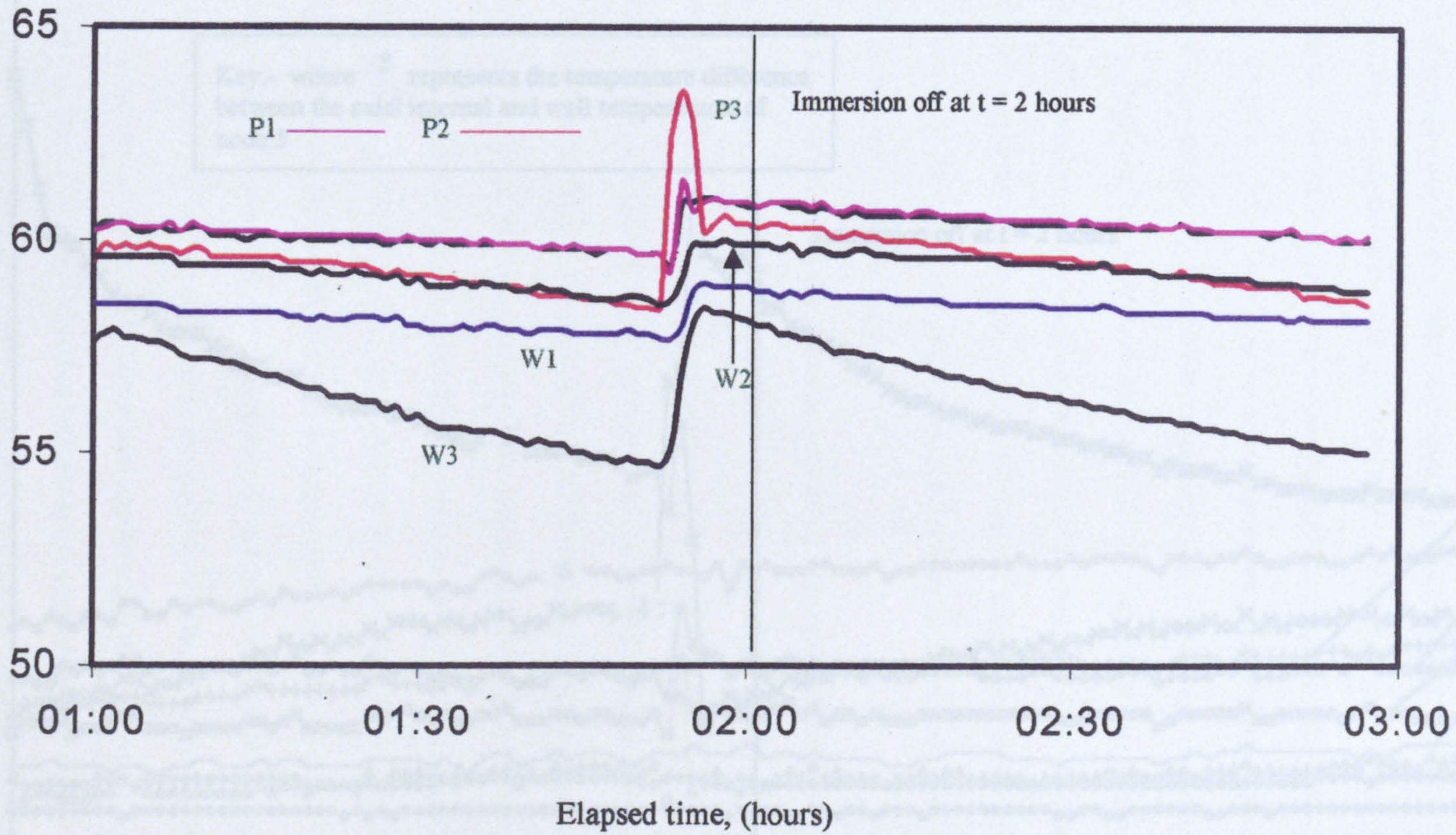

Figure 3.3.3 Plot of upper external wall and internal probe temperatures during the charging phase.

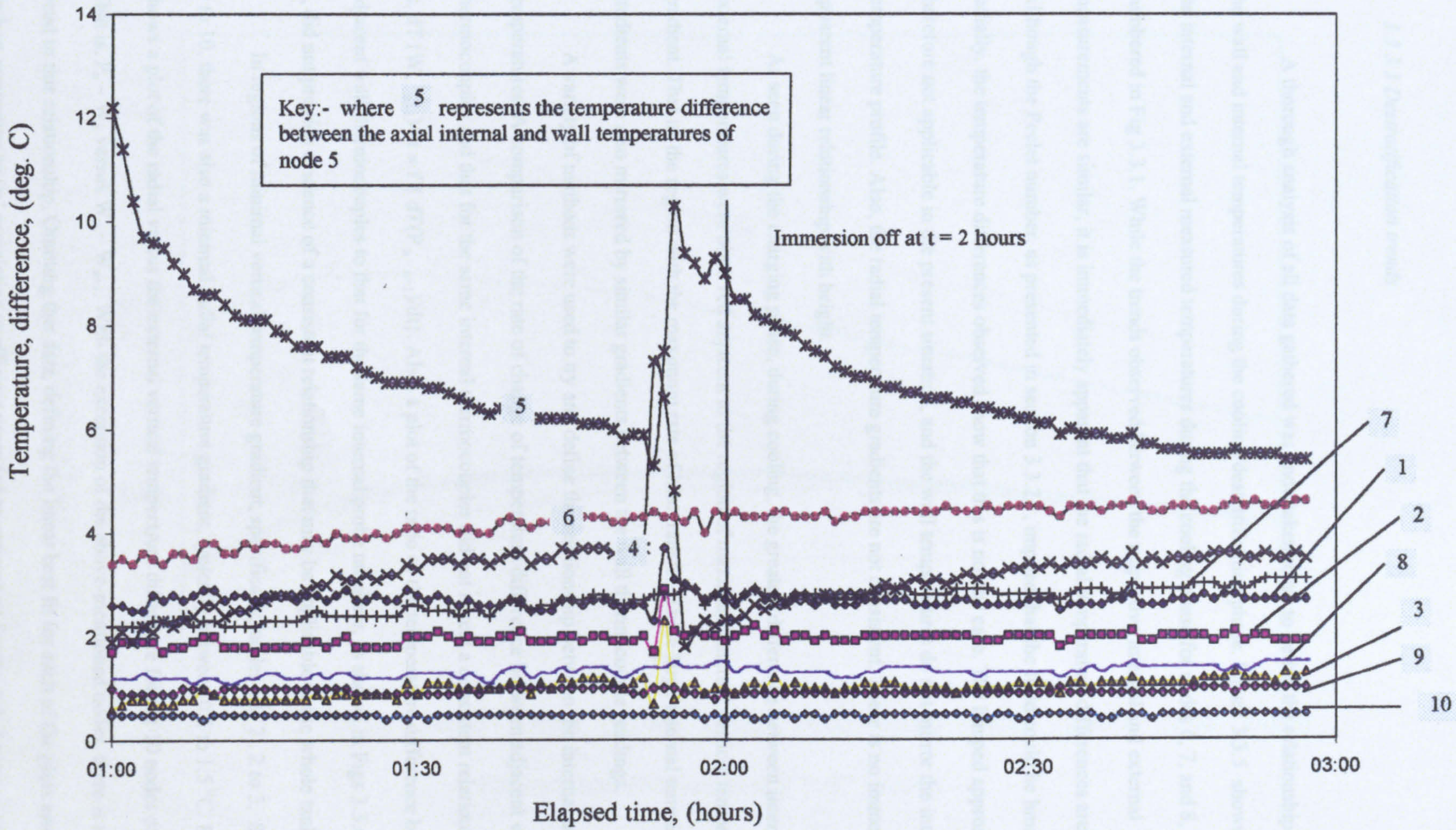
Key:- where 5 represents the temperature difference between the axial internal and wall temperatures of node 5
Immersion off at t = 2 hours
Temperature, difference, (deg. C)
Elapsed time, (hours)
14
12
10
8
6
4
2
0
01:00
01:30
02:00
02:30
03:00
5
6
4
7
1
2
8
3
9
10

3.3.3.3 Destratification trends

A thorough analysis of all data gathered was undertaken to try to define the relationship between the wall and internal temperatures during the cooling/destratification phase. Figure 3.3.5 shows a plot of the internal and external measured temperatures during the cooling phase for nodes 6, 7, and 8, as numbered in Fig 3.3.1. While the trends observed between the respective internal and external measurements are similar, it is immediately apparent that the radial temperature differences are dissimilar. Although the Peclet number, as presented in section 3.3.2.1, implied that the fluid could be lumped radially, the temperature differences observed show that this is not the case. The lumped approach is therefore not applicable in the present situation, and the wall temperatures do not mirror the internal temperature profile. Also, the radial temperature gradients are not consistent. There is no immediately apparent linear relationship with height.

As seen during the charging phase, during cooling, the greatest difference between internal and external temperatures were observed adjacent to the region of maximum internal vertical temperature gradient. That is, the region with the maximum rate of heat transfer. These large internal temperature gradients were also mirrored by similar gradients between the wall thermocouple readings.

A variety of methods were used to try and define the relationship between the internal and external temperatures. A comparison of the rate of change of temperature difference between adjacent wall thermocouples and that for the same internal thermocouples did not reveal a consistent relationship. That is, $dT(W_{n-n+1})/dt \neq f\{dT(P_{n-n+1})/dt\}$. Also, a plot of the ratio of the temperature difference between adjacent wall thermocouples to that for the same internal probe numbers, as shown in Figs 3.3.6a, b, and c, did not provide evidence of a consistent relationship that may be applicable to the whole tank.

In regions of minimal vertical temperature gradient, specifically, nodes 1 to 2 , 2 to 3, 8 to 9, and 9 to 10, there was also a minimal radial temperature gradient, typically between 0.5 to 1.5 °C. Figure 3.3.7 shows a plot of the radial versus the external vertical temperature difference for the 10 nodes of the tank. That is, $P_n - W_n$ versus $W_n - W_{n+1}$. With the exception of the above-mentioned nodes, there is an obvious trend in this relationship. Omitting this data, defining the linear best fit for each of the plots and weighting each in proportion to its' correlation coefficient provided an estimation for the radial temperature

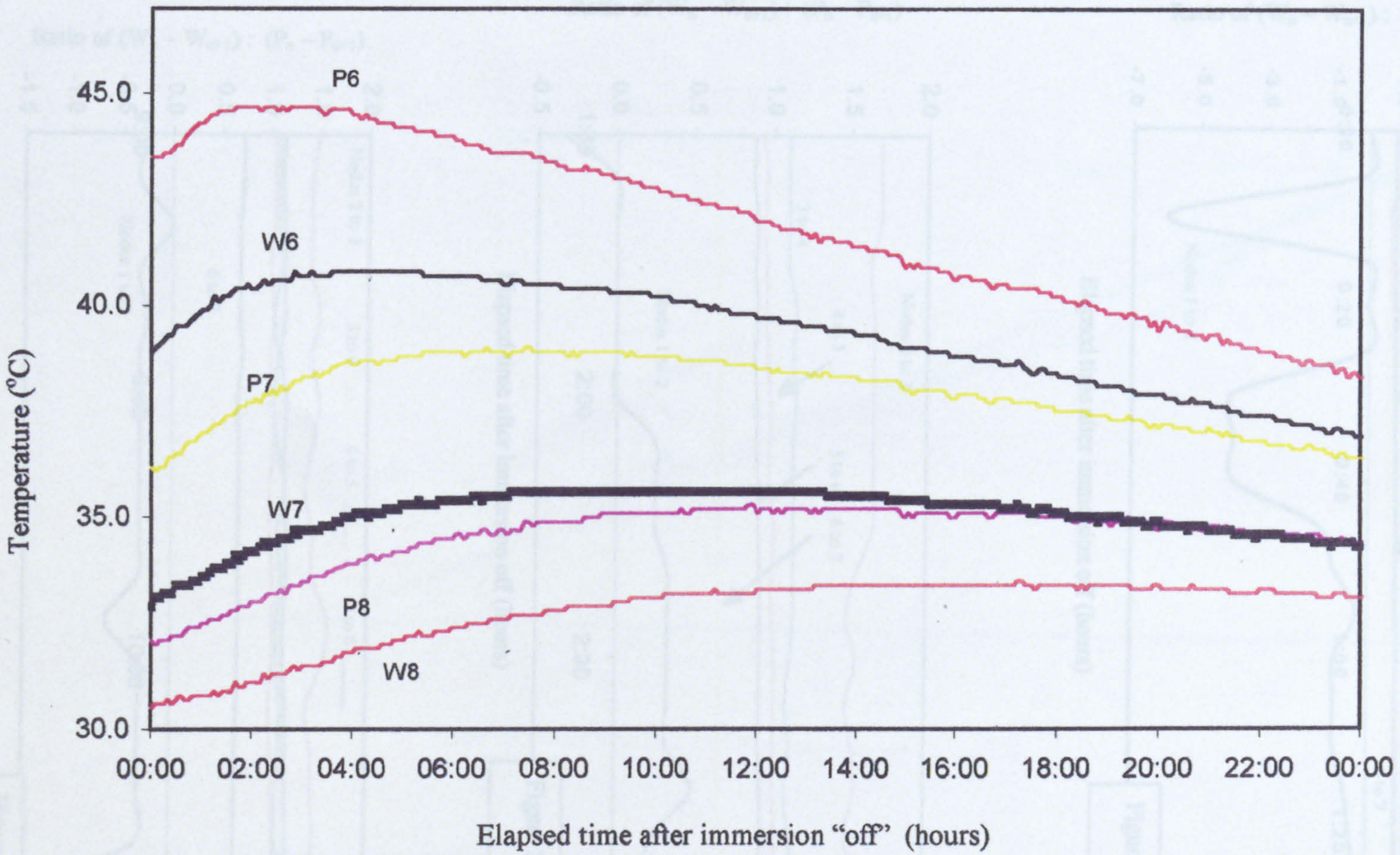

Figure 3.3.5 Internal and external measured temperatures for nodes 6, 7, and 8 during the cooling/destratification phase

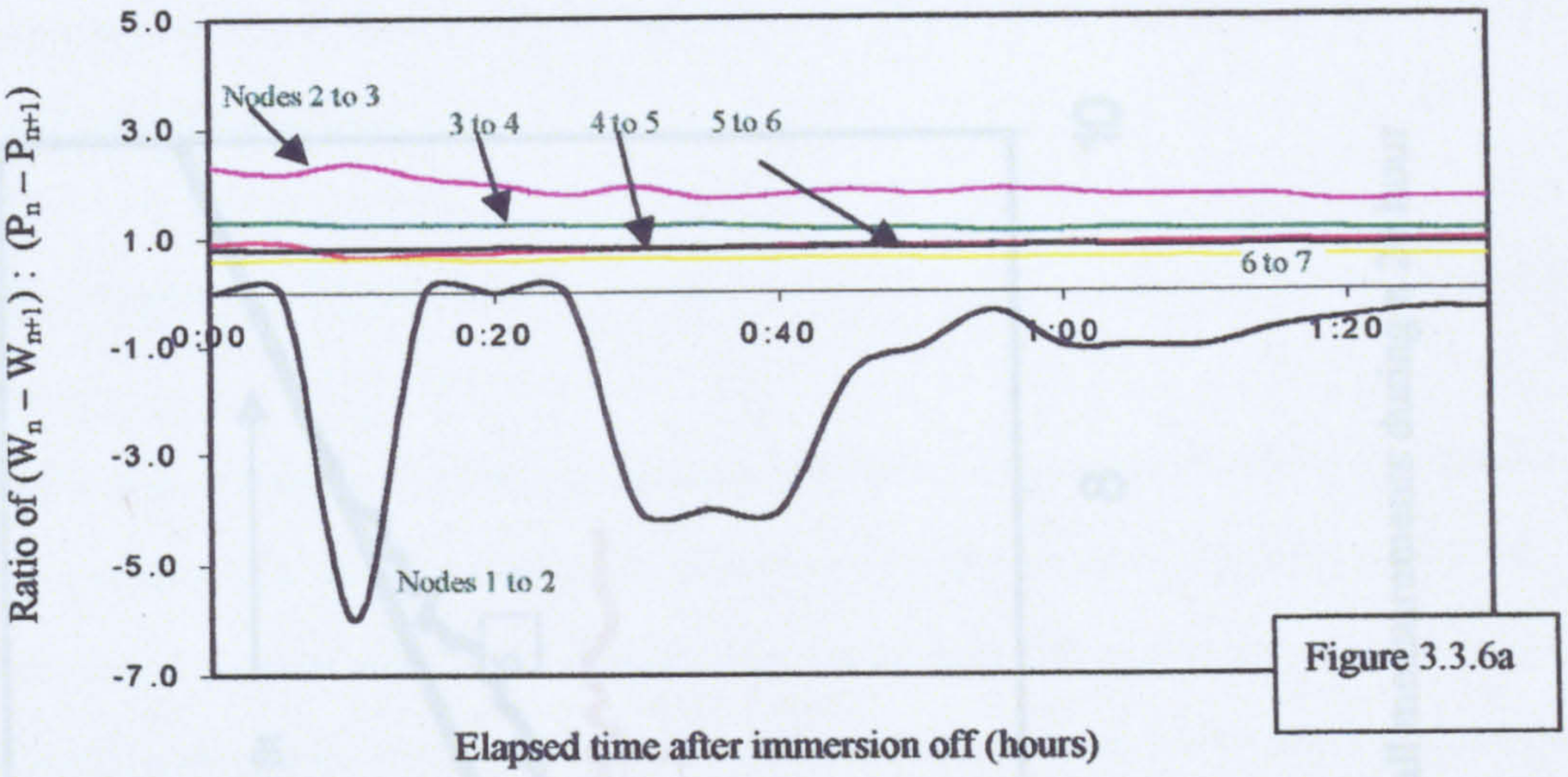

Figure 3.3.6a

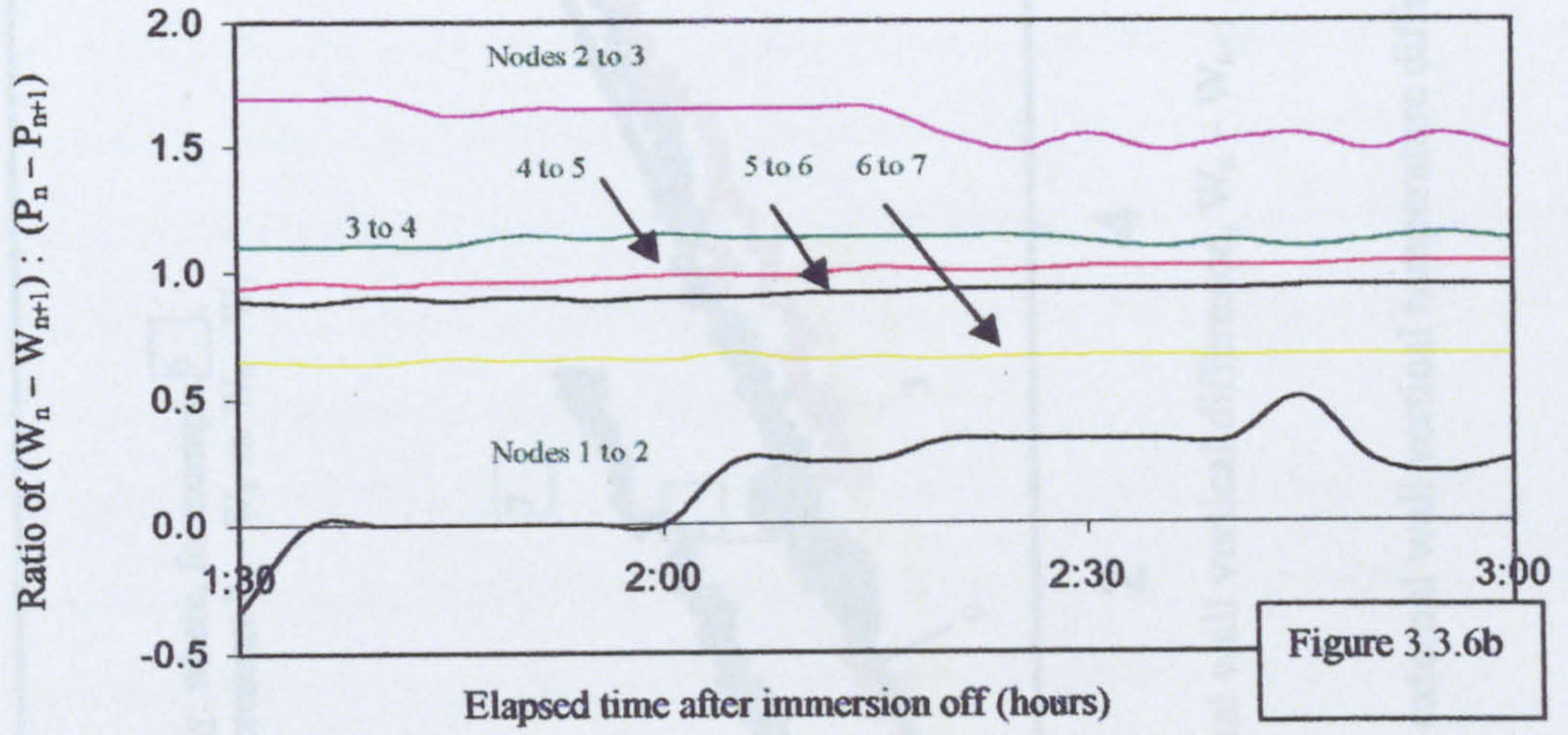

Figure 3.3.6b

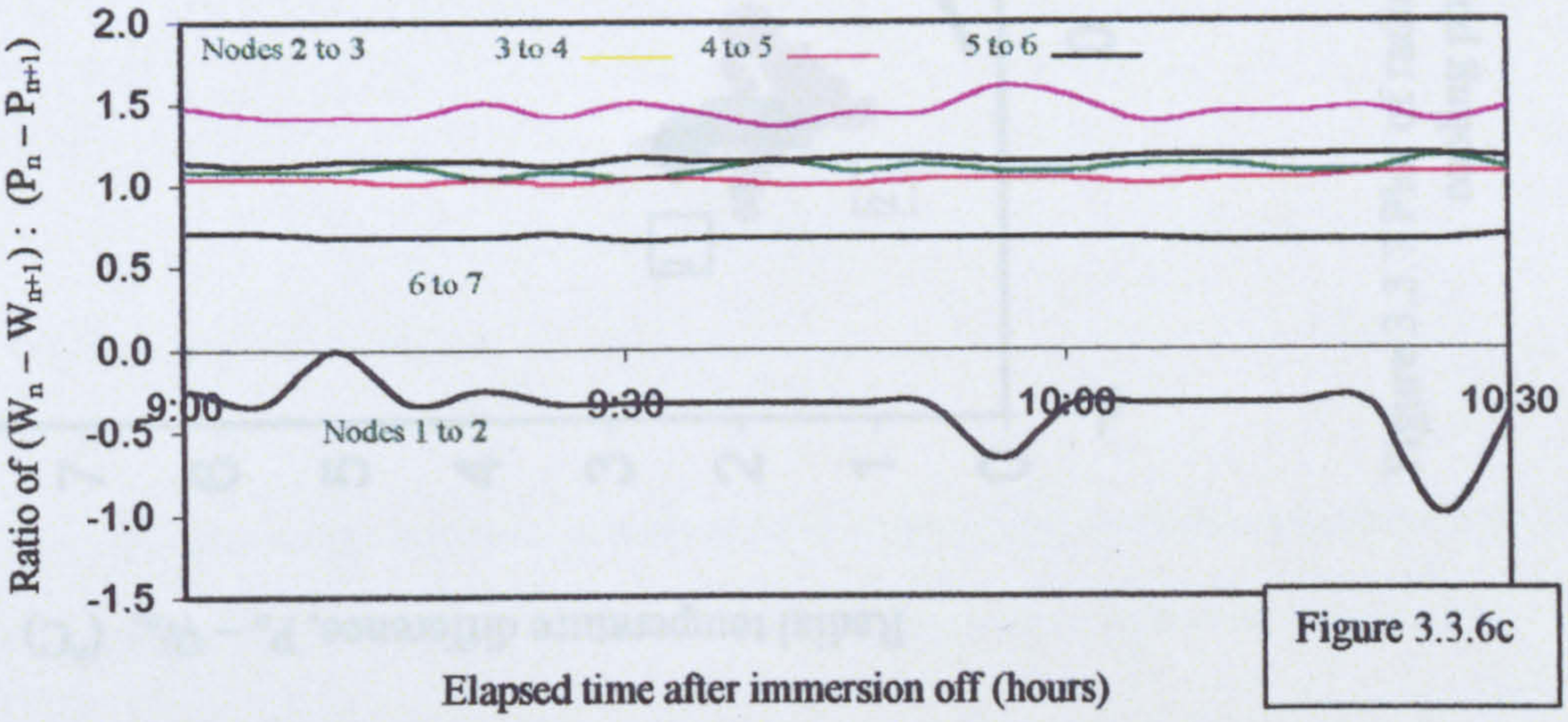

Figure 3.3.6c

Figures 3.3.6a,b, and c. Plots of the ratio of the difference in adjacent wall thermocouple temperatures to that for the same internal probe numbers

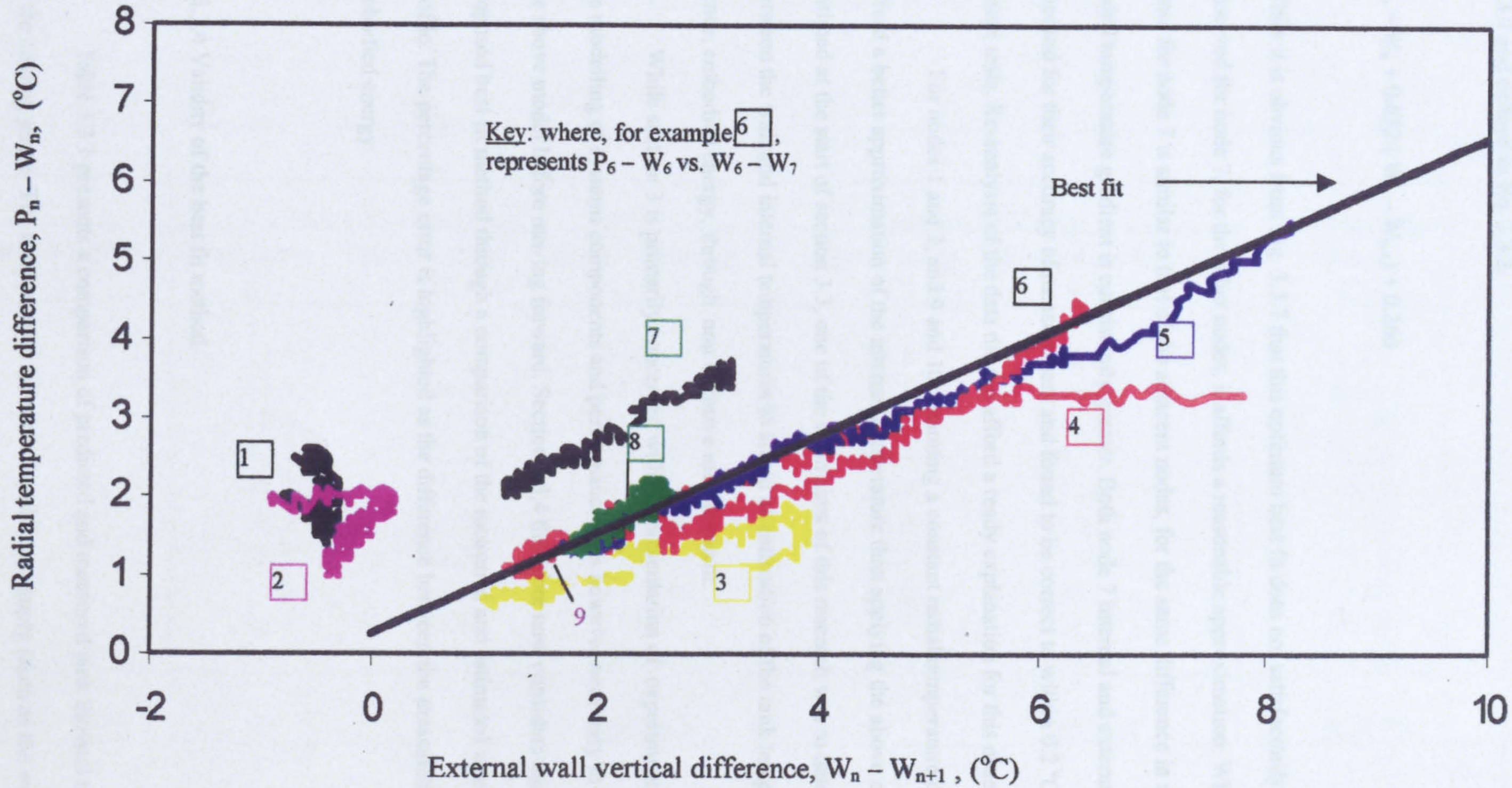

Figure 3.3.7 Plot of radial versus external wall vertical temperature difference for all measurements during a 24 hour cooling phase.

difference as a function of the respective vertical difference. This optimum best fit is highlighted in Fig 3.3.7 and defined in Eq. 3.3.2.

$$P_n = W_n + 0.632\,(W_n - W_{n-1}) + 0.260 \qquad (3.3.2)$$

While it is obvious from Fig. 3.3.7 that this optimum best fit does not satisfactorily reflect the relationship observed for node 7, for the other nodes, it affords a reasonable approximation. While the slope of the trend for node 7 is similar to that of the adjacent nodes, for the same difference in wall temperature, the radial temperature gradient is consistently greater. Both node 7 internal and external thermocouples were checked for their accuracy of measurement and found to be correct to within 0.2 °C for both, boil and freeze tests. Re-analysis of the data did not afford a ready explanation for this observed phenomenon.

For nodes 1 and 2, and 9 and 10, assuming a constant radial temperature difference of 1.5 °C will afford a better approximation of the internal temperature than applying the above optimum best fit. As outlined at the start of section 3.3, one of the main aims of this research was to determine the relationship between the wall and internal temperatures to afford an estimation of the tank temperature profile and hence, embodied energy, through non intrusive measurement.

While section 3 is primarily concerned with the presentation of experimental work, and section 4 the modelling of systems components and performance, it is however necessary to define the accuracy of the above model before moving forward. Section 3.3.4 therefore now considers the validity of the proposed best fit method through a comparison of the measured and estimated internal temperature profile. The percentage error is highlighted as the difference between the measured and estimated embodied energy.

3.3.4 Validity of the best fit method

Table 3.3.1 presents a comparison of predicted and measured tank internal temperatures at the start of the cooling phase. The temperatures for nodes 1 and 2 are simply taken as the wall temperature

Table 3.3.1 Comparison of predicted and measured internal tank temperatures and embodied energy.

T=0						
	Measured Values			Predicted Values		Percentage
Node Number	Wall temp. (°C)	Internal temp (°C)	Embodied Energy (kJ)	Internal temp (°C)	Embodied Energy (kJ)	Error (%)
1	57.3	60.1	2362.5	58.8	2331.0	1.33
2	58.0	60.1	2379.5	59.5	2364.9	0.61
3	58.7	60.1	2396.5	61.4	2427.0	-1.28
4	54.9	58.6	2267.9	60.3	2302.5	-1.53
5	47.2	52.6	1935.6	52.7	1938.2	-0.13
6	38.9	43.5	1513.6	43.0	1500.3	0.88
7	32.9	36.2	1191.0	34.7	1154.0	3.10
8	30.5	32.1	1033.3	32.0	1031.5	0.18
9	28.5	29.4	919.3	29.5	921.7	-0.26
10	26.7	27.4	827.1	27.7	834.4	-0.88
Totals			**16826.1**		**16805.4**	**0.12 %**
T= 3 hours			16668.5		16654.2	0.09
T= 7 hours			15855.9		15834.1	0.14
T=15 hours			14427.2		14443	-0.11

plus 1.5 °C, while those for nodes 9 and 10 assume a value of the wall temperature plus 1.0 °C. For nodes 3 to 8 the internal temperatures are calculated using Eq.3.3.2.

As the research has shown that there is a marked radial temperature gradient, the fluid in any node therefore cannot be assumed, as implied in section 3.3.1, to be at the one temperature. For the purpose of calculating the energy embodied within each node, the bulk fluid temperature is taken as the average of the respective wall and internal temperatures. Working to a base of 10 °C, the nodal energy is calculated on the basis of this average temperature, the nodal mass, and the specific heat capacity. The specific heat capacity is taken as having a constant value of 4.2 kJ/kg.k. As the data generated is primarily for comparison, this approximation for C_p, will not affect the percentage error. The percentage error is calculated as the measured energy less the predicted, divided by the measured. A negative error therefore represents an overestimation of nodal energy.

It can be seen that the maximum deviation is 3.10% for node 7. As the best fit line derived to define the internal/external relationship does not accurately represent the trend observed for this node, the predicted internal temperature is therefore a relatively poor approximation to the measured value. For all other nodes however, the proposed model predicts the internal temperatures and energies with a high degree of accuracy. In considering the totals presented for the measured and predicted energy, the overall error is 0.12%. A comparison of the total tank energies calculated after periods of 3, 7, and 15 hours respectively are highlighted at the foot of Table 3.3.1. As for the initial period, at T=0, there is a very close correlation between the measured and predicted energies as calculated in the manner outlined above. While the full data sets for the above periods are not presented, the percentage error for the individual nodes remained similar in magnitude to those given in Table 3.3.1. The percentage error for node 7 was observed to decrease with time. (@T=3 hours : 2.49%, @T=7 hours : 2.40%, @T 15 hours : 2.01%). As the tank cools and nodal temperatures converge, the measured temperature of node 7 will tend to conform, thus reducing model inaccuracy.

3.3.5 Conclusions

The modified Richardson number and Peclet number have been calculated for the tank operating within the FT-PV system. While the values obtained for these specific performance parameters implied that the fluid at least could be lumped radially, a comparison of internal and external temperatures has shown that this assumption is not valid in the present situation.

Through an analysis of experimental data, a simple model has been developed which enables an accurate definition of the tank internal temperature profile to be made form external measurement alone. Comparison of measured and predicted values has validated the application of this model during the cooling/destratification phase for the tank studied. The values obtained for the above-mentioned performance parameters imply that, during charging, fluid motion within the tank will be of an ideal piston form. Temperatures within the tank will not change rapidly. This model should also be applicable during charging. However, due to the rapid changes in temperature experienced within the tank during load/delivery and heating with electric immersion, the relationship between wall and internal temperatures is likely to be more complex than during destratification. The present model will therefore not be applicable during these periods. Further investigation will be required to define the internal external temperature relationships during these periods, and the required extend of their application preceding the event.

3.3.6 Errors

During cooling both the internal and external nodal temperatures change relatively slowly. Through selecting a logger interval of 5 minutes for this period it is highly unlikely that any interesting or unusual fluctuations in temperature have been missed.

Type "K" Nickel Chromium/Nickel Aluminium thermocouples were used throughout all experimental temperature measurement as their temperature range of operation was best matched to that required. The manufacturers, Radio Spares (2000), claim a virtually linear e.m.f / temperature curve for this thermocouple. (Sensitivity of 41 $\mu V/^{o}C$). As the Squirrel type data loggers are also calibrated on the

basis of a linear curve, this implies a negligible error in temperature measurement. In respect of measurement sensing and recording , for the data logger scale range of 0 – 300 °C, the displayed readings are sensitive to 0.1°C. This equates to a tolerance of +/- 0.05 °C. In calculating the embodied energy for a given node, where the fluid is at an average temperature of, for example 50°C, this tolerance implies a possible error of 0.12 % in the calculated value. For a lower bulk temperature of 20 °C and an assumed base temperature of 10 °C this equates to 0.5%. In section 3.3.4 the bulk fluid temperature is taken as the average of external wall and axial internal temperatures. This assumption implies a negligible temperature gradient across the tank thin copper wall, and a constant radial gradient. These assumptions are likely to incur a far greater error in the estimated nodal energy than that implied by logger tolerance and the thermocouple response curve.

In defining the best fit given in Eq. 3.3.2, the individual best fit lines were weighted in relation to their respective correlation coefficients. Figure 3.3.7 shows that there is obviously a linear trend for all nodes, with the exception of nodes 1, 2, 9 and 10. By weighting each nodal trend in relation to it's R^2 value, this removes some of the uncertainty from the averaged overall best fit. As can be seen from a comparison of the results given in Table 3.3.1, this averaged best fit provides an accurate estimation of the internal temperature. With the exception of node 7, the error is typically not greater than 1.5 % for any of the other nodes at any period.

3.4 PERFORMANCE OF THE NEW COLLECTOR

3.4.1 Introduction

As outlined in section 2.2 there are several ways in which the efficiency characteristic of a solar collector can be determined. An estimation of this characteristic derived from a consideration of the collector construction and material properties is given in section 4. Section 3.4 presents an experimental evaluation of the collector time constant and hydraulic characteristics. A new method for determining the collector efficiency characteristic from data collected under transient outdoor testing is outlined. Results are presented and the validity of the new method considered.

3.4.2 Determination of the collector hydraulic characteristic

A 2 m^2 prototype collector was constructed and used for all experimental work relating to the new system studied. A simple test apparatus comprising the collector, flow measurement and head gauge was assembled. The consensus of many authors, for example, Furbo and Shah (1996), Wuestling et al (1985) and Al-Ibrahim (1996), is that system thermal performance is optimised when the collector flow rate is approximately 0.2 l/min.m^2. For the above-mentioned 2 m^2 collector this implies an optimum flow rate of 0.4 l/min.m^2. The collector head loss was therefore measured for flow rates up to 1 l/min, in 0.1 l/min steps, with the procedure repeated three times to ensure a good spread of data and an accurate measure of the hydraulic characteristic. As can be seen in Fig 3.4.1 there is a linear relationship, as given in Eq 3.4.1, between flow rate and frictional pressure drop up to a flow rate of 0.8 l/min.

$$\Delta H = 0.6\,Q \qquad (3.4.1)$$

where the constant value of 0.6 has the units, m.min/l.

This linear relationship implies that the flow is laminar up to a flow rate of 0.8 l/min. Above this flow rate it will become turbulent.

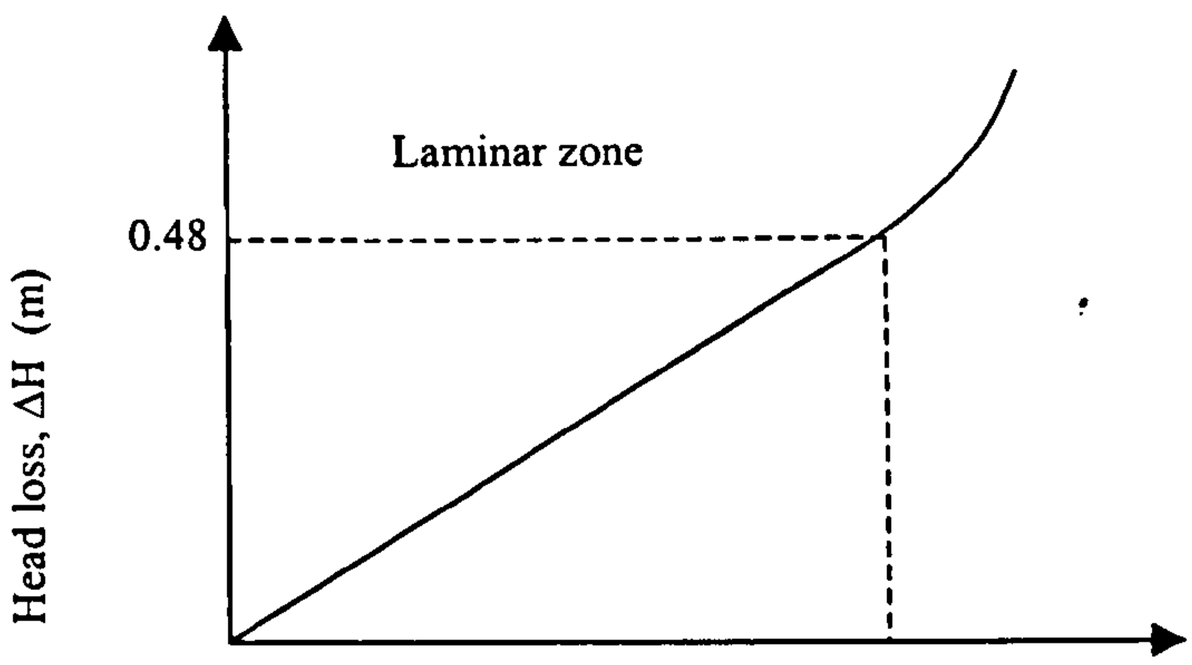

Figure 3.4.1 Form of the Flexsol collector hydraulic characteristic.

3.4.3 Measurement of the collector time constant

3.4.3.1 Introduction

The time constant of a solar collector is defined in section 2.2.4. Pierson and Padet (1990) stated that, while the time constant varied with flow rate for lower flow rates, it could be considered constant for collector mass flow rates greater than 0.06 kg/sec. Taking the density of water to be 1000 kg/m^3, this mass flow rate equates to a volume flow rate of approximately 3.6 l/min. While the above authors state that this rule cannot be applied to natural circulation systems, they do not specify the collector area considered, or the design. As such, it is not possible to define the flow rate within the collector tubes. In a header and riser type collector the flow is often distributed unevenly in the tubes, Duffie and Beckman (1991), whereas, assuming a constant fluid tube cross sectional area, it is constant for a serpentine configuration. Without clarification, the above rule cannot be applied to the present situation.

The most common method of testing used to determine the time constant of a given collector, as defined in BS 6757 (1986), Duffie and Beckman (1991), and Proctor (1984), involves subjecting the collector to a step change in irradiance and measuring the change in the collector outlet temperature. For

outdoor testing this is best achieved by shading the panel after a period of steady irradiance and monitoring the decrease in outlet temperature. An alternative method involves dark testing where the collector is subjected to a step increase in inlet temperature, and the outlet temperature again monitored.

Section 3.4 3. presents an experimental evaluation of the Flexsol collector time constant derived from the standard means of testing and compares these results to those obtained through subjecting the collector to a step change in flow rate.

3.4.3.2 Apparatus

Figure 3.4.2 shows a schematic of the test apparatus. For both test methods, the collector was set with a header tank and control valve to regulate flow rate. Flow rate was measured by means of a 1.5 litre measuring cylinder, with the flow rate taken as the average of three 30 second readings for each flow rate studied. Collector inlet and outlet temperatures, measured with K type thermocouples, and the global irradiance, being the sum of diffuse and beam irradiance, perpendicular to the collector plane, measured by a Kipp and Zonen type solarimeter, were logged at 5 second intervals using a Grant, Squirrel type data logger. (Details of the data logger and solarimeter are given in Appendix 1). Data files were downloaded into spreadsheet format. As collector cover transmissivity decreases for sun incidence angles greater than 30° to the collector plane normal, Duffie and Beckman (1991), all testing was undertaken during periods when this beam angle was less than 30°. The time available for testing was calculated from the beam angle equations presented by the above authors, and also measured by use of a solar protractor.

In the first instance, for a step change in flow, the flow rate was altered by means of the control valve only after both the collector outlet temperature and irradiance had been observed to be stable for the previous 10 minutes. The above mentioned parameters were logged and analysed. For testing by the shading method the same pre test conditions as above were observed prior to covering the collector with a thick reflective insulation board. An insulation board was used to stop the collector losing heat to the environment and so inducing error in the results.

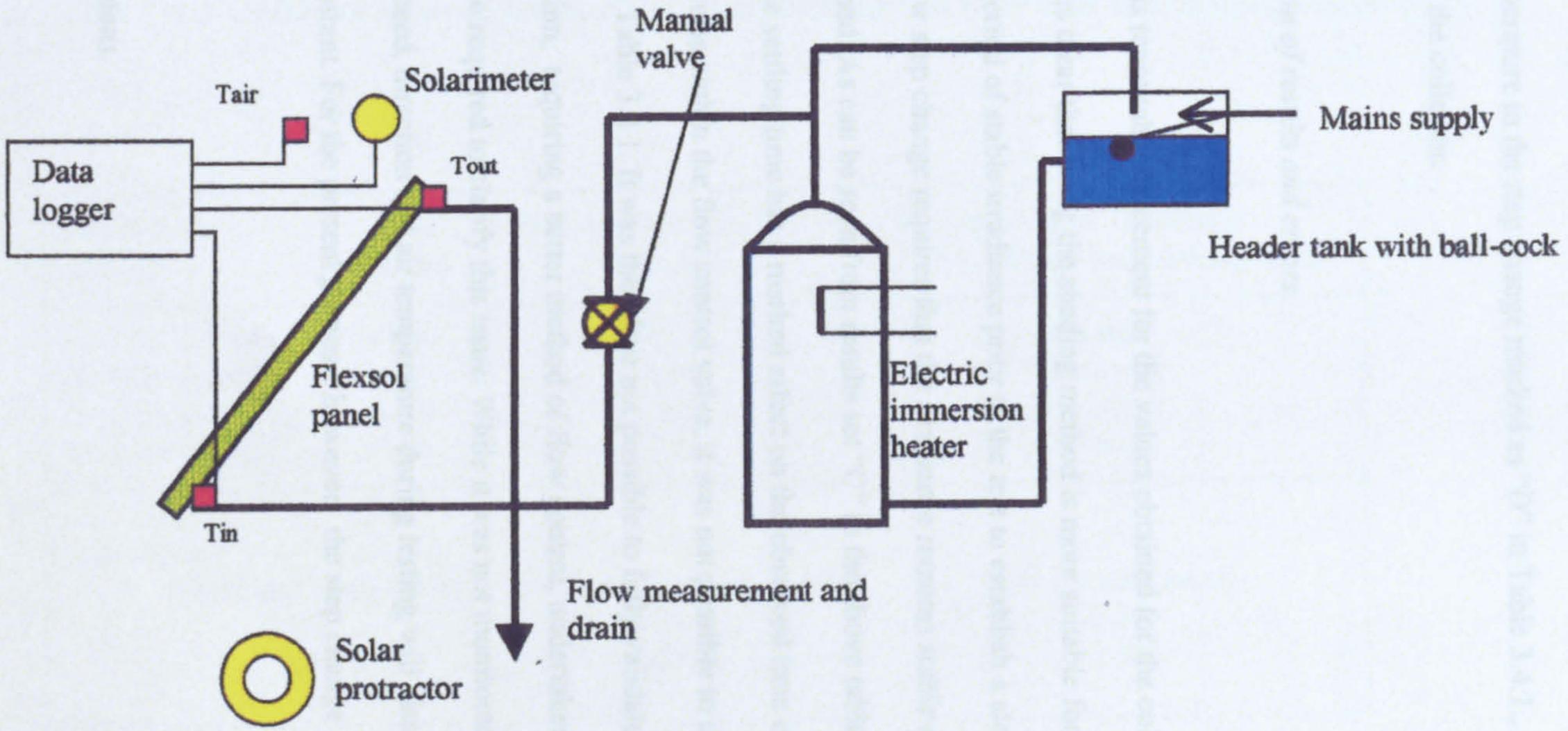

Figure 3.4.2 Collector efficiency characteristic test apparatus

3.4.3.3 Results

Table 3.4.1 shows a summary of the averaged results for the step change in flow rates examined, and the time constant as obtained by the afore-mentioned standard shading test method. The time constant is determined from a simple analysis of spreadsheet data. Fig 3.4.3a shows a plot of the response of the collector outlet temperature to the step change marked as "D" in Table 3.4.1., and Fig 3.4.3b that obtained for a full shading of the collector.

3.4.3.4 Discussion of results and errors

While there is reasonable agreement for the values obtained for the collector time constant from the two methods, it is clear that using the shading method is more suitable for outdoor testing. While both methods require a period of stable irradiance prior to the test to establish a steady collector outlet temperature, the flow step change requires that the irradiance remains stable until the new steady outlet temperature is reached. As can be seen from results set "C" in the above table, a large variance in the irradiance during the settling time has a marked effect on the observed time constant. In addition, due to the effects of hysteresis within the flow control valve, it was not possible to accurately reproduce the step changes outlined in Table 3.4.1. It was therefore not possible to fully validate these results. A more thorough investigation, requiring a better method of flow control, undertaken during conditions of stable irradiance, would be required to clarify this issue. While it was not monitored for the above investigation, a change in wind speed, direction and air temperature during testing will also have an effect on the calculated time constant. For the present purpose, however, the step change method is sufficiently accurate.

3.4.3.5 Conclusions.

Generally, the time constant is used as a measure of the required settling time and steady state measurement period for determining the efficiency characteristic of a specific collector. BS 6757 (1986) states that duration of both the afore-mentioned periods should be three times that of the time constant.

Table 3.4.1 Collector time constant for both step change in flow rate and shading methods

Step change (l/min)	τ (min)	Time to reach steady state (min)	Stability of Irradiance (% change over settling time)
A 0.58 to 0.34	4:10	9:55	1 % increase.
B 0.24 to 0.54	4:15	10:25	2.4 % decrease.
C 0.48 to 0.24	4:18	12:25	9.3 % decrease.
D 0.24 to 0.48	4:06	12:30	1.5 % increase.

From shading:

Initial irradiance (W/m^2)	Collector flow rate (l/min)	Time constant (min)
648	0.54	3:50
724	0.54	3:48

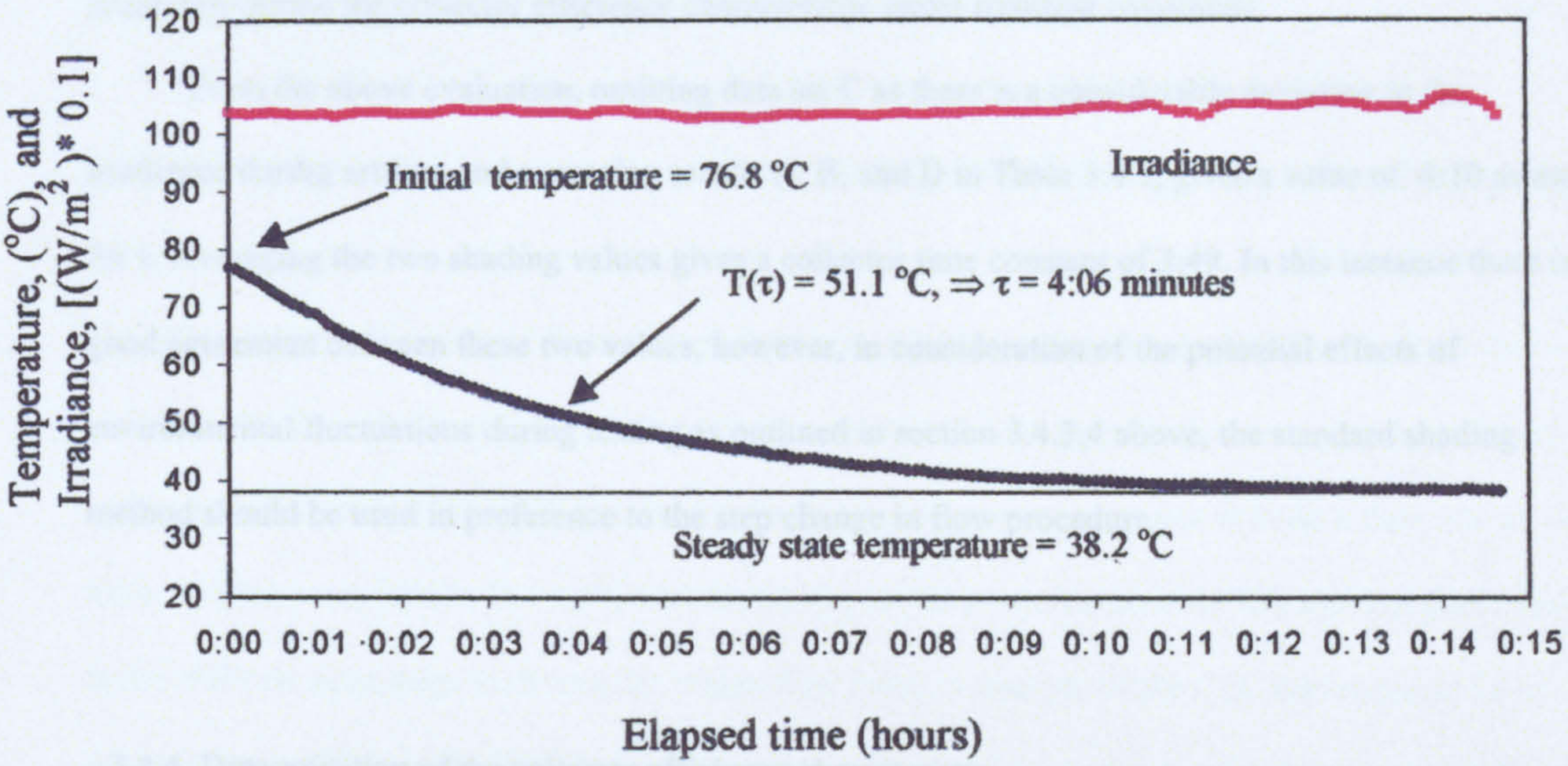

Figure 3.4.3a Response of collector outlet temperature to a step change in flow rate from 0.24 to 0.48 l/min.

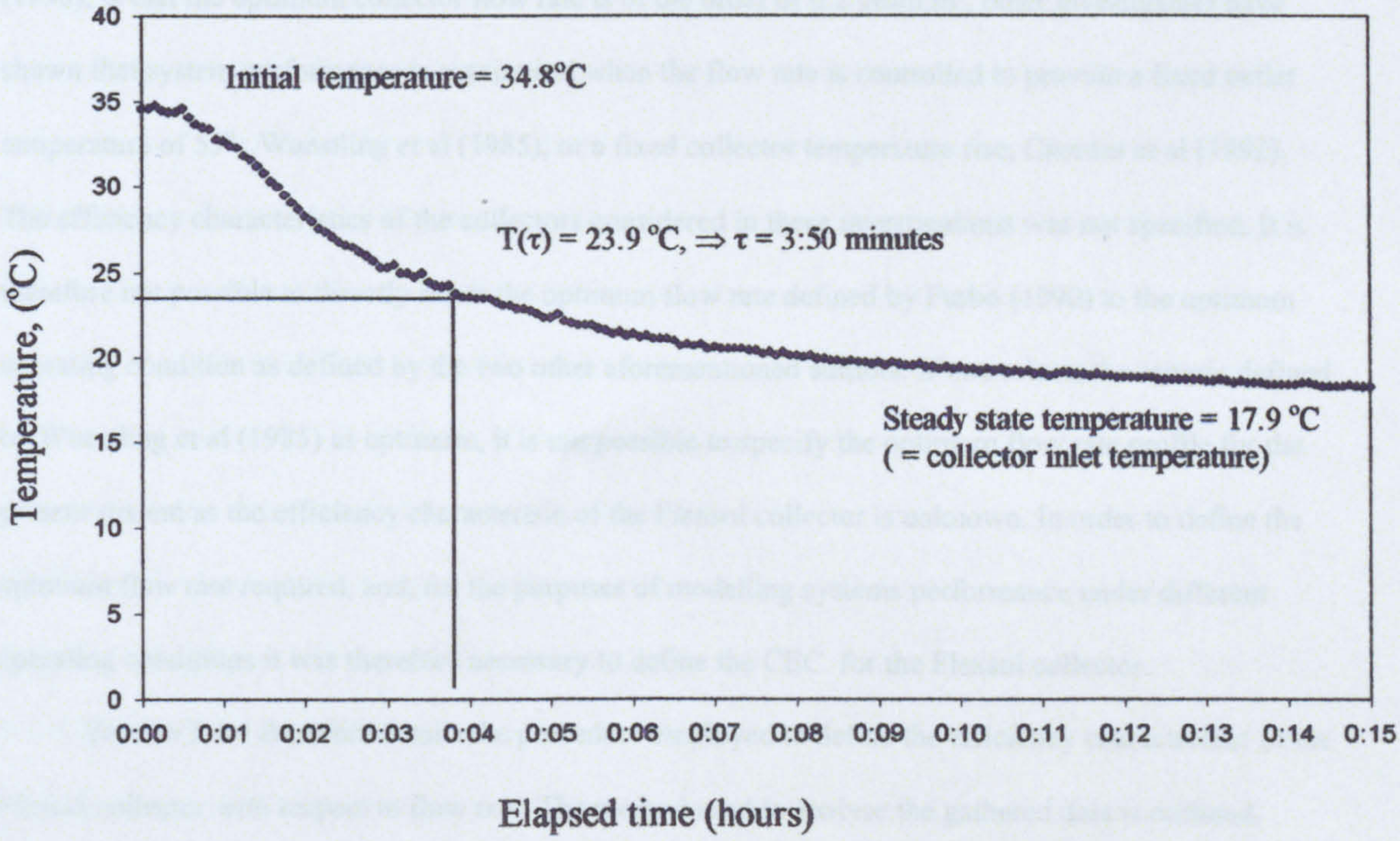

Figure 3.4.3b Response of collector outlet temperature to full shading of the collector

For a collector with a large thermal capacity, and hence time constant, such as is the case for collectors with integral storage, the defined steady state period implies that it will be more difficult to accurately define the collector efficiency characteristic under transient conditions.

From the above evaluation, omitting data set C as there is a considerable deviation in the irradiance during settling and averaging results A, B, and D in Table 3.4.1, gives a value of 4:10 minutes for τ. Averaging the two shading values gives a collector time constant of 3:49. In this instance there is good agreement between these two values, however, in consideration of the potential effects of environmental fluctuations during testing as outlined in section 3.4.3.4 above, the standard shading method should be used in preference to the step change in flow procedure.

3.4.4. Determination of the collector efficiency characteristic

3.4.4.1 Introduction

While the consensus of many of the researchers cited in section 2.3, such as, for example, Furbo (1990), is that the optimum collector flow rate is of the order of 0.2 l/min.m^2, other investigators have shown that system performance is maximised when the flow rate is controlled to provide a fixed outlet temperature of 55^o , Wuestling et al (1985), or a fixed collector temperature rise, Csordas et al (1992). The efficiency characteristics of the collectors considered in these investigations was not specified. It is therefore not possible to directly relate the optimum flow rate defined by Furbo (1990) to the optimum operating condition as defined by the two other aforementioned authors. If one selects the criteria defined by Wuestling et al (1985) as optimum, it is not possible to specify the optimum flow rate profile for the present system as the efficiency characterisic of the Flexsol collector is unknown. In order to define the optimum flow rate required, and, for the purposes of modelling systems performance under different operating conditions it was therefore necessary to define the CEC for the Flexsol collector.

Section 3.4.4 therefore details the procedure employed to define the efficiency characteristic of the Flexsol collector with respect to flow rate. The method used to analyse the gathered data is outlined.

Results are presented and the validity of this new method is considered. Both instrumentation and experimental errors are detailed.

3.4.4.2 Rationale

An initial calculation of the optimum flow / irradiance relationship, derived from a theoretical estimation of the collector efficiency characteristic (section 4.3), suggested that for a collector inlet and ambient air temperature of 15 °C, to produce the desired outlet temperature at full sun a flow rate of 0.42 l/min would be required for the $2m^2$ panel. However, for the purposes of modelling systems performance under different operating conditions, (ie higher flow rates), a measure of the CEC was required for a broader range of flow rates. Five flow rates were therefore studied to give a good indication of collector performance over this range, namely 0.15, 0.25, 0.35, 0.45, and 0.7 l/min. Again the system as shown in Fig 3.4.2 was used. In considering the results obtained from the inital time constant tests outlined in section 3.4.3, a sample interval of 20 seconds was selected for the logger.

As for the above measurement of the collector time constant, testing was resticted to periods where the beam angle of incidence was less than 30° to the collector surface normal.

For each test the flow was measured, as described above, at the start and end of each run. The collector inlet, outlet and ambient air temperature, and solarimeter readings were recorded. At the end of each testing period the logger data was downloaded and analysed. All initial runs for the five flow rates outlined above used unheated water from the hot water tank, as supplied from the mains. In order to provide a good spread of data, as specified in the standards, BS6757 (1986), a range of collector inlet temperatures, namely 20 °C, 30 °C, 40 °C, and 50°C, provided by the thermostatically controlled electric immersion heater in the supply tank, was utilised for each of the flow rates. Testing was undertaken on 3rd, 4th and 6th March 1999. As testing and data analysis progressed over this period judicious choices of flow rate and collector inlet temperature were made in respect of weather conditions to obtain data in the desired range for each of the flow rates. These choices were made to minimise testing time.

3.4.4.3. Analysis of data

Spreadsheets were designed to accept the raw data from the data loggers, and perform the required calculations and validity tests. As outlined in section 2.2.5, the methods employed by Wang et al (1987) and Amer et al (1997), require that variance limits of 20 °C/hr and 12 °C/hr respectively are imposed on the collector fluid average temperature. These limits imply that these methods are only applicable to slowly varying irradiance and are therefore not broadly suited to outdoor transient testing.

In the present case a limit was set such that only data gathered during periods when there was less than a 5% variance between the irradaince avereged over the previous 5 minutes and that for the 10 minute average was accepted. This limit was imposed to indicate that the irradiance had been reasonably steady for a 10 min period prior to a measurement point. In comparison with the temperature variance limits imposed by the above authors this limit, imposed over a shorter period with less variance in temperature acceptible, allows testing during periods of greater variation in irradaince. Where the above condition is met, this is recorded as "TRUE" in the column shown.

The efficiency of the collector is derived from a consideration of the energy balance as given in Eq. 3.4.1.

$$\eta = m_c C_p (T_o - T_i) / (G A) \qquad (3.4.1)$$

where: m_c and C_p are determined from the properties of water at the average of T_o and T_i.

While the "TRUE" result implies that the collector outlet temperature, T_o, will be reasonably stable, using instantaneous values of irradiance at this point in the above equation will not give an accurate measure of the collector efficiency values.

3.4.4.4 Selection of the optimum calculated value of collector efficiency based on the least Root Mean Square Error (RMSE)

In consideration of the results obtained from the initial time constant tests, it was considered appropriate to look at the efficiency characteristic in terms of 6 averaged values for irradiance and air temperature: namely averaged over the previous 1, 5, 8,10,12 and 15 minutes. Table 3.4.2 gives the results of this analysis, and considers the efficiency characteristic in relation to the correlation coefficient/ RMSE obtained for a best fit analysis of collector efficiency generated from the above mentioned averaging times.

The correlation coefficient is found to be greatest for the plots generated from data points obtained when using 12-minute averages for irradiance and air temperature. These plots therefore represent the most accurate estimation of the collector efficiency characteristic for the given flow. Figures 3.4.4.a, 3.4.4.b and 3.4.4.c show the data, best fit lines, and correlation coefficients obtained for 5, 12 and 15 minute averaged irradiance/air temperature respectively for a flow rate of 0.7 l/min. The increased spread in the data obtained using the 5 and 15-minute averaged values is immediately apparent.

3.4.4.5 Discussion of results.

Figure 3.4.5 shows the plot of the best-fit lines obtained using the 12 minute average values for three of the above flow rates, namely; 0.7, 0.35, and 0.15 l/min. (It should be noted that the legend key is to provide ease of identification and does not represent actual data points gathered.)

It can be seen that both the intercept and the slope of the characteristic curves increases as the flow rate increases. This is probably because both these parameters are a function of F_R, and F_R is a function of the fluid side surface heat transfer coefficient, Hausner and Fechner (1998). During periods of high irradaince, the characteristic will tend towards having a higher maximum efficiency, and a steeper slope.

With regard to the intended mode of system operation, as the CEC varies with flow rate, to maintain a steady outlet temperature, this implies that the optimum flow profile, as shown by Al-Ibrahim et al (1996), will be non-linear.

Table 3.4.2 Collector efficiency and root mean squre error for different periods of averaged irradiance

Flow (l/min)	I av 1min (R^2)	I av 5min (R^2)	I av 8 min (R^2)	I av 10 min (R^2)	I av 12 min (R^2)	I av 15 min (R^2)
0.70	$\eta = 0.656 - 3.69X$ (0.644)	$\eta = 0.653 - 3.60X$ (0.862)	$\eta = 0.648 - 3.47X$ (0.886)	$\eta = 0.656 - 3.59X$ (0.914)	$\eta = 0.665 - 3.75X$ (0.936)	$\eta = 0.689 - 4.10X$ (0.914)
0.45	$\eta = 0.575 - 2.87X$ (0.860)	$\eta = 0.583 - 3.52X$ (0.870)	$\eta = 0.612 - 3.14X$ (0.894)	$\eta = 0.641 - 3.24X$ (0.915)	$\eta = 0.626 - 3.20X$ (0.930)	$\eta = 0.596 - 2.85X$ (0.926)
0.35	$\eta = 0.678 - 4.32X$ (0.872)	$\eta = 0.638 - 3.44X$ (0.850)	$\eta = 0.637 - 3.41X$ (0.857)	$\eta = 0.626 - 3.13X$ (0.895)	$\eta = 0.618 - 2.94X$ (0.909)	$\eta = 0.603 - 2.49X$ (0.837)
0.25	$\eta = 0.516 - 0.97X$ (0.208)	$\eta = 0.557 - 1.85X$ (0.491)	$\eta = 0.556 - 1.85X$ (0.534)	$\eta = 0.566 - 1.99X$ (0.624)	$\eta = 0.590 - 2.41X$ (0.764)	$\eta = 0.633 - 2.8X$ (0.7861)
0.15	$\eta = 0.546 - 1.53X$ (0.495)	$\eta = 0.536 - 1.35X$ (0.635)	$\eta = 0.532 - 1.34X$ (0.637)	$\eta = 0.535 - 1.36X$ (0.644)	$\eta = 0.532 - 1.44X$ (0.673)	$\eta = 0.255 - 1.29X$ (0.628)

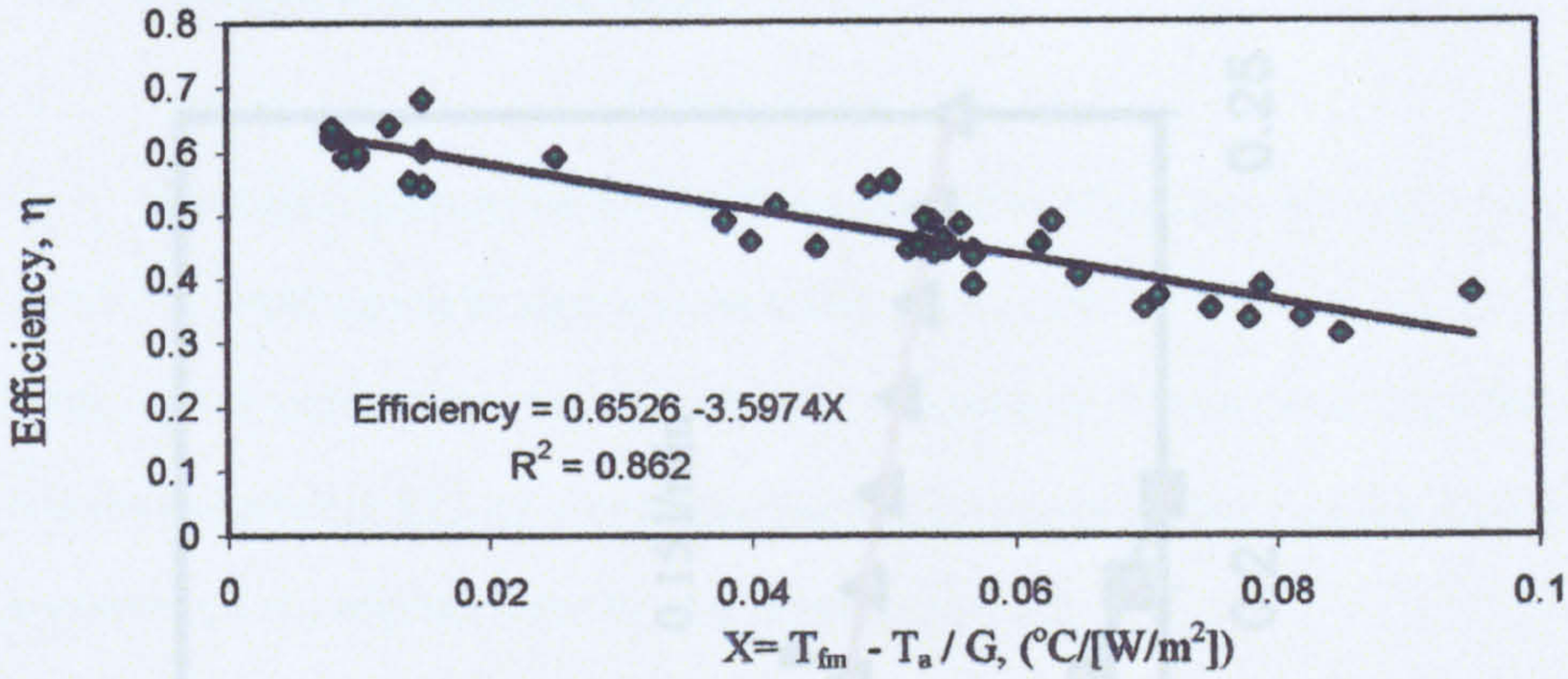

Figure 3.4.4.a Plot of efficiency characteristic for a collector flow rate of 0.7 l/min using 5 minute averaged irradiance values

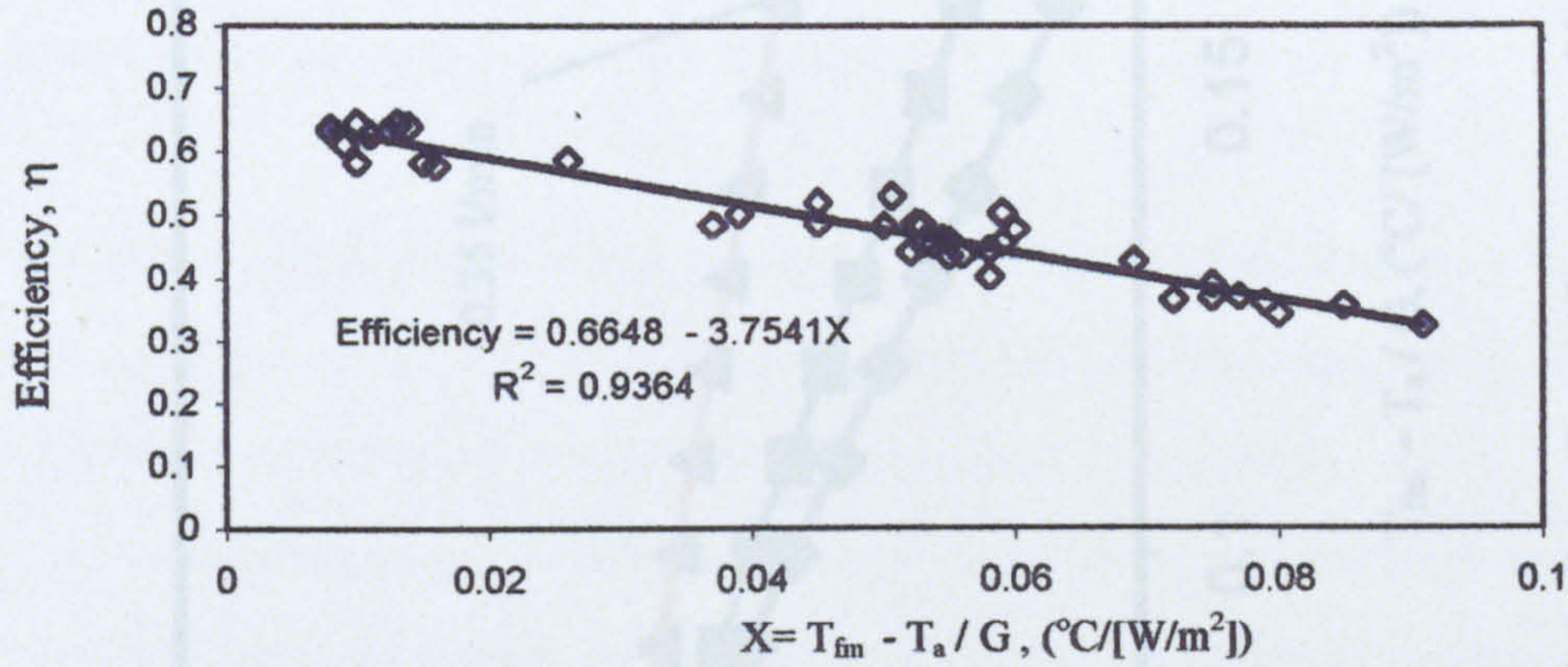

Figure 3.4.4.b Plot of efficiency characteristic for a collector flow rate of 0.7 l/min using 12 minute averaged irradiance values

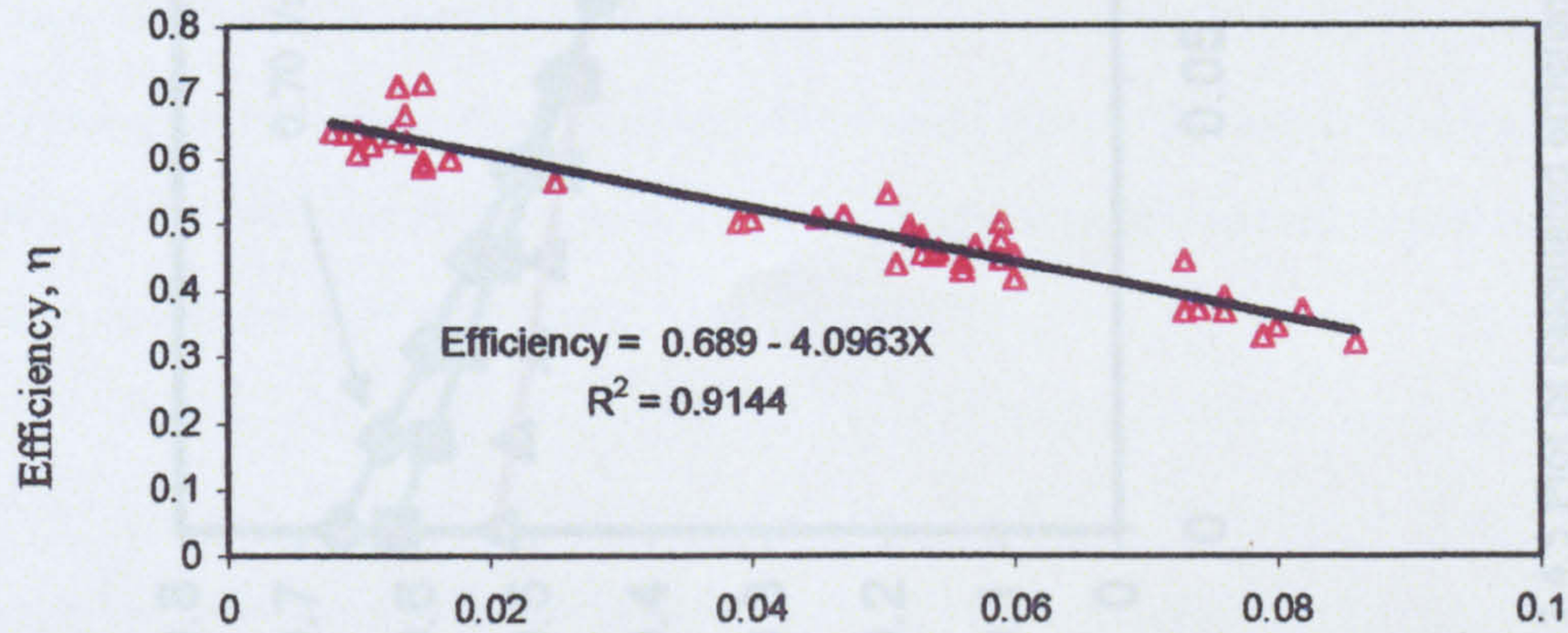

Figure 3.4.4.c Plot of efficiency characteristic for a collector flow rate of 0.7 l/min using 15 minute averaged irradiance values.

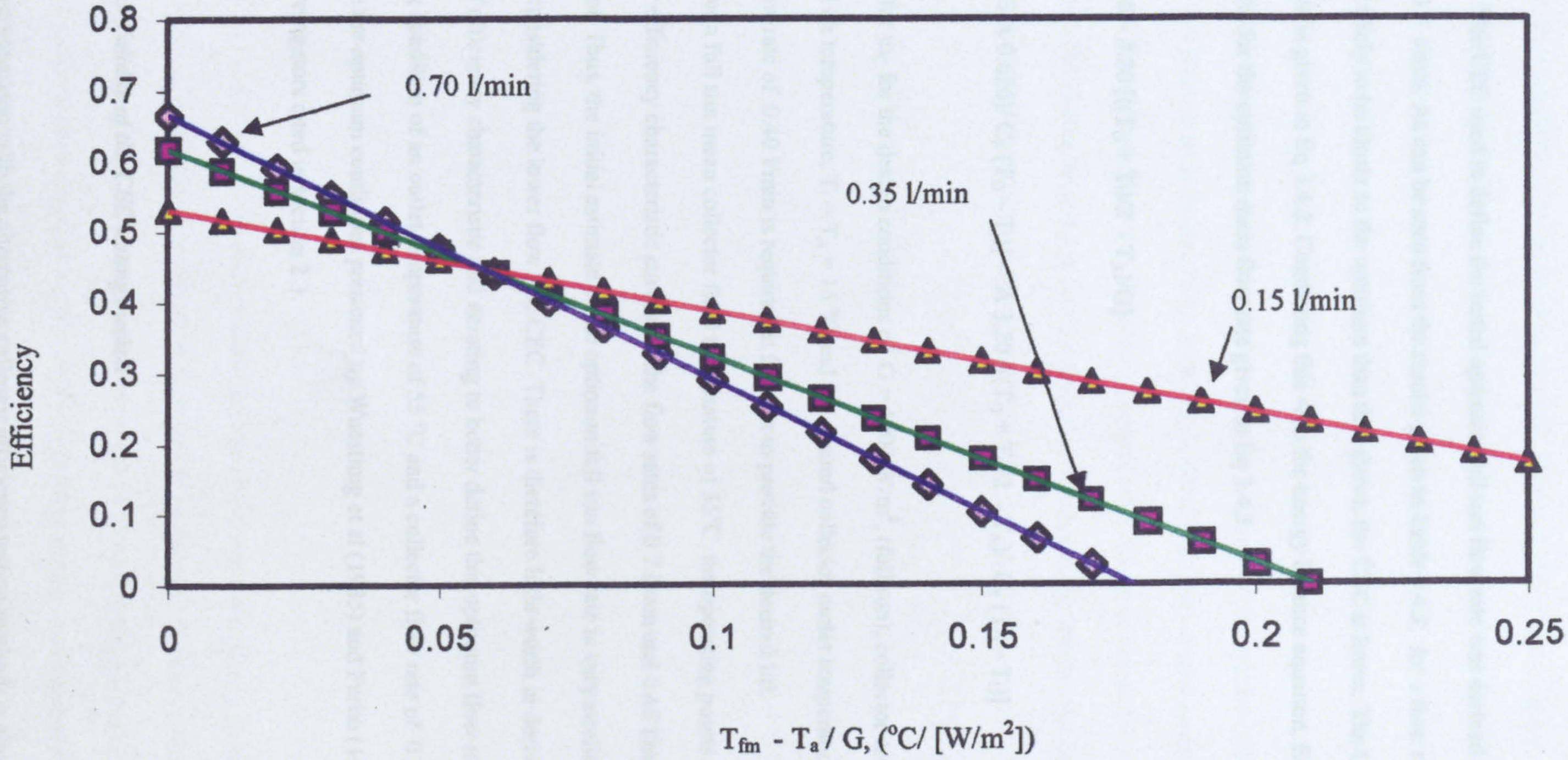

Figure 3.4.5 Plot of calculated efficiency characteristic for collector flow rates of 0.7 l/min, 0.35 l/min, and 0.15 l/min.

3.4.4.6 Optimum maximum flow rate.

The CEC used to define the initial optimum full sun flow rate was derived for a collector flow rate of 0.7 l/min. As can be seen from the results given in Table 3.4.2, for a flow rate of 0.45 l/min, which is likely to be closer to the optimum than that above, the CEC is lower. The CEC for a flow rate of 0.45 l/min is given in Eq 3.4.2. Combining this with the energy balance equation, Eq. 3.4.1, yields the expression for the optimum mass flow rate given in Eq 3.4.3.

$$\eta = 0.626 - 3.20\,[((T_O + T_I)/2 - T_A)/G] \tag{3.4.2}$$

$$m_C = [\,(G\,A\,0.626)/\,C_P\,(T_O - T_I)] - A\,3.20\,[((T_O + T_I)/2 - T_A)/\,C_P\,(T_O - T_I)] \tag{3.4.3}$$

Solving for m_C for the design conditions of $G = 1000$ W/m^2, (full sun), collector area $A = 2$ m^2, collector inlet and air temperature, $T_I = T_A = 15$ °C and the desired collector outlet temperature $T_O = 55$ °C, implies that a flow rate of 0.40 l/min is required at full sun to provide the desired lift.

For a full sun mean collector fluid temperature of 35°C the operating points on the respective collector efficiency characteristic curves for the flow rates of 0.7 l/min and 0.45 l/min are almost coincident. Thus, the initial estimate of the optimum full sun flow rate is very similar to that obtained through considering the lower flow rate CEC. There is therefore little worth in deriving interpolated values of efficiency characteristic and iterating to better define this optimum flow rate. The desired operating condition of an outlet temperature of 55 °C and a collector flow rate of 0.2 l/min.m^2 agree very well with the optimum conditions presented by Wuestling et al (1985) and Furbo (1990) and many of the other investigators cited in section 2.3.

3.4.4.7 Validity of the CEC testing method

In comparison with the alternative collector efficiency testing methods outlined in section 2.3 the above method, through utilising averaged values of irradiance and RMSE error analysis allows a greater

variance in irradiance than others specified during testing. This factor, in conjunction with the judicious choice of flow rate reduces the required testing time. However, this method does not consider the effect of wind speed on the CEC suggesting that it may not be so broadly applicable in different weather conditions. In addition, the apparatus and computations required are simpler than that specified for other methods of testing. The degree of applicability to a wider range of weather conditions has not been considered.

Only a comparison of the characteristic equations derived by this method with those obtained by testing in accordance with the standards, for example BS 6757 (1986), would establish the degree of accuracy of this method. However, the good agreement between the calculated and measured CEC's for a flow rate of 0.7 l/min, as given in Eqs. 3.4.4 and 3.4.5 respectively, implies that the method of testing employed does yield an accurate estimation of the CEC.

$$\eta = 0.667 - 3.70\,[\,(T_I + T_O)/2 - T_a)/\,G] \qquad (3.4.4)$$

$$\eta = 0.665 - 3.75\,[\,(T_I + T_O)/2 - T_a)/\,G] \qquad (3.4.5)$$

As can be seen from the figures given in Table 3.4.2, the correlation coefficient decreases as the flow rate decreases. This implies that there is a greater error in the CEC calculated for the lower flow rates.

3.4.4.8 Errors

By its very nature, under outdoor conditions there is never a completely steady state operating condition for a solar collector from which to draw data to profile the efficiency characteristic. Among other factors, the suns angle of incidence, air temperature and wind speed are continually varying. The analysis and criteria used for defining the validity of data points were designed to allow a large enough sample of data to be used in determining the characteristic while not allowing too loose an approximation

to steady state points. The high values obtained for the correlation coefficients reflect the accuracy obtained in using this method.

The data logger temperature scale, fixed at 0.1 °C increments, allows for an error of + / - 0.05 °C. Where there was only a very small temperature lift recorded between panel inlet and outlet, typically for the greater flow rates, the instrumentation tolerance can account for up to an error of 1 °C in the calculated value for $(T_O + T_I)/2 - T_A$. For a lift of 2°C an error of + / - 5 % may be incurred in the calculated efficiency. Of all data points used in all plots, only 25% have a lift of less than 3 °C, implying that only 25% of points have a possible error of 3.3% or greater. For all calculations, the mean fluid temperature is taken as the average of inlet and outlet temperatures. For a small lift, this may not be too inaccurate a method of estimation, but where the lift is greater, the average may be considerably greater than that calculated as the true temperature profile along the length of absorber pipe is typically convex. Without extensive study it is not possible to quantify this error, but suffice to say here that this will tend to give values that underestimate panel performance.

For each averaged data set, for the five flows studied, the correlation coefficient R^2 is seen to be reasonably constant with the exception of the lowest flow in each set. Many of the data used to generate these plots and best fit lines were taken from points with a very high outlet temperature. It was noted that when the outlet temperature exceeded about 75 °C the flow became very unstable due to dissolved air coming out of solution and causing slight resistance in the narrow guage connecting pipe. In addition, the measuring cylinder used to determine the flow rate had a 25 ml graduated scale. The scale was, however, as broadly spaced as to visually estimate the volume to within at least +/- 5ml. For lower collector flow rates, such as 0.15 l/min, taken as the average of 3 30 second measures, this equates to a potential error of 6.7%. At higher flow rates, for example 0.7 l/min, this is reduced to 1.4%. This potential increase in measurement error for the lower flow rates may, at least in part, account for the lower correlation coefficients observed in Table 3.4.2.

3.5 OPTIMISING THE COLLECTOR FLOW RATE PROFILE.

3.5.1 Introduction.

Al-Ibrahim et al (1996), through an analysis of PV- SDHW systems, stated that the flow rate profile required to optimise system thermal performance could be defined by a second order polynomial fit, as shown in Fig 3.5.1. While Wuestling et al (1985) and Csordas et al (1992) specified the optimum operating condition, (section 2.3.3.2), the specific design criteria employed by Al Ibrahim et al (1996) in the derivation of their optimum profile were not specified. This optimum profile was used by the above authors to define the characteristics of appropriate system components to best meet the optimum profile. These analyses were based on the assumption that the pump, operating in a system comprising a defined 6.5 m^2 collector, would operate at near optimum efficiency across the range of flows.

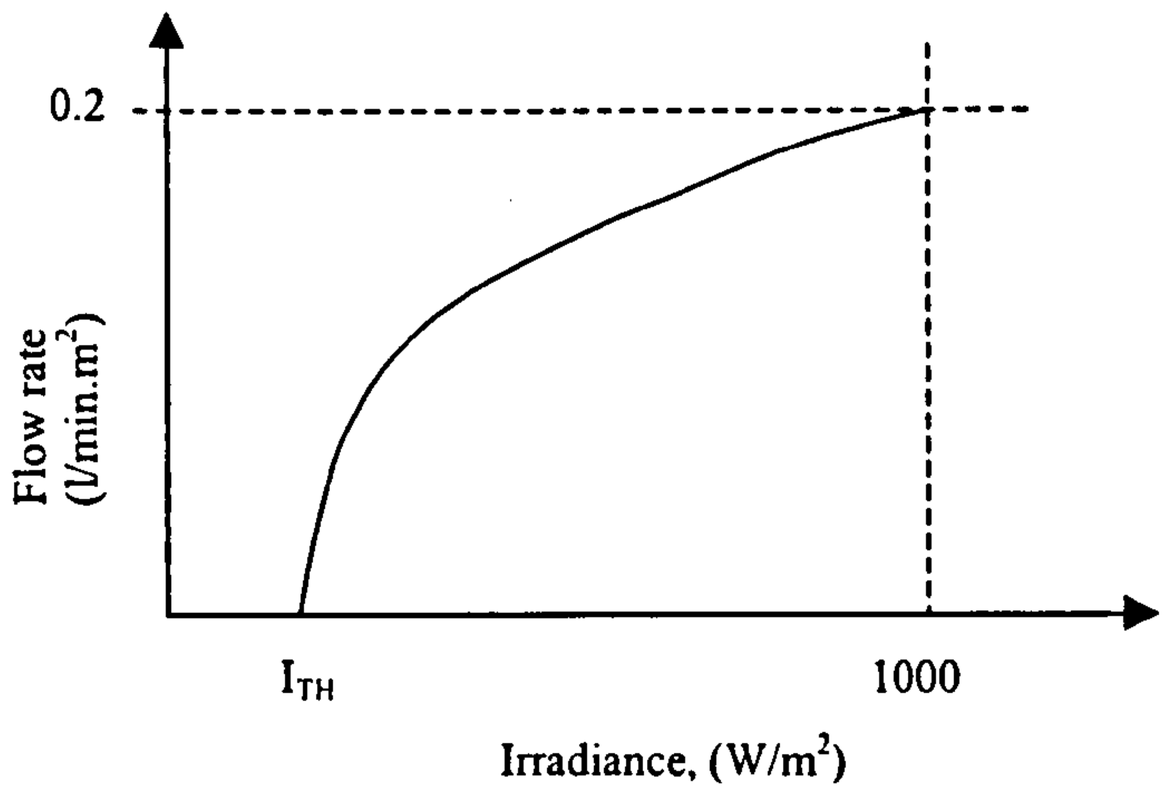

Figure 3.5.1 Optimum flow rate profile for a variable low flow solar water heating system.

(from Al-Ibrahim (1996))

From the above figure it can be seen that, ideally, the pump should cut in at a threshold irradiance, I_{TH}, below which there is no worthwhile heat to be gained, with the flow rate rising to a maximum at full sun. It has been shown in section 3.4 that, for the Flexsol collector, the calculated optimum maximum flow rate which will provide the design temperature rise at full sun is 0.40 l/min. While a fuller analysis of the

optimum flow rate profile for the present system is presented in section 4, an approximation for the ideal threshold irradiance can be obtained through considering the CEC for the lowest flow rate studied, namely, 0.15 l/min. Equation 3.5.1 gives the CEC for this flow rate.

$$\eta = 0.532 - 1.44\,[((T_o + T_i)/2 - T_A)/G] \qquad . (3.5.1)$$

Assuming an efficiency of 0 and substituting for the design temperature criteria yields a value of 54 W/m^2 for the ideal threhold irradiance.

Al-Ibrahim et al (1996 and 1998) defined the pump motor electrical characteristics required to achieve their optimum flow profile. In practice it is not always possible to buy off the shelf components that match the criteria for different systems. Through oversizing the PV module and pump and employing a suitable method of control, such as micro-processor based pulse width modulation, it would be possible to establish a flow profile that would produce the optimum operating conditions, namely the FCTR and SCOT strategies, as specified by Wuestling et al (1985) and Csordas et al (1992) for the present system. However, in respect of minimising component and control costs, the present work considers the potential of selecting and matching "off the shelf" optimum sized components, and the potential of simpler methods of control.

Section 3.5 therefore details the design process and the subsequent selection, configuration, and matching of system components through an analysis of their characteristics and interactions. Two simple methods of controlling the system flow rate are presented; namely physically shading the PV module to alter its electrical characteristic, and including additional electrical resistance in the electrical circuit. Through an experimental analysis, the suitability of each of these methods is considered in relation to its ability to meet the desired operating condition.

While section 4 focuses on system modelling, section 3.5 is primarily concerned with presenting the experimental work undertaken. However, in order to define certain parameters, such as the optimum full sun flow rate and the required degree of control, it is necessary to consider the modelling of components characteristics and interactions within the context of the experimental work.

3.5.2 Analysis of system component characteristics.

3.5.2.1 Hydraulic system characteristics

As for the hydraulic characteristic of the Flexsol collectof on its own, the hydraulic characteristic of the fluid system, namely the collector, associated pipe-work, fittings, and tank, was found to be linear up to a flow rate of 0.8 l/min. Equation 3.5.2 gives the flow versus head relationship for the hydraulic system, up to a flow of 0.8 l/min.

$$\Delta H = 0.9\ Q \qquad (3.5.2)$$

: where the constant value of 0.9 has the units (m min/litre).

3.5.2.2 Selection of a suitable PV module/pump pair, and module configuration

Equation 3.5.3 defines the fluid output power in terms of the required head and flow rate.

$$F_{PI} = \rho\ g\ H\ Q \qquad (3.5.3)$$

Operating at the design maximum flow rate of 0.40 l/min implies that the maximum fluid power input will be of the order of 0.024 Watts. To obtain an initial estimation of the required electrical input at this operating point, if one assumes a combined pump motor and hydraulic efficiency of between 5% and 10%, this implies that an input of between 4.8 W and 2.4 W is required.

Polycrystalline PV modules generally have a higher efficiency, and degrade more slowly than their amorphous counterparts. For initial testing they were therefore considered in preference to amorphous modules. One of the smaller commercially available polycrystalline modules is the 5 W BP module, BP (1999). On the basis of this modules specified electrical characteristics, (Fig 3.5.2) a selection of readily available pumps were tested for their suitability. While it was immediately apparent that several of these were quite unsuitable, a positive displacement diaphragm type met the desired

criteria. On testing, over a range of operating conditions, it was found to have the electrical characteristics given in Eqs. 3.5.4.a and 3.5.4.b.

For I_A < 0.1 Amps, $V = (6.76 * I_A) + 4.72$ (3.5.4 a)

For $I_A \geq 0.1$ Amps, $V = 53.5 * I_A$ (3.5.4 b)

While the pump started to draw current at 4.72 volts, no significant flow was realised until the applied voltage reached 4.87 V, at which point the pump drew a current of 0.022 A. For the present hydraulic circuit this applied voltage produced a flow rate of 0.02 litres/min.

Generally, pump electrical characteristics vary depending on the hydraulic system in which they are operating. However, the present pump, Charles Austen Model LD2, for the range of operating conditions studied, was found to have the consistent V-I characteristic outlined in the above equations.

The pump electrical load line as defined by Eqs. 3.5.4 a and 3.5.4 b, superimposed on the PV performance curve chart, as shown in Fig. 3.5.2., is therefore seen to have two slopes.

As can be seen from Fig 3.5.2 the chosen module is specified as having a full sun short circuit current of 0.3 Amps and an open circuit voltage of 21 Volts. For full sun, maximum power is generated at 0.29 A and 17 Volts.

Due to ease of rewiring, among other possible configurations, the 5Wp PV module may be considered as two separate 2.5 W_p modules that may be either series or parallel connected. Each 2.5 W_p module will produce maximum power at approximately 8.5 V and 0.29 A. Wiring in parallel will give the characteristics as shown in Fig. 3.5.3 plot A, whereas wiring in series will produce the curves B. Superimposing the pump load line, as given by Eqs. 3.5.4.a and 3.5.4.b, shows that the available electrical inputs for pumping are very different for the two module configurations. These operating point values, for the two configurations, are shown in Table 3.5.1.

Since with laminar flow, the resistance head is approximately proportional to flow rate, then the hydraulic power (product of flow and head) will increase by a factor of four for a doubling in flow rate. The collector efficiency characteristic equations outlined in section 3.4 imply that at 500 W/m^2 the optimum flow rate is approximately 0.18 litres/min, and for 1000 W/m^2, 0.40 litres/min. The required

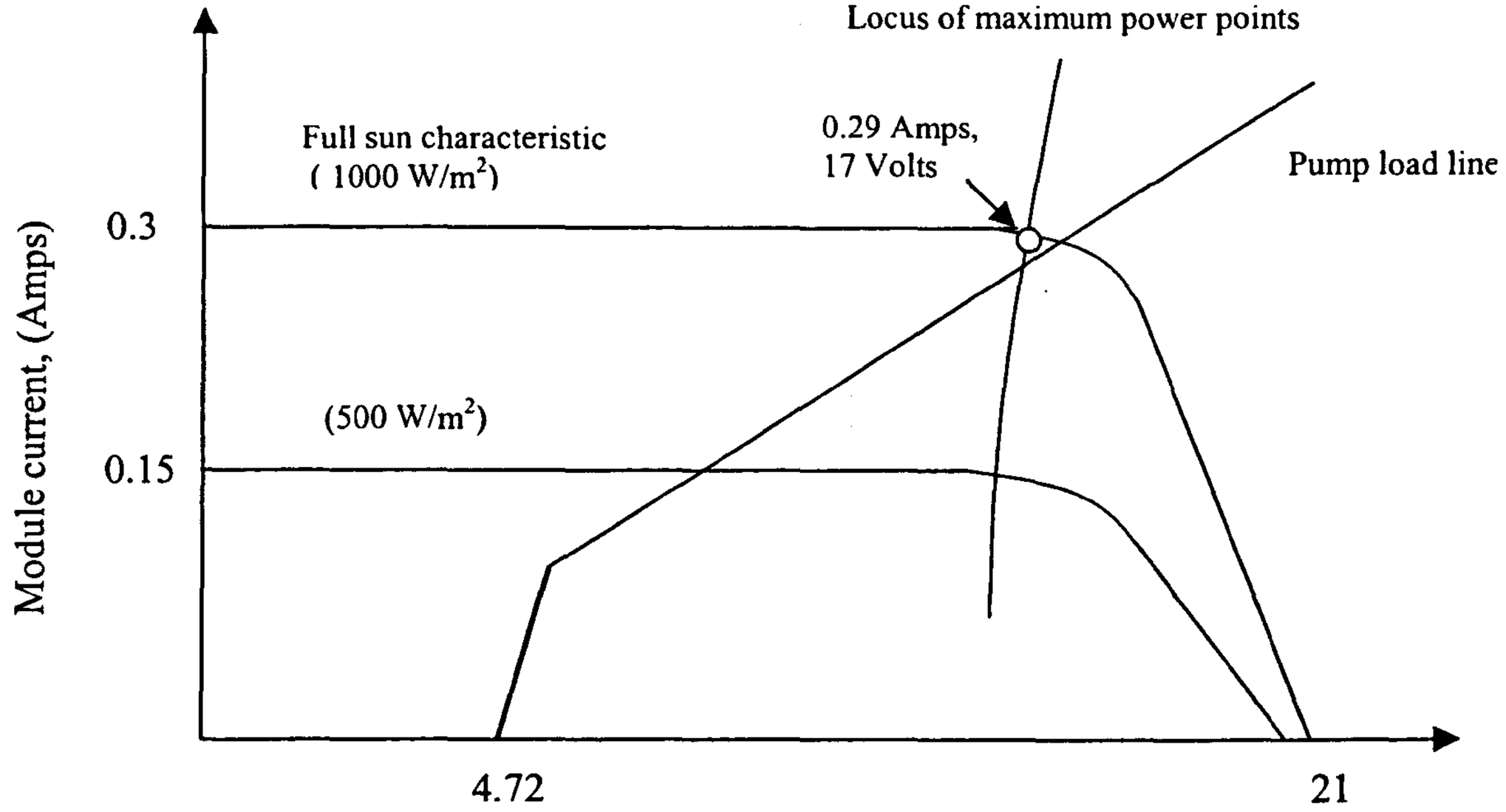

Figure 3.5.2. BP 5 Watt (peak output @ 1000 W/m^2) module characteristics, and Charles Austen pump model LD2 load line characteristics.

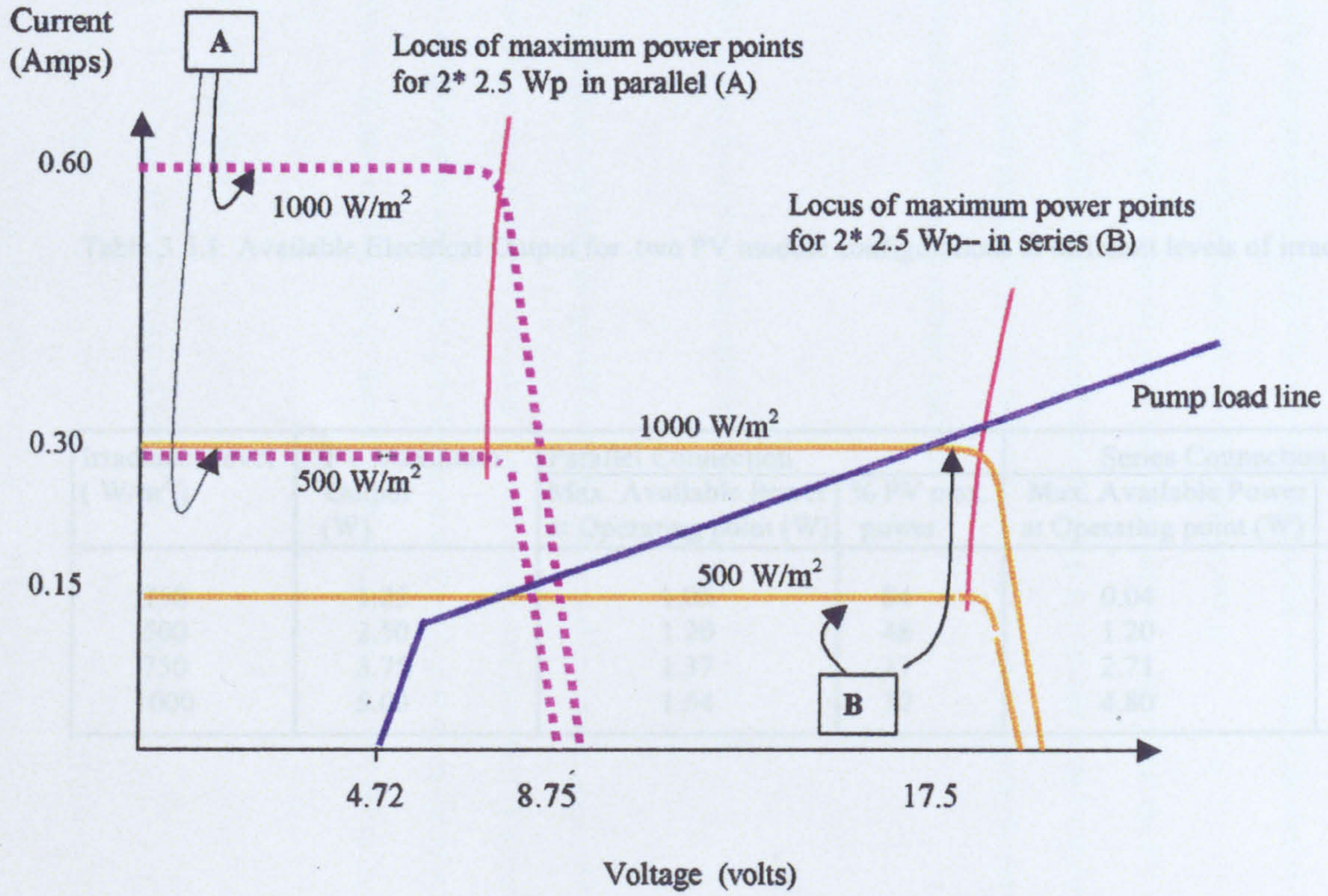

Figure 3.5.3 Current vs. Voltage Characteristic for 2 PV module configurations at two irradiance levels, namely Full Sun, (1000 W/m^2) and Half Sun, (500 W/m^2) and the Load Line for the Charles Austen pump model LD2

Configuration A, 2 *2.5 Wp in parallel (·····)
Configuration B, 2 * 2.5 Wp in series (——)

Table 3.5.1 Available Electrical Output for two PV module configurations at different levels of irradiance.

Irradiance level (W/m^2)	PV Maximum Output (W)	Parallel Connection		Series Connection	
		Max. Available Power at Operating point (W)	% PV max. power	Max. Available Power at Operating point (W)	% PV max
250	1.25	1.05	84	0.04	31
500	2.50	1.20	48	1.20	48
750	3.75	1.37	37	2.71	72
1000	5.00	1.54	30	4.80	96

hydraulic output will therefore necessarily increase by approximately a factor of 5, $[(0.40/0.18)^2]$ between these irradiance levels. A review of the pump performance specification sheet, Charles Austen (1999), although data is only given for two operational voltages, implies that the pump efficiency will be reduced at lower flows and voltages. On this basis, it is likely that the electrical input will have to increase by at least a factor of 5 between these irradiance values to provide the desired flow rate. Considering the values reported in Table 3.5.1 indicates that this criterion is more closely met by the series module configuration. In addition, as there is a minimal increase in available pumping power between 500 and 1000 W/m^2 for the parallel module, this implies that the flow rate will also not alter significantly between these levels. The series configuration was therefore chosen in preference to the parallel module as the more favourable for this application.

Initial testing of the selected pump indicated that it was likely that the PV module was oversized and that it would therefore require some form of control to regulate output and hence flow rate. In order to define the required degree of control for the PV module it was necessary to first determine the system flow rate versus applied pump voltage characteristic.

3.5.2.3 System flow rate versus applied pump voltage

The addition of a head gauge within the hydraulic system, and consideration of the additional resistance to flow imposed by its inclusion, allowed the system flow rate versus pump applied voltage profile to be determined. Analysis of profile obtained (Q vs. V_p) allowed the relationship to be defined in linear sections, operating with voltage based conditional limits as given in Eqs 3.5.5 a to 3.5.5 d.

If $4.72 < V \leq 5.0$ Then:

$$Q = (0.2 * V) - 0.945 \qquad R^2 = 0.9615 \qquad (3.5.5.a)$$

If $5.0 < V \leq 5.5$ Then:

$$Q = (0.852 * V) - 4.204 \qquad R^2 = 0.9965 \qquad (3.5.5.b)$$

If $5.25 < V \leq 7.0$ Then:

$$Q = (0.117 * V) - 0.153 \qquad R^2 = 0.9550 \qquad (3.5.5.c)$$

If V > 7.0 Then:

$$Q = (0.074 * V) + 0.138 \qquad R^2 = 0.9136 \qquad (3.5.5.d)$$

As can be seen in Fig 3.5.4 sectional linear fitting gives a better correlation coefficient than is afforded by fitting a single polynomial curve to the measured data.

Rearranging the above equations to find the flow limits defined by each, and applying a desired maximum design flow of 0.40 l/min, implies that an applied pump voltage of 5.40 volts is required at full sun to obtain the desired collector outlet temperature. Rearranging Eqs. 3.5.4.a and 3.5.4.b, and applying this maximum voltage condition implies a desired maximum, full sun, current of 0.101 amps.

Two simple control methods, namely physical and electrical shading were considered for their suitability in providing the desired temperature rise at full sun and with regard to the stability of the collector outlet temperature across the operational range of irradiance. An analysis of the effect of both these control methods on the combined PV module/pump performance, and the subsequent collector outlet temperature is now presented.

3.5.3 The effect of physical shading on the collector outlet temperature

3.5.3.1 The effect of physical shading the PV module output.

The module used comprises 4 columns of 9 cells all connected in series. Using black insulating tape, under direct beam irradiance (full sun), physically shading one column of cells by 50% by area, as shown in Fig. 3.5.5 was seen to reduce the circuit current by the same proportion. An analysis of the circuit current characteristic revealed that the current was not reduced by the same proportion for all irradiance levels. The effective percentage shading was seen to decrease with decreasing irradiance, that is, the measured current, calculated as mA/(kW/m^2) equivalent, was seen to increase at lower irradiance levels. Figure 3.5.6 gives a plot of the measured current as mA/(kW/m^2) equivalent against irradiance for two shading levels. The degree of shading is defined as the percentage reduction in current seen at full sun.

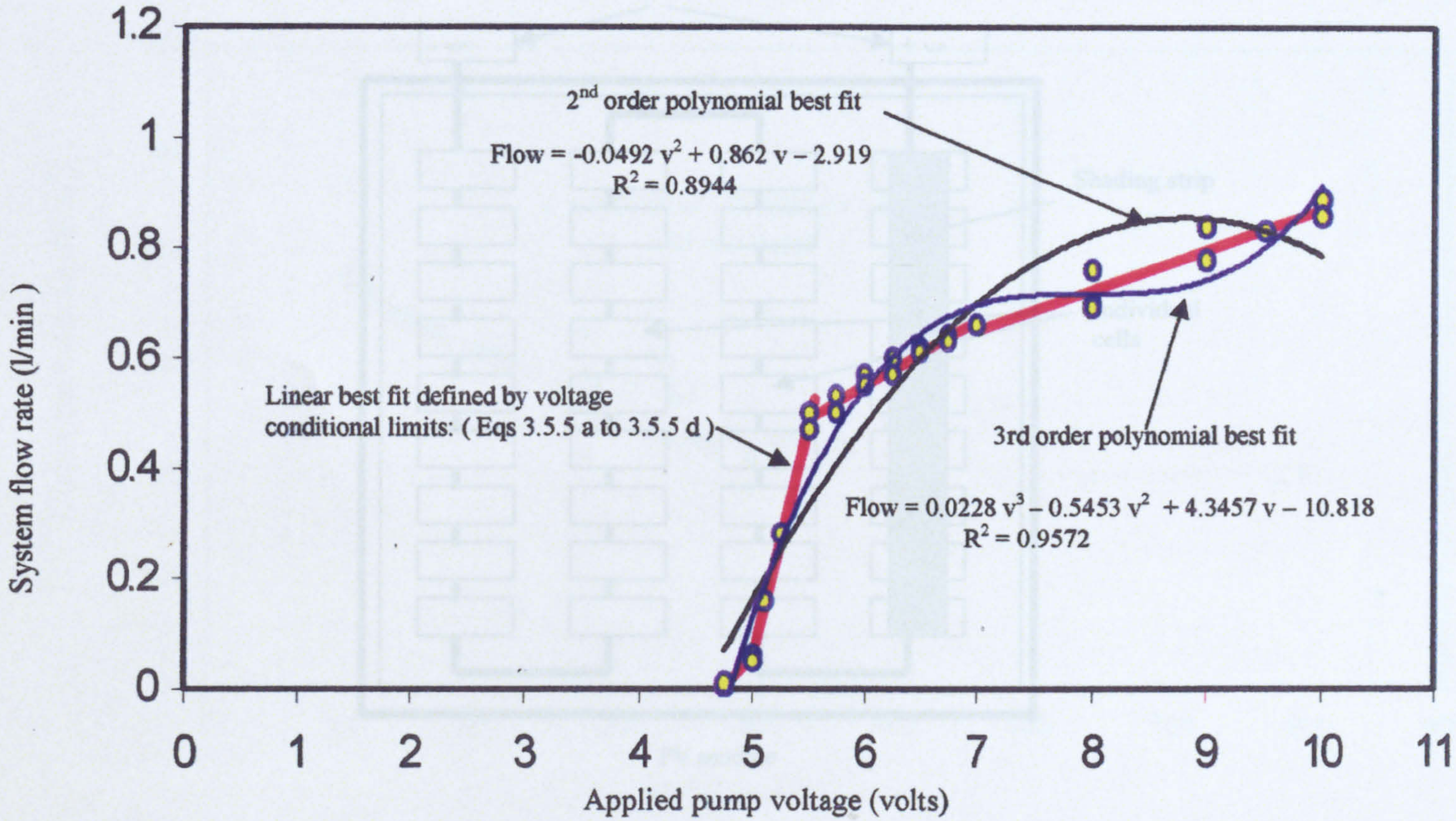

Figure 3.5.4 Plot of calculated flow rate versus applied pump voltage for three test runs with linear, second, and third order polynomial

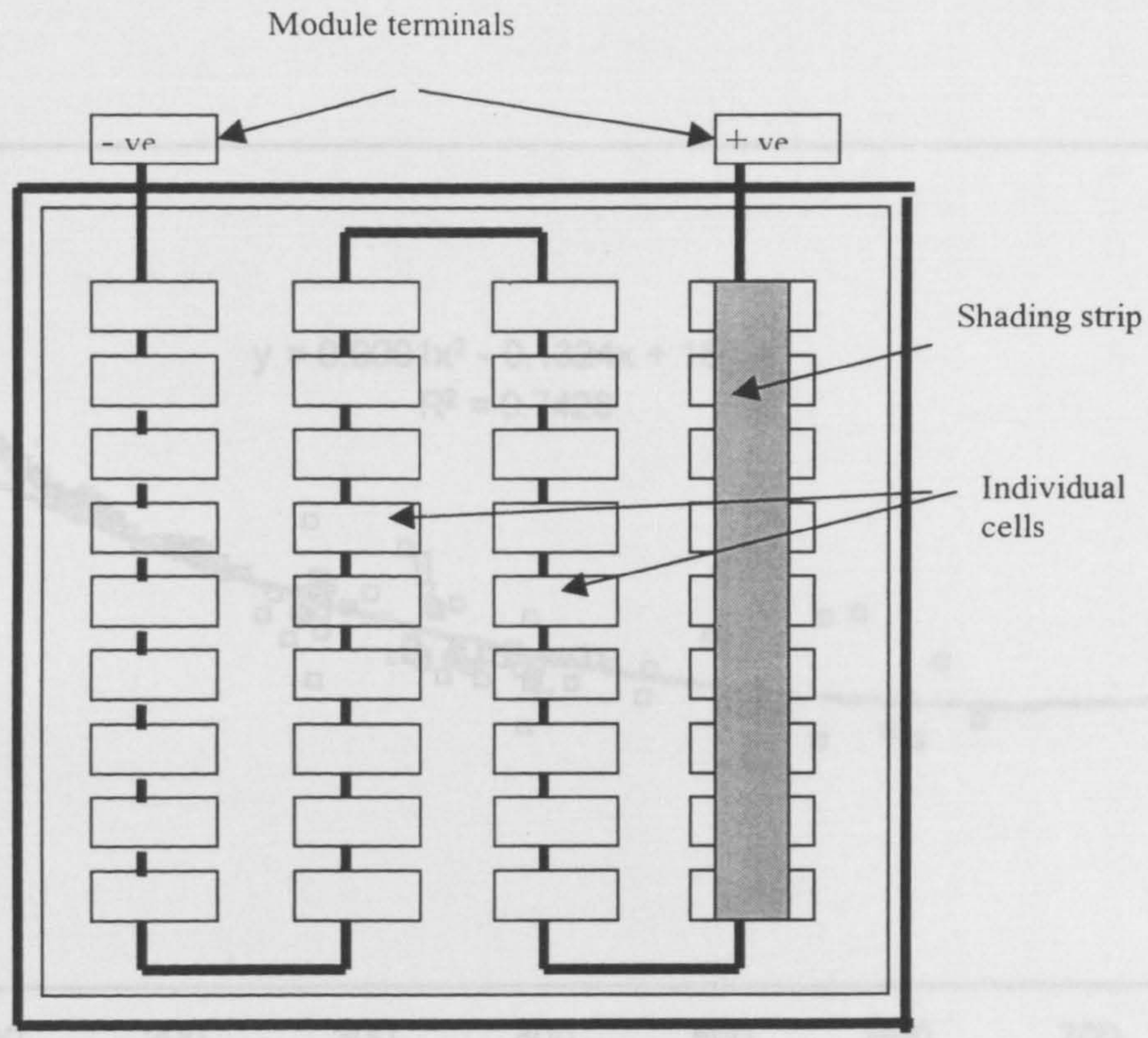

Figure 3.5.5 Schematic of fully series connected PV module showing shading method applied..

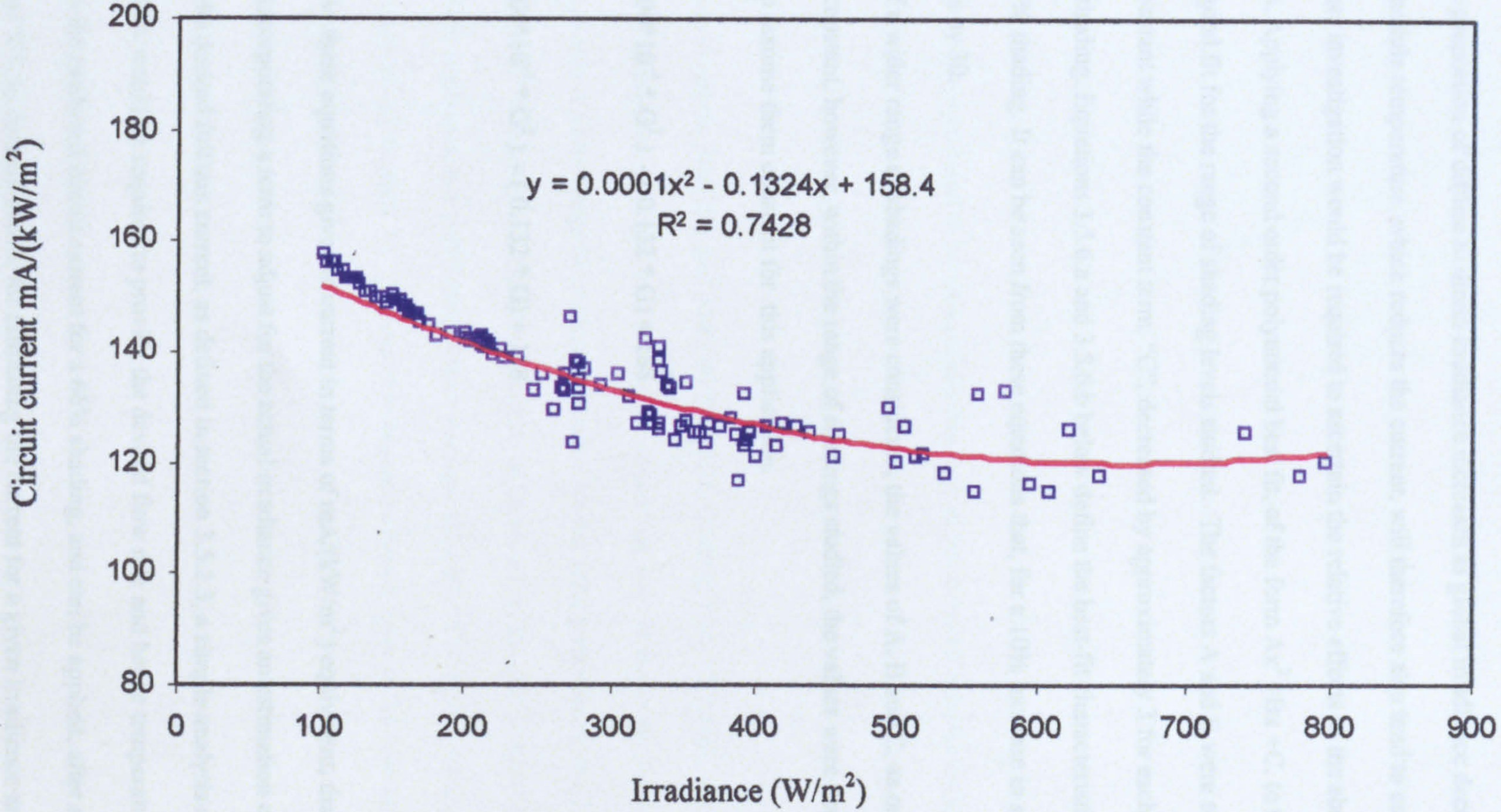

Figure 3.5.6 Circuit current defined as full sun equivalent, (mA/(kW/m^2)), versus irradiance for a 60% shading of the 5 Wp PV module.

As the shading tape is placed on the module cover, there is a small gap (2-3 mm) between the tape and the cell surface. This observed non-linear effect is most likely due to their being a higher proportion of reflected diffuse/scattered irradiance reaching behind the shading cover at lower irradiance levels as the proportion of diffuse to direct irradiance increases as global irradiance decreases. In addition, increasing module temperature, which reduces the current, will therefore also tend to cause the above noted effect. Further investigation would be required to ascertain the relative effects of the above mentioned mechanisms. Applying a second order polynomial best fit, of the form $Ax^2 + Bx + C$, to the data gathered, provided a good fit for the range of shading levels studied. The factors A and B were seen to remain relatively constant while the constant term, "C", decreased by approximately 3 for each additional percentage shading. Equations 3.5.6.a and 3.5.6.b below define the best-fit characteristic curves derived for 50% and 60% shading. It can be seen from these equations that, for a 10% increase in shading, the constant term reduces by 30.

If a wider range of shadings were considered, the values of A, B and C, as outlined above, would not remain constant, however, within the range of shadings studied, the values were considered close enough as to assume them constant for this application.

$$I_{AFs} = (1.00*10^{-4} * G^2) - (0.132 * G) + 188 \qquad (3.5.6.a)$$

$$I_{AFs} = (1.00*10^{-4} * G^2) - (0.132 * G) + 158 \qquad (3.5.6.b)$$

As these equations give the current in terms of $mA/(kW/m^2)$ equivalent, that is, full sun equivalent, incorporating a term to adjust for the actual irradiance gives an estimation of the circuit current. To provide the desired full sun current, as defined in section 3.5.2.3, a simple analysis revealed that a shading of 66% would be required to provide the desired flow rate and hence temperature rise. Equation 3.5.7 defines the predicted circuit current for a 66% shading, and can be applied, after adjusting the constant term "C", as defined above, for estimating the current for a given irradiance and shading.

$$I_A = \{(1*10^{-4} * G^2) - (0.132 * G) + 140 \} * (G/1000) \qquad (3.5.7)$$

3.5.3.2 Measured collector outlet temperature profile.

While the above analysis has been applied to define the required degree of shading for the design conditions at full sun. The ideal current required at lower levels of irradiance has not been specified. The method employed in modelling and predicting the collector outlet temperature profile with respect to the degree of physical shading of the PV module is presented in section 4. Section 3.5.3.2 presents only the measured temperature profile for different degrees of shading and compares this with the design criteria.

Figure 3.5.7 shows a plot of the measured collector outlet temperature versus irradiance for a 66% shading. It can be seen that the measured outlet temperature is reasonably stable for the midday period when the irradiance lies between 500 W/m^2 and 1000 W/m^2. However, between the measured cut in irradiance of 250 W/m^2 and 500W/m^2, between 10:00 am and 10:30 am, it is unacceptably high. The outlet temperature was found to be consistently too high at cut in for all subsequent measurement for this degree of shading. As the system is intended for heating domestic water these temperatures, up to 80 °C, as seen in Fig. 3.5.7, are dangerously high. As such, it is not advisable to use such a high degree of shading.

It would appear from the plot obtained for a 50% shading, Fig. 3.5.8, that, while it does not give the desired temperature rise at full sun, this degree of shading does however produce more useable temperatures over a wider range of irradiance. For a collector inlet temperature of 12 °C an outlet temperature of 45 °C is obtained. For greater angles of incidence of the sun's beam to the collector and lower average irradiance this outlet temperature decreases slightly. The higher collector outlet temperature observed at point "A" represents a stagnation temperature at the collector outlet after the cessation of pumping. Earlier analysis considered the threshold irradiance in terms of irradiance perpendicular to the plane of the PV module. As can be seen from Fig 3.5.8, the sun's beam angle of incidence has a marked effect on the threshold irradiance. This effect is considered in more detail in section 4.

Figure 3.5.9 also shows a plot of the outlet temperature profile for a shading of 50%. In the first instance, as shown in Fig 3.5.8, the storage tank supplying the collector was fully discharged prior to testing, providing the relatively constant inlet temperature observed. In the second case, Fig 3.5.9, a partially preheated tank, supplying a gently increasing inlet temperature was used. In this instance, the

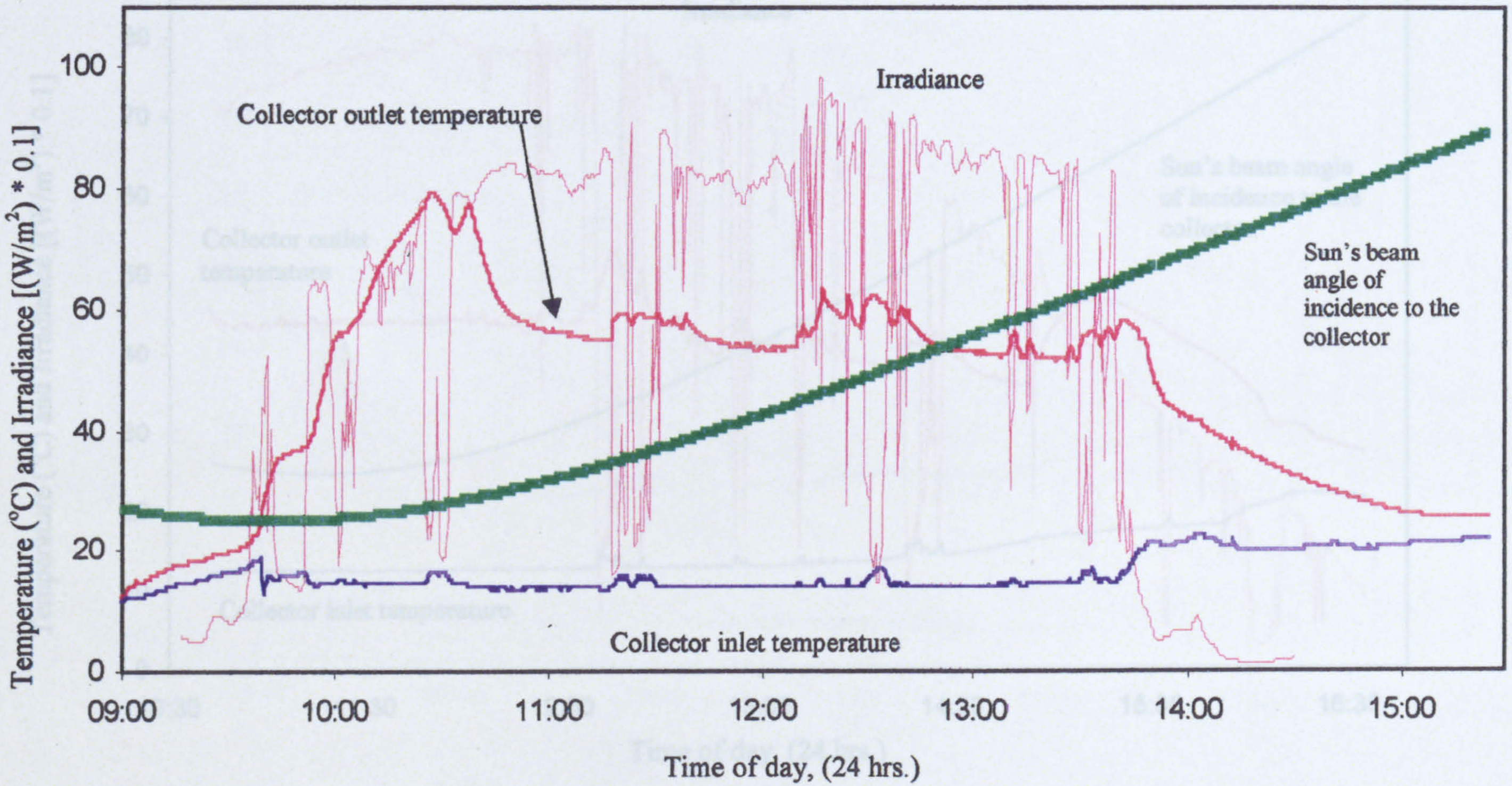

Figure 3.5.7 Irradiance and collector inlet and outlet temperatures for a 66% shading of the PV module (22nd October 1999)

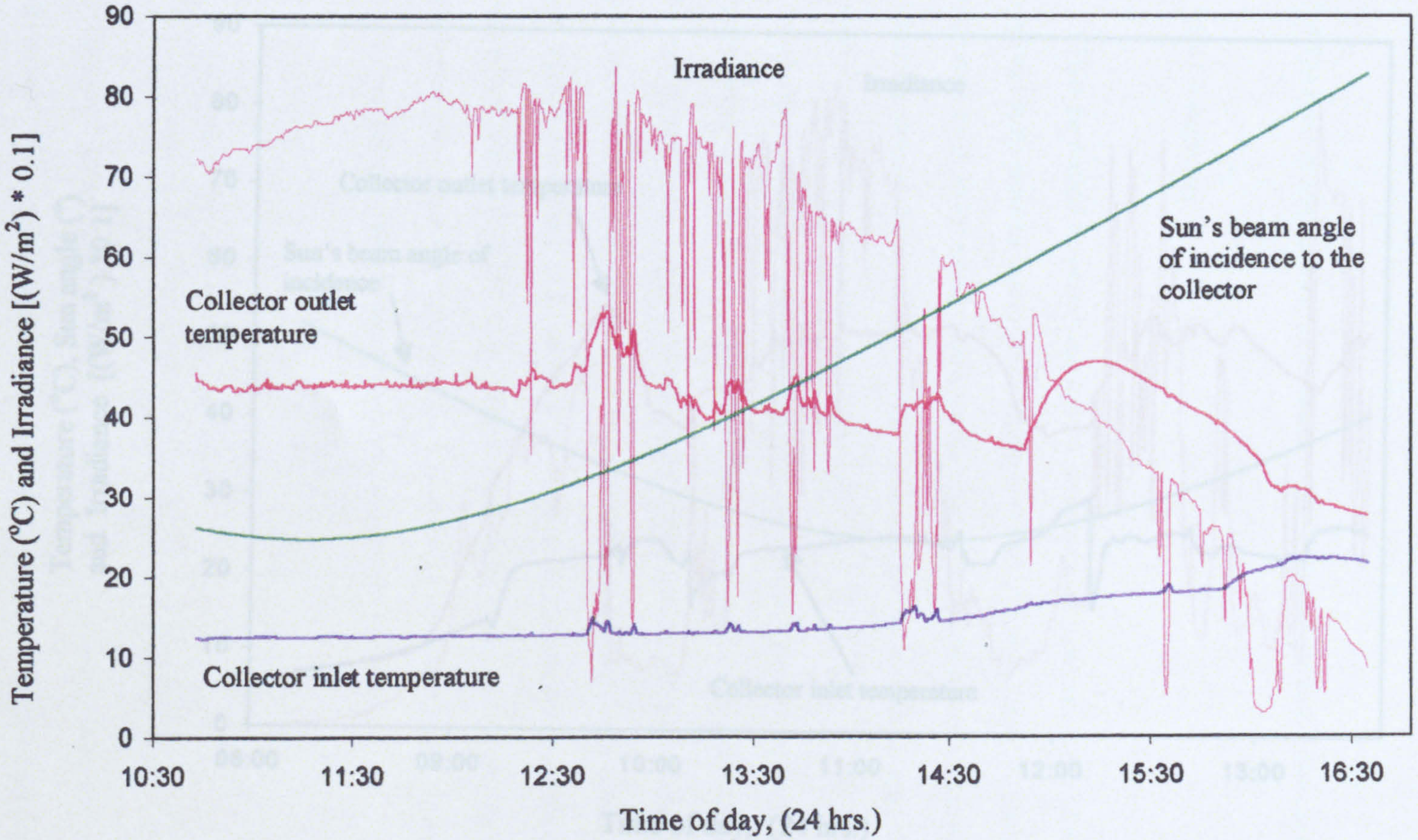

Figure 3.5.8 Irradiance and sun's beam angle of incidence, and collector inlet and outlet temperatures for a 50% shading of the PV module (26th October 1999)

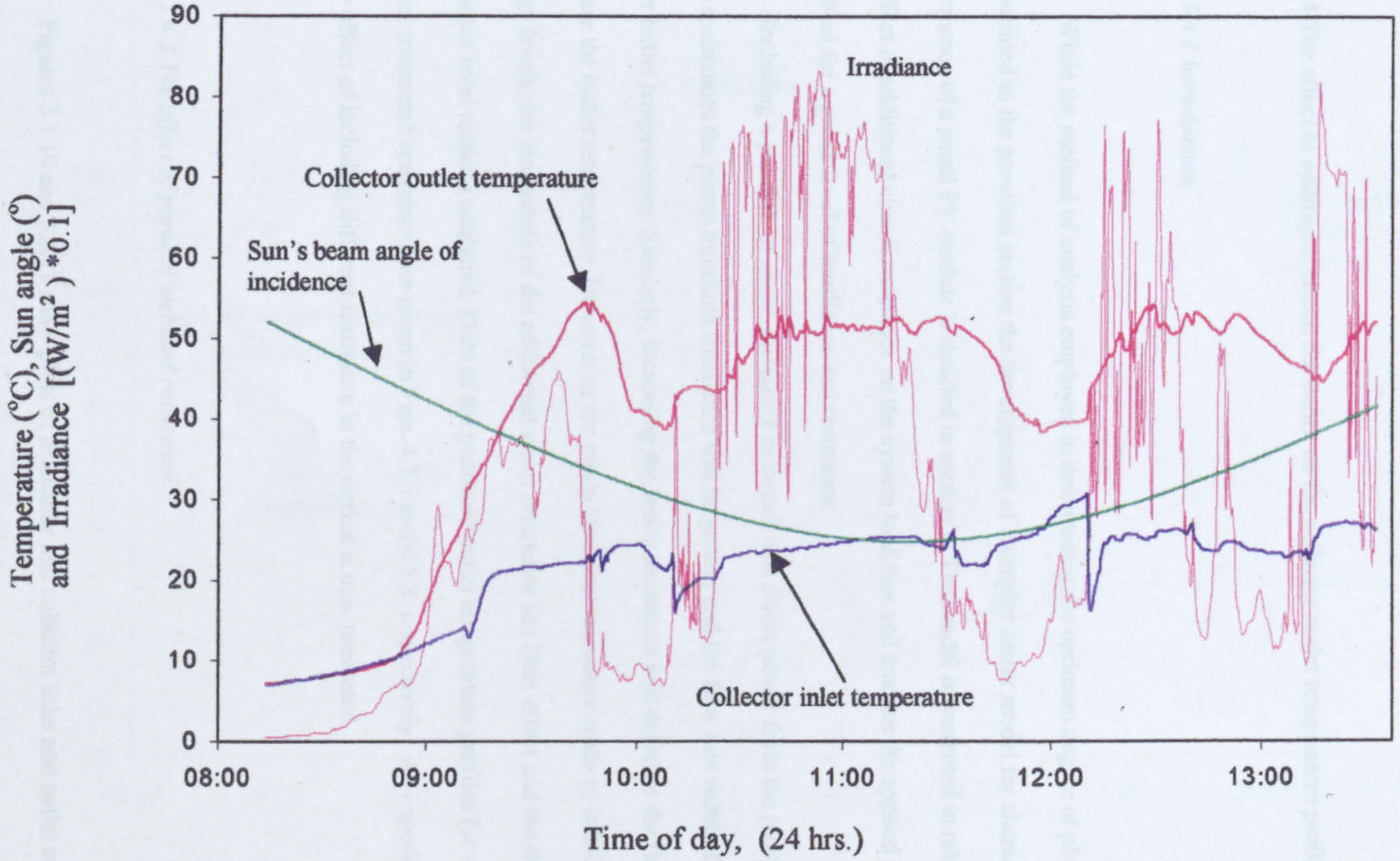

Figure 3.5.9 Irradiance and sun's beam angle of incidence, and collector inlet and outlet temperatures for a 50% shading of the PV module (28th October 1999).

design outlet temperature is achieved. Under normal operating conditions, where an electric immersion may be used to boost the tank temperature, and hence raise the collector inlet temperature, this degree of shading will tend to provide the closest to optimum outlet temperature profile.

3.5.4 The effect of additional circuit resistance on the collector outlet temperature profile.

3.5.4.1 Introduction

While the method of analysis employed in determining the optimum degree of physical shading was outlined in the previous section the development of a simpler linear model for characterising the performance of a small PV module is detailed in section 4. The model is presented in relation to defining the effect of additional circuit resistance on the system load line and enables the applied pump voltage to be solved for a given level of irradiance and resistance.

Including a parallel, or shunt, resistance in circuit will divert power from the pump. For smaller shunt resistances the pump threshold irradiance will be greater and the flow rate reduced, thus affording higher outlet temperatures. Similarly, increasing the series resistance will decrease the flow rate and increase the outlet temperature. However as the pump electrical resistance tends to infinity at cut in voltage levels, the magnitude of the additional series resistance has little effect and the threshold irradiance level remains unaltered. Plots of the predicted outlet temperature profiles for various series and parallel connected resistances are given in Figs. 4.5.5 and 4.5.8 respectively. An experimental analysis of the effect of including different resistance in the circuit is now presented.

3.5.4.2 The effect of parallel included resistance.

Figures 3.5.10 and 3.5.11 show plots of irradiance and collector inlet and outlet tempetrature profiles for additional parallel resistances of 58 Ω and 179 Ω respectively. Comparing section "A" of Fig 3.5.10 with section "C" of Fig. 3.5.11, where the average irradiance and collector inlet temperatures are

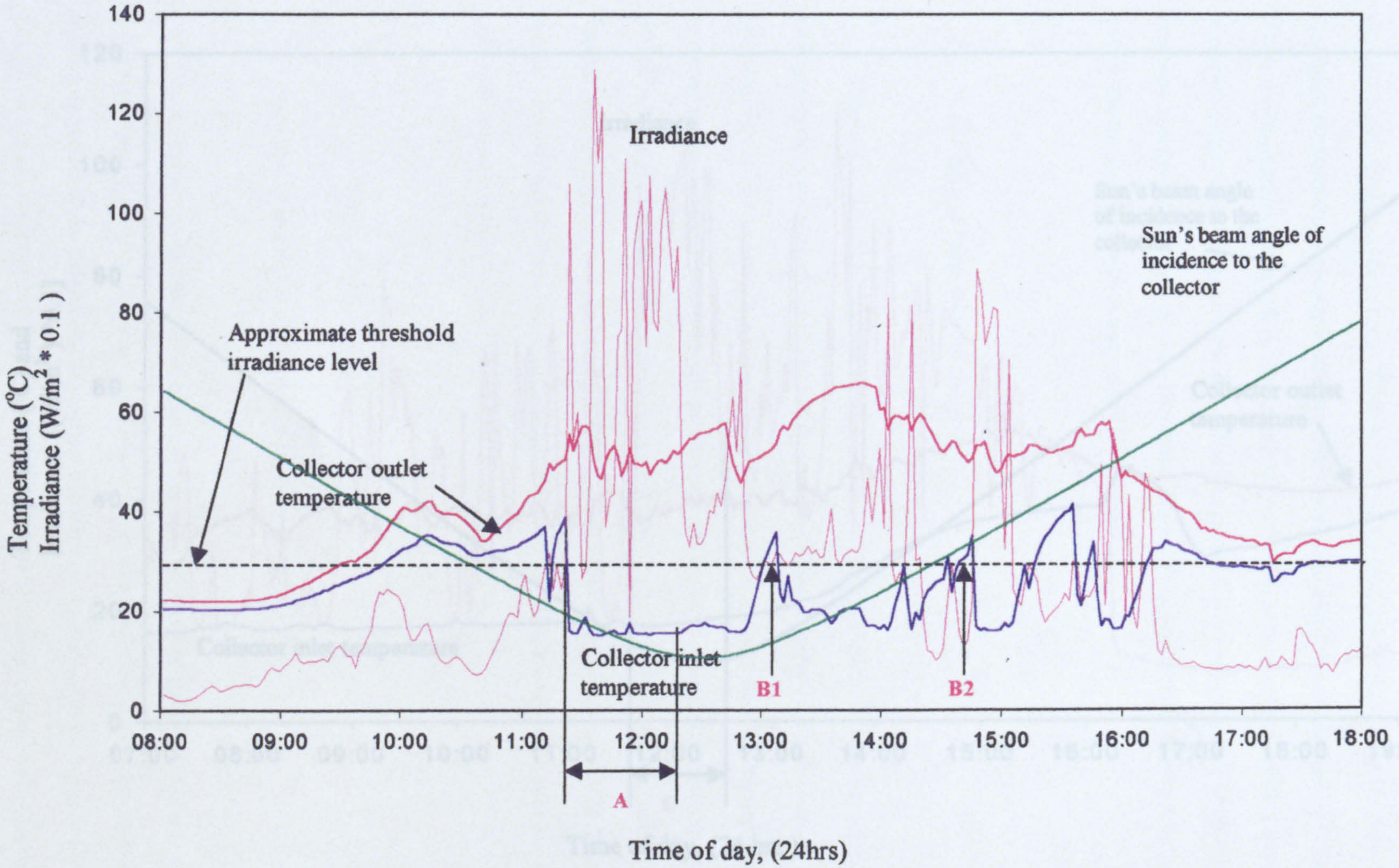

Figure 3.5.10. Irradiance collector inlet and outlet temperatures for a 58Ω resistor connected in parallel with the pump. (21st June 2000)

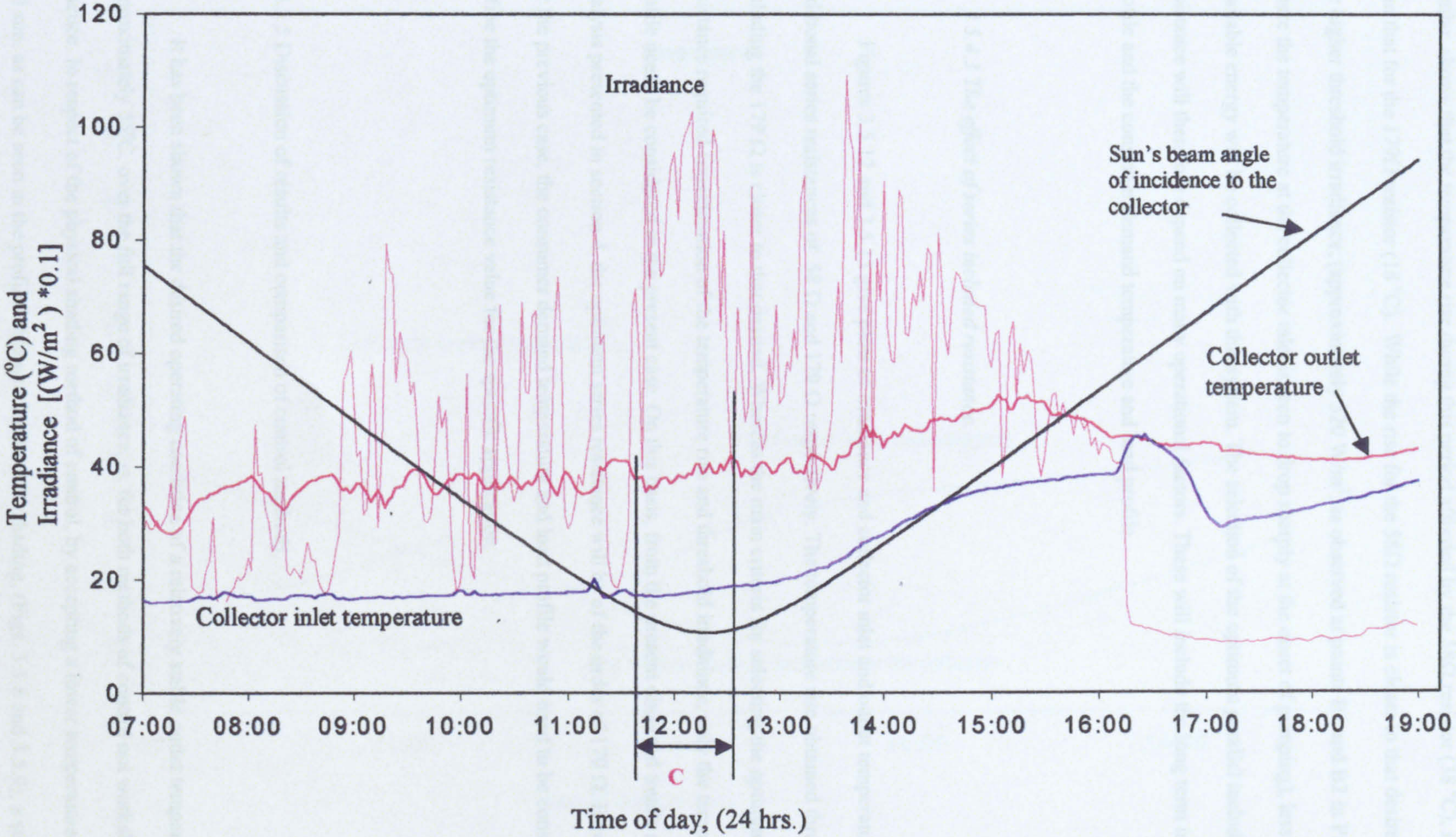

Figure 3.5.11 Irradiance and collector inlet and outlet temperatures with a 179 Ω resistor connected in parallel with the PV module (18th June 2000).

similar, shows that the temperature rise during this period afforded by the 58Ω resistor (38 °C), is greater than that for the 179Ω resistor (18 °C). While the rise for the 58Ω resistor is closer to that desired, due to the higher threshold irradiance, (approximately 320 W/m^2, as observed at points B1 and B2 in Fig 3.5.10 where the temperature at the collector inlet is seen to drop sharply at the onset of pumping), less of the available energy will be collected with this system. The selection of the optimum parallel included resistance will therefore depend on many operational factors. These will include the long term irradiance profile and the consumer demand temperature and load profile.

3.5.4.3 The effect of series included resistance.

Figures 3.5.12 and 3.5.13 give plots of irradiance and collector inlet and outlet temperatures for additional series resistances of 58 Ω and 179 Ω respectively. The temperature rise obtained through including the 179 Ω is closer to that desired. Whereas the main criteria for selecting the optimum parallel resistance required consideration of the temperature rise and threshold irradaince, only the temperature profile needs be considered in the present case. On this basis, from the present observed trends and the analysis presented in section 4, the optimum series resistance will be of the order of 170 Ω. However, as for the previous case, the consumer demand temperature and load profile would need to be considered to define the optimum resistance value for the specific application.

3.5.5 Discussion of results and comparison of control methods.

It has been shown that the desired operating condition of a relatively stable outlet temperature of approximately 55°C, over the full range of irradiance, is, for both methods of control not workable in practice. In respect of the physical shading method of control, by accepting a lower temperature rise at full sun, as can be seen in the profiles obtained for the 50% shading, (Figs. 3.5.8 and 3.5.9), a still useful outlet temperature can be obtained over a wider range than for the optimum full sun shading.

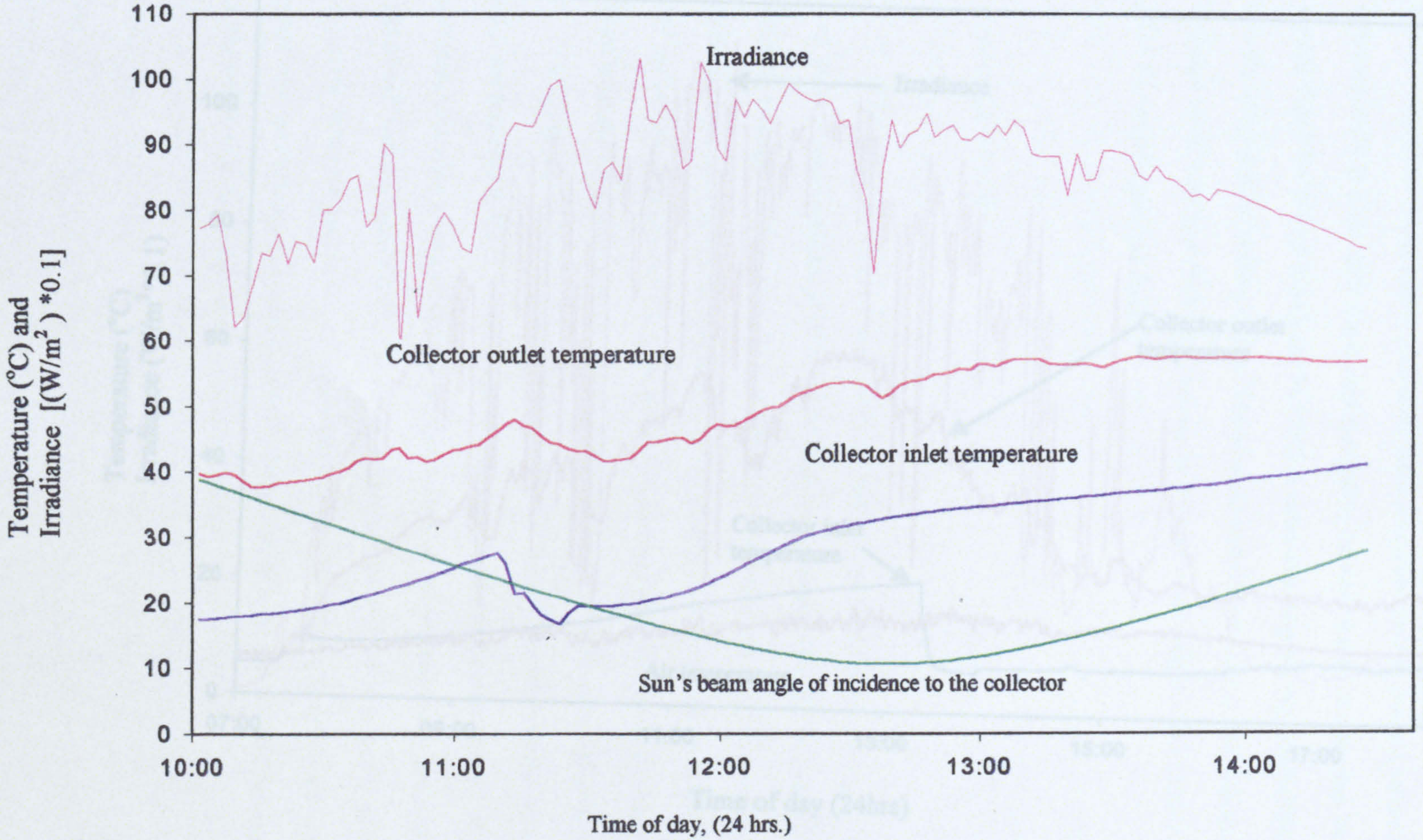

Figure 3.5.12 Irradiance and collector inlet and outlet temperatures with a 58 Ω resistor connected in series with the PV module (19th June 2000).

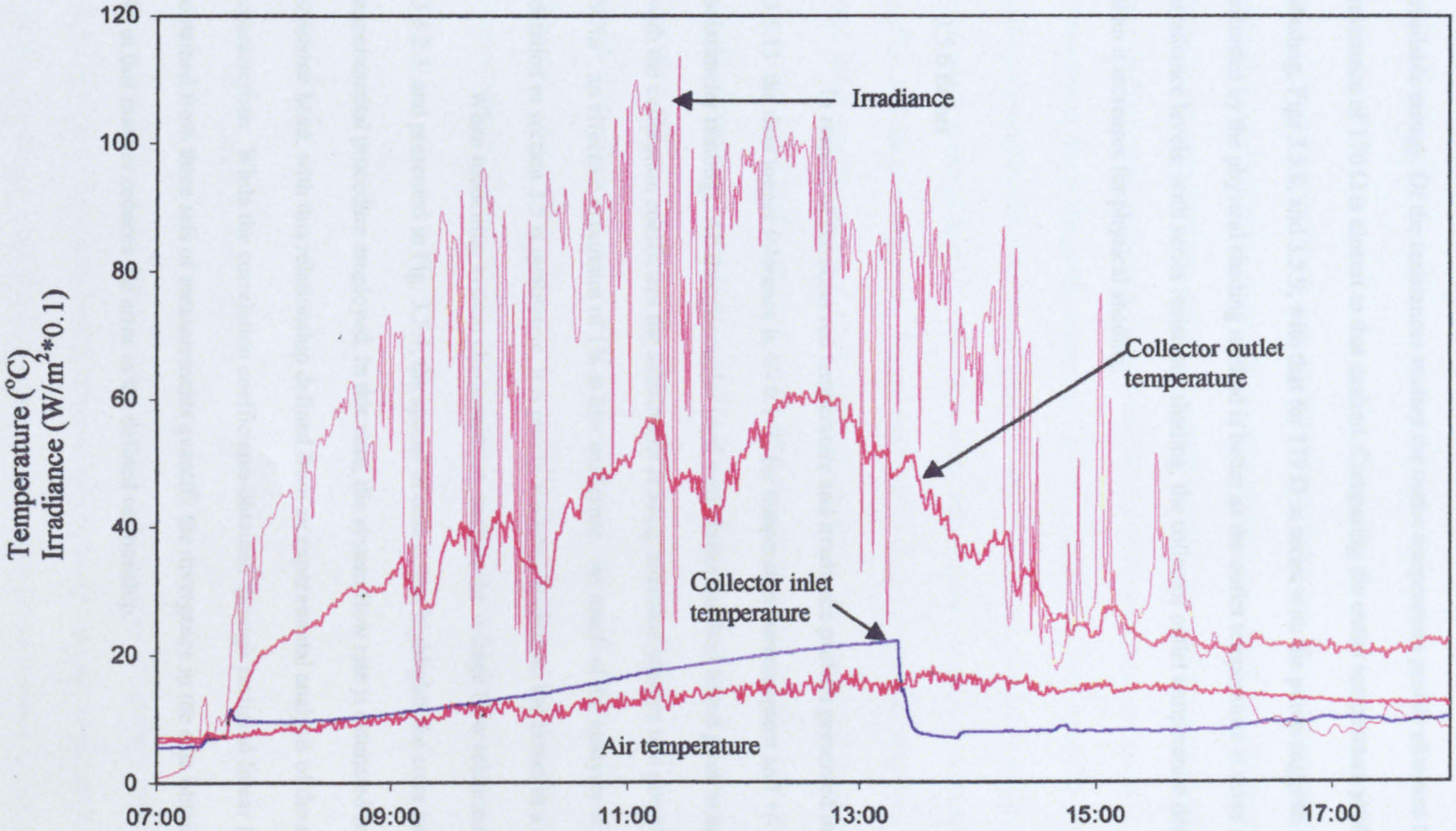

Figure 3.5.13 Irradiance, collector inlet and outlet temperatures, and air temperature for a 180Ω resistor in series with the pump (1st April 2001)

With regard to the effects of including additional resistance within the circuit it has been shown that adding resistance in series, due to lower threshold levels, allows the collection of more of the available energy. Of the resistances studied the outlet temperature profile obtained for the series included resistance of 170 Ω is closest to that desired. Comparing the outlet temperature profiles for the 50% shading, Figs 3.5.8, and 3.5.9, with that for 179 Ω in series with the pump suggests that the profile afforded by the physical shading method is better as the outlet temperature is more consistent. At lower irradiance levels, with series resistance shading, the collector outlet temperature decreases more rapidly than it increases for physical shading.

3.5.6 Errors

In respect of the observed temperature and irradiance profiles presented in Figs. 3.5.7 through 3.5.13 the data logger tolerance is +/- 0.1 °C for temperature measurement and +/- 0.005 mVolts for the solarimeter readings. All thermocouples used were freeze and boil tested prior to use. After conversion with the calibration coefficient the solarimeter reading tolerance equates to a potential error of +/- 0.97 W/m^2, an effective maximum of 1% at low irradiance. As much of the analysis of the experimental work detailed in section 3.5 is qualitative, it is purely academic to discuss the errors in a quantitative manner.

When modelling system characteristics, such as the voltage flow relationships detailed in section 3.5.2.3, and presented in Fig. 3.5.4, the spread of data points highlights the error incurred through the experimental procedure employed. In this case, the system flow rate is estimated from a measure of the dynamic head, with this relationship defined from an experimental analysis of the system hydraulic characteristic. While the correlation coefficients obtained through sectional linear fitting to the data obtained from three sets of measurements quantify the divergence in the data obtained, by applying a best fit in this manner reduces the error in the defined relationship.

3.6 COMPARATIVE TESTING OF SYSTEMS PERFORMANCE

3.6.1 Introduction.

The experimental work thus far detailed has shown that the outlet temperature profile as obtained through either the physical or electrical shading methods is not ideal. By reducing the degree of shading, physical, or series electrical, and thus accepting a slightly lower collector outlet temperature at full sun, a more stable profile is obtained. As the resistors used in the above analysis experienced high operational temperatures due to the power dissipated, (up to 3 W at full sun) their durability for the longer periods of testing required by the present comparative testing was in doubt. For future application it may be appropriate to mount them on a heat sink, or use a combination of smaller resistances to give a greater surface area for heat dissipation. For the comparative testing of the present system with a conventional 2 tank anti-freeze based system, a 50% physical shading was used on the PV module.

The effect on the perceived system performance of system design, performance indicators utilised, and the definition of collector area chosen, was considered in Section 2.5. Section 3.7 details the procedure employed to define the relative performance of the present FT-PV system with that of a standard anti-freeze based 2 tank solar water heating system. The rationale behind the selection of the load profile and method of immersion control applied to the two systems is outlined. Results are presented and discussed and the viability of the FT-PV system considered.

3.6.2 Rationale

3.6.2.1 Control of auxiliary input

Due to the requirement of frost protection at higher latitudes, in many retrofit solar domestic hot water systems a second tank, with a solar coil heat exchanger, is often installed. If the auxiliary energy source is electricity, a low level immersion heater is often left on untimed to raise the temperature to that required by the consumer. Where an application requires the constant availability of a full tank at the pre-set temperature this may not seem an unreasonable control strategy, however, in many cases, smaller

quantities of hot water are required at any one time. For the duration of testing the reference system was operated with the bottom immersion heater in the delivery tank left on untimed, (bottom not timed (BNT)). For this system the electricity consumption was recorded as the combined consumption of immersion, pump and controller. For a direct comparison, the FT-PV system was also initially operated in this mode. However, as is outlined in the following section, with respect to thermal performance, this is likely to be the worst case operating scenario for this system. To give a better indication of the overall performance of the FT-PV system, with respect to the reference system, the FT-PV system was also operated with the top immersion not timed, (TNT), for one period, and subsequently with the top immersion timed, (TT). In this last case, the top immersion timer was set to come on prior to the to pre-set draw off such that, during periods of low, or no solar input, there was enough time allowed for the auxiliary alone to provide the desired load. For each test run, both systems were operated for a period of 2 days in the desired mode prior to any data collection to allow for settling.

3.6.2.2 Effect of immersion control and load profile on systems performance.

Operating the FT-PV system with the bottom immersion untimed will tend to provide a higher collector inlet temperature than other modes of auxiliary control considered for this system. This in turn, as can be seen by considering the form of the collector efficiency characteristic as given in Eq. 3.6.1, will decrease the collector efficiency and therefore solar gain.

$$\eta = F_R\tau\alpha - F_RU_L[((T_o + T_I)/2 - T_A)/G] \qquad (3.6.1)$$

Although in this mode the collector will operate at a lower efficiency, it will tend however to provide water that is hotter than required. As such, from first considerations, there appears to be little benefit, other than topping up, from installing this system and operating in the BNT mode. In addition, if one defines system thermal performance in relation to the ability of the whole system to deliver water at the pre-set temperature, this would imply that, for this mode, there is less benefit still in installing this system.

Operating this system in the third mode outlined above, with the top immersion timed, TT, through providing the collector with cooler water for longer will tend to maximise the collector efficiency, and reduce unnecessary overnight heating/heat loss costs. One would therefore expect that, in this mode of operation, the FT-PV system should perform better than in the other modes. However, this mode will not be able to provide large volumes of hot water during periods of low irradiance.

For the reference system, operating with a separate solar tank, collector efficiency is not affected by the mode of auxiliary control. As the unstratified solar tank, for normal operation, is typically at a lower temperature than the delivery, or secondary tank, solar gain will generally be maximised through the provision of cooler water for the collector to work on. During periods of high solar gain and an evening peak load however, the preheat tank temperature will tend to increase thus reducing collector efficiency. Providing an evenly distributed load will tend to benefit the performance of having this second tank, while delivering the preheated water from the primary tank to the secondary only during/ after the delivery of load implies that there is the potential for greater heat loss and inefficient use of the solar pre-heated water than in a single tank system.

3.6.3 Systems description.

A schematic of the test apparatus developed for the comparative performance testing of the two above mentioned solar water heating systems is shown in Fig. 3.6.1. The FT-PV system is shown to comprise the freeze tolerant collector, the upper most half having a selective coating, and the PV module and pump. The collector supply and return pipes are connected directly to the mains cold feed and domestic hot water supply pipes respectively. These connections are made immediately adjacent to the storage tank which has both top and bottom electric immersion heaters available for "top up" heating. The reference system comprises a flat plate collector with a selective coating on the whole of the absorber surface. The collector is connected via an anti-freeze loop to a primary tank. Solar heat is transferred from the loop, via a heat exchanger to this tank, and thence to a second tank of the same configuration as the sole one in the FT-PV system. Whereas operation of the solar section of the FT-PV system is controlled

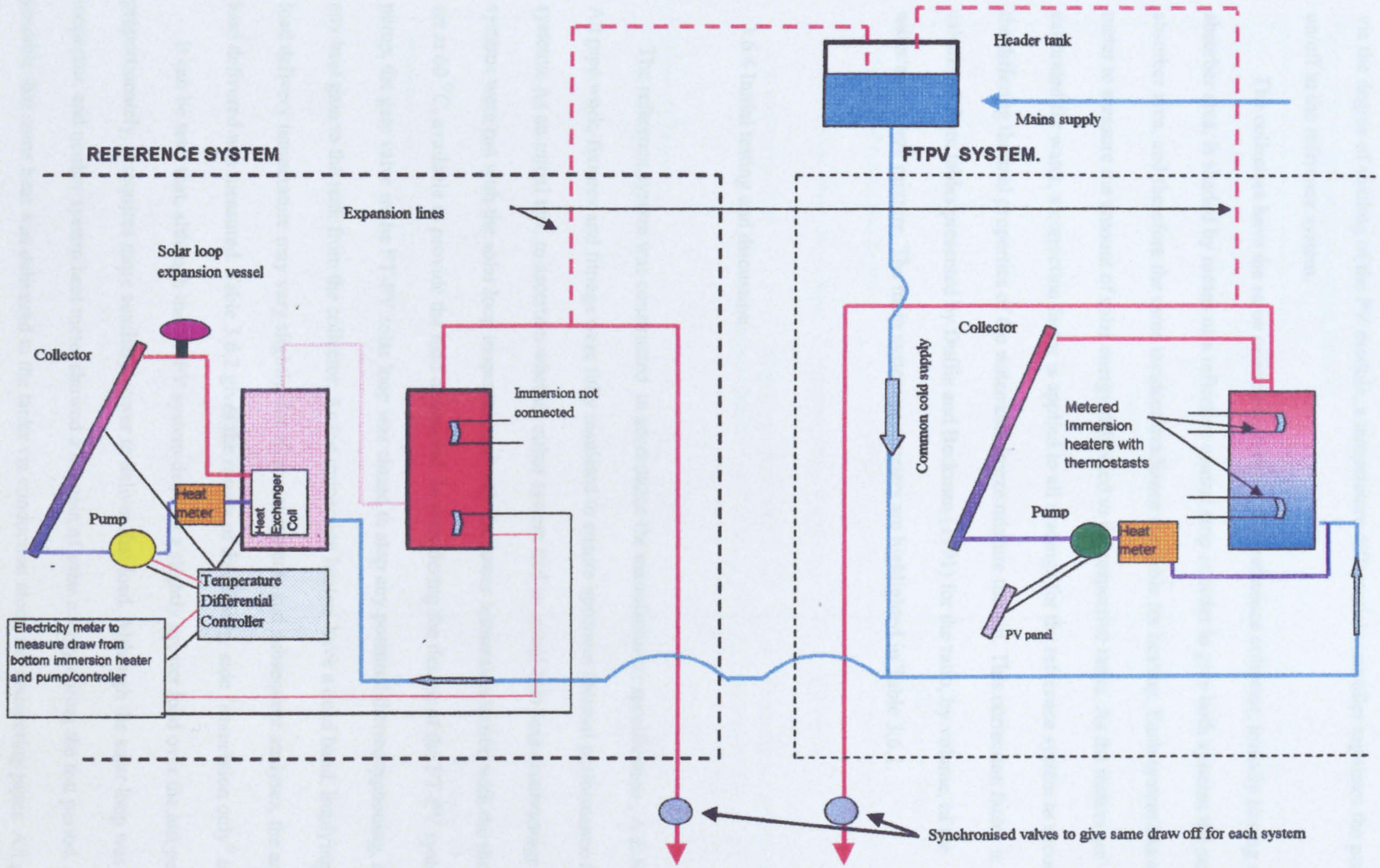

Figure 3.6.1 Comparative testing apparatus

via the degree of shading of the PV module, a temperature differential controller regulates the pump on/off in the reference system.

The collectors have the same orientation and tilt. The reference collector, initially having a greater absorber area, is shaded by means of a reflective central strip in order to give both systems the same absorber area, and therefore the same incident irradiance available for heating. Each system has a heat meter to measure the amount of solar energy delivered to the respective tanks. As the meters are calibrated for water, a correction factor is applied to all readings for the reference system to account for the differing thermal properties of the water/anti-freeze mixture therein. This correction factor is calculated from tables presented by Duffie and Beckman (1991) for the ratio, by volume, of the water/anti-freeze mixture. The main system parameters are highlighted in Table 3.6.1.

3.6.4 Initial testing and discussion

The reference system was constructed in accordance the manufacturers specification , A.E.S (1999). All pipe work, fixtures and fittings were fully insulated to ensure optimum thermal performance for both systems. As an initial test, to ascertain whether either system had an initial heat loss disadvantage, both systems were run with the solar loop inoperant, and only the lower immersion heater, with the thermostat set at 60 ^{o}C, available to provide the load demanded. In considering the design of the FT-PV system pump, the gate valve in the FT-PV solar loop was closed to stop any potential thermosyphoning, and limit any heat gain to the tank from the collector. As the immersion heaters have a dead band, implying that the load delivery temperature may vary slightly, for all measurements and subsequent analyses, the actual load delivered was measured. Table 3.6.2 gives the results of this side by side "immersion only" testing.

It can be seen that, although the FT-PV system delivers a slightly greater load over the test period, proportionately, it requires more auxiliary power to deliver that load. Although the solar loop was inoperant, and neither system heat meter showed a net gain of solar energy during the test period, it is still possible that some heat was delivered to the tanks via conduction along the connecting pipes. All pipe work and fittings within the reference system are copper whereas the FT-PV system uses narrow silicon

Table 3.6.1 Site and systems details

Location: Edinburgh, 55°57'N, 3°12'W

	FTPV system	Reference system
Absorber area (m^2)	1.95	1.95
Collector tilt (^{0})	45	45
Orientation	15° East of South	15° East of South
Heat transfer fluid	Water	Water/Anti-freeze (70/30 by volume)
Anti-freeze correction factor	N/A	0.956
Collector fluid flow rate (l/min)	Variable (max 0.4 l/min)	2.4 l/min
Flow control method	Shading of PV module (Cut in irradiance level 150 W/m^2)	Temperature differential controller. ON IF $\Delta T > 5°C$ OFF IF $\Delta T < 3°C$
Draw off times (15 minutes, daily)	8:00, 13:00, 18:00	8:00, 13:00, 18:00
Load (litres/draw)	35	35
Immersion thermostat setting (°C)	60	60
Storage tank volume (l)	116	Secondary 116 Primary 96
Immersion heater rating (kW)	3.0	3.0

Table 3.6.2. Results for both systems operating with only the bottom immersion, untimed.

Test period: 15:30 on 10/08/2000 to 15:30 on 15/08/2000 (5 days)							
Delivered load (kWhrs.)		Immersion Consumption (kWhrs.)		Thermal efficiency (%)		Electrical consumption as percentage of delivered load (%)	
FTPV.	Ref.	FTPV.	Ref.	FTPV.	Ref.	FTPV.	Ref.
27.43	26.69	37.20	34.35	73.7	77.7	135.7	128.7

tubes to connect the collector to the tank. The silicon has a lower thermal conductivity than the copper implying that there is a greater potential for heat gain to the reference system during this period of testing. During one period there was noted to be a temperature gradient of 20 °C across the heat exchanger of the reference system while the FT-PV system panel return pipe thermocouple showed a temperature of 70 °C adjacent to the top of the tank. With ambient air temperature in the test room typically 7 °C to 8 °C above mains water temperature it is also possible that additional heat was gained by the reference system through mains water sitting in the primary tank between draw off periods.

In consideration of the above, as both systems started with cold tanks at the beginning of the test period and contained a residual energy at the period end, the figures presented in Table 3.6.2. do not represent an accurate measure of the "auxiliary with no solar" for calculation of the solar fraction, nor an average thermal efficiency for the systems as operated in this mode. This initial test was intended to determine whether there was any major discrepancy in the heat loss and immersion characteristics of the delivery tanks of the two systems prior to fully operational comparative testing. Although these initial results are non-conclusive, if the relative operational performance of the two systems is such that the difference is similar to that observed in this preliminary test, these results may then be taken into consideration.

3.6.5 Comparative testing method.

The potential effects of the mode of immersion control selected and the draw off profile on the performance of the two systems was discussed in section 3.6.2.2. On the basis of these considerations, for each of the three modes of operation of the FT-PV system, the respective immersion heater thermostats were set to 60 °C and an evenly distributed load of 35 litres drawn from each system three times per day. This regime is summarised in Table 3.6.1. While other investigators using system performance simulation packages, such as TRANSYS have incorporated more realistic draw off profiles, for example, the RAND profile presented by Mutch (1990), Furbo (1990) showed that, while the draw off profile affected the performance of the systems studied, it did not affect their thermal performance ranking. In addition, the differences observed between the profiles presented by Mutch (1990), [America], and Papakostas et al

(1995), [Greece], implies that results derived from one profile are not transferable to a different season or global location.

For each of the three immersion modes testing the above regime was imposed for a period of at least 10 days to allow for a reasonable variation in irradiance and a more accurate appraisal of relative performance. As the solar fraction has been shown to be a potentially flawed performance indicator for the present systems, the electrical consumption of the respective systems was taken as the best indicator.

3.6.6 Presentation and discussion of results.

3.6.6.1 Collection efficiency

The results of the above mentioned comparative tests are presented in Tables 3.6.3a and 3.6.3b. Defining the collection efficiency as the solar energy delivered to the tank divided by the total incident solar energy available over the duration of the test period, it is immediately apparent from a comparison of the presented data that, irrespective of the immersion control mode selected for the FT-PV system, the reference system, for the same absorber area, has a higher collection efficiency. The reference system collector is quoted as having the efficiency characteristic defined by Eq. 3.6.2. (A.E.S, 1983).

$$\eta = 0.82 - 4.00 * [((T_i + T_o)/2 - T_a) / G] \qquad (3.6.2)$$

Although this characteristic was derived using water as the heat transfer medium, implying that both constant terms in Eq 3.6.2 will be reduced through using the water/anti-freeze mix stipulated by the manufacturers, it is likely that this collector will have a higher efficiency than the Flexsol collector.

As the FT-PV system operates with a variable flow rate, the average operational efficiency will be lower than that given for a flow rate of 0.4 l/min. In addition, at low irradiance levels, and hence lower flow, the heat loss from the FT-PV system will be greater due to the maintenance of a higher collector outlet temperature than would be realised by the constant flow reference system. For the FT-PV system, it can be seen that, with respect to the solar energy gain, the collection efficiency, as expected, is greatest when

Table 3.6.3a. Comparative systems performance data

Test period	Mode of operation		Total Solar Available (kWhrs.)	Solar Gain (kWhrs.)		Collection Efficiency (%)	
	FTPV	Ref.		FTPV.	Ref.	FTPV.	Ref.
5/05 - 18/05 2000	T.T.	B.N.T.	104.2	38.0	50.7	36.5	48.6
21/08 - 4/09 2000	T.N.T.	B.N.T.	70.8	22.0	31.5	31.1	44.5
21/05 - 2/06 2000	B.N.T.	B.N.T.	108.4	28.0	48.8	25.8	45.0

Table 3.6.3b. Comparative system performance data

Test period	Mode of Operation	Delivered Load (kWhrs.)		Electricity Consumption (kWhrs.)		Thermal Efficiency (%)		Electricity Consumption as Percentage of Delivered Load (%)	
	FTPV Ref.	FTPV.	Ref.	FTPV.	Ref.	FTPV.	Ref.	FTPV.	Ref.
5/05 - 18/05 2000	T.T. B.N.T.	66.7	69.5	40.7	79.2	84.8	53.4	**61.0**	**113.9**
21/08 - 04/09 2000	T.N.T. B.N.T.	68.6	64.2	55.1	71.3	89.0	62.5	**80.3**	**111.0**
21/05 - 02/062000	B.N.T. B.N.T.	65.3	62.1	61.8	62.9	72.6	55.6	**94.7**	**101.2**

the system is operated with the top immersion timed. In this mode, as outlined in section 3.6.2.2, the collector will generally receive cooler water for a longer period than in the other two modes, therefore maximising efficiency.

Figure 3.6.2 shows a plot of the FT-PV and Reference system tank top/delivery temperatures and immersion heater "ON" times, and the FT-PV system collector inlet temperature, during a period of testing with the FT-PV system operated in TT mode. Fig. 3.6.3 shows these same variables as measured with the FTPV system operated in BNT mode. As can be seen from comparison of these two figures, the FT-PV collector outlet temperature, due to increased inlet temperature, is higher for the BNT mode. For both systems, the load delivery temperature, as observed at points A and B in Fig 3.6.2, with the FT-PV system operating in TT mode, is close to the pre-set. However, comparison of the respective delivery temperatures observed at points C and D in Fig. 3.6.3 shows that, while this temperature is effectively constant for the reference system, the delivery temperature, as observed at point D for the FTPV system, is considerably greater than the pre-set demand temperature of 60 °C. For the BNT mode, as outlined above, after hot water has reached the bottom of the tank, and the collector inlet and outlet temperatures have risen, collection efficiency decreases and the load delivery temperature, and therefore energy, increase.

3.6.6.2 Thermal efficiency

For the purposes of this analysis the thermal efficiency is defined as the delivered energy divided by the total energy input. The total input is taken as the sum of the total auxiliary and the solar delivered to the tank. For the reference system, the figure for the total auxiliary input includes the energy consumed by the controller and pump. The combined consumption of the controller and pump, during the period of testing averaged 0.4 kWhrs./day. The controller alone, having a measured rating of 1.2 Watts, as compared to the specified rating of 40 Watts for the pump, contributes little to their combined consumption. Much of the pump output is dissipated as heat via the flow setter, and is therefore partially a positive heat input to this system.

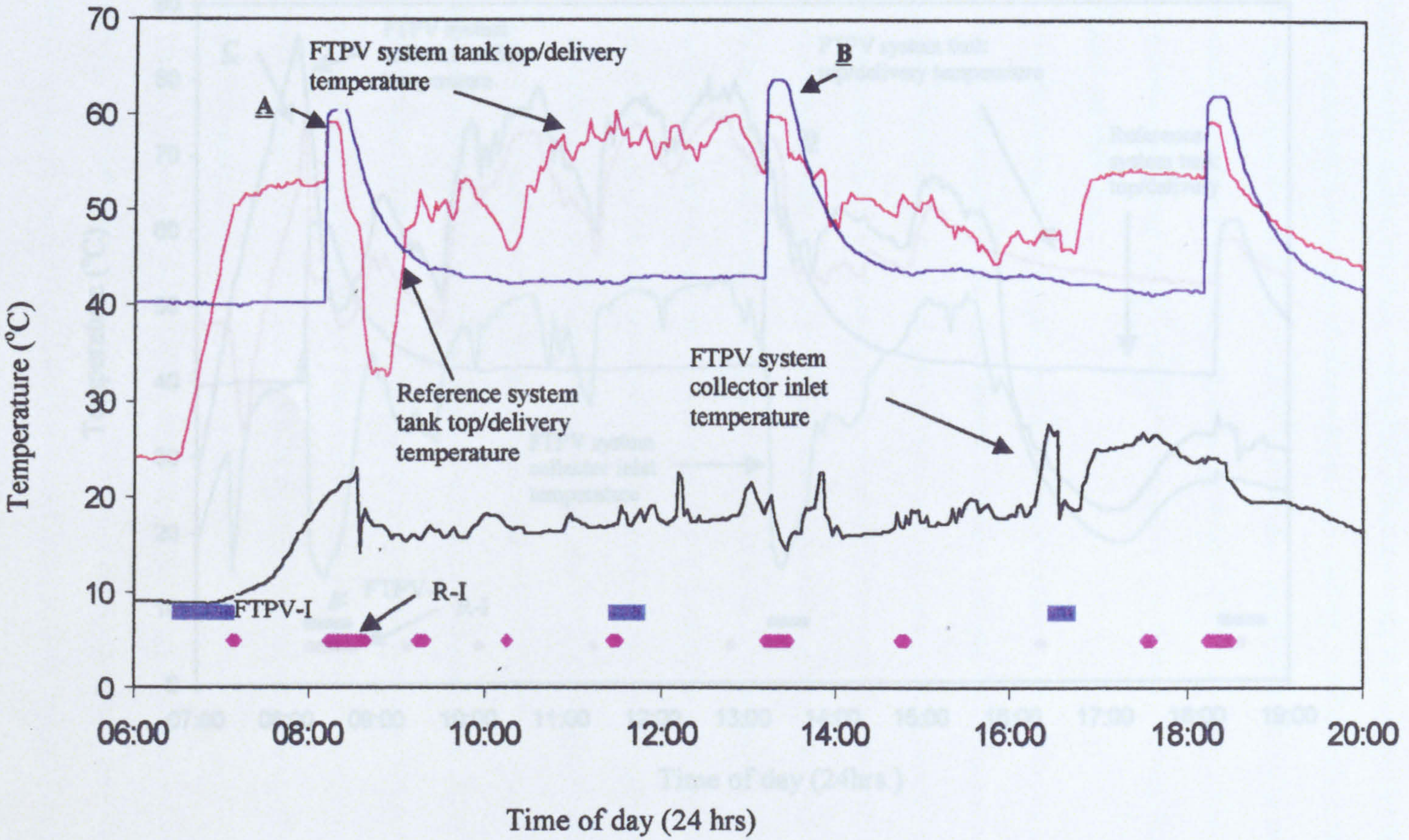

Figure 3.6.2. Tank top/outlet temperature profile and immersion on/switching record (FTPV-I and R-I), for both systems, with the FTPV system operated in TT mode. (17-05-00)

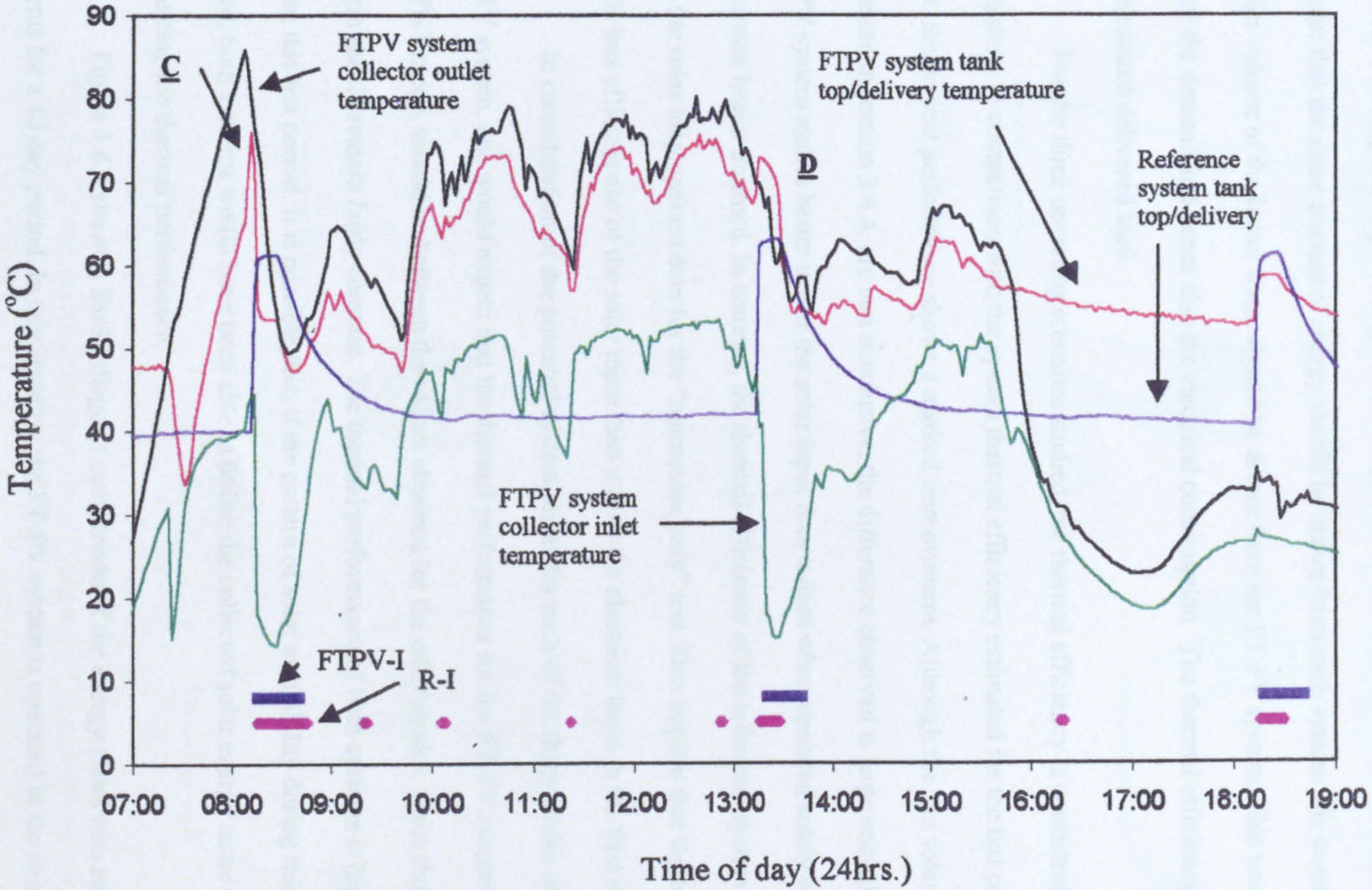

Figure 3.6.3 Tank top/ delivery temperature profile and immersion on/switching record (FTPVI and RI) for both systems, with the FTPV system operated in the BNT mode. (28-05-00)

If, as outlined in section 3.6.2.2, one considers thermal efficiency on the basis of the systems ability to provide water at the pre-set temperature, and neglects the delivery of heat above this temperature, this would imply a reduced delivery from the FT-PV system when operated in either the TNT or BNT modes. Hence, a lower overall thermal efficiency would be observed, and the perceived electrical consumption as percentage of delivered load would increase. Alternatively, if one were to consider that the same amount of energy should be drawn from each system this would imply that a smaller volume of the hotter water should be drawn from the FT-PV system. This would effectively reduce the demand and hence also the electrical consumption. The thermal efficiency is based purely on the measured delivered load.

For the three operating scenarios studied, the thermal efficiency is consistently better for the FT-PV system. In comparison with the system thermal efficiency estimated for the test period with no solar input, the present performance shows a marked improvement. Although the "no solar" values, as discussed in section 3.6.4, are non conclusive, the difference observed is large enough to imply that the FT-PV system makes better use of the solar input than it does when operated solely with the bottom immersion heater untimed. In contrast, the thermal efficiency of the reference system is seen to be lower with the solar loop operant than for the "immersion only" test. This implies that the reference system makes less efficient use of the solar input than it does the electrical input in the first instance.

In consideration of the potential system losses for each of the three modes of operation of the FT-PV system, one would expect that the thermal performance for the FT-PV system, when operated in the TNT mode, should be between the values obtained for the other modes, while that of the reference system should remain fairly constant. The thermal performance of both systems is higher than expected during this test period. It is possible that, if the pattern of solar availability during this period was morning biased, both systems would have been able to utilise the collected solar energy more efficiently, thus enhancing the thermal performance.

Figure 3.6.4 shows a Sanky diagram comparison of the energy flows into and out of both systems for a 13 day period. In this instance, the FT-PV system is operated in the most favourable mode, with the top immersion timed. It can clearly be seen that while the FT-PV system is less efficient at collecting the available solar energy, the electrical consumption is much lower than that for the reference system, (approximately 50 %). The system losses are much greater for the reference system partly

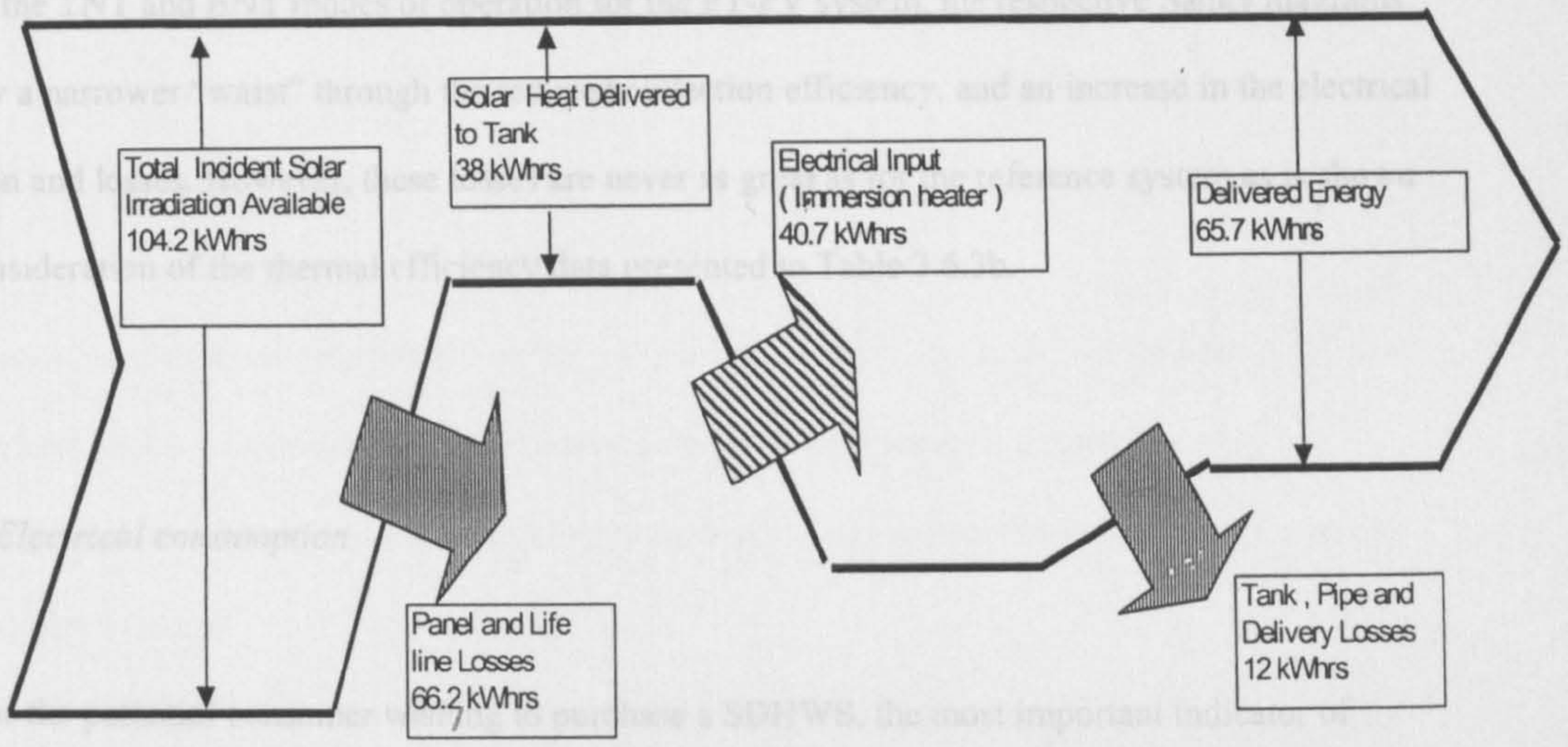

FTPV System

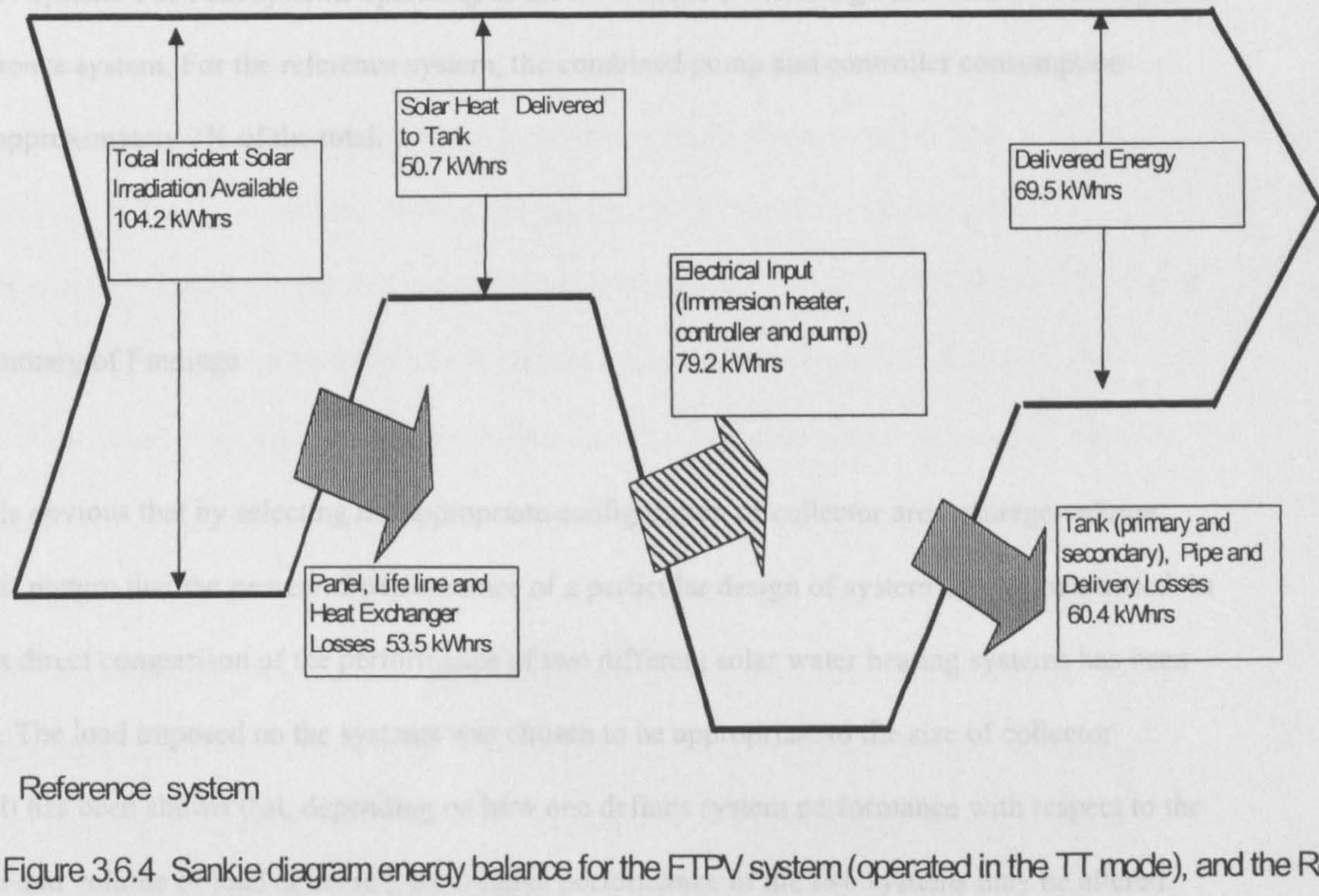

Reference system

Figure 3.6.4 Sankie diagram energy balance for the FTPV system (operated in the TT mode), and the Reference system, for the period 5/05/2000 to 18/05/200

through its operating with a two tank system, but also through operating with the bottom immersion heater untimed.

For the TNT and BNT modes of operation for the FT-PV system, the respective Sanky diagrams would show a narrower "waist" through the reduced collection efficiency, and an increase in the electrical consumption and losses. However, these losses are never as great as for the reference system as is shown through consideration of the thermal efficiency data presented in Table 3.6.3b.

3.6.6.3 Electrical consumption

For the potential consumer wishing to purchase a SDHWS, the most important indicator of performance is the auxiliary energy consumption, or saving. Considering the figures presented for the electricity consumed as a percentage of the delivered load, the FT-PV system consistently out-performs the reference system. For both systems operating in the BNT mode it offers a greater financial saving than for the reference system. For the reference system, the combined pump and controller consumption represents approximately 7% of the total.

3.6.7. Summary of Findings

It is obvious that by selecting the appropriate configuration of collector area, storage volume, and draw off pattern that the perceived performance of a particular design of system can be maximised. In this study, a direct comparison of the performance of two different solar water heating systems has been undertaken. The load imposed on the systems was chosen to be appropriate to the size of collector employed. It has been shown that, depending on how one defines system performance with respect to the temperature and volume of load delivered, the relative performance of the two systems may be altered. However, in the main, for the three modes of operation imposed on the FT-PV system, the FT-PV system has a better thermal efficiency and lower auxiliary demand. Although the FT-PV system has a better

thermal efficiency, there is little difference in the auxiliary demand when both systems are operated with the bottom immersion untimed.

3.6.8 Errors

The sources of external interference on the measurements obtained for the "immersion only" tests presented in section 3.6.4 have already been discussed. Section 3.6.8 presents a summary of instrumentation and measurement errors in relation to their effect on the perceived relative performance of the two systems studied.

As shown in Fig 3.6.1, both systems have identical integrated heat meters to measure the energy delivered to the tank. Raab Karcher combimeter type Q 1.5 meters were used for all heat measurement as these afforded the best accuracy of measurement for the flow rates and operational temperatures of each system. The heat meter specifications are given in Appendix I. Each heat meter comprises a flow meter and two temperature sensors which measure the supply and return to and from the collector, adjacent to the tank. As the heat meter is calibrated for water, a correction factor, as presented in table 3.6.1, is applied to the recorded value of the heat delivered to the tank by the anti-freeze based system.

The heat meters have a temperature measurement tolerance of +/- 0.05 °C. For the FT-PV system, operating with a greater temperature difference across the collector than the reference system, this represents a smaller measurement error. For a collector ΔT of 40 °C this tolerance represents a possible maximum error of 0.25%, whereas, for a reference system ΔT of 15 °C it may account for an error of 0.67%. The heat meters have a power recording range of 0.04 to 84 kW (at $\Delta T = 40°C$). For cooler collector inlet temperatures both systems collectors have a measured maximum output of approximately 1.2 kW. However, the daily operating average was found to be closer to 0.7 kW. During any typical operating period, the time during which either collector output will be less than the above-mentioned minimum of 0.04kW will be limited. This lower limit of measurable power output will therefore have a negligible effect on the cumulative totals of energy delivered to each tank. In consideration of the above mentioned temperature and power measurement tolerances, the data obtained from the heat meters should provide a true record of the energy delivered to the respective tanks over the periods of testing.

In respect of the readings taken for the auxiliary energy demand, the meters used for each system measured to 0.01 kWhrs. In consideration of the totals presented in table 3.6.3b, which have been rounded to 1 decimal place, for the lowest value recorded this represents a maximum possible error of 0.025%, {(0.01/40.7)*100}. Again this will have a negligible effect on the reported performance of both systems.

Section 3.6.6.2 considered the effect of the actual load delivery temperature on performance. For both systems the delivery temperature used in the calculation of delivered load was taken as the average temperature of the fluid leaving the tank during the draw off period. Where this was greater than the immersion pre-set temperature, the additional energy provided was included. As shown in Fig 3.6.3, when both systems are operated with the bottom immersion untimed, for the FT-PV system the delivery temperature frequently exceeds the pre-set. If this additional energy was discounted the delivered energy would be reduced. However, the FT-PV auxiliary demand would be unaffected and, in this respect, the relative performance of the two systems would be unaltered.

3.7 SUMMARY OF EXPERIMENTAL WORK

3.7.1 The effect of limescaling in the FT-PV system

Through the qualitative analysis of the potential effects of limescaling on the FT-PV system it has been shown that there are no additional detrimental effects to system performance through using the carbon-doped EPDM rubber pipe within the absorber.

3.7.2 Measurement of energy stored within the storage tank.

Through measurement of the tank midline axis and external wall temperatures during destratification, their relationship has been defined. The energy stored within the tank can therefore be accurately defined from the external wall temperatures alone. This negates the need for intrusive measurement and hence removes the risk of disturbance to flow within the tank and the potential effect of this on system performance.

3.7.3 Determination of the efficiency characteristic of the Flexsol collector.

A new method for determining the efficiency characteristic of the Flexsol collector under transient conditions has been presented. A least Root Mean Square Error method has been employed to determine the optimum averaging time for the measured irradiance. For a collector flow rate of 0.7 l/min., the efficiency characteristic derived in the above manner agrees well with that calculated from the semi-empirical method.

3.7.4 Optimising the collector flow rate profile and system performance.

A comparison of the optimum flow rate profile for the present system with that as defined by Al-Ibrahim et al (1996) is presented in section 4. However, it has been shown that the desired outlet temperature profile, for the design conditions specified, is not attainable in practice with the simple

control methods applied. Consideration of the plots of collector outlet temperature observed in Figs. 3.5.9, 3.5.10, and 3.6.4, where more realistic operational collector inlet temperatures are observed, implies that the design condition of a relatively stable outlet temperature of approximately 55°C is more readily achievable under real operating conditions. Even with the lesser degree of shading, (50% as opposed to 66%) the outlet temperatures observed are still higher than desired when the FT-PV system is operated with either the top or bottom immersions untimed. These higher temperatures are generally observed prior to a draw off period or later in the day. If the system is to be operated in either of the above modes it may therefore be appropriate to select a lesser degree of shading still. This will increase flow rate, lower outlet temperatures, and improve collector efficiency. Alternatively, a combination of altered shading and orientating the PV module slightly to the west of the collector could provide higher flow rates in the afternoon and therefore help to maintain the desired outlet temperature. This would increase solar gain. Further investigation is required to determine the optimum shading/collector outlet temperature with respect to the immersion pre-set temperature and load profile.

Investigations into the effect of the position of the auxiliary water heater on system performance in forced circulation SWHS, such as those undertaken by Morrison et al (1992), and Furbo and Shah (1996), and also for similar studies relating to the performance of thermosyphon systems, Michaelides and Wilson (1997), have shown that the solar fraction is maximised when the auxiliary supply is external to the solar tank. This has the effect of maintaining lower collector inlet temperatures, thus maximising solar gain, and reducing auxiliary demand for a specified load. The performance of the FT-PV system may therefore be improved through employing this strategy.

3.7.5 Comparative testing of systems performance.

Comparative testing of the FT-PV system with a standard anti-freeze based system has shown that, for the load profile imposed on both systems, the FT-PV system requires less auxiliary input. In respect of the auxiliary power drawn to provide the afore mentioned load, the performance of the FT-PV system is highly sensitive to the position and mode of operation of the electric immersion heater. However, irrespective of which immersion heater is used in the FT-PV system storage tank, for all modes of immersion control, the FT-PV system requires less auxiliary input, and is therefore cheaper to run.

REFERENCES

A.E.S. (1983), Communication from Cardiff University to Appropriate Energy Systems re: collector testing.

A.E.S., (1999), Appropriate Energy Systems, Solar Water Heating System Installation Guide. A.E:S Ltd, The Park, Forres, Scotland.

Al-Ibrahim A. M., Klein S.K., Mitchell J.W., Beckman W.A.(1998). Design procedure for selecting an optimum photovoltaic pumping system in a solar domestic hot water system. *Solar Energy* Vol. 64, Nos 4-6, pp.227-239.

Al-Ibrahim A.M., (1997), Optimum selection of direct coupled photovoltaic pumping system in solar domestic hot water systems. PhD Thesis, University of Wisconsin-Madison.

Al-Nimir M.A., (1993), Temperature distribution inside a solar collector storage tank of finite wall thickness. *Transactions of the ASME JSEE,* Vol. 115, pp 112 – 116.

Amer E.H., Nayak J.K., and Sharma G.K., (1997), Transient test methods for flat – plate collectors: review and experimental evaluation. *Solar Energy,* Vol. 60, No.5, pp 229 – 243.

B.P., (1999), Solar Electric Module Specification Data, www.bpamoco.com

B.S., (1986), British Standard 6757: Method of test for thermal performance of solar collectors. British Standards Institute.

Bowman N.T., Redferne W.B., and Eldessouky E., (1981), Stratified solar storage for use in domestic scale systems. *Sun at Work in Britain,* No. 12/13.

Bryant T., (1998), Personal Communication, Terry Bryant, Research and Development at Thames Water Board.

Charles Austen, (1999), Charles Austin Pumps Ltd. West Byfleet, Surrey. Pump model LD2 specification sheet.

Csordas G.F., Brunger A.P., Hollands K.G.T., and Lightstone, M.F., (1992), Plume entrainment effects in solar domestic hot water systems employing variable flow rate control strategies. *Solar Energy,* Vol. 49, No.6, pp 497-505.

Duffie J.A. and Beckman W.A. (1991) *Solar Enginering of Thermal Processes,* 2nd edn, Wiley Interscience, New York . ISBN 0-471-51056-4

Eldessouky E.A.E., (1985), Comparison of measured and predicted results for a domestic thermally stratified solar storage container. *Proceedings of INTERSOL '85.* 9th biennial congress of the ISES. Vol. 2, Bilgen E., Hollands K.G.T., Eds. Pergamon Press.

Furbo S., (1990), Attractive small marketed hot water solar heating systems using low flow operation. In *Proceedings of Northsun '90,* Reading, England, Sayigh A.A.M. (Ed), Pergamon Press, Oxford

Furbo S., and Shah L.J., (1996), Optimum solar collector fluid flow rates. In *Proceedings, EuroSun '96.* Section II-46. *Pub* ISES, DGS Sonnenenergie Verlags-GmbH, Munich.

Hahne E. and Chen Y., (1998), Numerical study of flow and heat transfer characteristics in hot water stores. *Solar Energy,* Vol. 64, Nos. 1 – 3, pp 9 - 18.

Hausner R., and Fechner H., (1998), Influence of the flow condition (laminar/ turbulent) in the fluid tube on the collector efficiency factor of a fin absorber. In *Proceedings of EuroSun 1998*, 14-17 September, Portoroz, Slovenia, Goetzberger A. and Krainer A. (Eds)Volume 2 Section III.2 13. The Franklin Company Consultants Ltd, Birmingham, UK.

Hoogendorn C.J., Bakker R.G., Herweijer E.J.J., and Plokker W., (1985), Thermal stratification in water vessels for energy storage.

Issa M., and Al-Nimir M., (1989), Temperature distribution inside hot water storage tanks of solar collectors. *Transactions of the ASME JSEE,* Vol. 111, pp 311 – 317.

Ledion J., Gueugnon Y., Ribal C., and Combaz P., (1993), Encrustation of the surface of plastic materials. *Techniques, Sciences, Methodes,* Vol. 88, Nos.7/8, pp 355 – 360. (In French)

Mavros P., Belessiotis V., and Haralambopolous D., (1994), Stratified energy storage vessels: characterisation of performance and modelling of mixing behaviour. *Solar Energy,* Vol. 52, No. 4, pp 327 – 326.

Michaelides I.M., and Wilson D.R., (1997), Simulation studies of the position of the auxiliary heater in thermosyphon solar water heating systems. *Renewable Energy,* Vol. 10, No.1, pp 35 – 42.

Morrison G.L., Gilliaert D., and Tebaldi P., (1992) Outdoor testing of solar water heaters- effects of load pattern and auxiliary boosting. *Solar Energy.* Vol. 49, No. 4. pp 299 – 308.

Mutch J.J., (1974), Residential water heating, fuel conservation economics and public policy. Rand corporation. R-1498-NSF.

Papakostas K.T., Papageorgiou N.E., Sotiropoulos B.A., (1995), Residential hot water use patterns in Greece. *Solar Energy,* Vol. 54, No. 6, pp 369 – 374

Pierson P., and Padet J., (1990), Time constant of solar collectors. *Solar Energy,* Vol. 44, No. 2, pp 109-114.

Proctor D., (1984), A generalised method for testing all classes of solar collector, parts I and II. *Solar Energy,* Vol. 32, No. 3, pp. 377 – 394.

Radio Spares (2000), On-line product information, http://rswww.com

Vliet G., and Baker D., (1992), Designing solar hot water systems for scaling environments. *ASHE JSES ITSES International Solar Energy Conference.* ISBN 0791807622.

Wang X.A., Xu Y.F., and Meng X.Y., (1987), A filter method for transient testing of collector performance. *Solar Energy.* Vol. 38, No. 2, pp. 125-134.

Wuestling M.D., Klein S.A., and Duffie J.A., (1985), Promising control alternatives for solar water heating systems. *ASME Journal of Solar Energy Engineering* Vol. 107.

4. MODELLING SYSTEM PERFORMANCE

4.1 INTRODUCTION

A model that can accurately simulate a physical system and predict the values of system parameters as a result of different operating scenarios is obviously a valuable design tool. The main aim of this study has been to design a simple computer model for simulating the performance of the FT-PV system, while maintaining the mathematical rigour required to provide accurate results.

If the simulation package is user friendly in terms of operation, and interpretation of results, it will stand a greater chance of being accepted in the broader market place. Presently, the majority of personal computers, and many networked computers, use the Microsoft Windows® operating system and associated Microsoft Office® (MO) software. While it is possible, via dynamic link libraries, to transfer data between the MO spreadsheet package, "Excel", and computationally more powerful programmes such as Fortran, all modelling has been undertaken in the Microsoft Excel/Visual Basic for Applications environment to maintain simplicity and broader applicability.

Section 4 details the development of a suite of short programmes that have been designed to predict the collector outlet temperature, with respect to the two methods of flow control detailed in sections 3.5.3 and 3.5.4, and to define the tank temperature profile during charging and destratification. The performance of these models is assessed through a comparison of predicted and experimental data.

While, within the limits of this project, it has not been possible to produce an extensive systems simulation package, the present work provides a foundation from which a fuller long-term performance model may be developed.

To provide an outline of the above-mentioned programs operating structure, a brief overview of the Microsoft Excel/Visual Basic for Applications environment is now presented.

4.2 THE VISUAL BASIC / MICROSOFT EXCEL ENVIRONMENT

Microsoft Excel/ Visual Basic for Applications (VBA) provides an environment that gives the user a greater flexibility in designing engineering simulation models using the spreadsheet format. Simpler formulae may be entered directly into spreadsheet cells whereas, for more complex calculations, analyses and data retrieval, programs and commands may be written in Visual Basic language in units termed "Macros". "Macros" are designed in the VBA platform that is provided behind the spreadsheet, to which access is gained by pressing the keyboard "Alt" and "F11" keys simultaneously.

The VBA platform enables easier data input, manipulation and management, than would normally be afforded by a stand-alone spreadsheet programme. The above mentioned "Macros" can be designed to import the required data in spreadsheet cells, perform the relevant calculations, and export the results to specified cells within the spreadsheet. They can also be used to open files out-with the Excel "Workbook" and retrieve relevant data. Through "Macros" it is therefore possible to communicate with other workbooks and programmes, for example, Fortran PowerStation, if necessary. In addition, customised User Input Forms, again designed in Visual Basic, can be presented in the spreadsheet environment, allowing easy input of key data and option choices. These Input Forms can be designed so that the relevant VBA programs are set running without the need for the end user to enter the VBA environment.

All computing and graphical facilities are therefore managed within an Excel Workbook, which can contain a number of spreadsheets, program design modules, live graphs and input forms. Figure 4.2.1 shows a schematic of the above-mentioned environment.

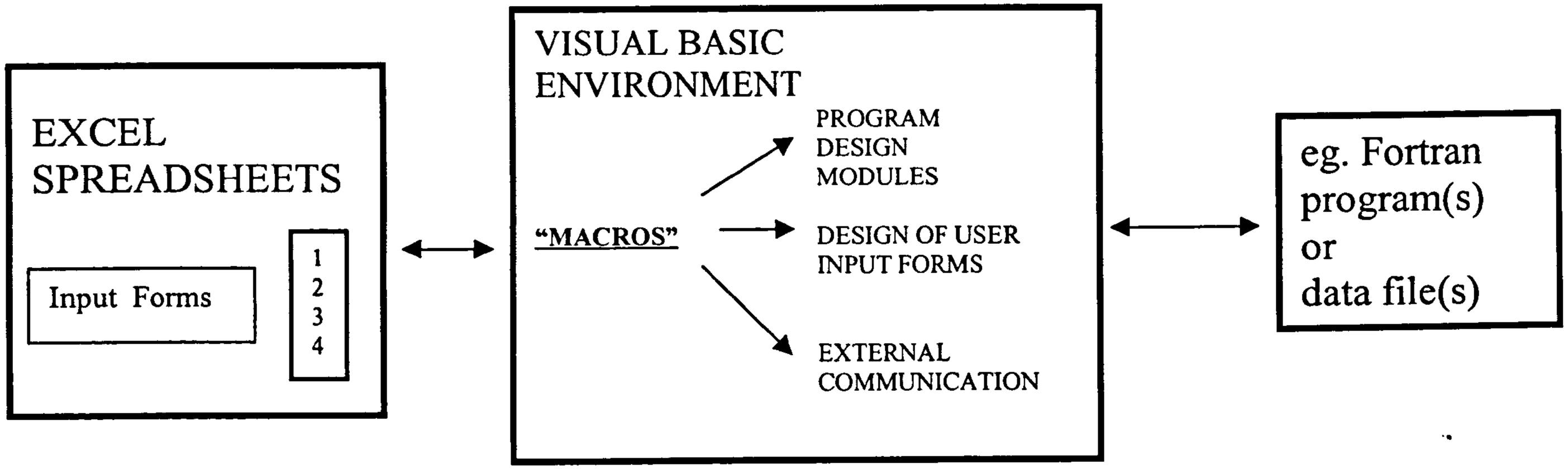

Figure 4.2.1 Schematic diagram of the Microsoft Excel/ Visual basic for Applications environment

4.3 DEFINING THE OPTIMUM COLLECTOR FLOW RATE PROFILE

4.3.1 Introduction

The concepts of an optimum collector flow rate, and subsequent optimum variable flow rate profile were introduced in section 2.3.3, and again, briefly, in section 3.5.1. In considering the design criteria of a constant collector outlet temperature of 55 °C, based on the design conditions of a collector inlet and ambient air temperature of 15°C, and the measured collector efficiency characteristics, (section 3.4) the optimum flow rate profile for the present FT-PV system is now presented.

4.3.2 The optimum profile.

In section 3.4 the collector efficiency characteristic (CEC) was calculated for 5 distinct flow rates. Considering the CEC to be of the form given in Eq. 4.3.1, and performing a regressional analysis with respect to flow rate, enables the parameters X and Y to be defined for any operational flow rate.

$$\eta = X - Y\,[((T_O + T_I)/2 - T_A)]/\,G \qquad (4.3.1)$$

While the above parameters have so far been presented in relation to the collector volume flow rate (l/min), considering them in relation to the system mass flow rate makes their application in the present analysis simpler. It is assumed that the density of water is constant at $\rho = 1000\ kg/m^3$. Figure 4.3.1 shows a plot of the parameters X and Y versus the collector mass flow rate, (m_C in kg/s). Applying a second order polynomial best fit to each curve yields the respective relationships and coefficients of determination given in Eqs. 4.3.2 and 4.3.3. Parameter X is dimensionless while Y has the unit W/m^2K.

$$X = -1479.7\ m_C^2 + 34.5\ m_C + 0.46 \qquad (R^2 = 0.9683) \qquad (4.3.2)$$

$$Y = -29007\ m_C^2 + 651.3\ m_C + 0.074 \qquad (R^2 = 0.9863) \qquad (4.3.3)$$

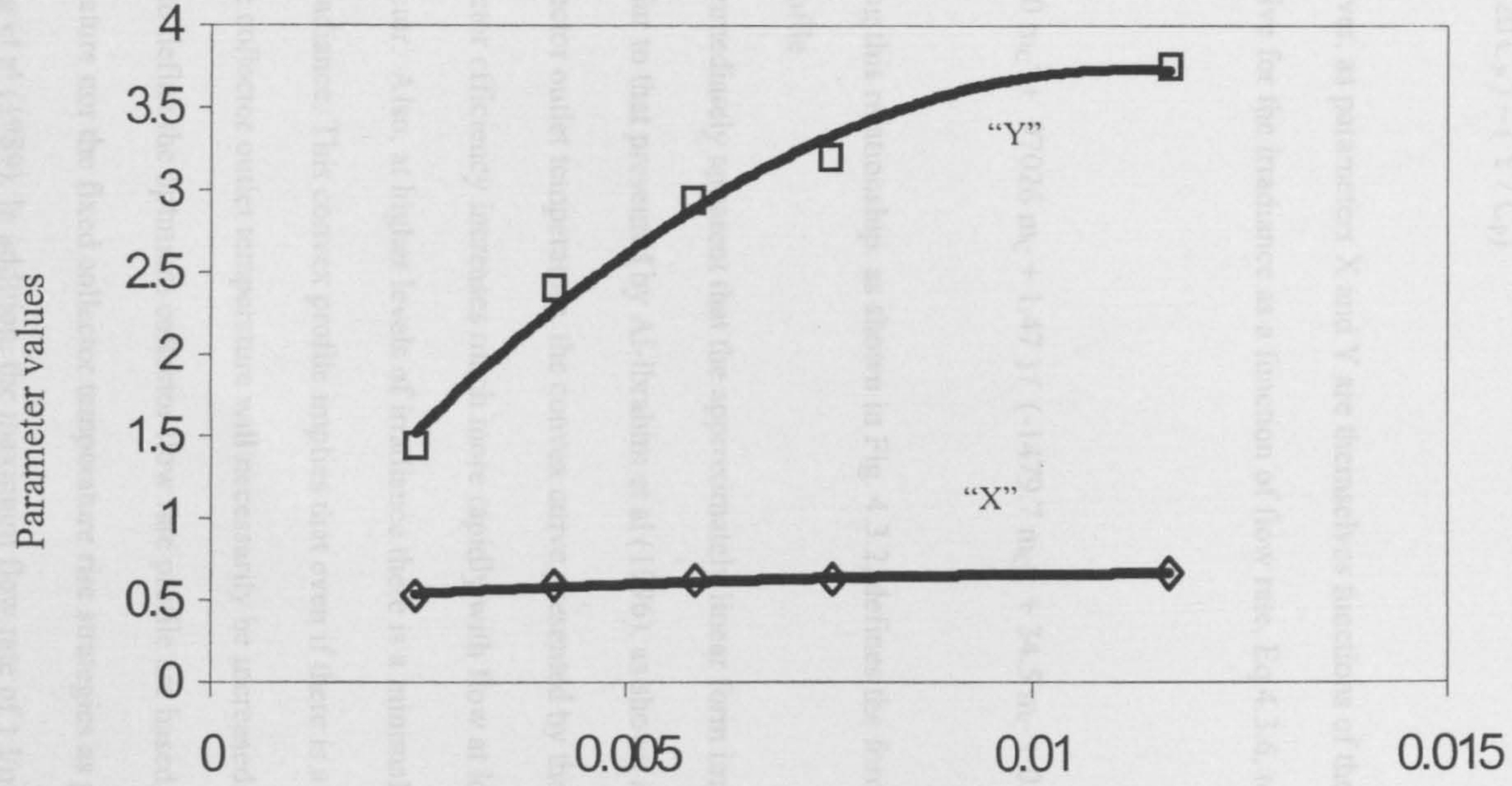

Figure 4.3.1 Plot of collector efficiency characteristic parameters versus collector mass flow rate

Substituting the above mentioned design conditions in Eq. 4.3.1, and combining this with the collector efficiency expression given in Eq. 4.3.4 below, yields an expression for the optimum collector flow rate as a function of irradiance. This relationship is given in Eq 4.3.5.

$$\eta = m_C (T_O - T_I) C_P / A_C G \quad (4.3.4)$$

$$m_C = (G X / 20 C_P) - (Y / C_P) \quad (4.3.5)$$

However, as parameters X and Y are themselves functions of the collector flow rate, m_C, it is simpler to solve for the irradiance as a function of flow rate, Eq 4.3.6, to obtain the form of the optimum flow profile.

$$G = (-580140\ m_C^2 + 97026\ m_C + 1.47) / (-1479.7\ m_C^2 + 34.5\ m_C + 0.46) \quad (4.3.6)$$

Plotting this relationship, as shown in Fig. 4.3.2, defines the form of the optimum flow rate versus irradiance profile.

It is immediately apparent that the approximately linear form implied by the above analysis is quite dissimilar to that presented by Al-Ibrahim et al (1996), as shown in Fig 3.5.1. To maintain a constant collector outlet temperature, the convex curve presented by the aforementioned authors implies that the collector efficiency increases much more rapidly with flow at lower flow rates than it does for the present collector. Also, at higher levels of irradiance there is a minimal increase in the optimum flow for increasing irradiance. This convex profile implies that even if there is a negligible increase in efficiency at this point, the collector outlet temperature will necessarily be increased. This therefore suggests that the criteria used to define the optimum collector flow rate profile are based on neither the constant collector outlet temperature nor the fixed collector temperature rise strategies as presented by Csordas et al (1992), and Wuestling et al (1989). In addition, the maximum flow rate of 1 l/min defined by Al-Ibrahim et al (1996), for the specified area and efficiency characteristic of that collector, implies an collector outlet temperature much greater than the defined load delivery temperature of 60°C.

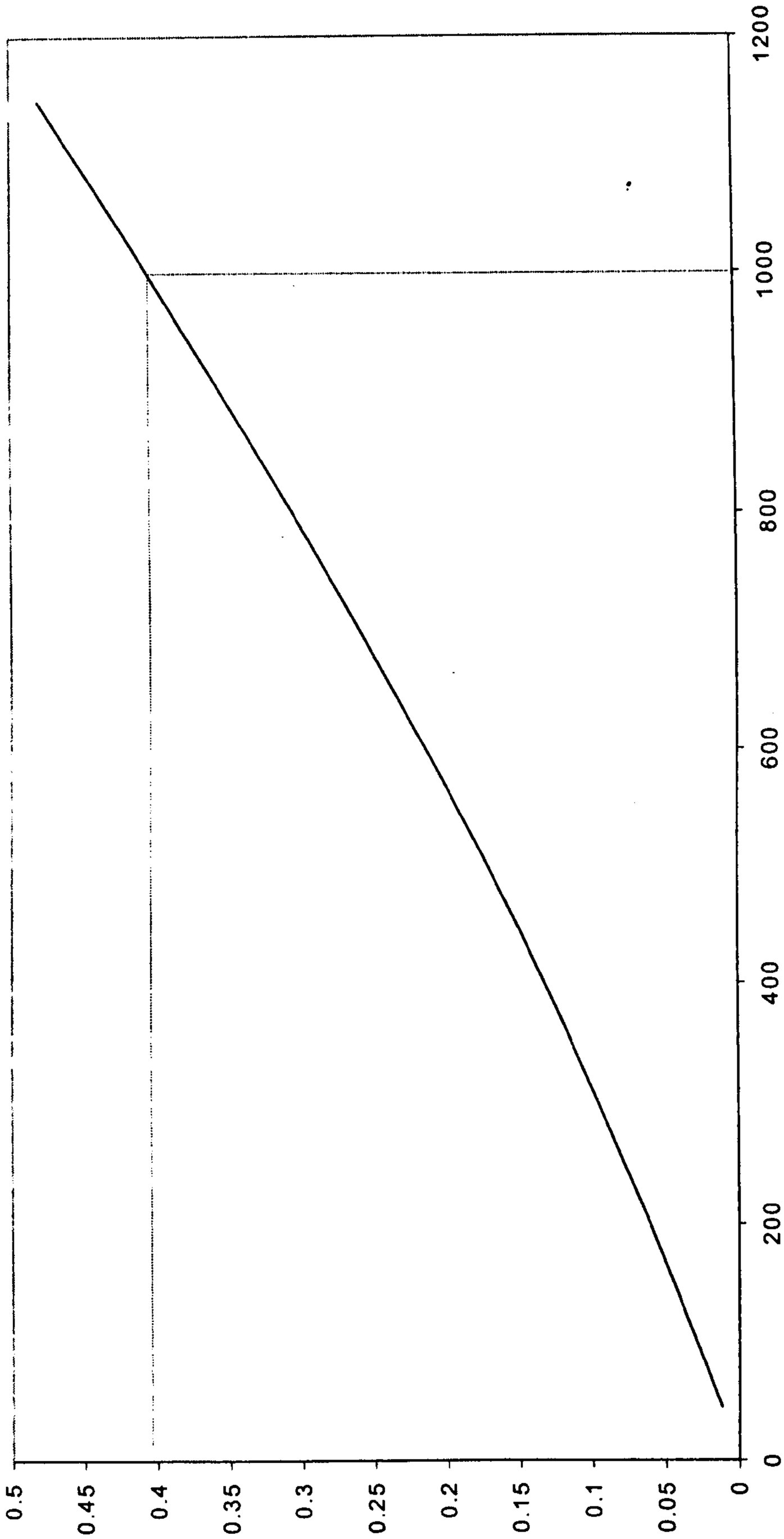

Figure 4.3.2 Plot of the optimum flow rate profile for the FT-PV system

4.4 MODELLING THE EFFECT OF PHYSICAL SHADING ON THE COLLECTOR OUTLET TEMPERATURE

4.4.1 Introduction

While section 4.3 considered the optimum flow profile for the present system and compared that with the form presented by Al-Ibrahim et al (1996), the experimental work detailed in section 3.5 considered collector/system performance in terms of the outlet temperature profile. This may be regarded as an indicator of the extent to which the flow rate was optimised for each of the methods and degree of control applied. Section 4.4 presents an overview of an algorithm that has been developed to define the collector outlet temperature profile as a function of the method and degree of control applied.

4.4.2 Estimation of the effect of physical shading on the collector outlet temperature

As presented in section 3.5, for the range of shadings studied, the relationship between irradiance and PV module current was found to be that as defined by Eq 4.4.1.

$$I_A = \{(1*10^{-4}\ G^2) - (0.132\ G) + (188 - [(\%\ \text{shading} - 50)*3])\} * (G/1000) \qquad (4.4.1)$$

As the pump load line lies to the left of the module maximum power point locus, for any degree of shading between 50% and 70%, Eq. 4.4.1 allows the module current to be defined for a given level of irradiance. As the pump electrical characteristics have previously been defined, (section 3.5.2.2), the voltage applied to the pump can therefore be determined for the above irradiance. From this operational voltage, using the voltage/flow rate relationships defined in section 3.5.2.3, the collector flow rate is thence defined.

Considering the collector efficiency characteristic to be of the form given in Eq. 4.3.1 and equating this with Eq 4.3.4 yields the expression for the collector outlet temperature given in Eq 4.4.2

$$T_O = [(2 A_C G X) - (A_C T_I Y) + (2 A_C T_A Y) + (2 m_C C_P T_I)] / [(2 m_C C_P) + (A_C Y)] \qquad (4.4.2)$$

As the parameters X and Y are dependant on the collector flow rate, suitable values must be chosen for application in the above equation to provide an accurate estimation of the collector outlet temperature. While the second order polynomial regression referred to in section 4.3 afforded a definition of the approximate form of the optimum collector flow rate profile, selection of the above mentioned collector efficiency characteristic parameters, including interpolated values for lower flow rates, based on conditional limits of flow rate, as given in table 4.4.1 was found to afford a better comparison with the measured collector outlet temperature.

Figure 4.4.1 shows a plot of the predicted collector outlet temperature profiles for 4 degrees of shading. The approximate irradiance threshold/pump cut in levels are also indicated.

4.4.3 Comparison of predicted with measured values.

Section 4.4.3 considers the adjustments that need to be made to the above-defined predicted steady state collector outlet temperature profiles in order to provide a more accurate estimation of the measured temperature profile.

4.4.3.1 Averaging the values of predicted outlet temperature.

The predicted outlet temperature profiles presented in Fig. 4.4.1 are calculated for steady state values of irradiance. The algorithm thus far presented does not take the collector time constant/ system thermal lag into consideration. For accurate comparison of predicted values with measured temperatures, this must be taken into account. It was shown in section 3.4 that the collector had a time constant (τ), of approximately 4:35 minutes, and that, in determining the collector efficiency characteristics, the most consistent data sets were obtained using a 12-minute average of previous irradiance values. The predicted

Table 4.4.1. Collector efficiency characteristics and conditional flow limits

Flow Rate (l/min)	Collector Efficiency Characteristic (experimental results)	Flow Range of Application (l/min)
0.70	$\eta = 0.66 - 3.80\ ([(T_O + T_I)/2] - T_a)/G$	$V_f > 0.575$
0.45	$\eta = 0.63 - 3.40\ ([(T_O + T_I)/2] - T_a)/G$	$0.40 < V_f \leq 0.575$
0.35	$\eta = 0.62 - 2.94\ ([(T_O + T_I)/2] - T_a)/G$	$0.30 < V_f \leq 0.40$
0.25	$\eta = 0.59 - 2.41\ ([(T_O + T_I)/2] - T_a)/G$	$0.20 < V_f \leq 0.30$
0.15	$\eta = 0.53 - 1.44\ ([(T_O + T_I)/2] - T_a)/G$	$0.125 < V_f \leq 0.20$
Interpolated values		
0.10	$\eta = 0.50 - 1.03\ ([(T_O + T_I)/2] - T_a)/G$	$0.075 < V_f \leq 0.125$
0.05	$\eta = 0.42 - 0.80\ ([(T_O + T_I)/2] - T_a)/G$	$0.020 < V_f \leq 0.075$

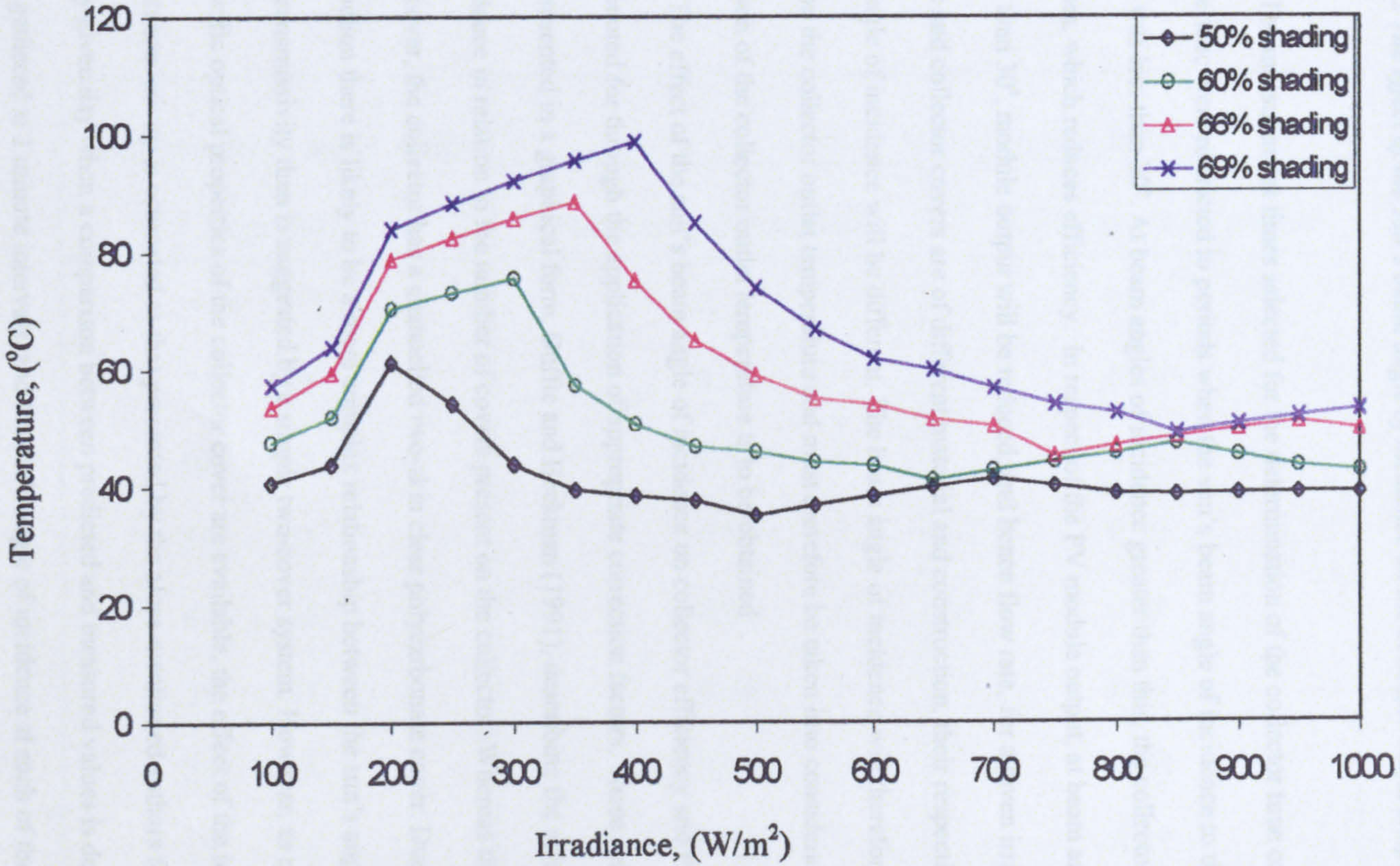

Figure 4.4.1 Predicted collector outlet temperature for four degrees of shading

values of outlet temperature are therefore calculated as the average of the instantaneous values for the previous 12 minutes.

4.4.3.2 The effect of the sun 's beam angle of incidence on the collector outlet temperature.

The measurement times selected for the determination of the collector time constant and efficiency characteristic were restricted to periods when the sun's beam angle of incidence to the collector surface normal was less than 30°. At beam angles of incidence greater than this, the collector cover transmissivity decreases, which reduces efficiency. In respect of the PV module output, at beam angles of incidence greater than 30°, module output will be reduced, and hence flow rate, for a given irradiance. As the PV module and collector covers are of different material and construction, their respective responses to the sun's angle of incidence will be different. The beam angle of incidence will therefore have a marked effect on the collector outlet temperature and must therefore be taken into consideration if an accurate prediction of the collector outlet temperature is to be obtained

The effect of the sun's beam angle of incidence on collector efficiency and PV module output may be accounted for through the application of appropriate correction factors. These correction factors are often presented in a graphical form, Duffie and Beckman (1991), describing the effect of the beam angle of incidence in relation to the number of covers present on the collector. Whereas the PV module has a single cover, the collector has a channelled two-skin clear polycarbonate cover. Due to the nature of this construction there is likely to be a more complex relationship between the sun's angle of incidence and cover transmissivity than is suggested by a simple two-cover system. However, as no data pertaining to the specific optical properties of the collector cover are available, the effect of the incidence angle on cover transmissivity is estimated as that presented by the afore-mentioned authors for a 2-cover system. For any given day when a comparison between predicted and measured values is desired, experimental data is gathered at 2 minute intervals, and the sun's angle of incidence at each of these intervals calculated using the equations presented by Duffie and Beckman (1991), {pages 11-15}.

Table 4.4.2 outlines the appropriate correction/multiplication factors to be applied to the collector and the PV module with respect to the calculated angle of incidence. For the collector, the

Table 4.4.2 . Sun angle of incidence correction factors for the Flexsol collector and PV module covers.

Beam incidence angle range (Degrees)	Multiplication factors	
	Irradiance to PV module	Collector ($\tau\ \alpha$) product
> 85	0	0
75 - 85	0.25	0.20
65 - 75	0.58	0.45
55 - 65	0.81	0.76
45 - 55	0.95	0.87
35 - 45	0.96	0.94
25 - 35	0.97	0.96
15 - 25	0.98	0.97
Up to 15	1.0	1.0

multiplication factor is applied solely to the positive term containing the $\tau\,\alpha$ product, whereas, for the PV module, it is simply applied to the observed irradiance, prior to any further calculation. Again, for application in the algorithm, conditional limits are set, as shown, to define the appropriate factors to be selected.

Figure 4.4.2 shows a flow chart of the steps, as outlined above, that are required to calculate the collector outlet temperature for the present case.

To highlight the effect of including the beam incidence angle correction factors on the accuracy of the predicted outlet temperature, Figure 4.4.3 shows a plot of the measured outlet temperature, and two predicted value data sets. The first of these predicted value sets, P1, does not include the above mentioned correction factors, whereas the second set, P2, does. At smaller beam incidence angles, plots P1 and P2 are seen to converge. However, if the correction factors are omitted, at higher beam incidence angles, particularly above 45°, the model grossly overestimates the outlet temperature.

4.4.3.3 Comparison of predicted with measured values

Figure 4.4.4 shows a plot of the measured and predicted outlet temperature for a 66% shading of the PV module. The measured values were presented earlier in Fig 3.5.7, with the irradiance, collector inlet and air temperatures, sun angle and degree of shading used as inputs for the present model. It can be seen that there is good agreement between the predicted and measured values throughout the day, with the predicted temperature rise across the collector typically within 5% of that measured for normal operation. The greatest divergence from the measured outlet temperature is observed at either end of the measurement period. This is now explained.

The model is designed primarily to calculate the flow and outlet temperature from the collector. The measured value of outlet temperature is that as measured at the collector outlet and does not always represent a delivered temperature. At lower irradiance levels when the pump is not running this measured temperature reflects the temperature of the stagnant water at the collector outlet. The algorithm presented considers that there is no useful net energy collected if the flow rate drops below 0.02 l/min, which is approximately 5 % of the design maximum. If this condition is met, the collector outlet temperature is

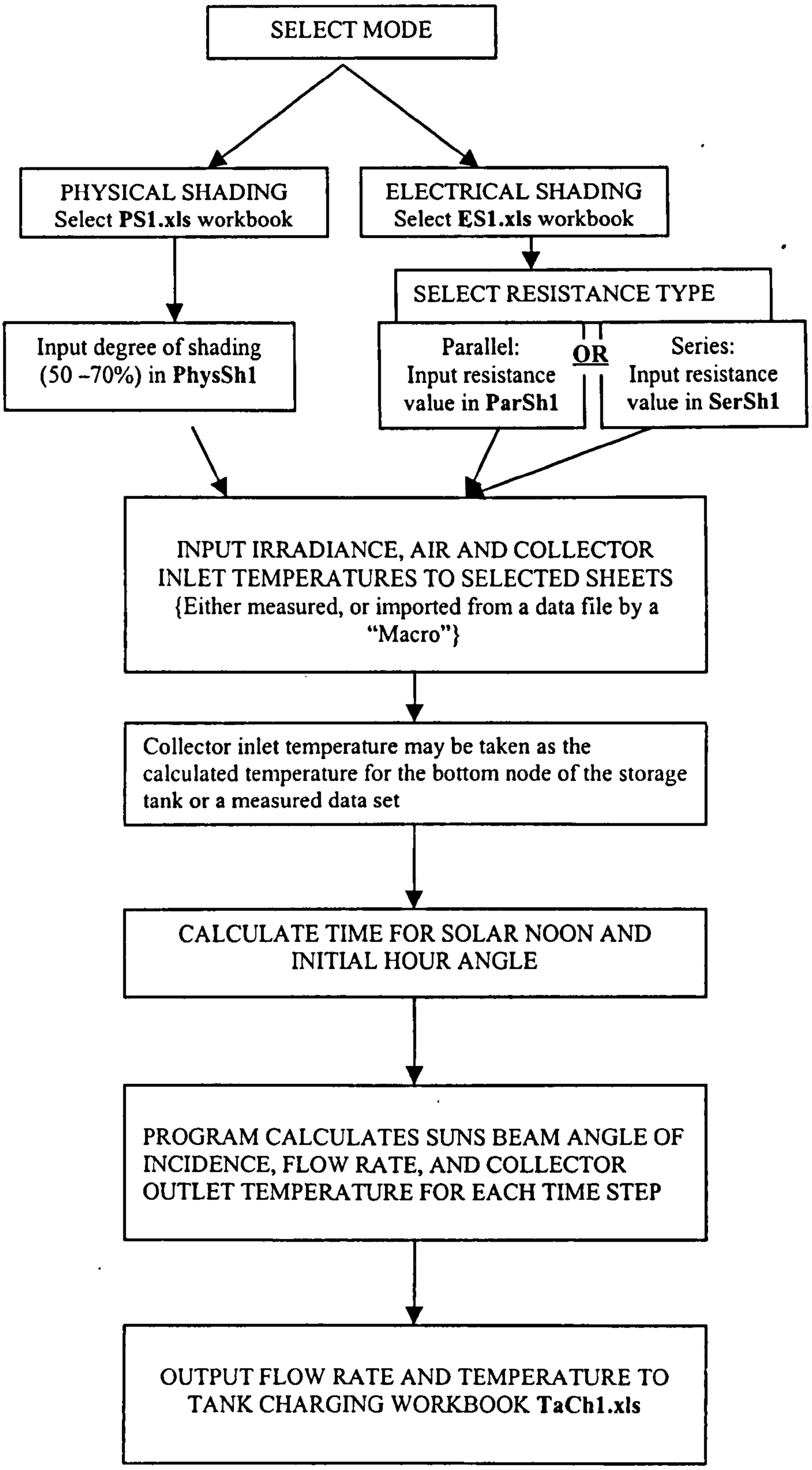

Figure 4.4.2 Flow chart of collector outlet temperature algorithm.

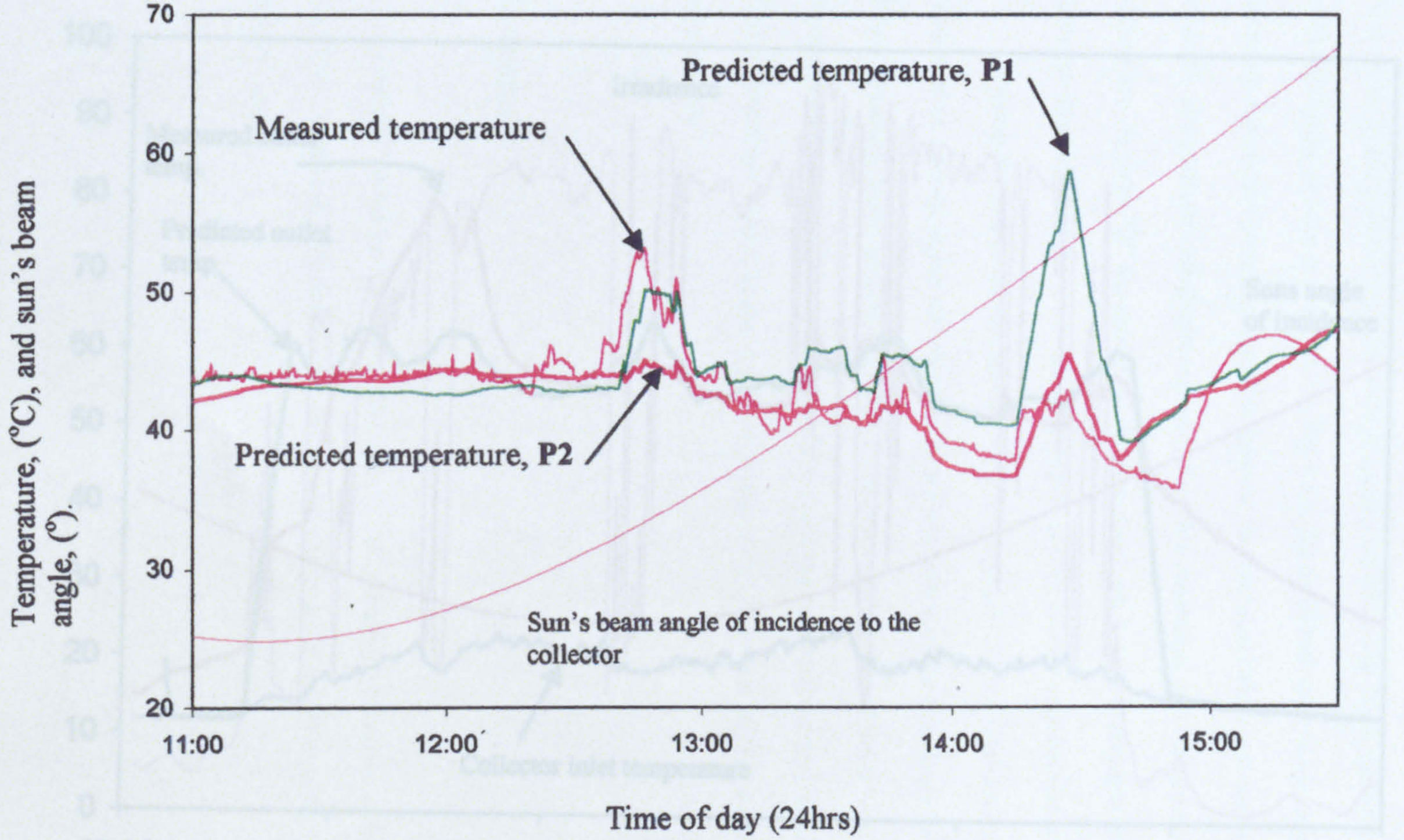

Figure 4.4.3 Plot of measured collector outlet temperature, and two plots of predicted temperature. Plot P1 , sun's beam angle effect not included. Plot P2 predicted outlet temperature including correction factors for beam angle effect

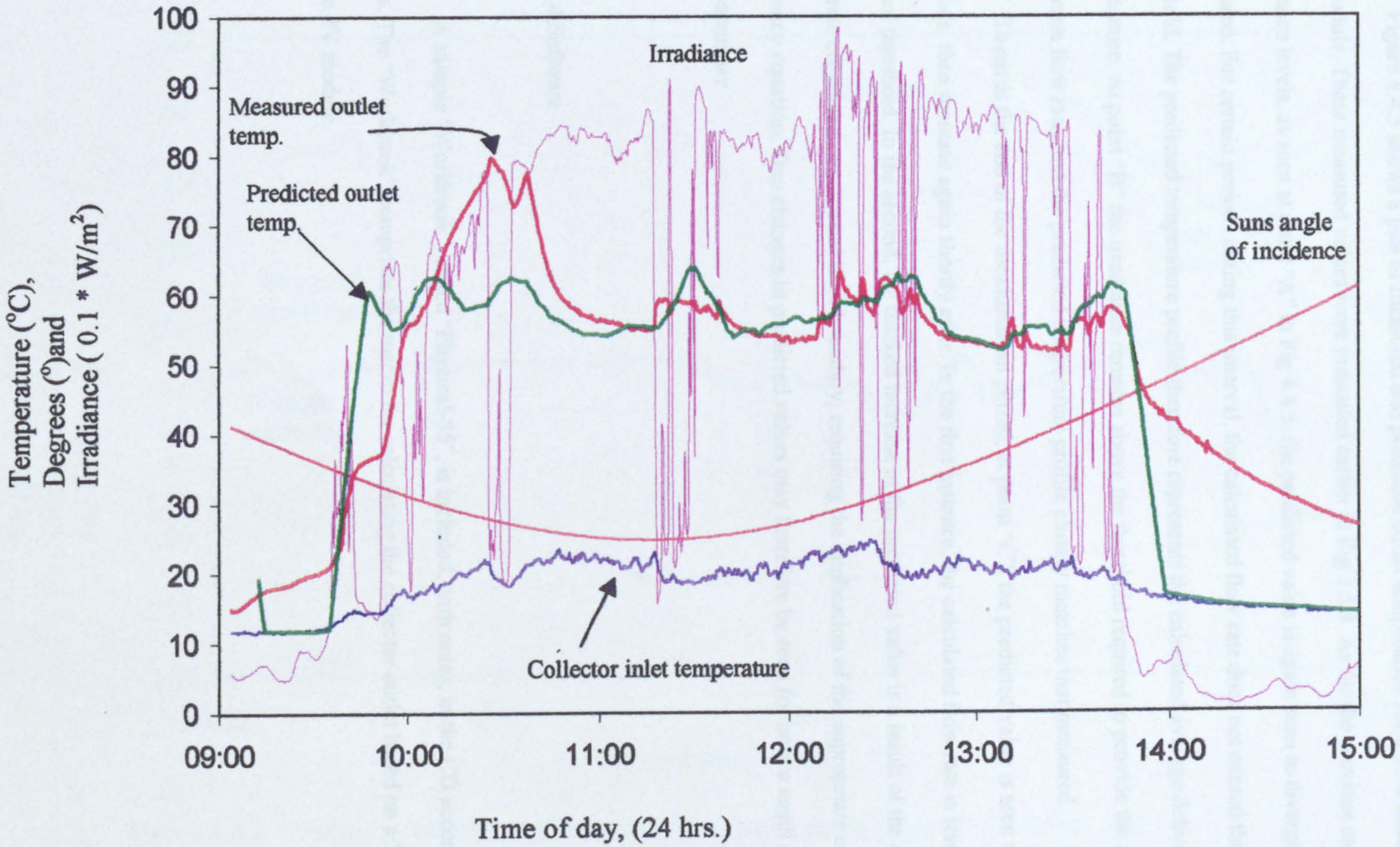

Figure 4.4.4 Predicted and measured outlet temperature for 22nd. October 1999 (66% shading)

defined to be the same as inlet, and the predicted value again calculated as the average for the previous 12 minutes. This produces the sharp rise seen in the predicted temperature at pump cut in, and the steep drop at cut out.

Figure 4.4.5 shows a plot of measured and predicted outlet temperature for a 55% shading of the PV module. These measured values were presented earlier in Fig 3.5.8. As for the previous case, at lower irradiance levels, as seen at point "A" in Fig 4.4.5, the predicted value is again seen to diverge from the measured. For certain periods during this interval, the calculated flow rate does not exceed the model threshold. The predicted temperature profile therefore represents the calculated average delivery temperature. At point "B" the irradiance remains above the threshold required to provide the defined minimum flow rate, and the predicted temperature profile closely matches that measured.

Towards the end of the measurement period, at point "C", the predicted value is seen to rapidly decrease, then increase again shortly after. In the first instance, the calculated flow rate is less than the defined threshold. In the second, the marked increase in the predicted value is a result of the calculated flow rate crossing a conditional limit boundary, requiring the application of the appropriate collector efficiency equation. Step changes in predicted values may therefore be seen for only a small change in one parameter.

4.4.4 Software

A sample "Workbook", called "Physical-55", is included, with notes, in the CD accompanying this thesis. The "Workbook" comprises the macro for calculating the collector outlet based on a 55% shading of the PV module.

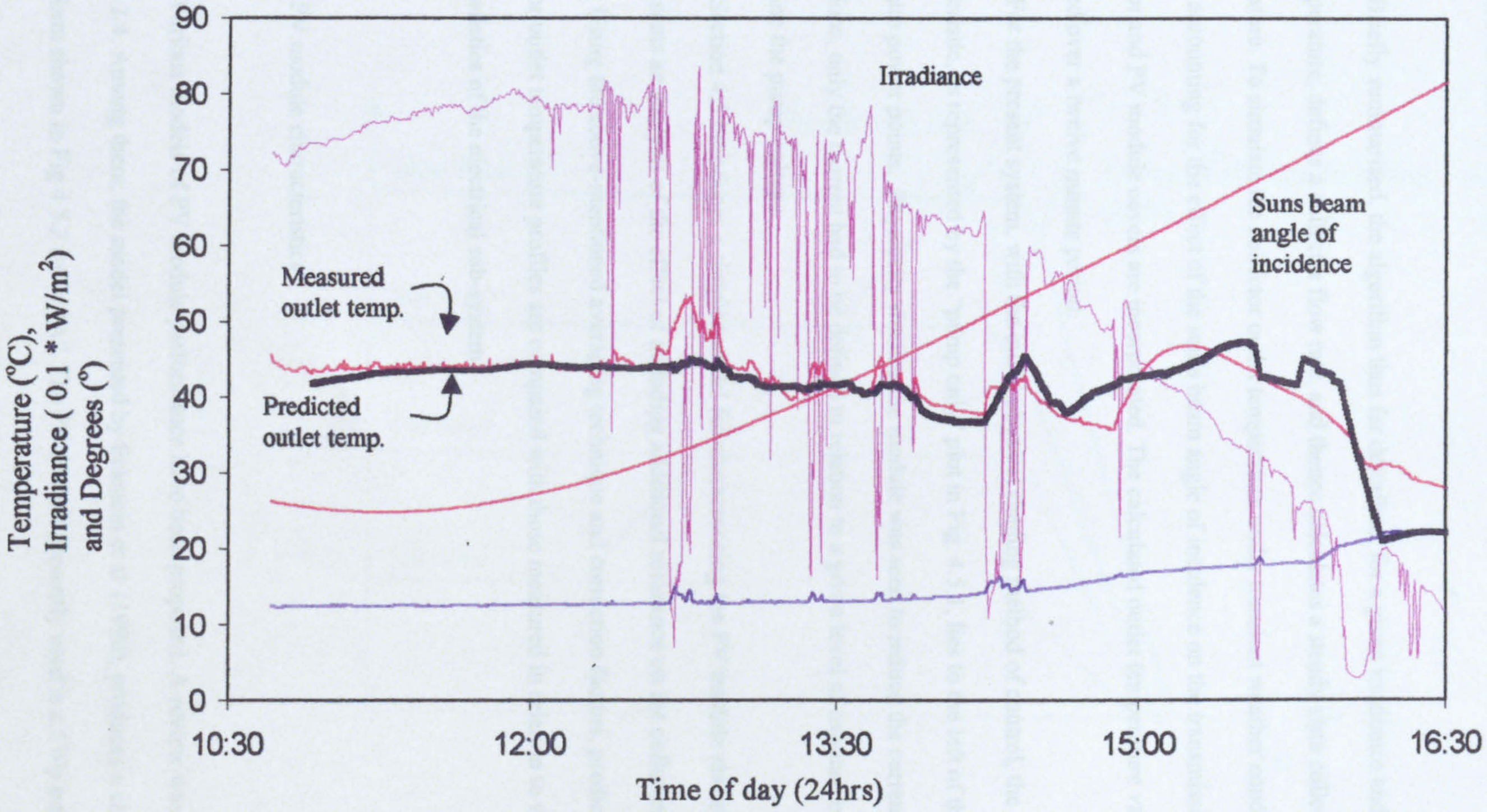

Figure 4.4.5. Irradiance, collector inlet temperature, sun's beam angle of incidence, and predicted and measured collector outlet temperature for 55% shading (28th October 1999)

4.5 MODELLING THE EFFECT OF ADDITIONAL CIRCUIT RESISTANCE ON THE COLLECTOR OUTLET TEMPERATURE PROFILE

4.5.1 Introduction

Briefly summarised, the algorithm thus far described, for a given irradiance and collector inlet and air temperature, defines a collector flow rate, and thence calculates a steady state collector outlet temperature. To simulate the collector outlet temperature under transient weather conditions, correction factors accounting for the effect of the sun's beam angle of incidence on the transmissivity of the collector and PV module covers are incorporated. The calculated outlet temperature values are then averaged over a twelve minute period.

For the present system, with the initial physical shading method of control, the pump load line characteristic, as represented by the "pump only" plot in Fig. 4.5.1, lies to the left of the locus of maximum power points. Physically shading the module was seen to reduce the current. For all tests and predictions, only the current had to be defined in relation to a given level of irradiance in order to determine the pump voltage.

Section 4.5 introduces a simpler model for characterising the PV module electrical performance, and presents an analysis of the effect of including additional resistance on the collector outlet temperature profile. Using the above-mentioned averaging technique and correction factors, predicted transient collector outlet temperature profiles are compared with those measured in relation to the altered resistance characteristics of the electrical sub-system.

4.5.2 PV module characteristics.

Various models of PV module performance have been proposed. A review was presented in section 2.4. Among them, the model presented by Eckstein et al (1990), produces a characteristic curve of the form shown in Fig 4.5.2 curve "A". The PV module presently used is a 5Wp polycrystalline unit

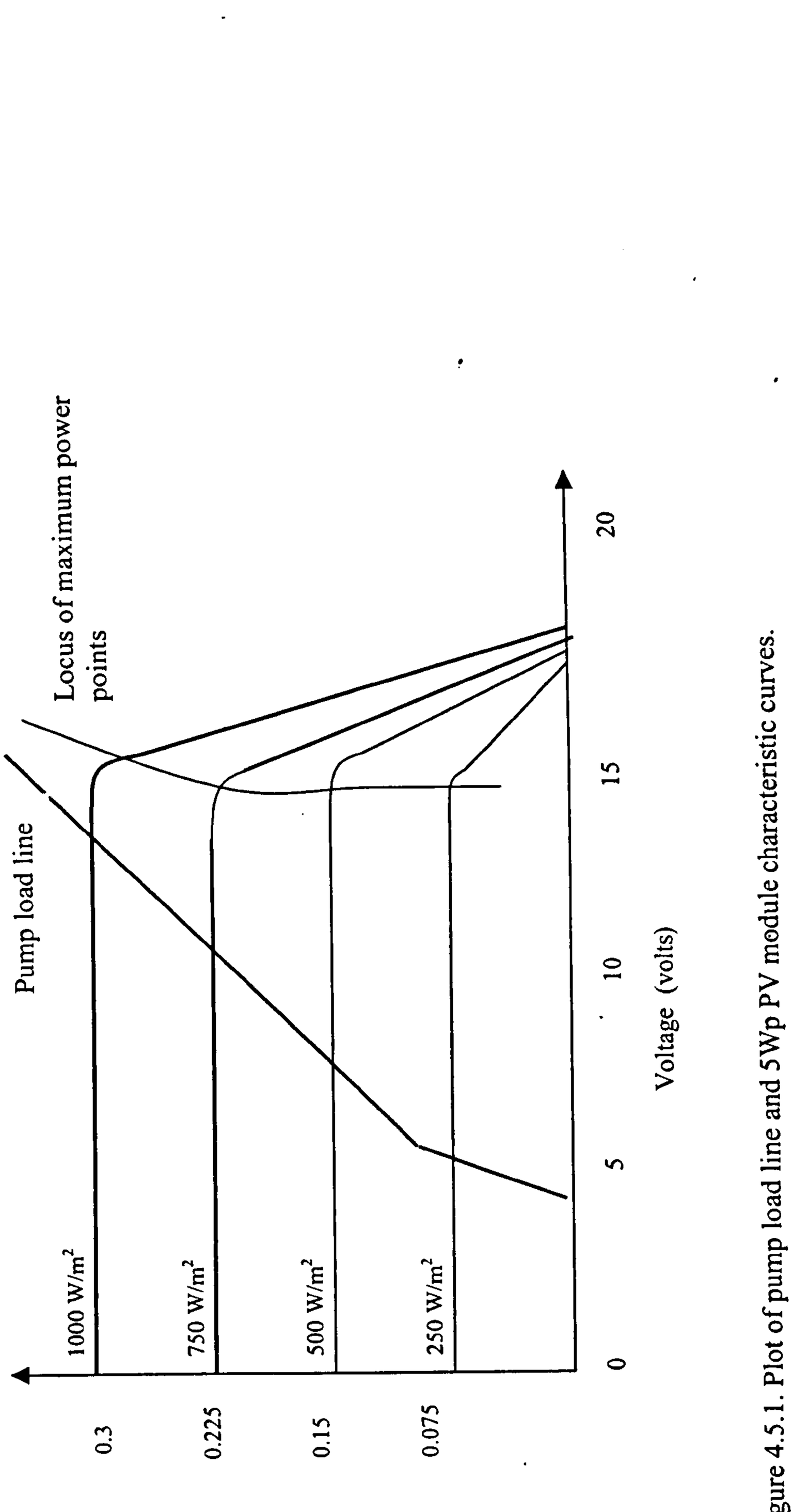

Figure 4.5.1. Plot of pump load line and 5Wp PV module characteristic curves.

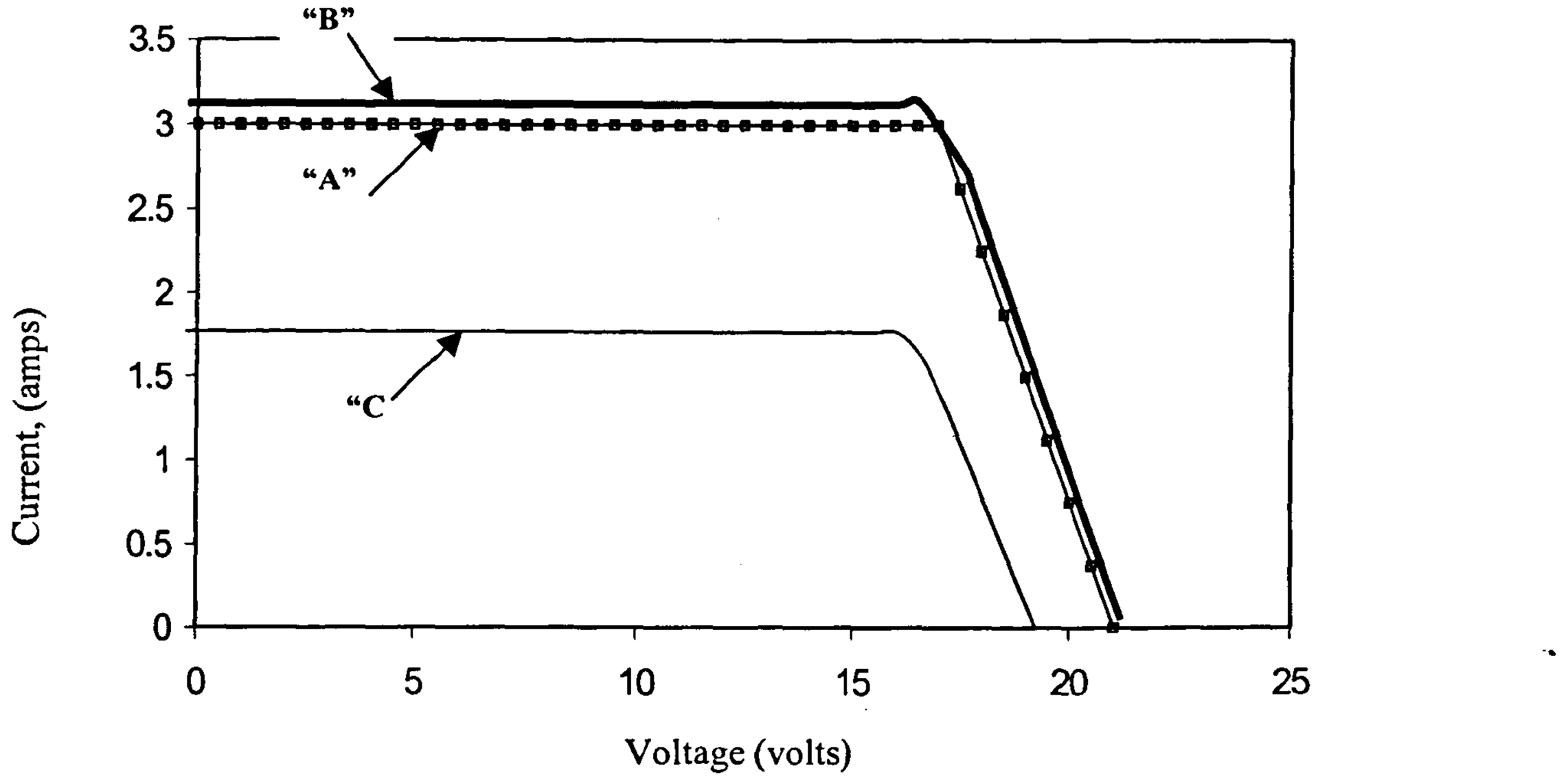

Figure 4.5.2. Comparison of manufacturers (curve "B") and present model characteristic (curve "A") curves, (40Wp module, type BP245/2), and the form of the characteristic curves generated by Eckstein's model. (curve "C")

with a full sun (1000W/m^2) short circuit current of 0.3 A and open circuit voltage of 21 V. While the manufacturers, BP (1999), supply only the above data for this module, and no characteristic curve, there are however plots provided for larger modules with the same open circuit voltage. A plot for the 40 Wp module, is given in Fig.4.5.2 curve "B".

To enable the pump voltage to be defined for a given included resistance and irradiance, a simpler linear model, represented by Eqs. 4.5.1a and 4.5.1b has been developed to give an approximation to the PV module characteristics.

$V_c <= 17.4 - (400 / G)$, Then $I_c = (I_{sc}/1000) * G$ (4.5.1a)

$V_c > 17.4 - (400 / G)$,

Then $I_c = ((I_{sc}/1000) * G) - [(V_c - [17.4 - (400 / G)]) * ((I_{sc}/4000)* G)]$ (4.5.1b)

The curve generated from Eqs. 4.5.1a and 4.5.1b is given by plot "C" in Fig. 4.5.2. Other than a slight divergence at the maximum power point, it can be seen that there is very good agreement with the Eckstein et al (1990) curve, and the form of that supplied by the manufacturers for the larger module. For the 5 Wp module, using Eqs. 4.5.1a and 4.5.1b, the family of curves derived using the supplied data is as shown in Fig. 4.5.3.

The voltage and current at the maximum power point for any given level of irradiance are represented by Eqs. 4.5.2a and 4.5.2b respectively. The maximum power available is defined as the product of I_{mp} and V_{mp}.

$V_{mp} = 17.4 - (400 / G)$. (4.5.2a)

$I_{mp} = 0.0003 * G$ (4.5.2b)

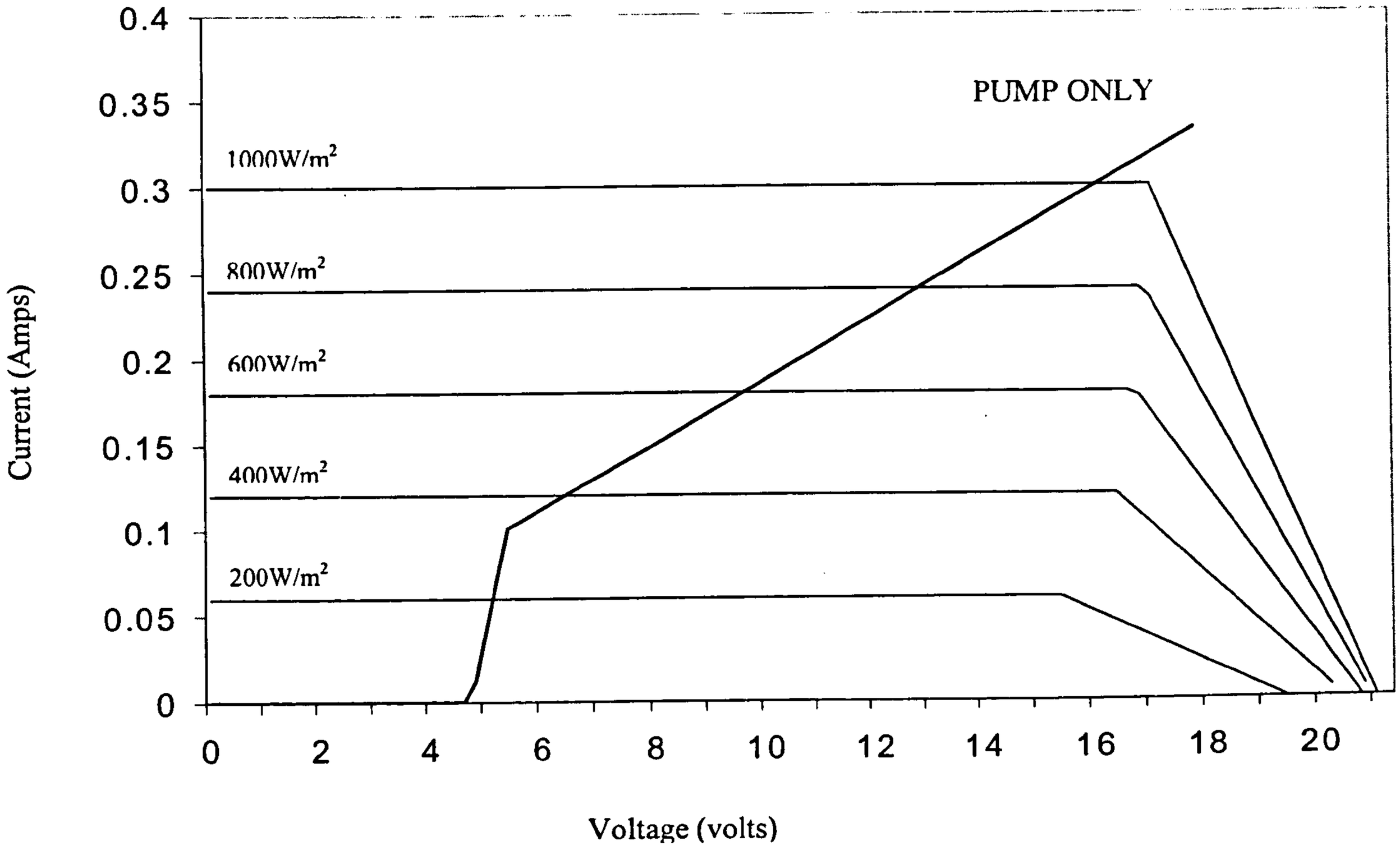

Figure 4.5.3. Plot of the family of curves generated by the model given in Eqs. 4.5.1a and 4.5.1b, for the 5Wp PV module.

4.5.3 The effect of additional circuit resistance on the pump load line and applied voltage.

4.5.3.1 Introduction

Based on the pump electrical characteristic, as given in Eqs. 4.5.3a and 4.5.3b, a series of equations and two subroutines have been developed in order to define the system load line characteristic that is obtained through including different resistances in the PV module/pump motor electrical circuit.

$I_p <= 0.1$ Then $V_p = (6.76 * I_p) + 4.72$ (4.5.3a)

$I_p > 0.1$ Then $V_p = 53.5 * I_p$ (4.5.3b)

Solving the derived load line equations simultaneously with the PV characteristic equations given in Eqs. 4.5.3a and 4.5.3b allows the pump voltage, and hence system flow rate to be defined for a given irradiance and resistance. Figure 4.5.4 shows a plot of the circuit load lines obtained for different series and parallel resistances. The effects of these different resistances on the collector outlet temperature profile are now considered.

4.5.3.2 Effect of additional parallel resistance

Introducing additional resistance in parallel with the pump motor has the effect of shifting the system load line to the left of the original "pump only" line. As this implies that all operating points will lie on the horizontal portion of the PV characteristic curve, the modelled circuit current will always be equal to the maximum for that irradiance, (0.0003 G for the 5Wp module). In comparison with the equations needed to define the pump voltage for series resistances, this greatly simplifies the set of equations needed to define the pump voltage as the PV characteristic equations conditional limits do not need to be considered.. Equations 4.5.4a, 4.5.4b, and 4.5.4c detail the sub-routine used to calculate the pump voltage based on the included parallel resistance and irradiance.

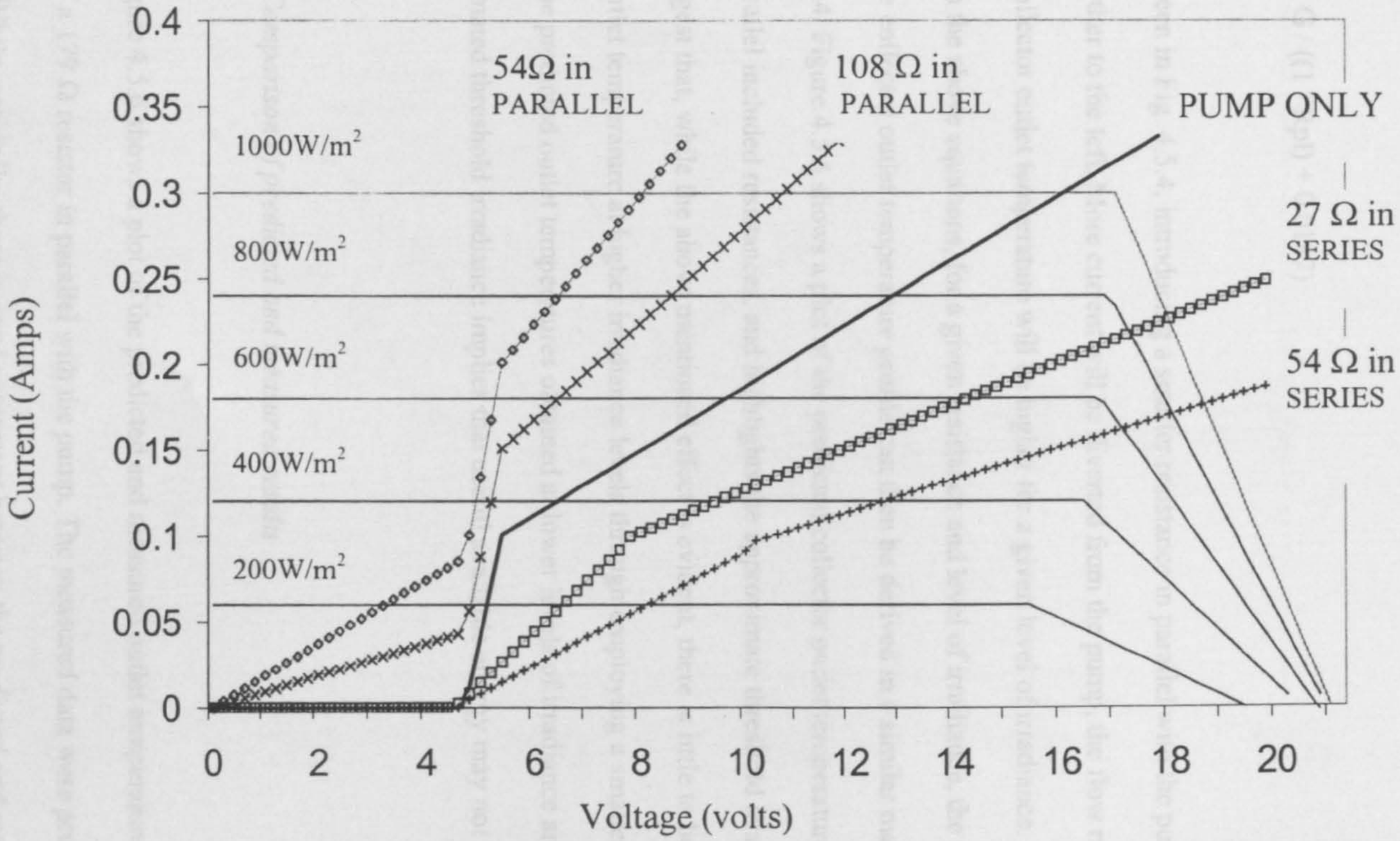

Figure 4.5.4 Plot of the "Pump Only" and circuit load lines for different series and parallel included resistances

If $G <= (15733.3 / Rpl)$

$$\text{Then } V_p = 0.0003\ G\ Rpl \tag{4.5.4a}$$

If $G > (15733.3 / Rpl)$ & $G <= ((17833.3 / Rpl) + 290.7)$

$$\text{Then } V_p = ((0.00203\ G\ Rpl) + (4.72\ Rpl)) / (6.76 + Rpl) \tag{4.5.4b}$$

Otherwise:

$$V_p = 0.0003\ G / ((1 / Rpl) + 0.0187) \tag{4.5.4c}$$

As seen in Fig. 4.5.4, introducing a smaller resistance in parallel with the pump motor shifts the load line further to the left. More current will be diverted from the pump, the flow rate will be lower, and hence the collector outlet temperature will be higher for a given level of irradiance.

From the above equations, for a given resistance and level of irradiance, the pump voltage can be defined. The collector outlet temperature profile can then be derived in a similar manner to that presented in section 4.4. Figure 4.5.5 shows a plot of the predicted collector outlet temperature profile for 3 different parallel included resistances, and highlights the approximate threshold irradiance for each. These profiles suggest that, while the above mentioned effect is evident, there is little to be gained in terms of increased outlet temperature at higher irradiance levels through employing a smaller parallel resistance. However, the predicted outlet temperatures obtained at lower levels of irradiance are unacceptably high, and the estimated threshold irradiance implies that useful available energy may not be collected.

4.5.3.3 Comparison of predicted and measured results

Figure 4.5.6 shows a plot of the predicted and measured outlet temperature profile for the inclusion of a 179 Ω resistor in parallel with the pump. The measured data were previously presented in Fig 3.5.11. While, generally, there is good agreement between the predicted and measured temperatures, the predicted temperature is seen to be slightly greater at lower levels of irradiance. This phenomenon was also observed in the comparative plots presented in respect of the physical shading outlet temperature

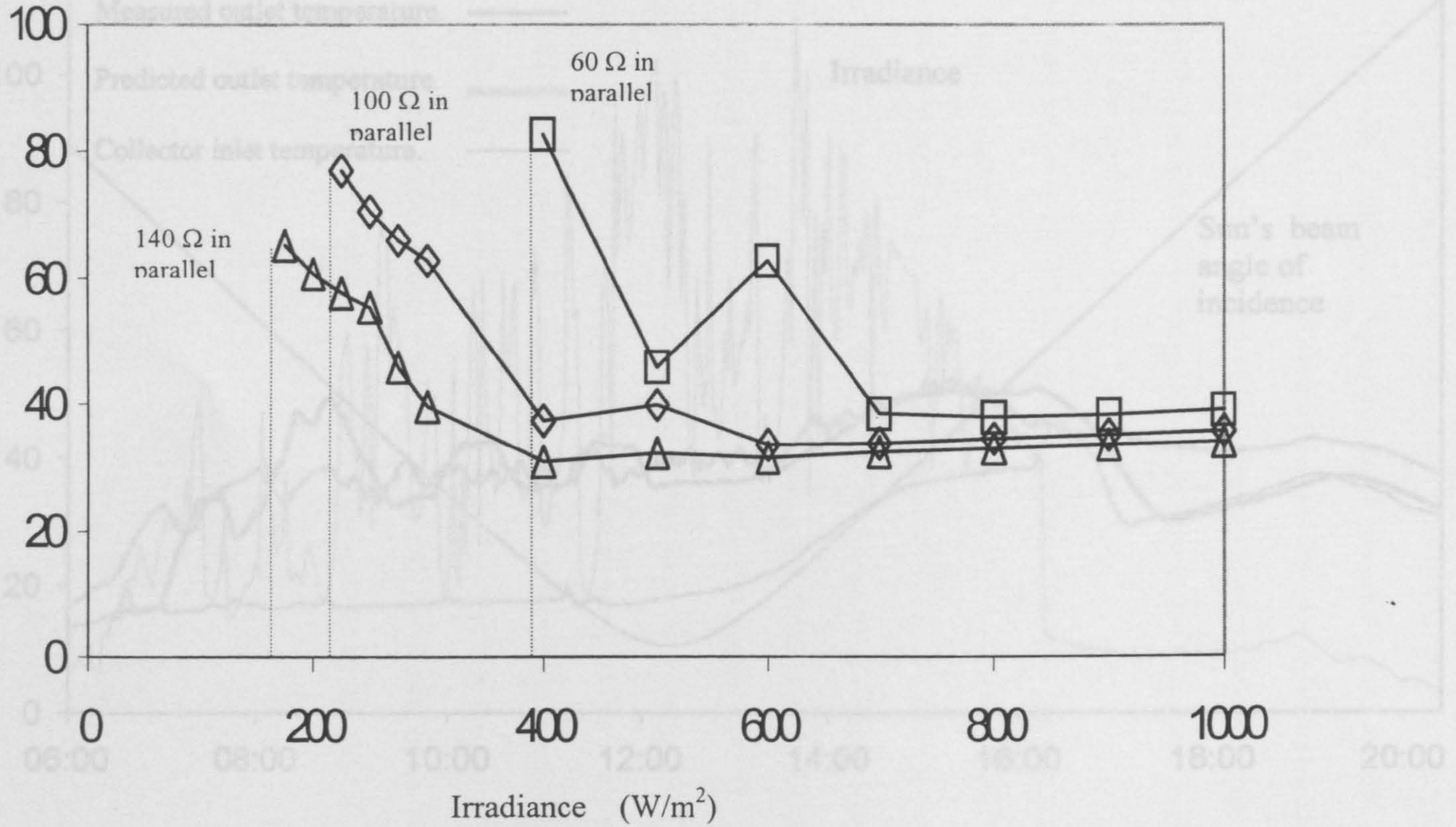

Figure 4.5.5. Outlet temperature versus irradiance profile for parallel included resistances. including approximate threshold irradiance levels

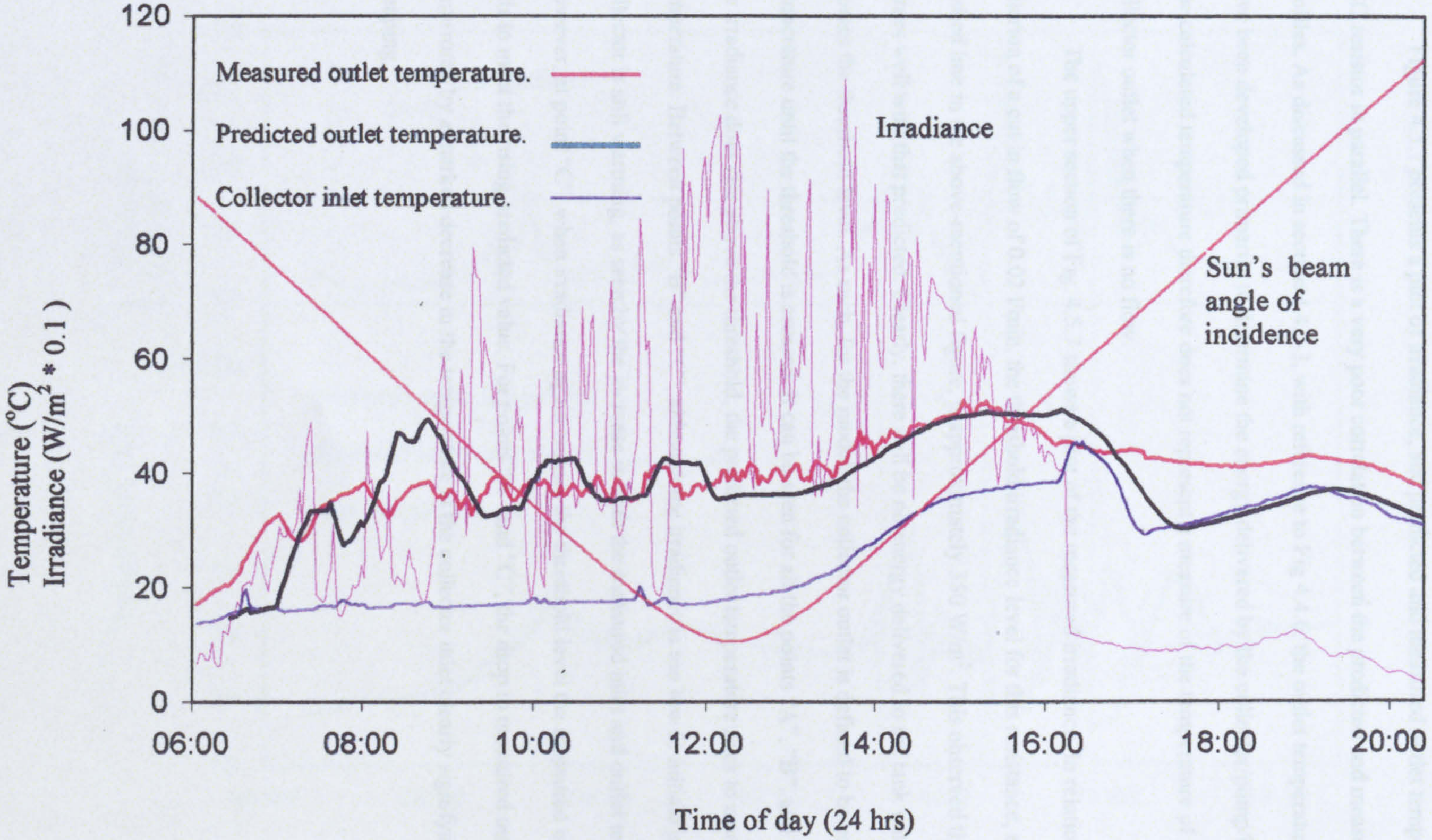

Figure 4.5.6 Irradiance, collector inlet and predicted and measured collector outlet temperatures for the inclusion of a 179 Ohm resistor in parallel with the pump (measured data gathered on 21st June 2000)

profiles. It is therefore likely that this is due to error in the defined pump voltage/flow rate relationship, or in the interpolated values for the collector efficiency characteristics used at lower flow rates.

Figure 4.5.7 presents a plot of irradiance, and predicted and measured outlet temperatures for a 58Ω resistor in parallel. There is a very poor correlation between the predicted and measured temperature profiles. As discussed in section 4.4.3.3, with reference to Fig 4.4.6, the outlet temperature algorithms have been developed primarily to determine the energy delivered by the collector/pump/PV sub-system. The calculated temperature therefore does not represent a measure of the temperature of the fluid at the collector outlet when there is no flow.

The upper section of Fig. 4.5.7 shows a plot of the measured irradiance. In relation to the defined criterion of a cut in flow of 0.02 l/min, the threshold irradiance level for this resistance, as shown by the dashed line in the above-mentioned figure, is approximately 350 W/m^2. This observed threshold level agrees well with that predicted. Clearly, there will be no energy delivered to the tank until the irradiance crosses the threshold level. As such, for the model, the collector outlet is defined to be equal to the inlet temperature until the threshold is crossed. It can be seen for all the points "A", "B", and "C" that when the irradiance does rise above the threshold, the predicted outlet temperature rises to meet the measured temperature. Between points "B" and "C", although the irradiance is too low to initiate pumping, the collector is still warming, as seen by the increase in both the measured inlet and outlet temperatures. However, at point "C", when irradiance again crosses the threshold level the measured outlet temperature falls to meet the rising predicted value. For points "A" and "C", the drop in measured outlet temperature is mirrored by a marked decrease in the temperature at the collector inlet clearly signifying the onset of pumping.

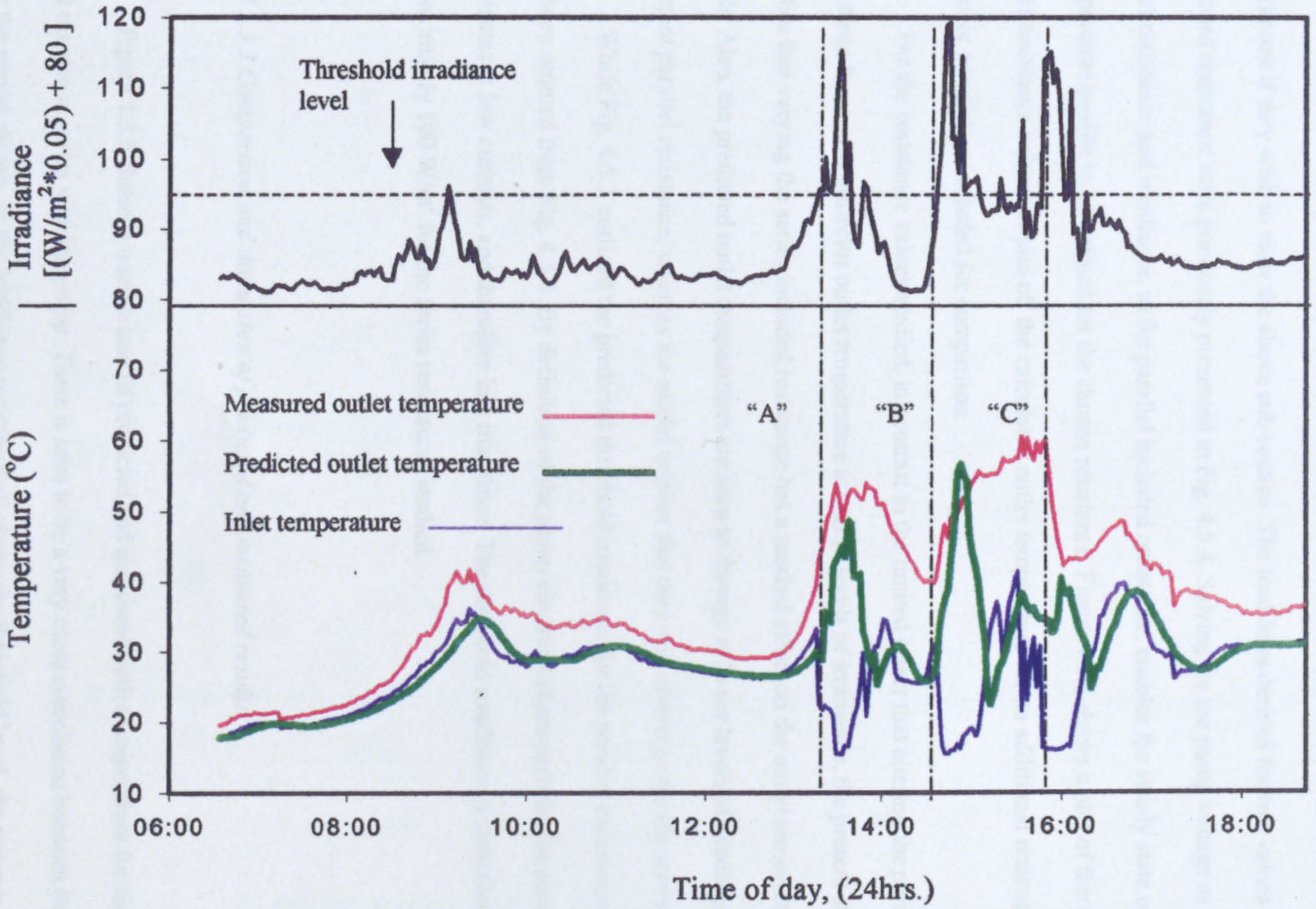

Figure 4.5.7. Plot of irradiance, collector inlet, and predicted and measured collector outlet temperature for a 58Ω resistor in parallel with the pump. (20th June 2000)

4.5.3.4 Effect of additional series resistance on the collector outlet temperature profile.

As discussed in the introduction to section 4.5.3, the sub-routine used to calculate the pump voltage based on the included series resistance and irradiance is much more complex than that given in Eqs. 4.5.4a, b, and c for parallel resistance. The reader is directed to the macro in the relevant "Excel" Workbook if they wish to view the above sub-routine. The load lines derived for two values of series included resistance were previously presented in Fig. 4.5.4. Solving for the pump voltage as a function of series resistance and irradiance, as for parallel included resistance, enables the steady state collector outlet temperature profile to be defined for the chosen resistance. Figure 4.5.8 shows a plot of this profile for 3 series resistance values. A plot of the calculated outlet temperature for no additional resistance, either series or parallel, is included for comparison.

For the resistance values studied, in contrast to the limited effect that altering the parallel resistance has on the collector outlet temperature at higher levels of irradiance, the present analysis implies that varying the series included resistance has a marked effect on the outlet temperature at these levels. Also, the predicted outlet temperatures are seen to diverge at lower levels of irradiance for different parallel resistance, whereas the model implies that they will converge for the series resistance.

While Fig. 4.5.5 outlined the predicted threshold irradiance for the parallel resistances studied, this has been omitted from Fig. 4.5.8. By definition of the pump electrical characteristic, the pump resistance dominates at low currents, and therefore low irradiance. The threshold irradiance is therefore found to be approximately 100 W/m^2 for the series resistances studied.

4.5.3.5 Comparison and discussion of predicted and measured results

Figure 4.5.9 shows a comparison of predicted and measured outlet temperature for inclusion of a 58 Ω resistor in series with the pump. There is seen to be a very close correlation between the two curves. Over the period shown, as the irradiance remains well above the threshold level, the pump is continuously operational, and the flow rate is greater than the defined cut out of 0.02 l/min. As flow is continuous, both the measured and predicted outlet temperatures therefore represent the collector delivery temperature. The

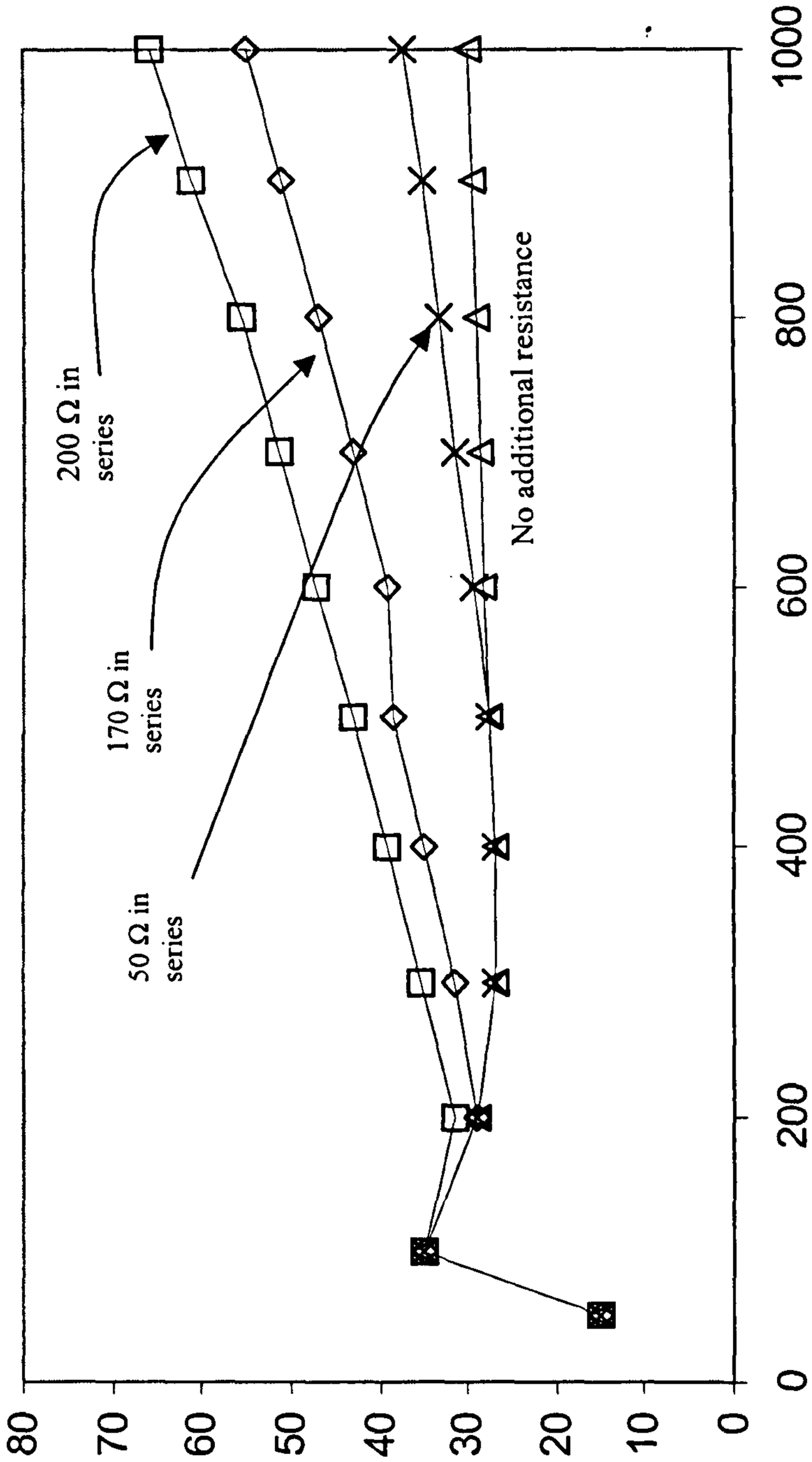

Figure 4.5.8. Outlet temperature versus irradiance profile for series included resistance. A plot of no additional resistance has been included to highlight the effect of series resistance.

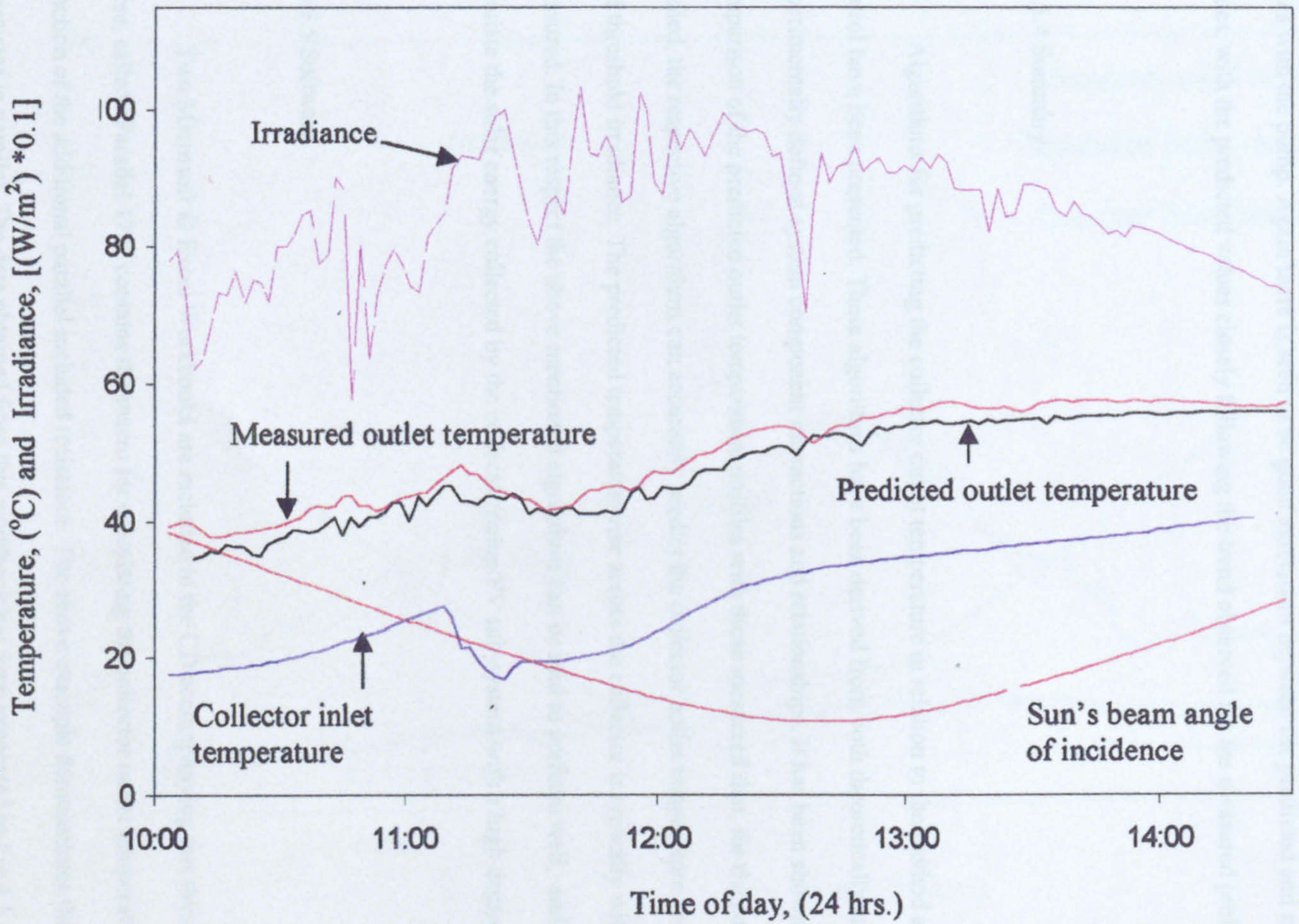

Figure 4.5.9. Plot of irradiance, sun's beam angle of incidence, collector inlet, and predicted and measured collector outlet temperatures for a 58Ω resistor in series with the pump. (22nd june 2000)

outlet temperature is higher than that presented for a similar resistance in Fig. 4.5.8 as the measured inlet temperature, used in calculating the predicted values presented in Fig. 4.5.9, is greater than that assumed for design (15°C) in Fig. 4.5.8.

Figure 4.5.10 presents a plot of irradiance, the sun's beam angle of incidence, the collector inlet and air temperatures, and the measured and predicted collector outlet temperature for a 179Ω resistor in series with the pump. Again there is seen to be good agreement between the predicted and measured values, with the predicted values closely following the trend observed for the measured profile.

4.5.4 Summary

Algorithms for predicting the collector outlet temperature in relation to the method and degree of control have been presented. These algorithms have been derived from both theoretically and experimentally defined system component interactions and relationships. It has been shown through comparison of the predicted outlet temperature profiles with those measured that, for the control methods studied, the respective algorithms can accurately predict the collector outlet temperature profile, flow rate, and threshold irradiance. The predicted temperature rise across the collector is typically within 5% of that measured. In this respect the above mentioned algorithms can be said to perform well, and therefore simulate the solar energy collected by the collector/pump/PV sub-system with a high degree of accuracy

4.5.5 Software.

Two Microsoft ® Excel Workbooks are included in the CD accompanying this thesis. The first of these, called "Parallel 179" contains the macro for calculating the collector outlet temperature as a function of the additional parallel included resistance. The above example demonstrates the case for a 179 Ω resistor in parallel. The data obtained from this workbook has been presented in Fig 4.5.6. The second, "Series-179" presents the macro and data for the inclusion of a 179Ω resistor in series with the pump motor. This data has been presented in Fig 4.5.10

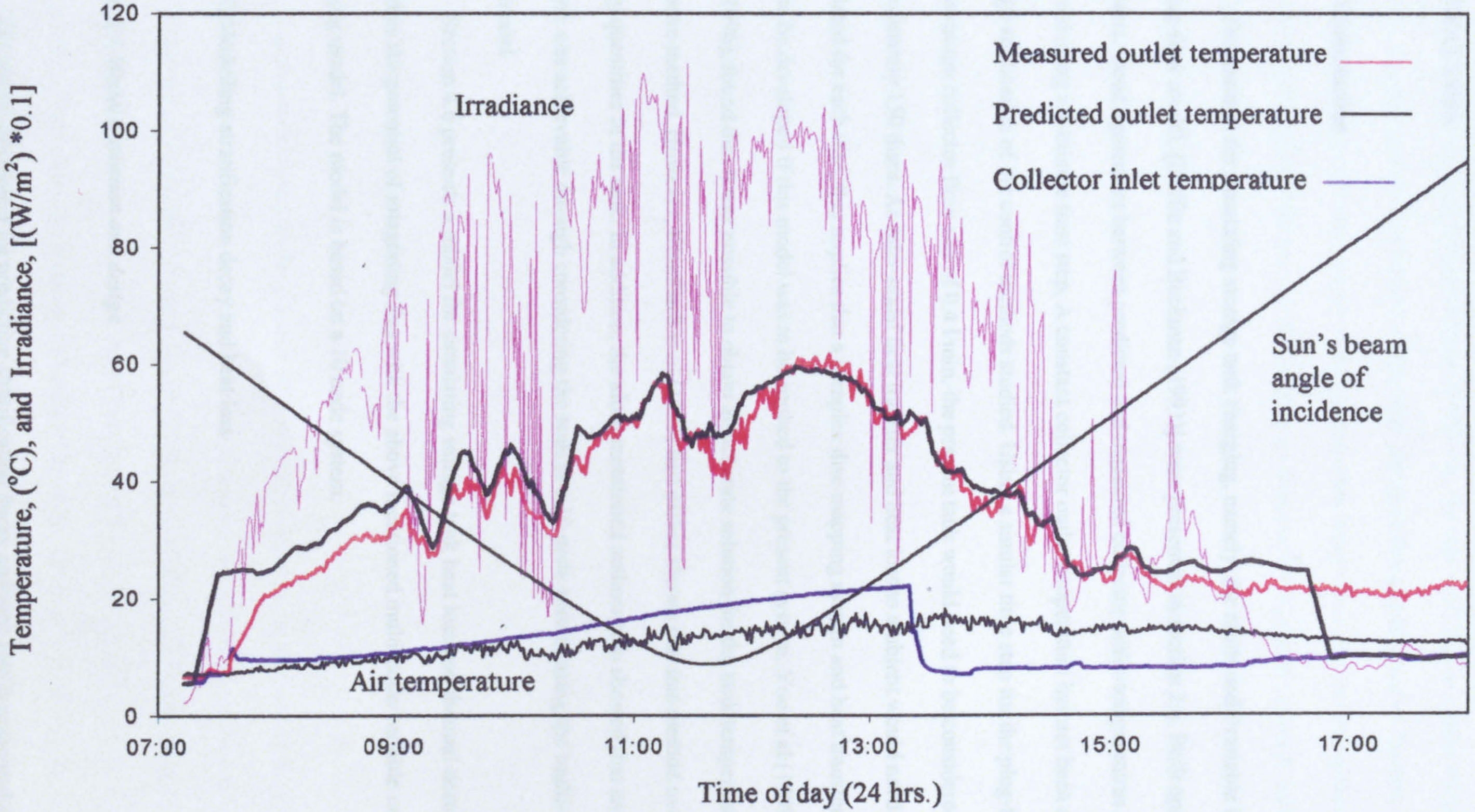

Figure 4.5.10 Plot of irradiance, air temperature, sun's beam angle of incidence, collector inlet, and measured and predicted collector outlet temperature for a 179 Ω resistor in series with the pump (20th April 2001).

4.6 MODELLING STORAGE TANK CHARGING, STRATIFICATION DECAY AND TANK HEAT LOSS

4.6.1 Introduction

Two models for simulating storage tank charging, namely, the multi-node/variable inlet model and the plug-flow model, [Duffie and Beckman (1991)] were presented in section 2.6. Both operate on a time step basis. Good agreement between predicted and measured collector outlet temperatures has been achieved using a 2-minute time step. A constant collector outlet temperature has not been achieved through application of the control methods studied. Using a similar time step for the plug-flow model, for the maximum collector flow rate of 0.4 l/min, the present tank would need to be considered as comprising approximately 150 discs. As inter-nodal heat transfer and heat loss to ambient would need to be calculated for each disc, this implies that a complex disc mapping system and heat transfer network would need to be developed if this model was to be applied to the present system. Yoo et al (1999), and Yoo and Pak (1996), found that it was possible to obtain an accurate solution for the tank temperature profile using the above method. However, Kleinbach et al (1993) had earlier shown that this method overestimated the energy quantities in the tank. In addition, the afore-mentioned authors also showed that an accurate solution was achievable through considering the tank as a 10 node system using the multi-node/variable inlet model.

Section 4.6 presents a model for simulating storage tank heat loss and thermal destratification and considers the potential of integrating this with the above mentioned multi-node/variable inlet tank charging model. The model is based on a 10 node system.

4.6.2 Modelling stratification decay and heat loss

4.6.2.1 Model operation and design

The model developed for predicting stratification decay and heat loss is presented in two sections. Firstly, the heat loss from the individual nodes to the environment is calculated through considering the

individual nodal external surface area and the sum of radial thermal resistances. These are, namely, the fluid, the fluid/tank wall surface heat transfer coefficient, the tank wall and insulation resistances, and the insulation external surface heat transfer coefficient. This provides an indication of the heat loss from each node in relation to the difference between the internal axial temperature and that of ambient. While the above-mentioned surface heat transfer coefficients are temperature dependant, average values have been used in the present analysis.

In respect of node 1, being the lowest, the tank is deemed to be sitting on a well insulated surface such that downward heat loss is negligible. Additional terms are included in calculating the heat loss term for node 10 to take account of losses from the top of the tank.

Ruey-Jong Shyu et al (1989) found that although exterior insulation could enhance axial conduction, the destratifying effects caused by axial conduction were small for a thin walled tank. In considering the present case of a copper tank with a wall thickness of 0.5mm, and in the interests of keeping the model simple, neither conduction along the outlet pipes, nor axial conduction through the tank walls has been incorporated.

The second of the two above-mentioned sections of the present model considers the heat transfer between adjacent nodes. The inter-nodal heat transfer equations derived are based solely on the nodal interface cross sectional area and the fluid thermal resistance and lumped capacitance. Figure 4.6.1 shows a schematic representation of the thermal resistance network considered in the present analysis. The algorithm developed from the above network is available in the macro in the relevant "Excel" Workbook in the accompanying CD.

4.6.2.2 Presentation of results.

The above-described model is given 10 measured, nodal axial, or external wall, temperatures as an input. Using the wall temperature profile as the model input/output allows a comparison with parameters that are more easily measured. Presently, the model has been adapted to output the wall temperature only. Once input data has been received, the "macro" containing the algorithm is run to give an output of the predicted individual nodal temperatures at 2 minute intervals. These data can be filtered and plotted to give a graphical representation of the tank wall profile for a more suitable time interval, for example,

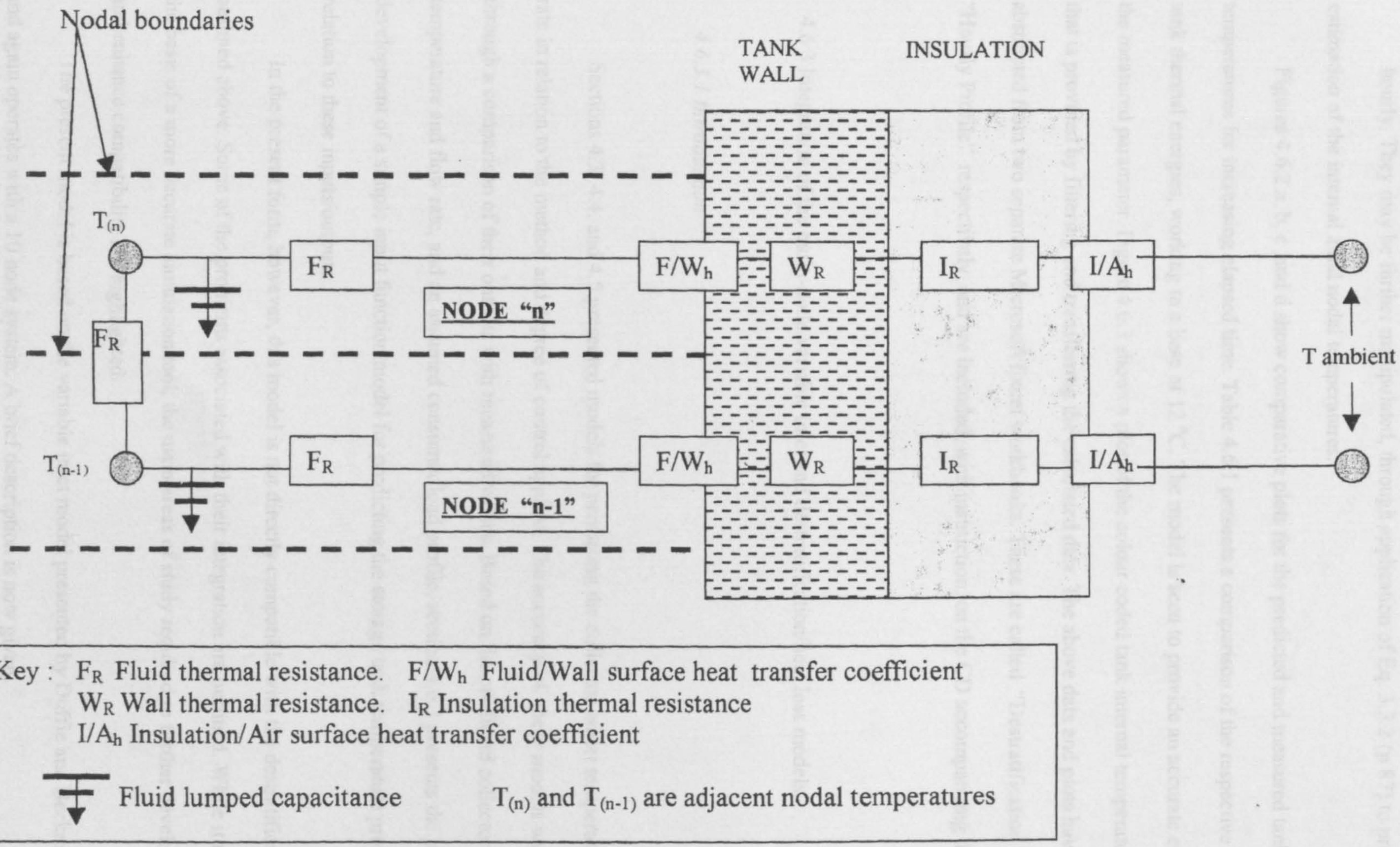

Figure 4.6.1 Tank thermal resistance network considered in the present analysis

hourly. They may be further manipulated, through application of Eq. 3.3.2 (p 87) to provide an estimation of the internal axial nodal temperatures.

Figures 4.6.2 a, b, c ,and d show comparative plots for the predicted and measured tank wall temperatures for increasing elapsed time. Table 4.6.1 presents a comparison of the respective nodal and tank thermal energies, working to a base of 12 °C. The model is seen to provide an accurate estimation of the measured parameter. Figure 4.6.3 shows a plot of the colour coded tank internal temperature profile that is provided by filtering and transferring the calculated data. The above data and plots have been abstracted from two separate Microsoft Excel workbooks. These are called "Destratification Model" and "Hourly Profile" respectively, and are included, with instruction, on the CD accompanying this thesis.

4.6.3 Integration of the multi-node/variable inlet and destratification/heat loss models.

4.6.3.1 Introduction

Sections 4.3, 4.4, and 4.5 presented models for predicting the collector outlet temperature and flow rate in relation to the method and degree of control applied. The accuracy of these models was verified through a comparison of their outputs with measured values. Based on the predicted collector outlet temperature and flow rate, and an assumed consumer load profile, section 4.6.3 presents the part development of a simple input function model for predicting the storage tank temperature profile in relation to these inputs/outputs.

In the present form, however, this model is not directly compatible with the destratification model outlined above. Some of the problems associated with their integration are outlined. While it may form the basis of a more accurate simulation tool, the main areas of study required to further develop the model and enhance compatibility are highlighted.

The present model is based on the variable inlet model presented by Duffie and Beckman (1991), and again operates with a 10 node system. A brief description is now given.

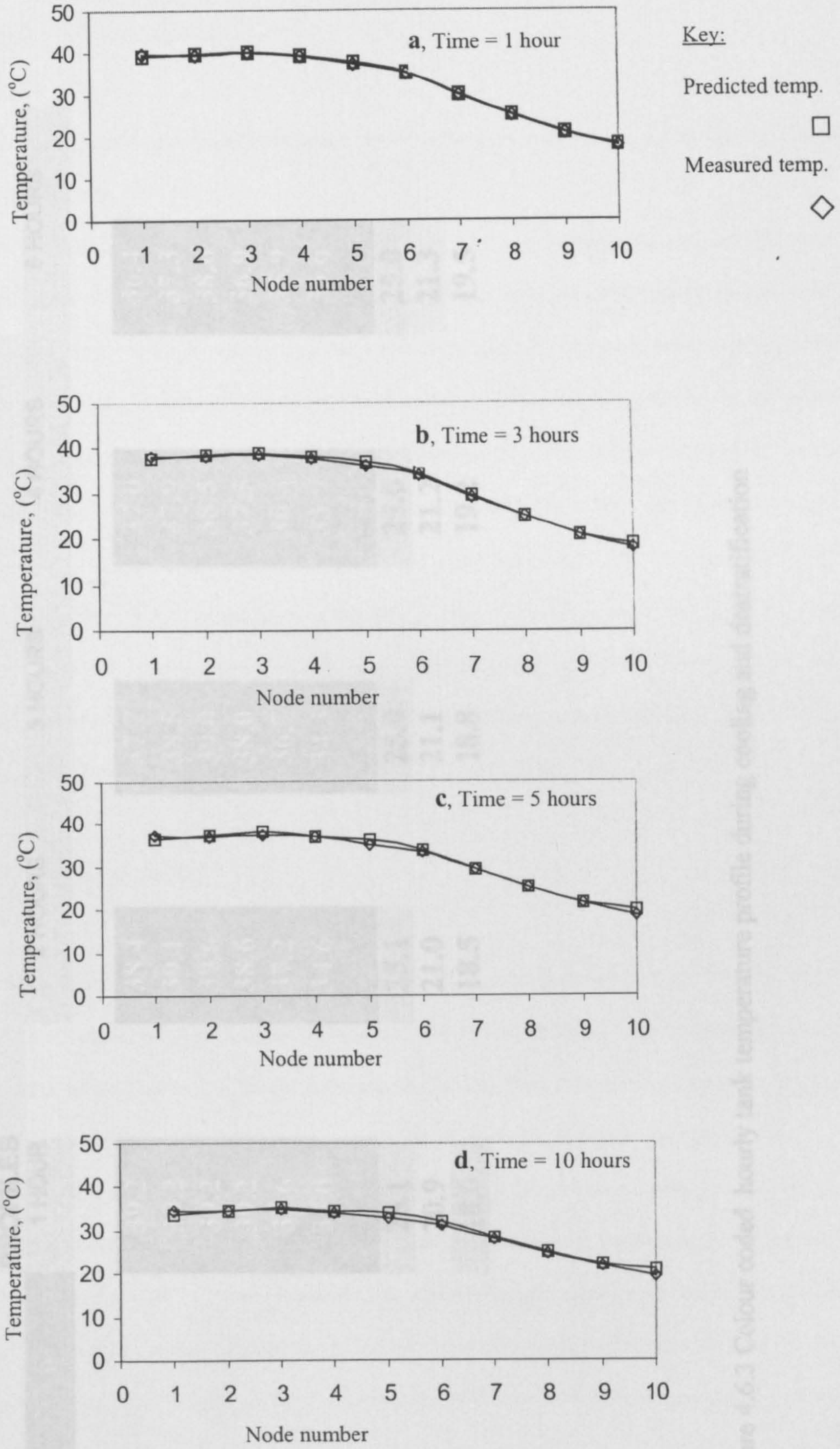

Figures 4.6.2a,b,c, and d. Plot of predicted and measured tank wall temperature profiles for increasing elapsed time.

PREDICTED TANK WALL TEMPERATURE PROFILES

ELAPSED TIME	1 HOUR	2 HOURS	3 HOURS	4 HOURS	5 HOURS
	39.2	38.4	37.7	37.0	36.4
	39.2	39.1	38.5	37.9	37.3
	39.2	39.6	39.0	38.5	38.0
	39.2	38.6	38.0	37.5	36.9
	37.6	37.2	36.7	36.3	35.9
	35.0	34.6	34.3	33.9	33.6
	30.0	29.8	29.6	29.5	29.3
	25.1	25.1	25.0	25.0	25.0
	20.9	21.0	21.1	21.2	21.3
	18.0	18.5	18.8	19.2	19.5

Figure 4.6.3 Colour coded hourly tank temperature profile during cooling and destratification

4.6.3.2 Model structure and operation

While the algorithm applied in the present analysis is for a ten node system, for simplicity, it is presented here for a five node tank.

When the calculated collector flow rate is greater than the program design threshold of 0.02 l/min, the model considers the placing of the collector outlet fluid in relation to the previous nodal temperatures within the tank such that the fluid is deemed, through buoyancy effects, to settle into the node with the temperature closest to, but lower than its own. The model is primarily based on considering the energy flows into and out of each node, or control volume, for each time step. Figure 4.6.4 shows a schematic representation of the flow and function relationship between each node. The program reads the collector outlet temperature, and sets the nodal flow functions accordingly. If, for example, the collector outlet temperature is 50 ^{0}C, with node 4 at 48 ^{o}C, and node 5 at 51 ^{o}C, the flow functions are set such that F4 = 1 , and F5, F3, F2, and F1 = 0. If there is load being drawn, then FL = 1. The nodal temperatures are calculated at the end of each time step in relation to the collector outlet temperature and flow rate, and also the inlet mains temperature and load flow rate.

4.6.3.3 Integration problems.

The main problems associated with combining the above models derive from the fact that, while the destratification model relies on a radial temperature gradient, the charging model assumes a uniform nodal bulk temperature. That is, it is based on the assumption that there is no radial temperature gradient. It was shown in section 3.3 that a radial temperature gradient does exist for the present tank.

The destratification model can accurately define the tank wall and internal temperature during the cooling phase. This may be used to define an average nodal temperature, or, assuming a linear gradient, the radial temperature profile. If a linear gradient is assumed, this implies that the same temperature may exist at different locations within the tank. To define where the inlet water will settle, assuming the above inlet/buoyancy theory holds true, would require knowledge of the rate of radial dispersion of the inlet jet in relation to tank vertical height.

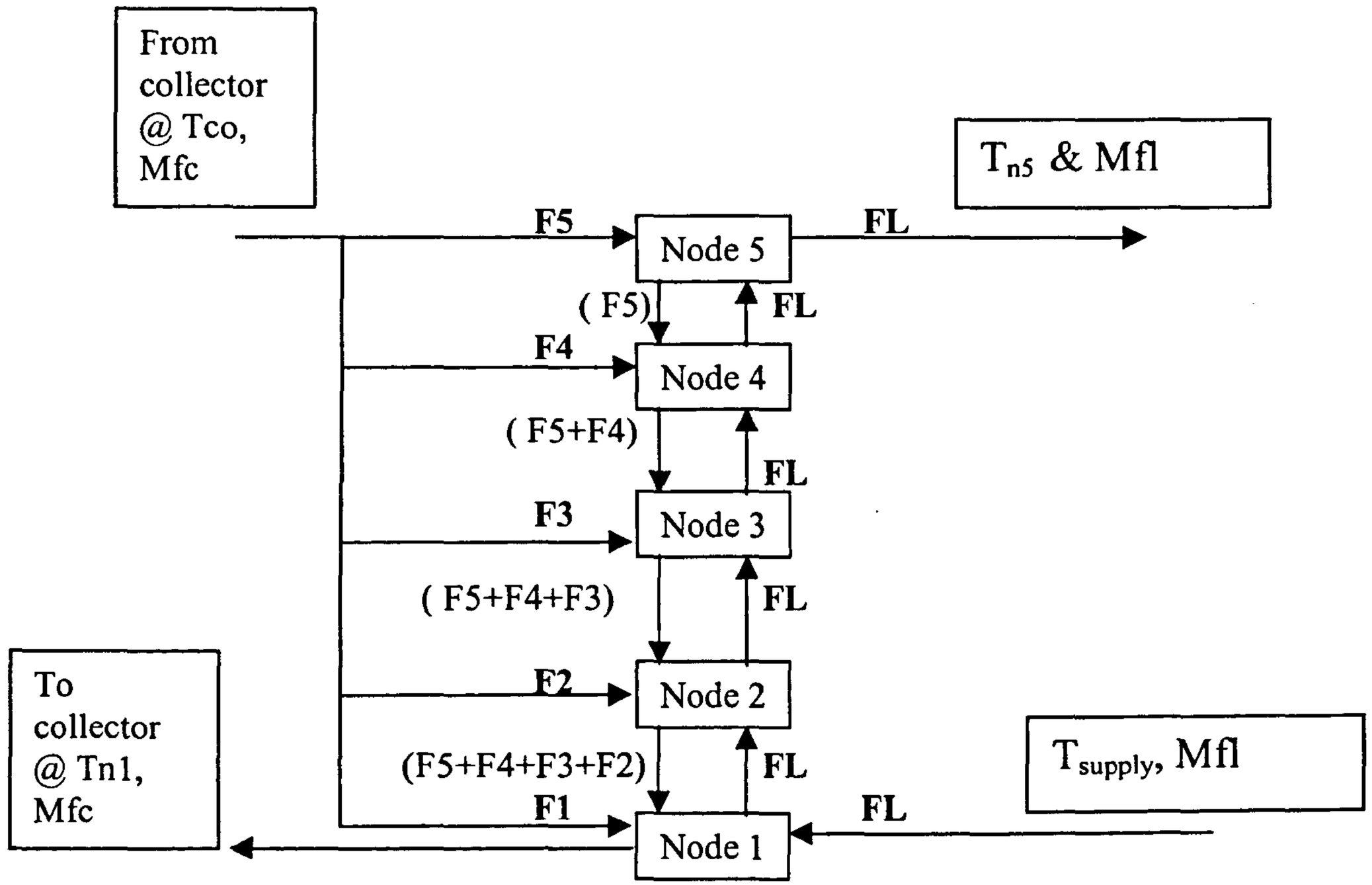

Figure 4.6.4 Schematic diagram of the variable inlet/multi-node tank charging/discharging model.

This is illustrated in Fig 4.6.5. If nodes 8 and 9 have the temperature gradients as shown, it can be seen that there are two positions within the tank that are at a temperature just less than the tank inlet temperature T_{in}; namely $T_{IN}.8$ and $T_{IN}.9$. For a lower inlet velocity, assuming a greater rate of radial dispersion, as represented by triangular section "A" in the above-mentioned figure, for the present model, the inlet water may settle at point $T_{IN}.9$. Alternatively, for higher inlet velocities, the inlet plume may penetrate more deeply into the tank, as shown by section "B", implying that the fluid may settle at point $T_{IN}.8$. The position at which the inlet water settles will have a marked effect on the tank temperature profile.

To provide an accurate solution for the settling location, a detailed study of the effect of inlet velocity on radial spread would be required. This analysis would also need to consider the effect of the difference in temperature between the incoming fluid, and that, primarily, in the tank upper region, on fluid buoyancy, mixing, and plume entrainment. Moreover, as higher inlet velocities are generally experienced at the tank inlet during load draw, mixing effects would also need to be considered.

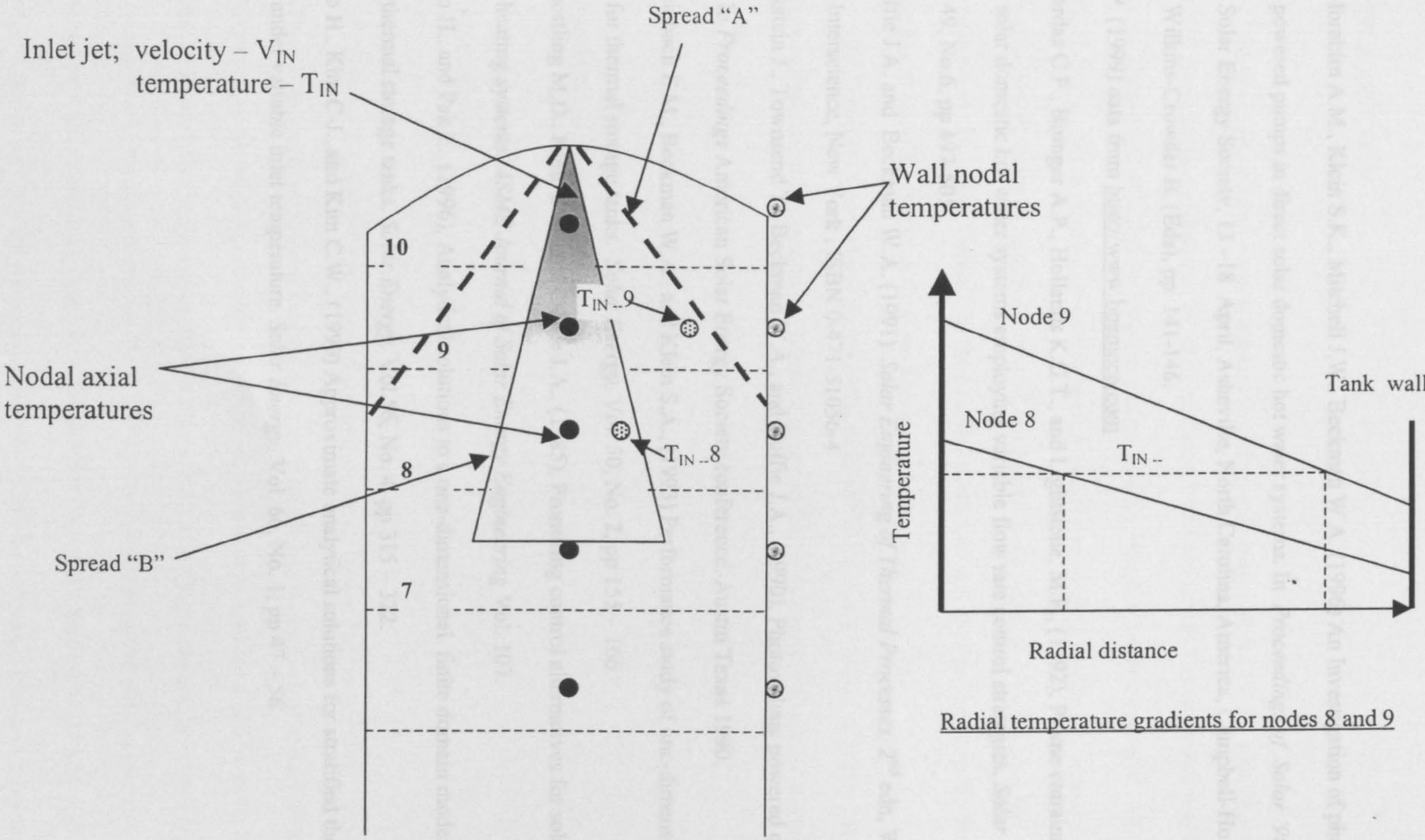

Radial temperature gradients for nodes 8 and 9

Figure 4.6.5 Radial temperature gradients and rate of radial spread of collector return/tank inlet fluid stream.

REFERENCES

Al-Ibrahim A.M., Klein S.K., Mitchell J.W., Beckman W.A. (1996) An Investigation of photovoltaic powered pumps in direct solar domestic hot water systems. In *Proceedings of Solar '96*, American Solar Energy Society, 13 –18 April, Asheville, North Carolina, America, Campbell-Howe R. and Wilkins-Crowder B. (Eds), pp. 141-146.

B.P. (1999) data from http://www.bpamoco.com

Csordas G.F., Brunger A.P., Hollands K.G.T., and Lightstone, M.F., (1992), Plume entrainment effects in solar domestic hot water systems employing variable flow rate control strategies. *Solar Energy,* Vol. 49, No.6, pp 497-505.

Duffie J.A. and Beckman W.A. (1991) *Solar Enginering of Thermal Processes,* 2nd edn, Wiley Interscience, New York . ISBN 0-471-51056-4

Eckstein J., Townsend T., Beckman W.A., and Duffie J.A., (1990), Photovoltaic powered energy systems. In *Proceedings* American Solar Energy Society conference. Austin Texas 1990.

Kleinbach E.M., Beckman W.A., and Klein S.A., (1993) Performance study of one-dimensional models for thermal storage tanks. *Solar Energy,* Vol. 50, No. 2, pp 155 – 166.

Wuestling M.D., Klein S.A., and Duffie J.A., (1985), Promising control alternatives for solar water heating systems. *ASME Journal of Solar Energy Engineering* Vol. 107.

Yoo H., and Pak E., (1996), Analytical solutions to a one-dimensional finite domain model for stratified thermal storage tanks. *Solar Energy,* Vol.56, No. 4, pp 315 – 322.

Yoo H., Kim C-J., and Kim C.W., (1999) Approximate analytical solutions for stratified thermal storage under variable inlet temperature. *Solar Energy,* Vol. 66, No. 1, pp 47 – 56.

5. ECONOMIC ANALYSIS

5.1 INTRODUCTION

Section 5 presents an economic analysis of the performance of the FT-PV system in respect of the potential financial saving that may be achieved through its installation. The environmental benefits, both in terms of displaced CO_2 and the efficiency of the system design, are also considered. All calculations and forecasts are based on the comparative testing results presented in section 3.6. While these results, for each of the three modes of immersion control, are given for a periods of 2 weeks, they have been extrapolated to obtain an estimation of the potential annual energy saving. The method used and assumptions made in estimating these savings are outlined.

While section 1 considered the potential of SDHWS for space heating at higher latitudes, the present analysis considers system performance solely in relation to heating water for washing and bathing.

5.2 ENERGY SAVING.

5.2.1 Introduction

Table 3.6.2 (page 141) presented the results obtained for the "immersion only" testing of both the FT-PV and Reference solar water heating systems. With the lower electric immersion left on untimed, the electrical consumption, as a percentage of the delivered load, was calculated as 136 % for the FT-PV system, and 129 % for the Reference. Tables 3.6.3a and 3.6.3b (pages144 and 145) gave the results for the comparative systems performance. The FT-PV system collection efficiency and electrical consumption were shown to be sensitive to the position of, and the method of control applied to, the immersion heater. The present analysis therefore considers the potential savings in relation to the position and method of control of the immersion heater.

As solar availability is not constant throughout the year, the monthly solar gain will vary. For each of the modes of operation studied, the data presented for the electrical consumption as a percentage of the given load will therefore also vary. It would therefore be incorrect to base an estimation of the potential saving directly on the measured electricity consumption for the test periods defined. The annual consumption is therefore calculated assuming the measured collection efficiency and system thermal performance to be constant for each of the immersion modes studied.

5.2.2 Annual energy/load demand

The above-mentioned comparative tests used 2 m^2 collectors, with the volume of hot water delivered reflecting the load that would be imposed on the larger commercial system. The proposed commercial FT-PV system comprises a 2.8 m^2 collector. For the present analysis, a daily load of 45 l/person at 60 °C is assumed. Assuming an annual mains water inlet temperature of 12 °C, for a four person household, this load equates to an annual demand of 3679 kWh. Using the immersion only to provide this load implies an annual consumption of 5004 kWh for the FT-PV, and 4746 kWh for the Reference systems respectively.

5.2.3 Annual solar gain and electrical consumption.

As stated in section 5.2.1 the collection efficiency is assumed constant for each of the immersion modes studied. This implies that, for an annual incident solar irradiance of approximately 926 kWh/m^2, [data for Glasgow, collector facing S.E. at a tilt of 45 °, Page and Lebens (1990)] for an FT-PV system with a 2.8 m^2 collector, operating with the top immersion timed (TT collection efficiency = 36.5 %), the collector will deliver approximately 1014 kWh to the tank. In this immersion mode, the FT-PV system was found to have a thermal efficiency of 85 %. For the above annual demand, this implies a required annual thermal input of 4328 kWh. The required electrical input will therefore be 3314 kWh/year, implying a potential saving of 1689 kWh. Carrying out a similar analysis for the FT-PV system operating

with the bottom immersion untimed, and also for the Reference system yields the data presented in table 5.2.1

5.2.4 Annual energy and financial savings.

As can be seen from the data presented in the above-mentioned table, the potential annual energy saving is greatest for the FT-PV system operating with the top immersion timed. The annual financial saving will therefore be dependant on the mode of immersion control applied. The above data are based on a comparison of the estimated required electrical input for the two systems, with that required when operating with the immersion only and no solar input.

The present cost per unit of electricity for the domestic consumer is, on the cheapest quoted tariff, (Scottish Power plc – direct debit scheme May 2001) 6.873 p/kWh. plus a standing charge of 11p/day, and 1.12 p/kWh with a similar availability charge of 9.9 p/day for gas. Obviously the payback period will depend on the primary fuel used. Both the larger FT-PV and Reference systems have an approximate installed cost of £2000. The FTPV system is more simple to install than the Reference, and can therefore be more readily self-assembled. As the FT-PV kit costs about £1600 (Solar Twin (2001)), self-installation would further reduce the payback period.

5.2.5 Displacement of Carbon Dioxide.

As outlined in section 1, in addition to saving energy, installing a solar water heating system also reduces CO_2 emissions. For the FT-PV system, the potential annual energy saving is almost halved if the system is operated with the bottom immersion untimed. The amount of CO_2 displaced would therefore also be halved. Assuming that the sole primary energy source is coal, with a calorific value of 23.2 MJ/kg, and a combined conversion/transmission efficiency of 30%, the predicted annual energy saving of 1680 kWh implies an annual reduction in CO_2 output of approximately 3204 kg.

Table 5.2.1 Estimated solar gain, electrical input required and potential annual saving.

Immersion Mode		Potential Solar Gain (kWh)		Electricity Required (kWh)		Annual Saving (kWh)	
FT-PV	Reference	FT-PV	Reference	FT-PV	Reference	FT-PV	Reference
Top Timed	Bottom Not Timed	1014	1350	3324	5539	1680	**-793**
Bottom Not Timed	Bottom Not Timed	716	1250	4351	4636	653	110

If government was to introduce incentives to encourage the uptake of SDHWS, at a national level the implementation of the FT-PV systems could make a significant contribution towards reducing CO_2 output.

5.3 DISCUSSION OF RESULTS

5.3.1 Validity of the data presented and conclusions

The measured collection efficiency, defined as the solar energy delivered to the storage tank divided by the total incident solar available, is relatively consistent for the Reference system for the three comparative testing periods detailed in section 3.6, (48.6, 44.5, and 45.0 %). While these efficiencies are consistently greater than those measured for the FT-PV system, the Reference system thermal efficiency is much lower. That is, this system, under the operating conditions imposed during comparative testing, makes very poor use of both the solar and electrical heat inputs; (thermal efficiency calculated as 77.5% for the immersion only test falling to 53.4 % during the period of testing with the FT-PV system operated with the top immersion timed). The thermal efficiency is consistently greater for the FT-PV system. On this basis the data presented in table 5.2.1 for the annual energy saving for the Reference system (-793 kWh.) implies that the annual cost of heating water would be increased through installing the Reference system. As the present measure of thermal efficiency is sensitive to the proportion of solar input, as shown by the above mentioned data, the earlier assumption of a constant annual thermal efficiency is therefore not valid in this case.

Generally, both collection and thermal efficiency increase with system size. Collector losses are reduced, and, as larger storage tanks have a lower surface area to volume ratio, heat loss is also reduced. In addition, if a more evenly distributed load is imposed, standing losses are also reduced. It is therefore likely that the larger commercial Reference system will provide a worthwhile contribution to water heating energy demand. This also applies to the FT-PV system. In consideration of the above, an accurate estimation of the payback time would require longer term system performance monitoring than has been undertaken in the present work.

In respect of payback, for the FT-PV system, the benefits of using a timed immersion are apparent. The payback period for the anti-freeze based Reference system would be greatly reduced if a single tank with immersion control was used in preference to the present two tank system.

CONCLUSIONS and FURTHER WORK

1. Effect of limescale on the FT-PV system.

The experimental results presented in section 3.2 imply that, in comparison with a standard collector with copper fluid tubes, the EPDM based Flexsol collector is no more likely to suffer from the detrimental effects of limescaling. However, the extrapolation of these results to provide a long-term system performance forecast is open to question.

Further work is required to ascertain the long term effects of limescale on both the collector and the pump. As it is difficult to quantify the increased rate of deposition from accelerated testing, this will perhaps be best achieved through the long term monitoring of systems deployed in areas with hard water.

2. System flow analysis.

Both the collector and system dynamic characteristics, and the pump voltage/flow rate relationships, as defined in section 3.5.2, refer only to the prototype system. While they facilitated an accurate derivation of the degree of control required to provide the desired collector outlet temperature at full sun, this cannot be applied directly to the commercial system which comprises a 2.8 m^2 panel. The same method as presented in the above-referred section may be applied to the commercial system to define the pump voltage required to provide the desired full sun flow rate. While this larger collector will be common to all commercial systems, the length of connecting pipe will vary. The effect of additional pipe length on the system hydraulic characteristic must therefore be included to make the above method more broadly applicable.

3. Collector efficiency testing.

A new method of collector efficiency testing using time averaged values of measured instantaneous irradiance has been presented. The experimentally defined characteristic correlates well with that obtained using the semi-empirical method for the same flow rate. The collector outlet temperature profile has been modelled using the above-mentioned experimentally defined efficiency characteristics. There is good agreement between the measured and predicted temperature profile. This further validates the collector testing method proposed. However, to fully validate this method, a comparison with the characteristic as defined by an officially recognised standard collector test method would be required.

4. Optimised system performance

For a defined collector inlet and ambient air temperature of 15 °C, the design condition of a stable collector outlet temperature of 55 °C is not achievable with the methods of control studied. By accepting a reduced outlet temperature, using the physical shading method, a more stable profile is obtained. As can be seen from the temperature profiles observed during the different periods of comparative testing, for the same degree of control (e.g. a 55% shading of the PV module), the collector outlet temperature is highly sensitive to which electric immersion, upper or lower, is on, and its' method of control, (BNT, TNT and TT). If the load profile is such that the collector inlet remains close to mains temperature, an acceptable outlet temperature profile is achievable in practice.

For the prototype system, the PV module was somewhat oversized. This implies that it may be possible to smooth the outlet temperature profile by means of a positive feedback pulse width modulation, (PWM), control system. For the physical shading method, collector outlet temperature was generally seen to increase with decreasing irradiance. Pump efficiency decreased with flow rate. A PWM control system would allow the PV module to supply more power to the pump at these lower irradaince levels, to reduce outlet temperature, while throttling output at higher levels. The effect of collector thermal capacitance

would also need to be incorporated into the processor control program. In addition, the design of such a control system could allow the selection of the collector outlet temperature by the user. During periods of high consumption the solar contribution can be increased through accepting a lower outlet temperature, whereas, if load demand is low, the outlet temperature may be set closer to the load pre-set.

5. System components modelling

5.1 PV module characteristics.

A simple model characterising the performance of the PV module has been presented. This model has neglected the effect of module temperature on output. This model was combined with that developed to define the circuit electrical load characteristic in relation to additional circuit resistance in series, and in parallel, with the pump motor. This combined model has been used within an algorithm developed to predict the collector outlet temperature profile. The good agreement seen between the predicted and measured profiles implies that the afore-mentioned PV characteristic model, while simpler than those reviewed, performs with sufficient accuracy for the present purpose. The same can be said of the model developed to define the pump motor voltage in relation to the degree of physical shading applied to the PV module.

While the application of the physical shading model is limited to between 50 % and 70% shading, the algorithm for defining the pump voltage in relation to the additional resistance and irradiance has a broader applicability.

The respective algorithms for the above-mentioned models are easily viewed by accessing the macros (section 4.2) in the relevant Excel Workbook on the CD accompanying this thesis.

5.2 Storage tank modelling

A model for predicting heat loss and destratification in a hot water storage tank has been developed. Comparison with a measured profile has shown that this model works well. However, as it has

been designed for a tank of specific dimensions it must be further developed to accommodate other tanks. In respect of modelling storage tank charging, the difficulties of integrating the above cooling model with the preferred charging model have been highlighted.

6. System performance

While it has been shown that it is not possible to fully optimise the collector flow rate using the control methods applied, it is possible to approach the desired operating condition. Using the physical shading method the performance of the FT-PV system has been compared with that of a standard anti-freeze based system. While the collection efficiency of the FT-PV system was found to be affected by the position and control of the electric immersion, for all control modes, to provide the same load, the FT-PV system required less auxiliary heating.

The periods of testing were limited to approximately 14 days, with the same load profile applied to each system over the duration. To provide a fuller understanding of the above systems relative performance, longer testing periods, and the effect of different load profiles, would be required. This would have the additional benefit of providing more detailed information on which to estimate the respective payback periods. The thermal penalty incurred in the Reference system through using a separate solar preheat tank has been shown to put this system at a disadvantage. The effect of this penalty may be determined through side-by-side comparative testing of the two above systems with a third comprising a combined solar coil and immersion. The development of an intelligent immersion controller would be of great advantage to any SDHWS operating with an auxiliary electric immersion heater.

7. Performance simulation.

The models thus far presented have been shown to accurately predict the collector outlet temperature and flow rate as a function of the method and degree of flow control applied. The heat loss and destratification model has also been shown to work well. To provide a fuller performance simulation model, the above-mentioned tank charging model must be integrated with that for destratification. In

addition, the tank model will need to consider heat input from the electric immersion, and the mixing associated with its operation. Heat loss from the collector feed and return connecting pipes will also need to be considered. The comparative performance data presented in section 3.6 could be used to validate the performance of any proposed model.

APPENDICES

APPENDIX I

Equipment Specifications

I.1 Solarimeter details

I.2 Squirrel Data Logger specifications

I.3 Raab Karcher Heat meter

I.1 Solarimeter details

Type: Kipp and Zonen

Model: CH 11

Serial N°: CH11861376

Sensitivity: $5.17 * 10^{-6}$ V/W.m^2

Data logger scale: 0 to 20.00 mV

Logger tolerance: +/- 0.005 mV

Irradiance equivalent: = +/- 1 W/m^2.

I.2 Squirrel Data Logger Data.

Manufacturer: Grant Instruments, Cambridge, CB2 5QZ, England.

Type: 1203 series, (Two off)

Serial N^{os}: N°1 – 1203 – 01635, N°2 – 1203-00808

Temperature scale used: 300.0 °C.

Tolerance: +/- .05 °C.

I.3 Raab Karcher Heat meter.

Heat meter type: Combimeter Q

Model: 1.5 (Two off)

Serial N^{os}: 9801947 (FT-PV system) and 9801943 (Reference system)